GRINDING OF Si_3N_4 CERAMIC USING NANO-PARTICLES SUSPENDED IN VEGETABLE OIL BASED LUBRICANTS

YUSUF SULEIMAN DAMBATTA

FACULTY OF ENGINEERING
UNIVERSITY OF MALAYA
KUALA LUMPUR

2018

GRINDING OF Si_3N_4 CERAMIC USING NANO-PARTICLES SUSPENDED IN VEGETABLE OIL BASED LUBRICANTS

YUSUF SULEIMAN DAMBATTA

THESIS SUBMITTED IN FULFILMENT OF THE REQUIREMENTS FOR THE DEGREE OF DOCTOR OF PHYLOSOPHY

FACULTY OF ENGINEERING
UNIVERSITY OF MALAYA
KUALA LUMPUR

2018

UNIVERSITY OF MALAYA

ORIGINAL LITERARY WORK DECLARATION

Name of Candidate: Yusuf Suleiman Dambatta

Matric No: KHA150111

Name of Degree: Doctor of Philosophy

Title of Project Paper/Research Report/Dissertation/Thesis: "GRINDING OF Si_3N_4 CERAMIC USING NANO-PARTICLES SUSPENDED IN VEGETABLE OIL BASED LUBRICANTS "

Field of Study: Manufacturing systems

I do solemnly and sincerely declare that:

(1) I am the sole author/writer of this Work;
(2) This Work is original;
(3) Any use of any work in which copyright exists was done by way of fair dealing and for permitted purposes and any excerpt or extract from, or reference to or reproduction of any copyright work has been disclosed expressly and sufficiently and the title of the Work and its authorship have been acknowledged in this Work;
(4) I do not have any actual knowledge nor do I ought reasonably to know that the making of this work constitutes an infringement of any copyright work;
(5) I hereby assign all and every rights in the copyright to this Work to the University of Malaya ("UM"), who henceforth shall be owner of the copyright in this Work and that any reproduction or use in any form or by any means whatsoever is prohibited without the written consent of UM having been first had and obtained;
(6) I am fully aware that if in the course of making this Work I have infringed any copyright whether intentionally or otherwise, I may be subject to legal action or any other action as may be determined by UM.

Candidate's Signature   Date:

Subscribed and solemnly declared before,

Witness's Signature   Date:
Name:
Designation:

[GRINDING OF Si_3N_4 CERAMIC USING NANO-PARTICLES SUSPENDED IN VEGETABLE OIL BASED LUBRICANTS]

ABSTRACT

Silicon nitride (Si_3N_4) ceramic is highly desired in various engineering applications due to its exceptional properties. However, machining the Si_3N_4 ceramic suffers huge setbacks due to various degree of damages inflicted on the ceramic during grinding operations. Due to the significance of lubrication methods in the outcome of the grinding operations, there has recently been increase need for alternative lubrication techniques for grinding of the advanced engineering ceramics. Several findings from previous works indicated that the nanofluid MQL technique is a viable option of lubrication in the grinding process. Studies have shown that the Minimum Quantity Lubrication (MQL) method has better tribological ability than the flood cooling lubrication system during grinding of advanced engineering ceramics. Furthermore, the MQL technique (a highly efficient and eco-friendly lubrication method), is being used to reduce the different types of surface and subsurface damages, while significantly reducing the consumption of lubricants. This work involves optimization and experimental study on the performance of the Silicon dioxide-based MQL nanofluids in both conventional and ultrasonic assisted grinding of Si_3N_4 ceramic. The MQL nano-lubricant utilized was prepared by suspending silicon dioxide (SiO_2) nanoparticles in biodegradable vegetable oils. The MQL nanofluids were used to conduct grinding operations on the Si_3N_4 ceramic, using different process parameter settings. The results of the tangential and normal grinding forces, surface quality was analyzed using Taguchi and ANFIS modelling technique. Moreover, the effect of the grinding parameters i.e. feed rate, depth of cut, type of diamond wheel and lubrication type, were investigated on the output parameters (grinding forces, workpiece surface roughness, surface damages and wheel wear). Furthermore, the adaptive neuro fuzzy inference system (ANFIS) prediction method was used to predict and analyze the

variation of the input parameters with the performance parameters. The developed ANFIS prediction model was found suitable for predicting the performance of the grinding operations. The findings in this work indicate that by increasing the nanofluid concentration, there is resultant decrease of the grinding forces, with subsequent improvement of the surface quality. In addition, it was found that that the introduction of the ultrasonic vibrations onto the workpiece material during grinding operations helps to reduce grinding forces and surface roughness significantly. The self-sharpening phenomenon found in the ultrasonic assisted grinding (UAG) process was found responsible for the improved machining performance of the UAG process. Hence, hybridizing the UAG process with biodegradable oil based nanofluids in the MQL technique was found to improve the machining performances of the grinding process, achieving better performance as the non-biodegradable lubricants. As such, the combined setup of the MQL nanofluid system with the Ultrasonic grinding system is vital for improved performance during machining of Si_3N_4 ceramic.

Keywords: Ultrasonic assisted grinding (UAG), Silicon nitride, Nanofluid, Adaptive neuro-fuzzy inference system (ANFIS), Minimum quantity lubrication (MQL).

ABSTRAK

Seramik silikon nitride (Si_3N_4) sangat dikehendaki dalam pelbagai aplikasi kejuruteraan kerana sifatnya yang luar biasa. Namun demikian pemesinan seramik Si_3N_4 adalah amat sukar disebabkan pelbagai tahap kerosakan yang dikenakan ke atasnya semasa operasi pencanaian. Disebabkan kaedah pelinciran memainkan peranan yang penting dalam menentukan hasil operasi pencanaian, justeru kebelakangan ini terdapat peningkatan permintaan untuk teknik pelinciran alternatif dalam pencanaian seramik kejuruteraan termaju. Hasil beberapa kajian sebelum ini menunjukkan bahawa teknik MQL cecair nano adalah pilihan pelinciran yang sesuai dalam proses pencanaian. Kajian juga menunjukkan bahawa kaedah Minimum Quantity Lubrication (MQL) mempunyai keupayaan tribological yang lebih baik berbanding sistem pelinciran penyejukan banjir dalam pencanaian seramik kejuruteraan maju. Selain itu, teknik MQL (kaedah pelinciran yang sangat cekap dan mesra alam) digunakan untuk mengurangkan pelbagai jenis kerosakan permukaan dan bawah permukaan, serta mengurangkan penggunaan pelincir secara signifikan. Kerja ini melibatkan kajian pengoptimuman dan experimentasi prestasi pelincir nano MQL berasaskan Silikon dioksida ke-atas pencanaian konvensional dan pencanaian ultrasonik berbantu seramik Si_3N_4. Pelincir nano MQL yang digunakan disediakan dengan menggantung zarah nano silikon dioksida (SiO_2) dalam minyak sayuran terbiodegradasikan. Pelincir nano MQL digunakan dalam operasi pencanaian seramik Si_3N_4 dengan tetapan parameter proses yang berbeza. Hasil penggergajian secara tangen dan normal serta kualiti permukaan dianalisis menggunakan teknik pemodelan Taguchi dan ANFIS. Selain itu, kesan parameter pencanaian iaitu kadar suapan, kedalaman potongan, jenis roda berlian dan jenis pelinciran, diperhatikan pada parameter output (daya pencanaian, kekasaran permukaan bahan kerja, kerosakan permukaan dan kehausan roda). Selain itu, kaedah ramalan neuro kabur adaptif sistem (ANFIS) digunakan untuk meramal dan menganalisis variasi parameter input dengan parameter prestasi. Model ramalan ANFIS yang dibangunkan didapati sesuai untuk meramalkan prestasi operasi pencanaian. Penemuan dalam karya ini menunjukkan bahawa dengan meningkatkan kepekatan pelincir nano, kekuatan daya mencanai dapat dikurangkan disamping kualiti permukaan dapat ditingkatkan. Di samping itu, pengunaan getaran ultrasonik ke atas kerja bahan semasa operasi pencanaian didapati membantu mengurangkan kekuatan daya pencanaian dan kekasaran permukaan secara signifikan. Fenomena penajaman kendiri yang terdapat dalam proses UAG didapati memain peranan dalam peningkatan prestasi pemesinan proses UAG. Oleh itu, hibridisasi proses UAG dengan pelincir nano berasaskan minyak terbiodegradasikan dalam teknik MQL didapati dapat meningkatkan prestasi pemesinan proses pencanaian berbanding pelincir yang tidak boleh dibiodegradasikan. Oleh sedemikian, persediaan gabungan sistem pelincir nano MQL dengan sistem pencanaian ultrasonik adalah penting untuk prestasi pemesinan seramik Si_3N_4 yang lebih baik.

Keywords: pencanaian ultrasonik Berbantu, Silikon nitrida, Pelincir nano, Adaptive neuro-fuzzy inference system (ANFIS), Pelinciran kuantiti minimum.

ACKNOWLEDGEMENTS

Firstly, I would like to give my overwhelming gratitude to Allah (the most glorified and the most high).

I would also like to express my profound gratitude to my supervisors Professor Dr. Ahmed Aly Diaa Sarhan, Dr. Sayuti Bn Ab Karim and Professor Dr. Hamdi Bin Abd Shukor, for their tremendous support, encouragement and guidance throughout my research work.

I am highly grateful to my Mom Hajiya Binta Zakariyya for her prayers and endless support throughout my life. May Allah grant her Aljannatul Firdous.

I would like to sincerely appreciate the advice, supports and care provided by my siblings Dr. Shu'aibu S. Dambatta, Dr. Murtala S. Dambatta, Dr. Abdullahi S. Dambatta, Engr. Ali S. Dambatta, Pharm. Abubakar S. Dambatta, Aisha S. Dambatta and Dr. Sunusi S. Dambatta.

Finally, my sincere gratitude goes to Kano state Government of Nigeria and Senator Engr. (Dr.) Rabiu Musa Kwankwaso for providing me with sponsorship for my master's program in Malaysia.

YUSUF.

TABLE OF CONTENT

LIST OF FIGURES

LIST OF TABLES

LIST OF SYMBOLS AND ABBREVIATIONS

V_s : Wheel speed

T : Period of grinding for a single grit

ω : Angular speed of the wheel

V_f : Feed rate

f : Frequency of vibration

A : Amplitude of oscillation

R : Wheel's radius

C_l : Length of lateral crack

a_p : Depth of cut

K_c : Fracture toughness of the work material

ζ : Proportionality coefficients

F : Grinding force

Ra : Surface roughness

E : Young's modulus

H : Hardness

δ : Successive cutting-point spacing

ds : Wheel's diameter

V_c : Cutting speed

μ_0 : Constant which depends on property of workpiece

V_m : Amount of monoclinic phase present

σ_r : Residual stress

E: Modulus of elasticity

CHAPTER 1: INTRODUCTION

1.1 Introduction

Engineering ceramics have seen rapid rise in their applications across wide range of industries, such as automotive, aerospace, nuclear industry, refractory insulators, electrical/electronics, and defense industries. The extensive application of the engineering ceramic materials is attributed to their excellent physical, mechanical and chemical properties (Agarwal et al., 2005; Agarwal et al., 2008; Samant et al., 2009; Thoe et al., 1998; Uhlmann et al., 2010). Ceramics are characterized by high melting point, low density, excellent resistance to thermal shocks, resistance to oxidation reactions, very high hardness, high strength at elevated temperatures, chemical stability, low thermal and electrical conductivities, low friction, and high wear resistance (Agarwal et al., 2005; Agarwal et al., 2008; Wang et al., 2007). Typical types of the engineering ceramics used for biomedical and aerospace applications includes silicon nitride (Si_3N_4), alumina (Al_2O_3), and 3-YTZP (zirconia).

Conventional grinding (CG) is the utilized technique for machining of advanced ceramics. The CG process has so far been used to obtain improved surface integrity, and high dimensional accuracy/tolerance (Denkena et al., 2008; Zemzemi et al., 2014). Studies indicate that grinding accounts for more than 23% of the machining methods of advanced materials and ceramics in industries, whilst consisting more than 80% of the costs in the manufacturing process (Huang et al., 2003; Malkin, 1989; Xue et al., 2013). This led to the mass exodus towards investigations aimed at improving the performance of the grinding process in other to obtain a more economical and reliable manufacturing process (Agarwal et al., 2008; Cao et al., 2014; Zhong et al., 2004).

Previous works have shown that the utilization of brazed diamond wheels in grinding operations could be used to improve both the machining efficiencies, and the part quality during grinding operations. Moreover, several factors also affect the performance of the diamond wheels in grinding operations. They include bonding strength, grain projections and grinding efficiency (Chattopadhyay et al., 1991). According to the findings of Chen et al. (2009), the energy expended during material removal of grinding operations arise mainly due to the sliding and ploughing actions occurring in the grinding region. Hence, by appropriately controlling the sliding and ploughing ability of the wheel, the energy used in the grinding process could be greatly reduced.

Recently there has been more focus on hybrid cutting processes for machining of ceramic components. They include processes like ultrasonic assisted grinding (UAG), Laser assisted thermal grinding (LAG), etc. The hybrid processes, as observed from previous research works have brought about significant improvements to the efficiency, and surface quality during machining of advanced materials (Moriwaki et al., 1995; Xin-honga et al., 2006; Yanyan et al., 2009). The hybrid machining process can henceforth be regarded as a favorable machining method for the ceramic materials (Cao et al., 2014).

The extensive application of the advanced engineering ceramics in various fields has recently seen a rapid rise due to their exceptional properties. However, a major drawback to their applicability is the difficulty encountered in the process of machining the ceramics. The grinding process which is thus far the most economical method of machining ceramics, is often associated with high grinding forces, enormous heat generation, surface and subsurface cracks, and excessive use of hazardous lubricants. In other to reduce the occurrence of these unwanted phenomena, it is necessary to study and optimize the parameters of the grinding process. This work is a crucial step aimed at significantly reducing lubricant consumption, and subsequently lowering the deformations obtained during manufacturing of advanced ceramics.

1.2 Problem statement

Even though the engineering ceramics have highly desired physical, mechanical and chemical properties, the difficulty encountered while machining them results to great limitation to their extensive usage in various engineering fields (Agarwal et al., 2008). In addition, during grinding of the brittle materials, there is high occurrence of residual deformations (surface and subsurface) such as macro and micro-cracks, which deteriorates the quality of the manufactured components (Tan et al., 2008). As such, the need to improve on the machining process of these materials is highly important, especially improving machining efficiency and obtaining defect free components at lower costs (Huang et al., 2003; Xue et al., 2013).

Recent research works have indicated that the MQL process helps to significantly improve the performance of the grinding operations. Several types of nanoparticles such as TiO_2, SiO_2, Al_2O_3, MoS_2, graphene, graphene-oxide and diamond are being used to produce nanofluids that have been effectively applied to the MQL process. The use of nanofluid is aimed at improving lubrication during grinding operations. The SiO_2 nanoparticles have excellent properties like high hardness, high bending strength and relatively inexpensive, and fewer studies have been done to investigate the performance of SiO_2 based nanofluids during grinding of advanced ceramics. Specifically, the use of the SiO_2 based nanofluid during MQL grinding of advanced ceramics has not been extensively investigated. In addition, the SiO_2 nano lubricant has been found to perform excellently in other manufacturing process like milling, turning and drilling process due to its ability to withstand the high impact force in these processes (Sayuti et al., 2014). Also, the superior stiffness of the SiO_2 compared to other nano particles gives it better smoothening capability during grinding operations, such that it significantly helps to reduce the coefficient of frictions and power consumed during machining (Ooi et al., 2015).

Although the UAG process has a lot of advantages compared to CG, it is yet associated with many limitations such as micro-cracks, subsurface damages, residual stress, and in some cases reduced surface quality (Lauwers, 2011). As such, an in-depth investigation of the effects of the UAG process parameters on the performance of the process during grinding of ceramic materials was required. By appropriately optimizing the UAG process, the productivity and widespread application of advanced ceramic materials could be achieved (Agarwal et al., 2008; Jianhua et al., 2014; Lauwers et al., 2010).

From the literature review for machining of the difficult to materials, the following research gaps have been identified;

- Advanced engineering ceramics exhibit very high hardness which makes them to be classified under difficult-to-cut materials. As such, the grinding process which accounts for about 23% of machining these advanced ceramics needs to be improved, in other to reduce the finishing costs and increase efficiency.
- Common grinding methods are coupled with many limitations such as high grinding forces, poor surface quality, higher sub-surface damages, high tool wears, micro-cracking. These unwanted performances should be reduced to minimum for the improved applicability of the advanced engineering ceramics.
- Conventional lubrication methods involves use of excessive amount of lubricant which are hazardous to both the environment and the health of the operator. Hence, the performance of SiO_2 nanofluids in MQL grinding of advanced ceramics should be explored. This is because the nanoparticles are cheap and readily available.
- In addition, less number of active grains participate in grinding operation. Most of the diamond grains on the grinding wheels perform rubbing actions, thereby increasing the friction and generating heat. This limitation could be eliminated using high frequency lateral vibrations during the feed.

1.3 Objectives

- To compare the performance of vegetable oil-based nanofluid in minimum quantity lubrication with conventional flood cooling lubrication techniques during grinding of Si_3N_4 ceramics.
- To determine the performance of different types of vegetable oils in minimum quantity nanolubrication grinding of Si_3N_4 ceramic.
- To evaluate the performance of SiO_2 nanoparticles suspended in eco-friendly oils during grinding with minimum quantity nanolubrication
- To investigate the effect of applying lateral ultrasonic vibrations on Si_3N_4 ceramic during grinding operations with minimum quantity nanolubrication using different types of eco-friendly oils.

1.4 Scope of study

This research focus on analysis of grinding process parameters and the performance response from the grinding operations. The main aim is to provide required improvements to the grinding of advanced engineering ceramics. The solution to several problems and defects generated during the grinding operations. The proposed solutions involve improving the lubrication systems and the grinding mechanisms. The performance of the grinding process was measure in terms of grinding forces and surface quality. The results of grinding forces and surface roughness were mapped using artificial intelligent (AI) method (i.e. ANFIS modelling). The mapping was done in other to develop AI prediction models for the performance of the grinding process. The utilization of SiO_2 based nanofluids in MQL grinding of Si_3N_4 ceramic was studied extensively, and the optimum parameter settings were obtained.

Studies of previous literatures have shown that the use of UAG to machine advanced engineering ceramics will ensure sustainable production of ceramic materials.

Additionally, an improved machining set-up formed by hybridizing the MQL nanolubrication system with the UAG process was proposed.

Summarily, this works covers the following aspects:

- Taguchi experimental designs for optimization of the grinding process.
- Study of the effect of different process parameters in the grinding of the Si_3N_4 ceramic.
- Performance improvement due to utilization of MQL nanolubrication in the conventional grinding the advanced ceramics.
- Performance evaluation of different types of vegetable oils in MQL grinding of ceramics.
- Design of ultrasonic horn configuration to achieve 2D elliptical vibratory motion during the UAG process.
- Hybridization of ultrasonic assisted grinding set-up with the MQL nanolubrication system.

1.5 Outline

This section provides an outline on how the thesis was structured. The thesis was reported in an article style format and comprises of six chapters. The article style format is such that each chapter consists of a brief introduction of the study, general literature review, methodology, result analysis and discussion, and a concise summary.

Chapter 1 of this thesis provides an understanding and significance of this study. Moreover, a brief introduction and history of grinding advanced ceramics was provided. The problem statement, research gaps and objectives are also provided.

Chapter 2 contains explanations on previous studies done on grinding of advanced ceramics. The evolution of the machining processes used in cutting ceramics was also explained comprehensively. Additionally, an insight into the limitations and possible improvements to the machining of advanced ceramics was provided.

Chapter 3 reports the findings from comparison of MQL nanolubrication with conventional flood cooling techniques. It consists of experimental investigation of the effects of different grinding parameters on the performance of grinding process. Taguchi L_{16} experimental design was used to optimize the responses of the grinding process. ANFIS modelling was then used to predict and analyze the relationship between the input and output parameters. The wheel and workpiece surface characteristics were also analyzed accordingly.

Chapter 4 gives an experimental analysis and optimization of SiO_2 based nanofluid in MQL grinding process. The grinding experiment was conducted using different grinding and MQL parameters based on Taguchi L_{16} design of experiments. The results of the tangential, normal grinding forces, and surface quality were analyzed using SN ratio analysis and ANFIS prediction modelling techniques. Lastly, the surface integrity of the Si_3N_4 ceramic was also analyzed.

Chapter 5 deals with an experimental analysis to study the effect of applying ultrasonication and MQL nanolubrication using SiO_2-based nanofluids produced using different types of vegetable oils. The tangential, normal grinding forces and surface quality were used to analyze the performance of the grinding process.

Chapter 6 the final section outlines the conclusions from all the findings of this work. In addition, future investigations and recommendations are provided in this section.

Lastly, the list of references and publications were also provided.

CHAPTER 2: REVIEW ON ULTRASONIC ASSISTED GRINDING OF ADVANCED MATERIALS FOR BIOMEDICAL AND AEROSPACE APPLICATIONS

2.1 Introduction

This section presents a review on ultrasonic assisted grinding (UAG) of advanced materials, specifically investigating the effects of ultrasonication on material removal rates (MRR), grinding forces and grinding energy, tool wears and surface/subsurface damages. It compares the performance of UAG of ceramics and super alloys for biomedical, and aerospace applications, with the performance of the conventional grinding (CG) techniques. The effects of the UAG process parameters on the MRR, grinding ratio, tool life, residual stresses and surface/subsurface damages were also investigated. Previous studies on the performance of the UAG process in the machining of brittle and ductile materials have shown that the introduction of the ultrasonic system to the grinding process helps to increase the material removal rates significantly, and consequently reduces the surface roughness, grinding forces and subsurface damages. The self-sharpening phenomenon found in the UAG process was realized to be responsible for the improved machining performance of the UAG process. Furthermore, the application of biodegradable lubricants (vegetable oil based) to the grinding process was also found to improve the machining performances of the UAG process, achieving almost the same performance as the non-biodegradable lubricants. As such, the use of the biodegradable lubricants in the grinding process was encouraged due to its economic benefits, and environmental friendliness.

2.2 Literature Review

Advanced engineering ceramics and super alloys such as alumina, silicon nitride, zirconia, and Inconel have seen rapid rise in their applications across wide range of industries, such as automotive, aerospace, nuclear industry, refractory insulators, electrical/electronics, and defense industries because of their excellent physical, mechanical and chemical properties Agarwal et al. (2005); (Agarwal et al., 2008; Samant et al., 2009; Thoe et al., 1998; Uhlmann et al., 2010). They are characterized by: high melting point, low density, good resistance to thermal shocks, resistance to oxidation reactions, very high hardness, high strength at elevated temperatures, chemical stability, low thermal and electrical conductivities, low friction, and high wear resistance (Agarwal et al., 2005; Agarwal et al., 2008; Wang et al., 2007).

Cutting is the most popular and feasible process for manufacturing ceramics and super alloys. Some methods used to fabricate or cut the super hard materials includes forming, grinding, shearing, etc. Interests in machining of the advanced ceramic materials have substantially grown due to their widespread usage in precision components (Agarwal et al., 2005; Arunachalam et al., 2004).

An important requirement during the manufacture of ceramic parts is the reliability of the machining process. In spite the significant advancements made in near-net shape technologies, the abrasion grinding method using diamond or cubic boron nitride (CBN) wheels is still the predominant method of machining the ceramic components (Qu et al., 2000). Conventional grinding (CG) utilizes the gliding action of a super-hard tool over the workpiece at very high speeds. This process has been utilized in advanced machining to obtain improved surface integrity, and high dimensional accuracy/tolerance in different engineering materials (Denkena et al., 2008; Zemzemi et al., 2014). Grinding has been estimated to account for more than 23% of machining advanced materials and ceramics in industries, whilst consisting more than 80% of the costs in the manufacturing process (Huang et al., 2003; Malkin, 1989; Xue et al., 2013). The various limitations associated with the CG process led to the mass exodus towards investigations, aimed at improving the performance of the grinding process economically, reliably, etc. (Agarwal et al., 2008; Cao et al., 2014; Zhong et al., 2004).

Due to the properties of the ceramic materials such as high hardness, low fracture toughness, and brittleness, the ceramic materials were classified under difficult to machine materials. Also, compared with their metallic counterparts, the ceramic materials are much harder and hence more prone to brittle fractures (Chen et al., 2015; Pei et al., 1995; Tesfay et al., 2016; Xiao et al., 2014). The setback mainly associated with grinding of the ceramic materials is their brittleness which results in high cutting forces, edge-chipping and micro fractures during the process of cutting (Ahmed et al., 2012; Choi et al., 2007; Xiao et al., 2014; Zeng et al., 2005). The limitations associated with the cutting of ceramics materials are among the major impediments to their widespread usage (Agarwal et al., 2008). Moreover, different kinds of deformations such as sub-surface damages, micro-cracks (Agarwal et al., 2008; Kirchner, 1984), pulverized layer (Zhang et al., 1994), plastic deformations, and tool/wheel wear are also found in the CG process. These deformations were also found to be accompanied by high grinding forces and heat generation (Xu et al., 1995).

Recently there has been more focus on hybrid cutting processes used in the cutting of the ceramic components. They include processes like ultrasonic assisted grinding (UAG), laser assisted thermal grinding (LAG), ultrasonic assisted turning, etc. The hybrid processes, as observed by previous research works have brought about significant improvements to the efficiency, and surface quality during machining of the advanced materials (Moriwaki et al., 1995; Xin-honga et al., 2006; Yanyan et al., 2009). The hybrid machining process can henceforth be regarded as a favorable machining method for the ceramic materials (Cao et al., 2014).

Several investigations have been done to understand the effects of ultrasonic vibration during the grinding of hard and brittle materials. The outcome of these investigations highlights that the surface roughness, material removal rates, and strength of the ground components were improved significantly by the ultrasonication of the grinding process.

Furthermore, the grinding forces, and tool wears were found to be decreased considerably by the ultrasonic vibrations (Akbari et al., 2008; Brecher et al., 2010; Gao et al., 2009; Gong et al., 2010; Suzuki et al., 2007; Vicario et al., 2007; Zeng et al., 2005).

Ultrasonic assisted grinding involves simultaneously applying ultrasonic vibrations to the workpiece in two directions, it is developed such that it combines the impact of material removal phenomenon of ultrasonic aided lapping with high-speed abrasive grinding (Pei, 1995; Uhlmann et al., 2007). In UAG process, the ultrasonic vibrations are produced by transforming electrical signals from piezo-electric or magnetostrictive converters into linear motions (Marinescu et al., 2006; Thoe et al., 1998). It has proved to be a cost-effective method of machining super hard materials (Akbari et al., 2008; Brehl et al., 2008; Choi et al., 2007; Feucht et al., 2014; Gao et al., 2009; Ma et al., 2005; Yanyan et al., 2009). The UAG process has been widely used in the cutting of super-hard materials such as structural ceramics, glass, super alloys, metallic composites and carbonated plastic composites (Brecher et al., 2010; Lv et al., 2013).

Although the UAG process has a lot of advantages compared to CG as elucidated, it is yet associated with many limitations such as micro-cracks, subsurface damages, residual stress, and in some cases reduced surface quality (Lauwers, 2011). However, an in-depth investigation of the effects of the UAG process parameters on the performance of the process during grinding of advanced materials was required, so as to optimize the machining process. By so doing, the productivity and widespread usage of the advanced ceramic materials would be increased considerably for the aerospace and biomedical applications (Agarwal et al., 2008; Jianhua et al., 2014; Lauwers et al., 2010).

This section provides a comprehensive review of the current achievements, and limitations of the UAG process with emphasis on the current limitations to provide grounds for future research works. It assesses the basic principles and performance of the ultrasonic assisted grinding process, in comparison with the CG process regarding productivity, physical properties, part quality etc.

2.2.1 Grinding wheels used in cutting superhard materials

The tool used to perform the grinding operations is referred to as the grinding wheel. Grinding wheels are important parts of the grinding process, and are made up of many tiny abrasive grains held by abrasive bonding material as illustrated in the structure of grinding wheel shown in **Figure 2.1**. The bonding material does not participate in cutting during the grinding process; its primary function is rather to hold the grains together. Standard grinding wheel bonds includes vitrified bond, resinous bond, silicate bond, shellac bond, rubber bond, metallic bond, and electroplated bond. The abrasive grains (superhard material) and bond (fixative material) are the main components of the grinding wheel. The space between the abrasive may be partially or wholly filled with the bond material. Also, the performance of the grinding wheel was a function of abrasive material, abrasive grain size, bond material, porosity, concentration and the strength of abrasive-bond. The abrasive grains are characterized by higher hardness, wear resistance, toughness, friability etc. The main parameters of the grinding wheel are grain size, bond material type, and wheel structure. The categories of abrasives mainly used as grinding wheels are either natural or synthetic. The artificial abrasives most commonly used are aluminum oxide, silicon carbide, cubic boron nitride, and diamond. Furthermore, the choice of the wheel types depends on the characteristics of the workpiece material, desired tolerance and the surface quality required. For instance, the conventional wheels i.e. Al_2O_3 and SiC are the primary abrasives used when grinding alloy materials such as steel, while the super-abrasive wheels i.e. diamond and CBN, have the ability to grind extremely hard materials such as ceramics, glass, and super alloys (Kalpakjian et al., 2014).

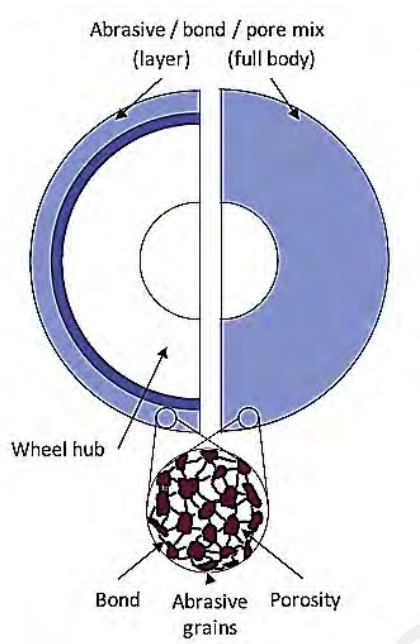

Figure 2.1: Structure of grinding wheels (Winter et al., 2015).

The concentration is a parameter that indicates the proportion of abrasives on the grinding wheel. The amount of abrasive found on the wheel number was scaled to give the concentration number (s), using the exact concentrations (Vg) as shown in **Table 2.1**.

Table 2.1 : Concentration number for various abrasives

Abrasive	**Concentration number (S)**
Diamond	$s = 4 \times V_g$
CBN	$s = \frac{100}{24} \times V_g$
Conventional Abrasive	$s = 64 - \frac{V_g}{2}$

2.2.2 Advanced biomedical and aerospace materials

Several applications in biomedical engineering require the use of advanced materials such as and ceramics (e.g. alumina, zirconia, Silicon nitride etc.), metallic based (e.g. Titanium alloys, SS, Co—Cr alloys etc.), and matrix composites. **Table 2.2** shows the biomedical fields in which the bioceramics are commonly used.

Table 2.2: Types of ceramics used in biomedical applications (El-Meliegy et al., 2011).

Application	Type of ceramic material used
Orthopaedic load bearing	Alumina, partially stabilized zirconia
Dental orthopaedic	Bioactive-glass, alumina, partially stabilized zirconia
Dental implants	Alumina, Bioactive-glass, hydroxyapatite
Spinal surgery	Bioactive glass ceramics, Hydroxyapatite
Alveolar ridge	Alumina, Bioactive glass ceramics

The biomedical engineering fields where these advanced materials are utilized includes; dentistry, ophthalmology, orthopaedics, plastic and reconstructive surgery, neurosurgery, veterinary medicine and surgery. The materials utilized often need to be characterised by high bioactivity, highly corrosion resistance, high strength, and in some cases the ability to undergo osseointegration (Shi, 2006). In general, the biomedical materials are classified as either bio-tolerant, bio-inert or bioactive as shown in **Table 2.3**.

Table 2.3: Bio-materials and their classifications (Shi, 2006).

Bio-tolerant materials	Bio-inert materials	Bioactive materials
Stainless steel	Titanium	Bio-glass
Vitallium	Titanium alloys	Tri-calcium phosphate
Poly-methyl methacrylate (PMMA)	Carbon	Hydroxyapatite
	Alumina	A-W glass ceramic
	Zirconia	
	Titania	
	Si_3N_4	

The advanced materials used for aerospace applications include metals, ceramics and composites. The metallic materials have been dominant as aerospace structural materials since the 1920s. However, since early 1990s, high strength ceramic and composite materials are being increasingly used in many aerospace applications. Studies have shown that the percentage of composites used in the airframes have grown from about 2% up to 27%. Also, the aircrafts are usually composed of about 5–15% high strength steels, which are usually found in highly critical parts such as landing gear components. Another type of aerospace material is the super alloys which are made up of nickel, iron–nickel or cobalt based alloys. The super alloys are used to manufacture aerospace components that operate at high temperatures (above 1000°F) such as compressors, turbines, and combustors (Cotton et al., 2002; Williams et al., 2003).

Figure 2.2 illustrates the evolution of amount of materials used in aerospace applications. It could be seen that over time, the conventional metals are being replaced by materials such as ceramics, composites, titanium and nickel alloys. The composites materials are gaining widespread popularity in the aerospace industry because of their properties which include lower density, higher modulus, high temperature resistance and reliability. Additionally, the aerospace industries have seen a rise the utilization of materials such as fiber reinforced plastics (FRP) and fiber reinforced metals (FRM) (Buhl, 2012).

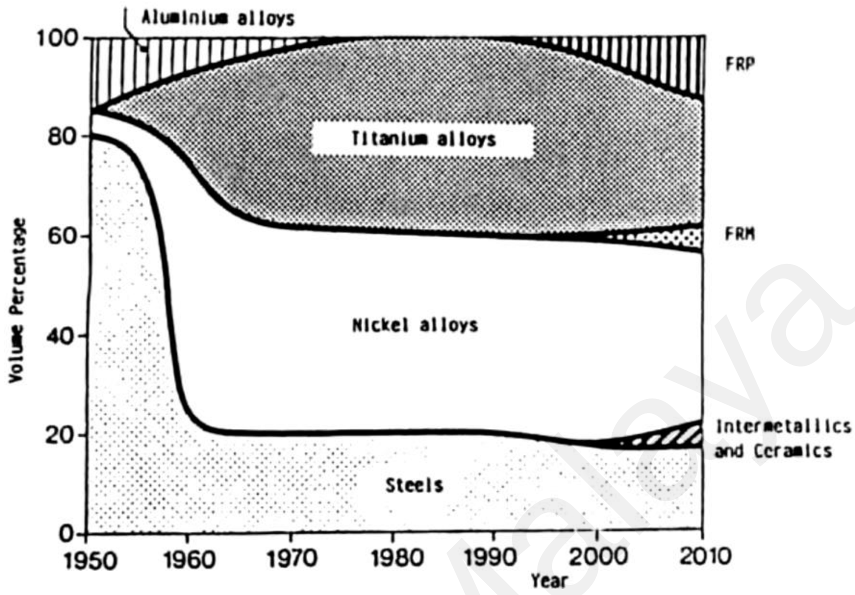

Figure 2.2: Evolution of aerospace materials since 1950s (Buhl, 2012).

Metals are used as biomedical materials because of their excellent mechanical properties and fair biocompatibility. Metals exhibit excellent strength and resistance to fracture, which are crucial for the medical applications requiring load bearing. Among extensive varieties of metallic materials, a number of them exhibit good biocompatibility and not hazardous to the human body. They include stainless steels, cobalt alloys, titanium alloys, and noble metals. Some of their properties which makes them extremely desired are shown in **Table 2.4**. The titanium-based alloys are more preferred for use as biomedical implants due to their excellent biocompatibility. However, stainless steel is currently more utilized because it is cheap. Also, the Cobalt-based alloys are often desired when the implantation requires very high wear resistance, but stainless steel has a very poor corrosion resistance which it less reliable when used as an implant (Niinomi, 2002; Speidel et al., 1992).

Table 2.4: Property Comparison of metallic based advanced biomedical materials (Shi, 2006).

Alloys	Density (g/cm3)	Young's modulus (GPa)	Yield strength (MPa)	Corrosion resistance
Ti and its alloys	4.5	79-116	485-1034	High
Stainless steel	7.9	190	221-1213	Low
Co-based alloys	8.3-9.2	210-253	448-1500	Excellent

The ceramic materials are characterized by high hardness, high strength at elevated temperatures, high chemical stability, and high wear resistance. Due to these outstanding properties, the grindability of the ceramic materials is poor compared to the metallic materials. Studies have shown that CG is mostly used to machine heat treated turbine blades in aerospace components. When the machining operation requires a significant amount of material removal, a rough grinding operation followed by a finish grind is used to produce the components. Also, the high temperature resistant materials are sensitive to the level of energy used during CG. As such various degrees of deformations such as surface and subsurface cracks, wheel wear and excess wheel loading are found on the machined components (Campbell Jr, 2011). Also, studies have shown that the machining of the ceramic materials is associated with lower material removal rates, chipping actions, high grinding force etc. Moreover, (Gates et al., 1999) reported that more efforts are being channeled toward improving the machinability of the ceramic materials. Several methods that could help to reduce the manufacturing costs are also being considered such as development of new machining techniques with optimal lubricating conditions. In addition, studies have shown that the utilization of ultrasonic vibrations during the grinding operations significantly reduces the occurrence of deformations with resultant increase in material removal, the UAG process could be an effective alternative for machining the aerospace and biomedical materials.

2.3 Fundamentals of Ultrasonic Assisted Grinding

UAG is a machining method which has recently been used in the grinding of various ceramic components. It is a technology that is considered to have a great potential in machining of super-hard and brittle materials. The ultrasonic vibrations have been used together different conventional or advanced machining techniques, so as to achieve higher process performances. Some of the hybrid processes such as the UAG have reached advanced stages, and are been used for large scale production of components in the industry. **Table 2.5** illustrates the current advances in the hybridized ultrasonic machining processes. It could be seen that the ultrasonic vibration assisted grinding is being utilized in various stages of product development from concept developments to mass productions. The UAG process has gained high desirability in industries due its high precision and ability to produce almost defect free surfaces (Lauwers et al., 2014).

The UAG was first introduced in the late 1950s and has since been used to machine various types of super hard materials (Brehl et al., 2008; Isaev et al., 1961). Moreover, in the early 1980s as a result of the difficulties encountered in machining the difficult to cut materials, the ultrasonic grinding process was considered a possible machining technique for these materials. This is because studies have shown that by using the UAG to machine stainless steel, glass or ceramics, the tool life is greatly increased, thus providing economic advantage during the machining process (Brehl et al., 2008; Moriwaki et al., 1991; Moriwaki et al., 1992). However, the 2D UAG systems came into light in the mid-1900s, and have since then been more extensively used to machine the super hard materials. The 2D UAG process is characterized by lower grinding force, higher surface quality and lower wheel wears (Brinksmeier et al., 1999; Moriwaki et al., 1995; Shamoto et al., 1994). Nowadays, the UAG process is being used to obtain precise cutting and higher surface quality in stainless steel, glass and ceramic materials. Also, studies have shown that the UAG process is increasingly being used to achieve high precision cutting in biomedical and aerospace materials such as ceramics and composites (Shi, 2006). The UAG process as shown in **Table 2.5** has grown from concept development stage to applications for mass productions. This could be attributed to the increased productivity and reduced deformation associated with the UAG process.

Table 2.5: Advances in assisted machining systems (Lauwers et al., 2014).

Vibration assisted processes	Fundamental research stage	Concept development	Prototype development	Production testing	Mass production
Vibration assisted turning					
Vibration assisted milling					
Vibration assisted drilling					
Vibration assisted grinding					
Vibration assisted polishing					
Vibration assisted EDM					
Vibration assisted forming					

The ultrasonic vibration found in the process refers to the high-frequency oscillations occurring between frequency ranges of 20-60 kHz (Ding et al., 2014). The vibrations are produced with the aid of either piezoelectric or magnetostrictive transducers (Pei, 1995). In UAG system, the setup of the CG process is integrated together with an ultrasonic system, thereby resulting to a complex multi-mode operation characterized by a spindle speed Vs, feed rate Vf, amplitude of vibration A, and vibration frequency f, as shown in **Figure 2.3a**. The UAG involves a very high-frequency 2D oscillation along the directions perpendicular to the feed direction, which results in oscillatory motions about the feed direction characterized by elliptical trajectory (Denkena et al., 2008). The 2D ultrasonic vibrations are produced via application of ac voltage to the piezoelectric material, which converts the electrical energy into mechanical energy. The resulting signal is then boosted, and channeled onto the workpiece via a horn, causing it to vibrate along the longitudinal and bending axes, creating elliptical movements as it vibrates (Chen et al., 2016; Liang, Z. Q. et al., 2010). Moreover, the reversal of the cutting direction during the vibrations, results in plastic flow of chips during the cutting cycle, thereby causing an in-process lubrication, and allowing for more penetration of the lubricants (Li et al., 2006; Liang, Z. Q. et al., 2010; Suzuki et al., 2003). Summarily, the UAG machining system involves complex movements of the abrasive grits resulting in three types of motion i.e. rotational, linear, and 2D oscillation about the wheel axis. The path traced out by a single abrasive grit during both the CG and UAG processes is illustrated in **Figure 2.3b**. it could be seen that the UAG process covers a larger cutting area (Li, S. et al., 2016).

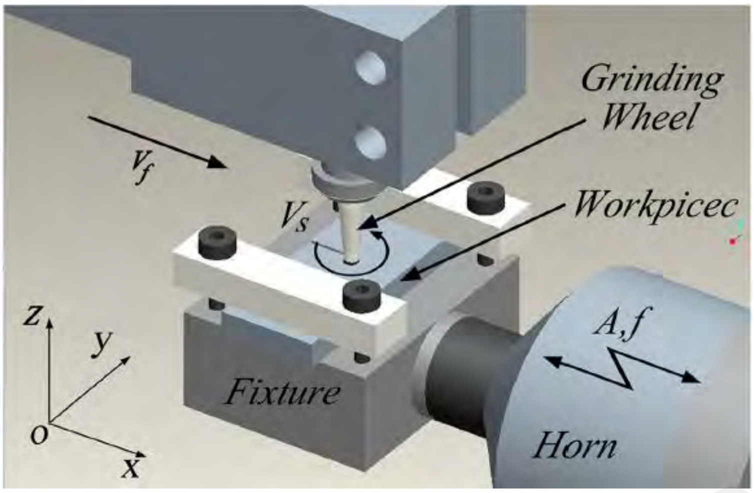

(a)

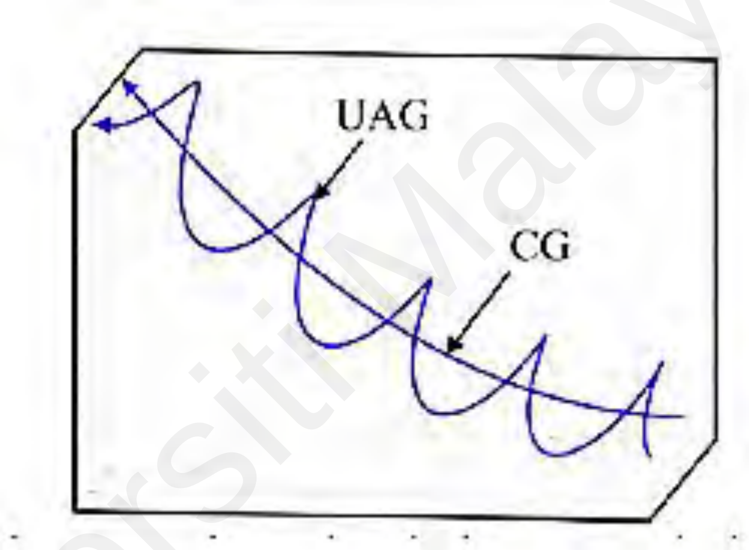

(b)

Figure 2.3: (a) UAG grinding system (Jian-Hua et al., 2015) (b) grain path in UAG (Liang, Z. Q. et al., 2010).

The grinding system is made of two sections namely the ultrasonic system and the tool, as shown in **Figure 2.4a** (Jianhua et al., 2014). The former consists of the ultrasonic generators, transducer, booster, horn and the workpiece holder as shown in **Figure 2.4b** (Liu et al., 2008), while the latter is usually made of diamond, CBN, or any other super hard grinding wheel (Yanyan et al., 2009).

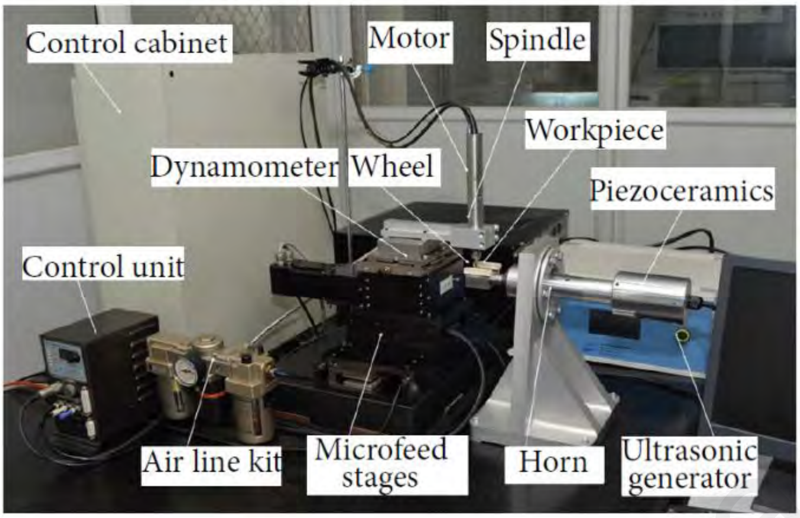

(a)

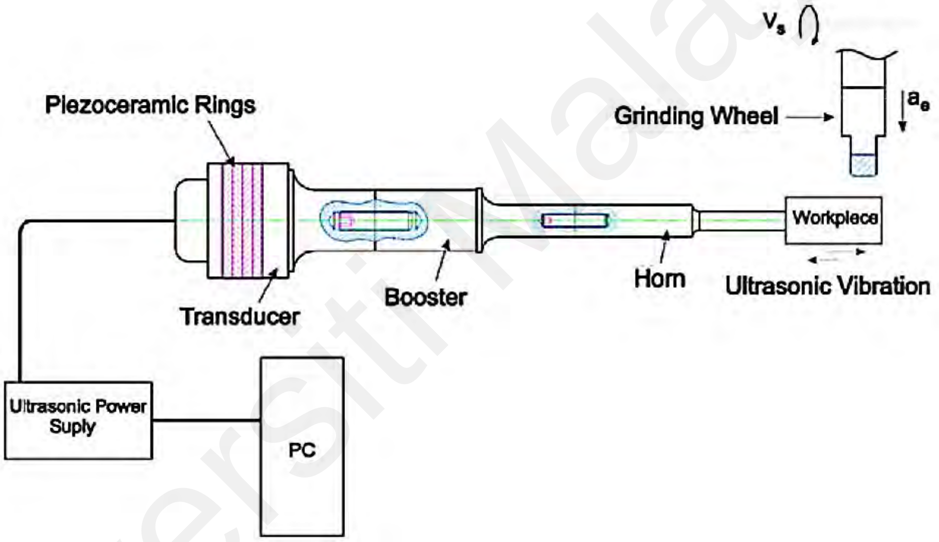

(b)

Figure 2.4: Ultrasonic assisted grinding (a) experimental setup (Jianhua et al., 2014) (b) illustration of workpiece holder.

2.3.1 Processing principle: Ultrasonic assisted grinding

The processing principle of the UAG entails using a high speed grinding wheel (tool) made up of super hard materials like diamond and CBN, operating at a specified depth of cut to machine the advanced materials. The tool is made to glide against the less harder workpiece material which is attached to an ultrasonic system vibrating at ultrasonic frequencies, having peak to peak vibration amplitudes up to 20µm (Agarwal et al., 2008;

Li, S. et al., 2016; Saljé et al., 1986; Tawakoli, Taghi, Azarhoushang, Bahman, et al., 2009).

Wang, Lin, and Zhang (2014) relate that there are 3 types of movements found in the UAG process. During the oscillation process, there exists a circular wheel motion, then a linear motion due to feed and harmonic oscillations resulting from the ultrasonic vibrations. Based on these three types of motions, it was found that the length traced by a single diamond grain during a single cut over a given period can be obtained using **Equation 2.1**;

$$\mathrm{L} = \int_0^{t_1} \sqrt{((V_f + V_s)^2 + (2\pi f A\cos\,(2\pi f t_1))^2 + (V_s sin\omega\, t_1)^2}\ dt_1 \tag{2.1}$$

Where V_s is the wheel speed, t_1 is the period of grinding for a single grit, ω is the angular speed of the wheel, V_f is the feed rate, f is the frequency of vibration, and A is the amplitude of oscillation.

Similarly, Wang, Lin, Wang, et al. (2014) came up with a mathematical model for the frequency of vibration in the UAG process. Their model gives the optimal resonance frequency for the UAG technique by considering the optimal performance of the process parameters. **Equation 2.2 and 2.3** present the mathematical model for the optimum frequency of vibration;

$$\mathrm{f} = \frac{t_1(V_s+V_w)-2C_l}{4C_l t_1} \tag{2.2}$$

$$\mathrm{f} = \frac{arccos R - \mathrm{ap}_{/R(V_s+V_w)} - 2\omega\zeta_1(F_{/k_c})^{3/4}}{4\,arccos\,R - \mathrm{ap}/R\zeta_1(F/K_c)^{3/4}} \tag{2.3}$$

Where R is the wheel's radius, C_l is the length of lateral crack, a_p is the depth of cut, K_c is fracture toughness of the work material, ζ_1 & ζ_2 are the proportionality coefficients, and F is the grinding force (Wang, Lin, Wang, et al., 2014; Zhao et al., 2006).

By using the above theoretical models, the total length traced by the grit and the desired frequency of vibration of the ultrasonic unit could be obtained using the machining parameters.

2.3.2 Classifications of Ultrasonic Assisted Grinding

The ultrasonic grinding process is divided into two modes i.e. vibrating tool or vibrating workpiece. Depending on the mode in which the workpiece or tool is been vibrated, the UAG process could be classified as either one-dimensional (1D) or two-dimensional (2D) UAG system. The 1D-UAG occurs when the ultrasonic vibrations are applied either along the wheel's rotational axis, or perpendicular to it (Cao et al., 2014). Studies have shown that the performance and operational characteristics of the 1D-UAG process is highly affected by the direction of the oscillations, which could be either perpendicular, or axial oscillations along the direction of the feed. When the vibrations are along the wheel's axis, it is called 1D Axial-UAG (1D-AUAG) and when it is perpendicular, it is referred to 1D vertical-UAG (1D-VUAG). The axial type has proven to produce superior surface roughness (Cao et al., 2014; Denkena et al., 2008), and fewer deformations on the workpiece surfaces (Liang et al., 2012). Moreover, reports have shown that with the introduction of 1D vertical vibrations, the grinding process witnessed a decrease in the grinding forces (Chen et al., 2016; Wu et al., 2003). Also, the 1D axial UAG process was found to perform better regarding accuracy and tolerances (Spur et al., 1996; Uhlmann et al., 2006). However, the 1D axial UAG was reported to exhibit high rate of tool wear and deterioration of the surface quality (Wu et al., 2003).

In the 2D-UAG, the workpiece is vibrated along two axes, thereby creating an elliptic or circular geometry (Ding et al., 2014; Peng et al., 2011). The 2D-UAG sometimes referred to as elliptical-UAG, involves triggering ultrasonic oscillations of the workpiece material concurrently along 2 horizontal directions. The system operates such that a vertical vibratory motion was integrated with the horizontal linear movements of the 1D-UAG. This enables the workpiece material to exhibit a tiny circular or elliptical form of motion during its movement along the cutting direction. **Figure 2.5** illustrates the path traced out during the 2D-UAG process, which takes the form of a sequence of overlapping ellipses. This results in a highly complex motion that requires a more complicated design, thereby making the 2D-UAG system to be more expensive than the 1D-UAG (Brehl et al., 2008). Previous research works have currently focused on the 2D-UAG, this is because literatures have shown that there was greater reductions in the grinding forces, and residual stresses during the 2D-UAG process (Li et al., 2006).

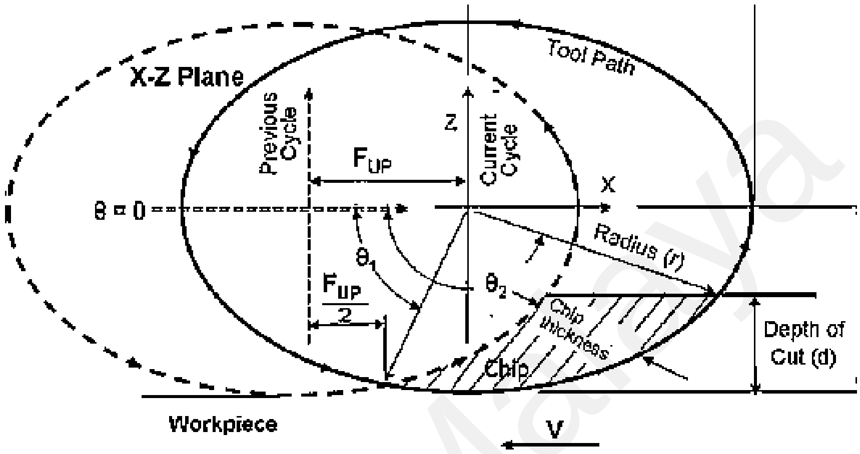

Figure 2.5: Two-dimensional UAG (2D UAG) (Brehl et al., 2008).

The grinding forces obtainable in the different types of UAG processes compared to the CG method are shown in **Figure 2.6**. It was found that the 2D-UAG process conflates the performances of both 1D-AUAG and 1D-VUAG. The amplitudes of vibration in each of the processes is shown in **Figure 2.6**, illustrating the mode and direction of motion present in the grinding operations. The elliptical-UAG was found to produce a better machining result among all the UAG processes, capable of realizing higher surface integrity, and lowest grinding forces. However, the cost of its initial set up is very high, making the 1D-VUAG more preferable as a result its economic advantages (Chen et al., 2016; Guo et al., 2011; Pei, 1995; Vanparys et al., 2008).

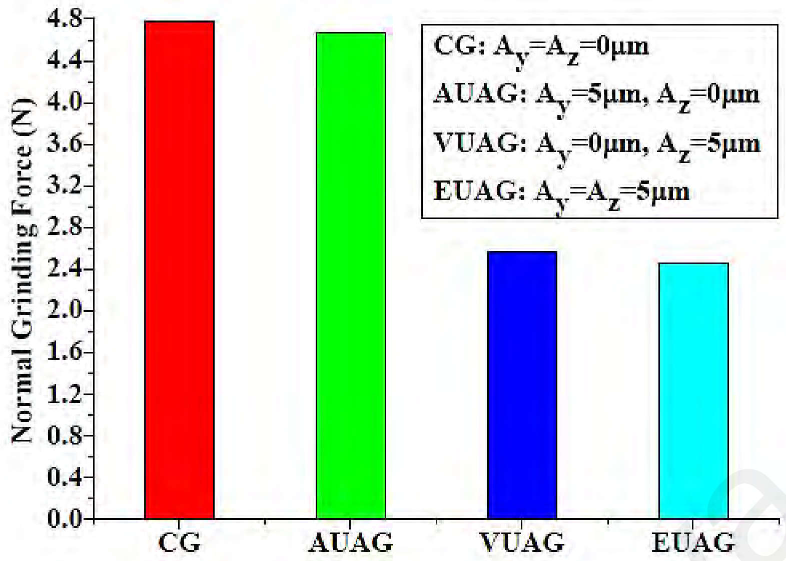

Figure 2.6: Grinding force in UAG processes (Chen et al., 2016).

2.4 Mechanism of material removal

The UAG method, just like the CG process employs either ductile mode, brittle mode and/or plastic flow as its mechanism of material removal (Dornfeld et al., 2006). Huang et al. (2003) studied the performance of high-speed grinding of ceramic materials such as alumina, alumina–titania, and yttria partially stabilized tetragonal zirconia(Y-TZP). They investigated the material removal process, and found that it was characterized by grain ejections, and propagation of lateral cracks along the grain peripheries. It was concluded that the mechanism of material removal in ceramic components involved both brittle fractures, and ductile grinding modes.

Brittle fracture is similar to creating cavities on the surface of the material using a hard indenter, it is often accompanied with two types of cracks i.e. lateral and median cracks. The former was found to be solely responsible for material removal, while the latter was associated with strength degradations, and deformations. The brittle fracture also involves materials material removal via nucleation, and propagation of voids and cracks, through micro-chipping or crushing actions (Kirchner, 1984). Studies have shown that the micro-cracks caused by the brittle fractures are formed from the lateral cracks. Furthermore, the material removal mechanisms in the brittle grinding mode was found to occur as a result of the proliferation of the lateral cracks, thereby creating crater-like geometries on the machined surfaced (Cook et al., 1990). Also, the deformations produced during the brittle mode machining has been found to give rise to various types of micro-cracks, phase transformations, and residual stresses. These deformations were found to be detrimental to the strength, and performance of the ceramic components (Maksoud et al., 1999). This setbacks were considered to hinder the extensive use of the ceramic materials in the fields of biomedical and aerospace engineering (Hammel et al., 2014; McNamara et al., 2014; Shen et al., 2015).

Recently, there has been increase in the cutting of super hard and brittle materials using ductile grinding mode. This has led to extensive research works aimed at improving the performance of the grinding process (Gao et al., 2006; Zhong et al., 2009). Bifano, Dow, et al. (1991) proposed a theoretical model for determining the critical cutting depth dc during the ductile grinding mode of the super hard materials. They came up with a model for critical cutting depth dc, for the UAG process as shown in **Equation 2.4**. As illustrated, it was found that the critical depth of cut depends on both the fracture toughness of the material being cut, and its hardness. This critical depth of cut for ceramics in UAG process was found to be 25µm, while in the CG process it was 15µm (Warnecke et al., 1995; Zhao et al., 2005).

$$dc = b\,\frac{E}{H}\left(\frac{K_C}{H}\right)^2 \qquad (2.4)$$

Where E is the young's modulus, H is hardness, K_c is the fracture toughness and b is a constant which depend on the material type and varies between 0.1-1.0.

Li, S. et al. (2016) explained the mechanism of material removal in the grinding process, using the interactions of a single abrasive grit. **Figure 2.7** shows macro and micro material removal methods found during the grinding operation. The method was characterized by chips whose maximum undeformed thickness and length was given by tm and lc respectively. The mathematical relationship between the cutting parameters is given by **Equation 2.5** (Dai et al., 2015) & **Equation** 2.6 (Agarwal et al., 2008). The maximum undeformed chip thickness and chip length could be seen to depend on the process parameters. That is to say, maximum undeformed chip thickness is directly proportional to the feed rate, spindle speed and depth of cut. Similarly, the length of the chips was found to depend on the depth of cut, and the diameter of the grinding wheel.

$$\text{tm} = 2\delta \frac{V_W}{V_c} \sqrt{\frac{a_p}{d_s}} \tag{2.5}$$

$$\text{lc} = \sqrt{a_p d_s} \tag{2.6}$$

Where δ is the successive cutting-point spacing, d_s is the wheel's diameter, V_f is the feed rate, and N_s is the spindle speed.

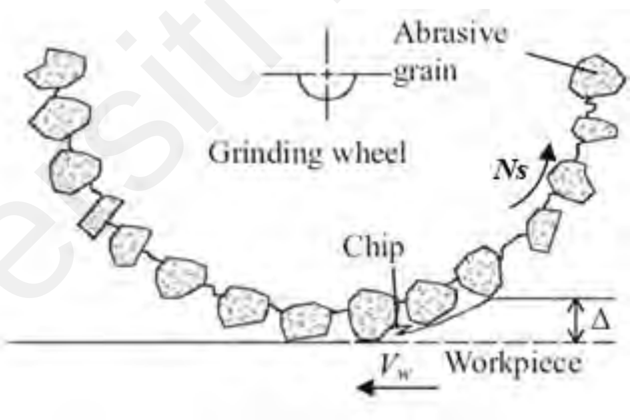

(a)

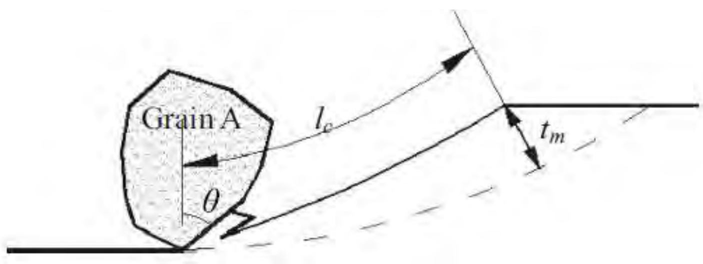

(b)

Figure 2.7: (a) Macro grinding behavior (b) Microchip formation by single abrasive grain (Dai et al., 2015).

Several investigations were conducted in other to analyze the plasticity of brittle materials. The formation of the median cracks and lateral cracks, and their propagations during the grinding process is illustrated in **Figure 2.8**. At the point of contact between the grits, and the workpiece material, it was found that there exist an elastic zone which was formed as a result of plastic deformations. At the base of the boundaries between the generated cracks, it was also found that there is a region characterized by high residual stress, this region is referred to the plastic zone (Kizaki et al., 2016). As the grinding force continues to increase with increase in grinding passes, the median cracks (which propagate perpendicularly into the material) is formed just at the bottom of the plastic zone along the direction axial to the load. Furthermore, when the grinding force was reduced, the lateral cracks were seen to expand and propagate downward (Jianhua et al., 2014; Lawn et al., 1979; Marshall et al., 1985).

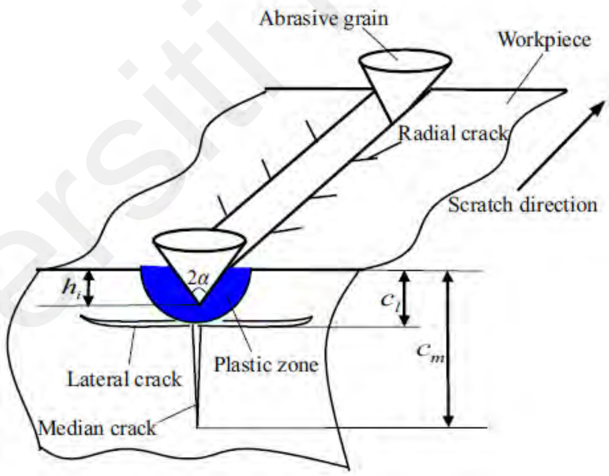

Figure 2.8: Plasticity of brittle materials (Wang et al., 2015).

Yan et al. (2006) report that the interaction between the abrasive grits and the work material resulted in median and lateral cracks. Moreover, previous works have endeavored to build theoretical models for the mechanism of material removal in the CG process (Arif et al., 2011; Bifano & Fawcett, 1991). The basis for the developed models was that the material removal mechanism was highly influenced by the median cracks (Nakamura et al., 2003). However, it was also reported that material removal by lateral cracks is commonly found in scratched grooves (Marinescu, 2006). The length of lateral cracks C_l and the corresponding depth C_h are respectively shown in **Equation 2.7 & 2.8**;

$$C_l = \zeta_1 \left(\frac{P_m}{K_c}\right)^{\frac{3}{4}} \tag{2.7}$$

$$C_h = \zeta_2 \left(\frac{P_m}{H}\right)^{\frac{1}{2}} \tag{2.8}$$

Where ζ_1, ζ_2 are the proportionality constants, K_c is the fracture toughness of the workpiece, and P_m is the grinding force.

Similarly, Lawn et al. (1979) showed that the extent of the median cracks could be obtained using **Equation 2.9**.

$$C_m = \mu_0 \frac{K_{IC}^2}{H^2} \tag{2.9}$$

Where μ_0 is a constant which depends on workpiece characteristics, H is its hardness, and K_{IC} is its fracture toughness.

Similarly, in another research work, it was found that the motion of the abrasion grains during the grinding process was characterized by two kinds of material removal mechanisms i.e. brittle or plastic flows. In ceramic materials, the volume of material removed by the single abrasive grit (V_b) during brittle flow could be obtained using **Equation 2.10** (Chen et al., 2016);

$$V_b = \frac{1}{2}\pi C_L^2 \, Vt \tag{2.10}$$

Where $V_t = \sqrt{V_x^2 + V_y^2}$ is the nominal tangential grinding speed, V_x and V_y are the components of relative velocity of the abrasive grain along X and Y-axis, C_L is the length of cracks.

In general, it was found that during any UAG operation, there are more individual grains on the grinding wheel participating in the scratching off the surface of the workpiece. This increase grain participation during UAG makes the achievable cutting depths in the UAG process to be much higher than that of the CG process. Gao et al. (2006) studied the performance of ductile mode cutting of Al_2O_3, zirconia-toughed alumina (ZTA) and nano-ZrO_2 using both CG and UAG processes. They found that the material removal rate in the UAG process was highly improved compared to the CG process. The higher depth of cut achievable in the UAG process was observed to be the reason for higher material removal rates in the process (Molaie et al., 2016).

2.4.1 Effect of process parameters on material removal rate

Several investigations have been done on how the grinding process parameters affect the performance of the process. The variation the performance grinding process with the process parameters have been studied extensively in both the CG, and UAG processes. It was observed that there were significant improvements regarding productivity, and also grinding quality in the UAG process compared to the CG. Moreover, in CG, investigations have shown that the presence of friction and rubbing actions results to significant loss of energy in form of heat. This heat dissipation was found to be highly reduced by the ultrasonication in the UAG process, with a resultant increase in the material removal rates (Prabhakar et al., 1992; Spur et al., 1996).

Lee et al. (1997) investigated the fundamental operations of the UAG of ceramic composites. They developed a theoretical model for the material removal rate (MRR) in the UAG process. Moreover, it was found that the MRR was affected by the process parameters such as the amplitude of vibration, grain sizes, feed rate and wheel speeds (Park et al., 2012; Zhou et al., 2002). Furthermore, KUO et al. (2012) studied the ultrasonic assisted machining of glass using diamond wheels. In their work, they investigated the effects of both feed rate and depth of cut on MRR, the effectiveness of the UAG process was also analyzed. It was observed that the UAG process produces a significant reduction to the grinding forces and performance compared to the CG process.

Yan et al. (2006) analyzed the material removal rates of UAG process. They found that an increase in any of the parameters (such as wheel grit size, wheel speed, type of wheel, vibration amplitudes and frequency) would result in higher existence of microcracks, and resultant increase of MRR. **Figure 2.9** compares the MRR in both the CG and UAG processes. It illustrates how increasing the wheel speed, and grit sizes (W10 & 270#) will result in an improved MRR in both CG &UAG processes. Moreover, the increase of MRR was found to be higher in the UAG process, confirming the results from previous researchers.

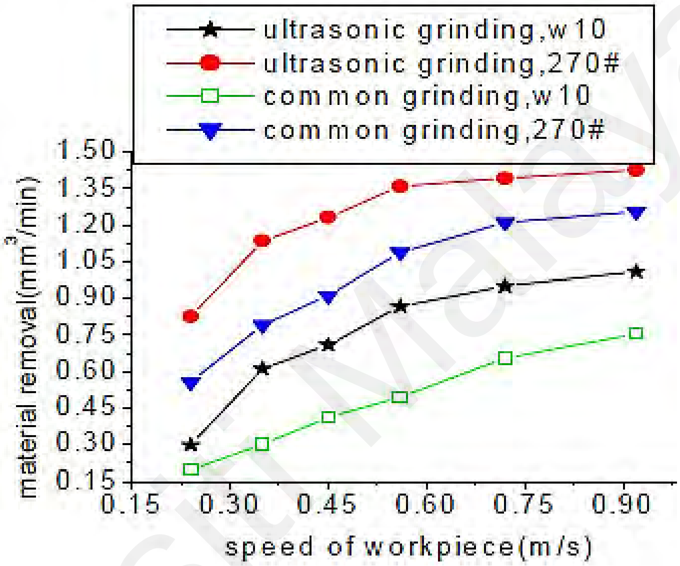

Figure 2.9: Effect of grit size (W10 & 270#) and wheel speed on MRR in both UAG and CG (Yan et al., 2006).

Similarly, Gao et al. (2006) studied the material removal mechanisms during the grinding of alumina, zirconia toughened zirconia (ZTA) and Nano-zirconia. They conducted diamond-grinding experiments with and without ultrasonication of the workpiece materials. They found that by increasing the cutting depth during UAG process, the MRR was twice that obtained in the CG process. This increase in MRR was attributed to the plastic flow behavior, which was prevalent in the UAG process. For example, during the grinding of ZTA ceramics, when the depth of cut was 6μm, the MRR was about 0.3mm3/min in CG and 0.7mm3/min in UAG process as illustrated respectively in **Figures 2.10a & 2.10b**.

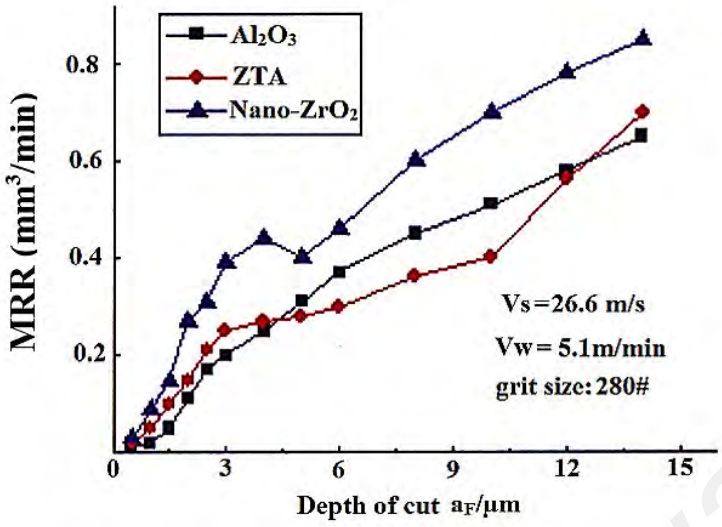

(a)

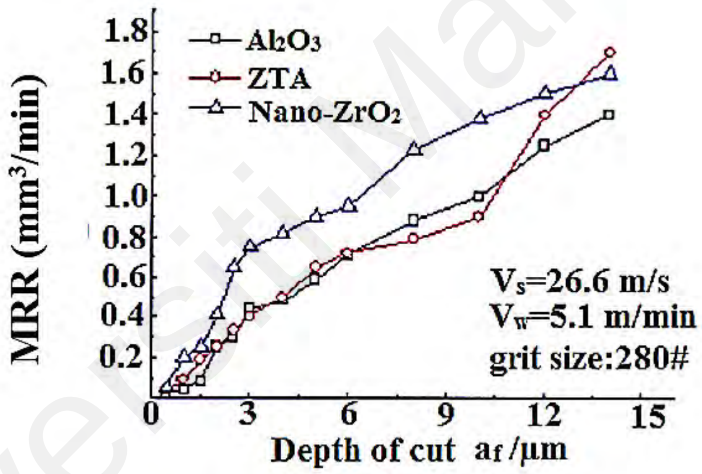

(b)

Figure 2.10: Effect of depth of cut on MRR (a) Common grinding and (b) Ultrasonic assisted grinding (Gao et al., 2006).

Qu et al. (2000) also reported a 62% improvement in MRR while machining Pyrex glass using diamond as a tool in the UAG process as compared with CG process. Moreover, Suzuki et al. (2000) also observed that In the UAG process, the MRR could increase 8 times compared to the MRR of the CG process.

2.5 Grinding forces and grinding energy

Studies have shown that in comparison with the CG process, the grinding forces and grinding energy are significantly reduced by the ultrasonic vibrations during UAG process (Gao et al., 2009; Wang, Lin, Wang, et al., 2014; Zahedi et al., 2015).

The specific grinding energy E, is defined as the ratio of the grinding power to the volumetric removal rate. In other words, the specific grinding energy is the energy utilised to remove a unit volume of material during the grinding operation. As given by **Equation 2.11**, the power P depends on the tangential forces F_t, and spindle speed V_s, while the volumetric material removal rate Q_w depends on other grinding parameters such as diameter of the wheel d_g, cutting depth a_p, and feed rate V_f (Adibi et al., 2014; Sayuti et al., 2012).

$$E = \frac{P}{Q_W} = \frac{F_t \times V_s}{d_g \times \mathrm{ap} \times V_f} \tag{2.11}$$

The specific grinding energy E, in the UAG process has been found to be lower than that in the CG process (Agarwal et al., 2008). Studies by (Li, S. et al., 2016) have shown that in the UAG process, the specific grinding energy has an inverse relationship with the depth of cut, wheel speed and amplitude of vibration.

Zahedi et al. (2015) built a UAG set up which was used to vibrate an alumina–zirconia (AZ90) ceramic material ultrasonically along the axial direction, and grinding it using a diamond tool. The specific grinding energy was found to reduce by more than 35% compared with the CG process. This was attributed to the increased participation of more diamond grits on the wheel during the grinding activity, and also the self-sharpening phenomenon which helps to produce newer cutting edges as the number of grinding pass increases (Malkin, 1989).

Moreover, the grinding forces along the tangential (f_t), axial (f_a), and normal (f_n) directions were modelled theoretically as shown in **Equation 2.12, 2.13 and 2.14** respectively;

$$F_t=k_x (MRR)M_x + F_{to} \tag{2.12}$$

$$F_a=k_y (MRR)M_y+ F_{ao} \tag{2.13}$$

$$F_n=k_z (MRR)M_z+F_{no} \tag{2.14}$$

Where, M_x, M_y, M_z, k_x, k_y and k_z are constants which depends on the property of the work material and grinding wheel. F_{to}, F_{ao} and F_{no} are the frictional components of the forces along the tangential, axial and normal directions respectively (Fan et al., 2006).

Also, Chen et al. (2016) found that the grinding forces in the UAG process are highly influenced by the wheel speed. In their work, they realized that any increase in the wheel speed would result to improved MRR during grinding of the brittle materials. As such, once the MRR and empirical constants are established, the theoretical models from **Equation 2.12, 2.13, and 2.14** could be used to obtain the grinding forces of the process. **Figure 2.11** shows the variation of the grinding forces with amplitude of vibration during UAG process. The axial force could be seen to be the lowest among all three grinding forces, while the normal grinding force was the highest. Further studies have shown that the force exerted along the normal direction F_n is greater than both axial force F_a and Tangential force F_t during grinding process (Jianhua et al., 2014). Specifically, Fn was realized to be seven times larger than F_a (Liu et al., 2008). Moreover, F_t was found to be responsible for the heat produced during the grinding operations, as such it is advisable to reduce the tangential forces by optimizing the process parameter settings (Nik et al., 2012). Jianhua et al. (2014) investigated the effect of ultrasonication on the grinding forces during the UAG process. In their work, they ground silica glass with an electroplated diamond wheel. Results from their experimental and hypothetical model shows that the axial and tangential grinding forces reduces as the vibration amplitude was increased. The lowest magnitude for all the forces was recorded at amplitude of about 7μm.

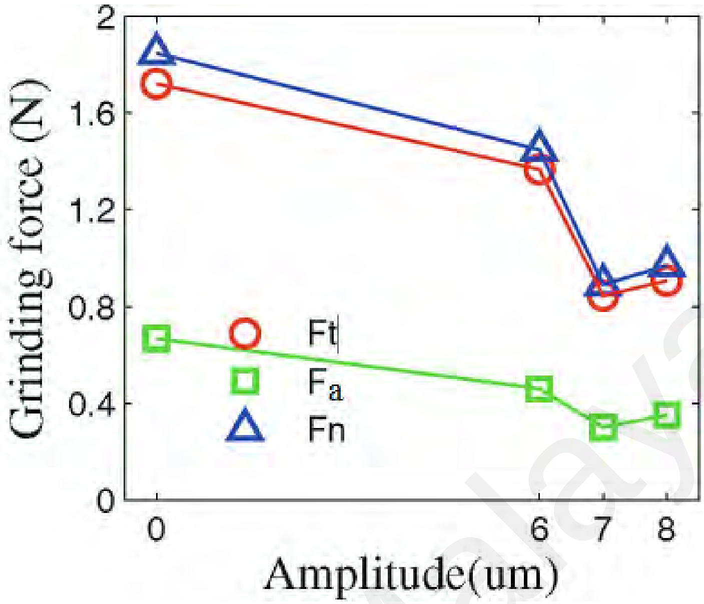

Figure 2.11: Effects of ultrasonic amplitude on grinding force in UAG(Vf= 100 μm/s, = 2μm, Vs = 18000 r/min) (Chen et al., 2016).

Moreover, some research works have indicated that the grinding forces could be reduced substantially when UAG is utilized in place of the CG process as shown in **Table 2.6** (Jianhua et al., 2014; Tawakoli, Taghi & Azarhoushang, Bahman, 2009). Also, there seems to be a high risk of tempered and burnt regions on the work material, when the frequency of oscillation was very small as reported by (Akbari et al., 2008; Hanasaki et al., 1994). As such, the frequency of oscillation should always be greater than 25 kHz to avoid these deformations. **Table 2.6** shows the variation of the grinding forces with the main process parameters in both the CG and UAG processes. It could be seen that the variation percentage of the tangential grinding force is proportional to the wheel speed, depth of cut, and feed rate, and the percentage in the UAG process is much smaller than in the CG process. Furthermore, the variation percentage of the normal grinding force when the wheel speed and feed rate were increased was higher in the UAG process compared to the CG process. Generally, it could be asserted that the ultrasonic oscillations helps to lessen the effect of the spindle speed on the normal grinding force. However, the oscillations were found to increase the effect of both depth of cut and feed rate on the grinding forces (Jianhua et al., 2014).

Table 2.6: Percentage variation of the grinding force in UAG and CG process (Jianhua et al., 2014).

S/N	Ex. Number		Variation percentage (%)	
			UAG	CG
1	Wheel speed	F_n	-39.6	-52.3
		F_t	-15.9	-17.4
2	Depth of cut	F_n	179.0	99.2
		F_t	61.9	96.2
3	Feed rate	F_n	270.5	258.3
		F_t	32.9	42.0

Previous research works have shown that the grinding force is an important process parameter in the grinding process. This is because it highly affects the material removal rates, and the surface quality of the products from the grinding process. Also, investigations have shown that the predominant type of grinding forces found in the UAG are the normal force and tangential forces. The former was found to be mostly associated with grinding damages like micro-cracks and subsurface damages (Zhang et al., 1995), while the latter was found to be responsible for the energy expended during the grinding process (Zhang et al., 2014). Hence, adequately reducing the grinding forces was considered to be a necessary method of improving the performance of the UAG process.

Wang, Lin, Wang, et al. (2014) reported that during UAG operations, the grinding force decreases with the increase of vibration amplitude, frequency of oscillation, and spindle speeds. The extent of reduction of the grinding forces during the grinding of the brittle materials in UAG process was also found to depend on the property of the material being cut (Moriwaki et al., 1995; Zhang et al., 2006). Moreover, The grinding forces in the UAG process were found to be lower compared to the grinding forces in the CG process (Feng et al., 2014).

Also, in a separate research work by Cao et al. (2014), the prevention of the sliding and ploughing actions during the grinding operation was found to be an option to reducing the grinding forces. Investigations conducted by previous researchers on the superimposition of the ultrasonic vibrations on either the tool, or the workpiece during grinding shows an uneven distribution of forces along the normal, tangential, and perpendicular directions. As a result of this, it was concluded that the ultrasonic vibrations causes a considerable reduction of the grinding forces, which in effect was found to lead to improved surface, and sub-surface quality of the workpiece materials (Spur et al., 1996; Zhang et al., 2006). Generally, the high reduction of the grinding force in the UAG process as compared to the CG process gives the UAG process an upper hand in the manufacturing industries for advanced ceramic and super hard materials (Moriwaki et al., 1995).

Xiao et al. (2016) proposed a theoretical model for obtaining the grinding force in the UAG process based on brittle-ductile mode material removal mechanism. The brittle and ductile modes were classified depending on the critical depth of cut used. The results of their work showed that the grinding force is inversely proportional to the wheel speed and amplitude of vibration (see **Figures 2.12a & b**) which corroborates with results of (Zhao et al., 2005). However, the grinding force was found to be directly proportional to the feed rates and cutting depths as shown **Figures 2.13a & b** (Wang et al., 2014). Also, the developed model was found to be highly accurate, with an average relative mean error of

14.40%. The grinding forces was found to be much higher in the UAG process compared to the CG process.

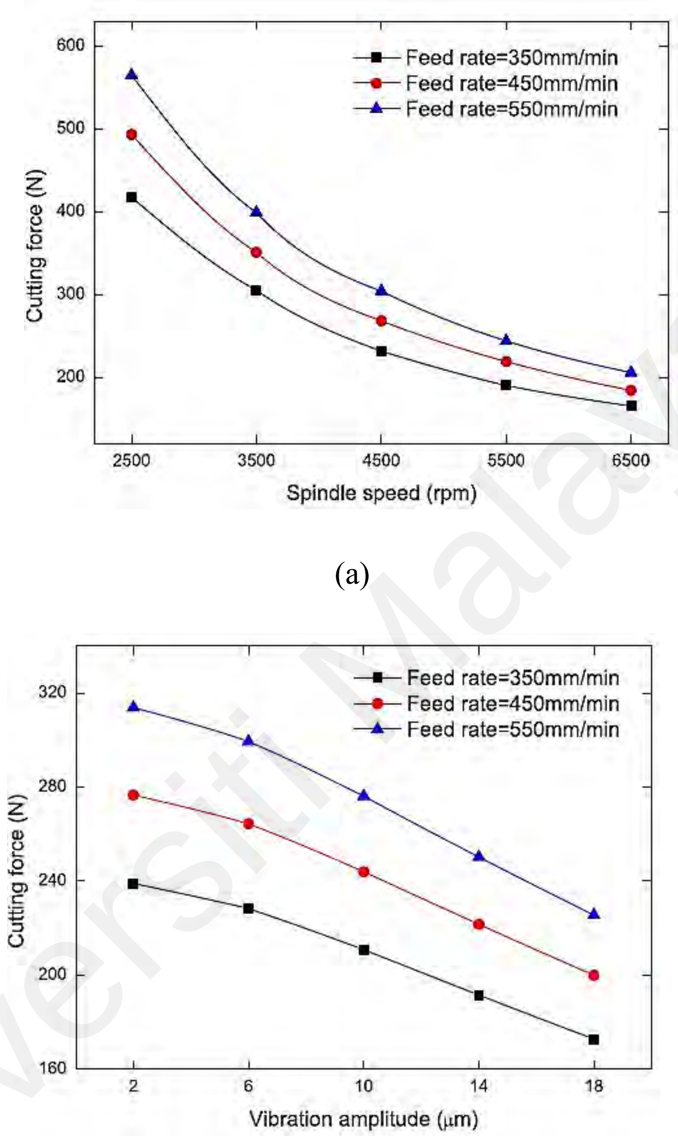

(a)

(b)

Figure 2.12: Grinding force vs (a) wheel speed (b) amplitude of vibration (Xiao et al., 2016).

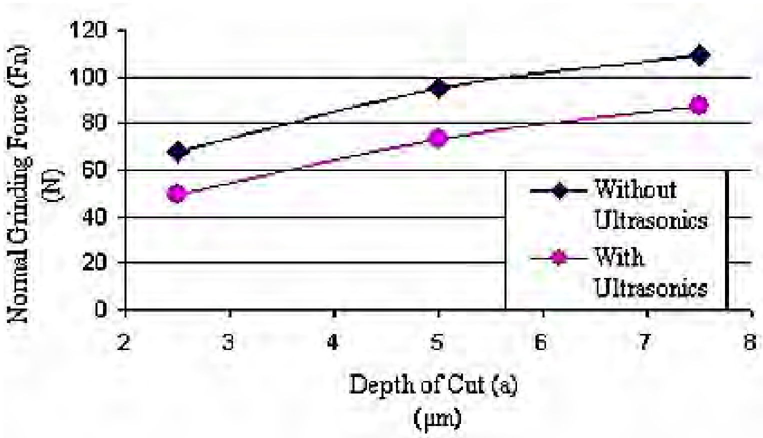

(a)

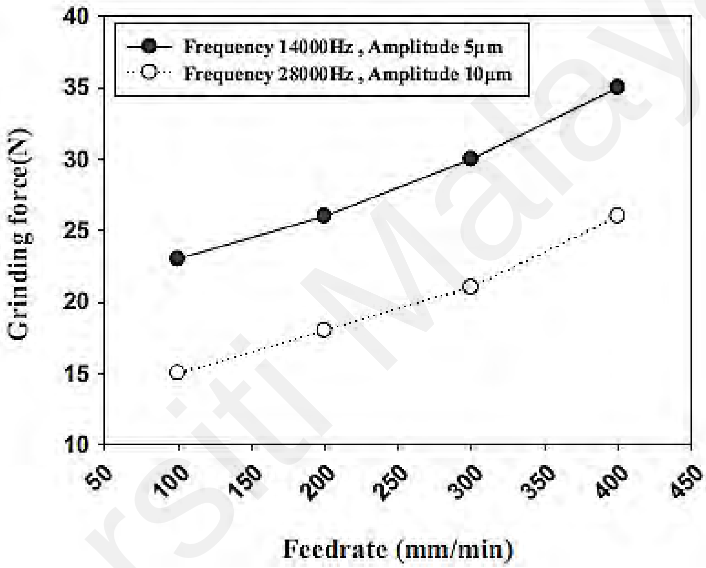

(b)

Figure 2.13: Grinding force vs (a) depth of cut (Akbari et al., 2008) (b) feed rate (Wang, Lin, Cao, et al., 2014).

Similarly, results from investigations have shown that the normal and tangential grinding forces obtainable in the UAG process were respectively decreased by 42.5% and 40 % compared to those obtained in the CG process (Arif et al., 2011; Li, S. et al., 2016; Nomura et al., 2007). This result shows that the introduction of ultrasonic vibrations significantly reduces the grinding forces, which is similar to the findings of (Spur et al., 1996; Zhang et al., 2006). **Figure 2.14a & b** shows the variation of both the normal and tangential forces with the depth of cuts in CG and UAG process. As illustrated in the figures, it could be explained that both grinding forces in the UAG process are directly proportional to the depth of cut, with the normal grinding force having higher magnitude (Liang, Z. et al., 2010).

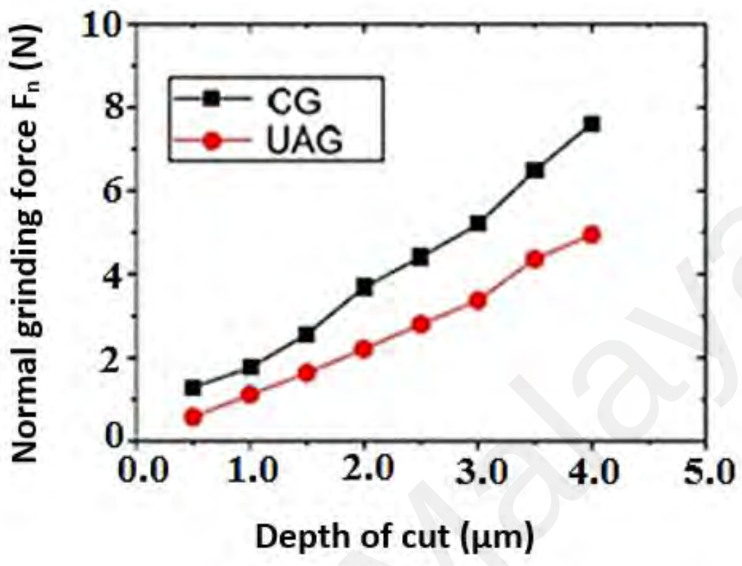

(a)

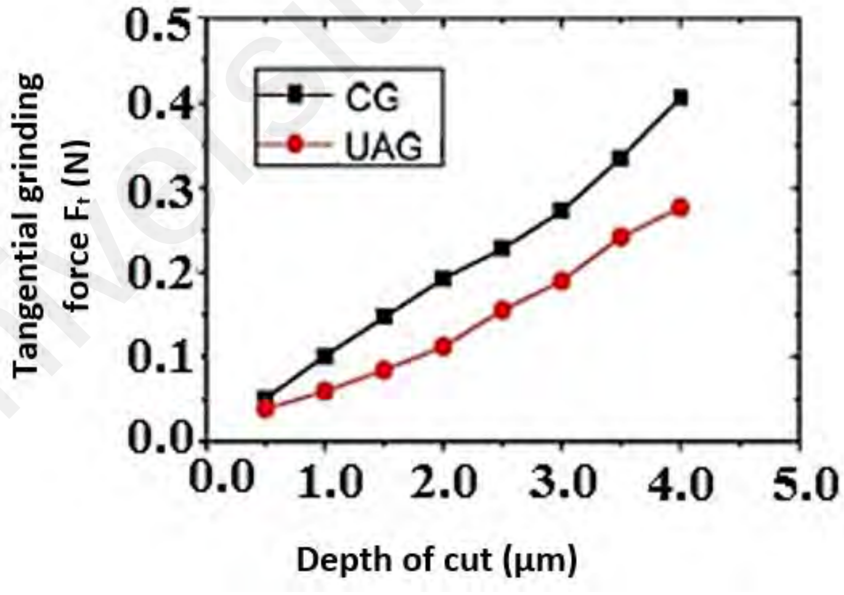

(b)

Figure 2.14: Depth of cut vs (a) Normal cutting force (b) Tangential cutting force (Liang, Z. et al., 2010).

Considering the number of passes during the grinding process, the extent of reduction of the particular grinding force was found to increase in the UAG process as the number of grinding pass increases. This rise was attributed to the increased tool micro fractures occurring at higher grinding passes (Feng et al., 2014). Also, it was found that in the 1st grinding pass, the decrease of the specific normal and specific tangential grinding forces compared to those obtained in the CG process, was about 32% and 34% respectively, as shown in **Figures 2.15a & b**. Moreover, in the 60th pass, the extent of reduction of the forces in the UAG process was found to be about 61% and 52 % for the specific normal and specific tangential grinding forces respectively. This almost double percentage reduction of the grinding forces was attributed to the occurrence of self-sharpening phenomenon in the UAG process at higher grinding passes (Ding et al., 2014).

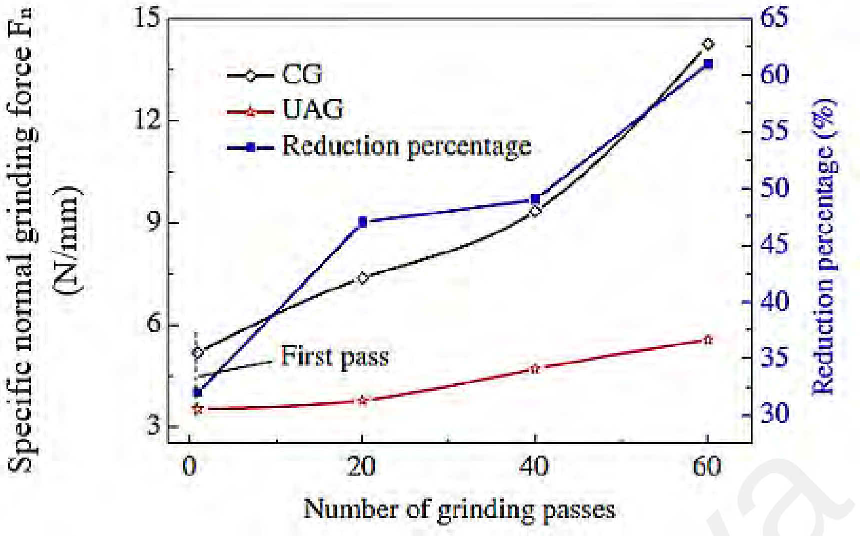

(a)

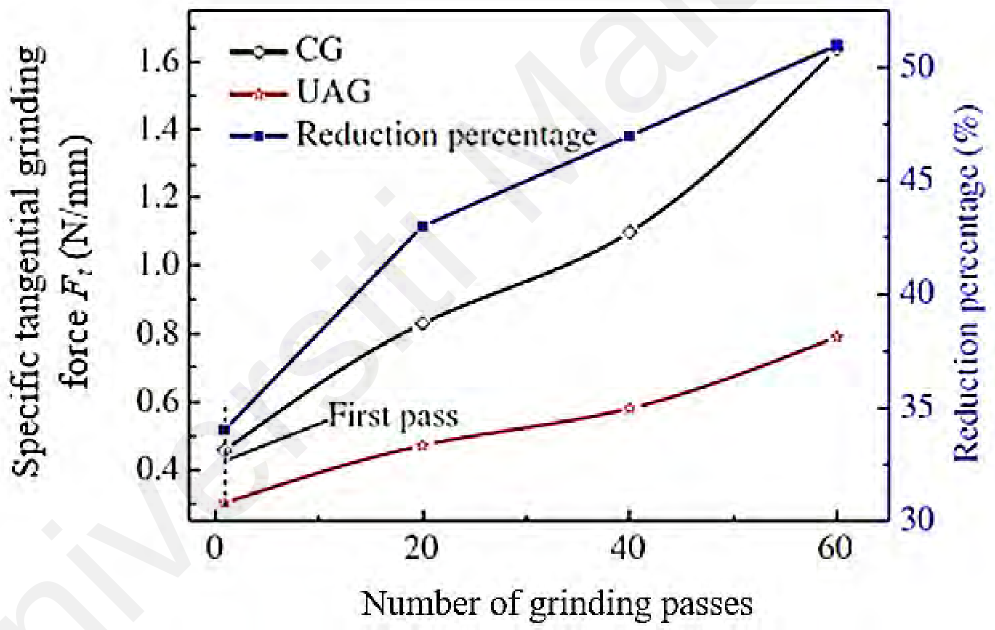

(b)

Figure 2.15: (a) Specific normal grinding forces vs grinding passes (b) Specific tangential grinding forces vs grinding passes.

The UAG setup was found to produce less wear with a resultant 45% increase in the G-ratio. This G-ratio is the ratio of the material removal volume to the tool wear, and it depends on the type of grinding wheel and their properties such as wheel diameter and wheel width (Gupta et al., 2001). The G-ratio in CG process is often very high at the beginning of the grinding operations, rising from 0 up to 10.5. After a significant number of grinding passes, the G-ratio steadily decreases and stabilizes at 9. However, in the UAG process, the trend of variation of the G-ratio was found to be opposite that of the CG process. That is to say as the grinding pass increases, the G-ratio was found to decrease sharply. Also, the value of G-ratio was found to be much lower in the UAG process compared to the CG process (Bhaduri et al., 2012; Liang et al., 2012).

Similarly, Tawakoli et al., (2009) also stated that the grinding forces found in the UAG process was lower compared to that in the CG process. The ultrasonication was found to result in less wear of the diamond wheels, leading to improved tool life, and subsequently making the UAG process more efficient and economical. However, the CG process which is characterized by high grinding forces, is also associated with frequent wear out of the abrasive grits. The frequent wears happening makes the wheel to require incessant truing/dressings which seem to be time-consuming. Furthermore, during the grinding operations in the UAG process, there appears to be increased micro fractures around the tip of the grinding tool, this was found to produce the new cutting edges and increased tool sharpness (Ding et al., 2014; Fathima et al., 2003; Jackson et al., 2001).

Studies in the UAG process relating the grinding force with the process parameters shows that the grinding force depends mostly on the depth of cut, the vibration amplitude, and worktable feed rates (Jianhua et al., 2014; Wang et al., 2014). The high depths of cut achievable in the UAG process was also found to cause a significant reduction of the grinding forces (Zhou et al., 2002).

Also, the extent of reduction of the grinding forces in the UAG process as compared to the CG was found to be within the range of 20% to 50% (Akbari et al., 2008; Denkena et al., 2008; Ding et al., 2014; Feng et al., 2014; Mahaddalkar et al., 2014; Negishi, 2003; Shamoto et al., 1999; Spur et al., 1996; Suzuki et al., 2000). Moreover, (Tawakoli et al.,

2009) noticed a slightly higher increase of the percentage of grinding forces in the UAG process. In their work involving dry cutting of 42CrMo4 using the diamond tool, they realized that there was a decrease of about 60% of the normal grinding force in the UAG process. A similar observation was also made by Uhlmann et al., 2007; Wang et al., 2014).

Wang et al., (2014) examined another UAG system that was modeled such that the ultrasonic vibrations occur along the longitudinal directions of a Titanium alloy (Ti_6Al_4V) workpiece. They found that the grinding force was inversely proportional to both the amplitude of vibration and frequency. Similarly, the grinding force was also observed to be directly proportional to the depth of cut and feed rate, but inversely proportional to the spindle speed. **Figures 2.16a & b** shows how these parameters affect the grinding force, it could be seen that when both amplitude of vibration and frequency were doubled, the cutting force was halved. This trend was found to continue as the grinding depth and wheel speed were increased.

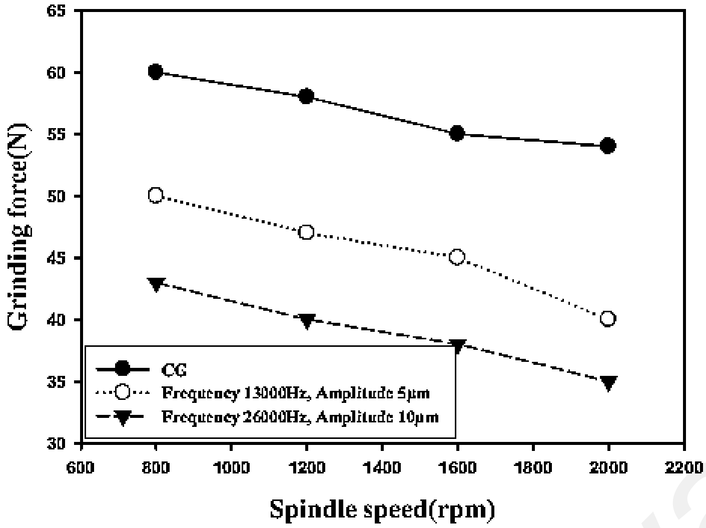

(a)

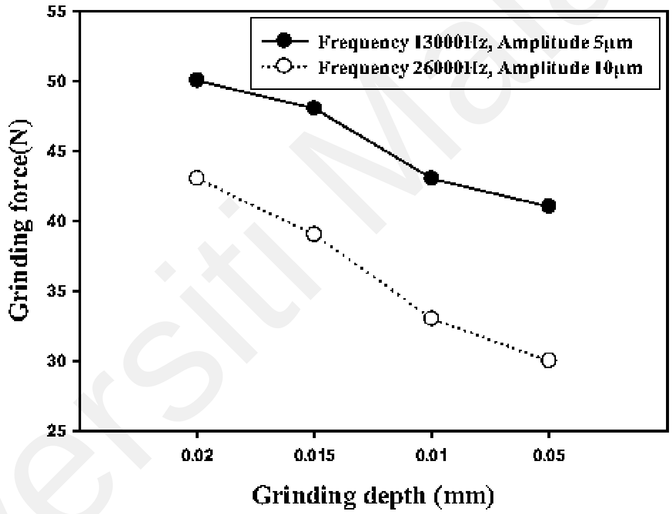

(b)

Figure 2.16: Grinding forces in process vs (a) wheel speed (b) grinding depth (Wang et al., 2014).

Moreover, in the UAG process, the diamond grains were found to possess higher impact energy, which helps them to puncture deeper into the work materials. This high energy also enables the increase of brittle fractures, which consequently results to decrease of the grinding forces (Akbari et al., 2008).

Molaie et al. (2016) illustrated the reduction of the normal and tangential grinding forces in CG and UAG processes. As seen from **Figures 2.17a & b**, the utilization of the different bio-degradable nano-lubricants on both processes resulted to lower grinding forces. The extent of reduction seems to be more pronounced in the normal grinding force, with average reduction ranging from 39% in dry grinding, to more than 60% in the paraffin mixed with 6% nano particles. Also, the tangential force has been found to reduce by more than 58% due to application of nano lubrication. Hence, the suspended nano particle lubricants were found to be capable of reducing the grinding forces significantly, and the extent of reduction was found to be higher in the UAG process than the CG process.

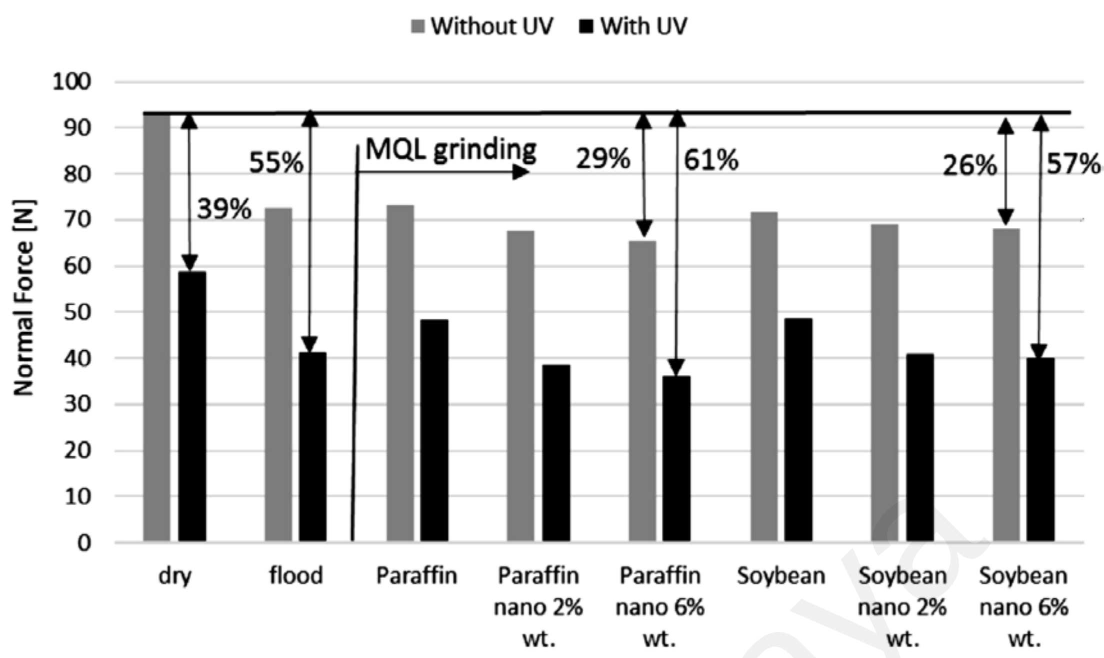

(a)

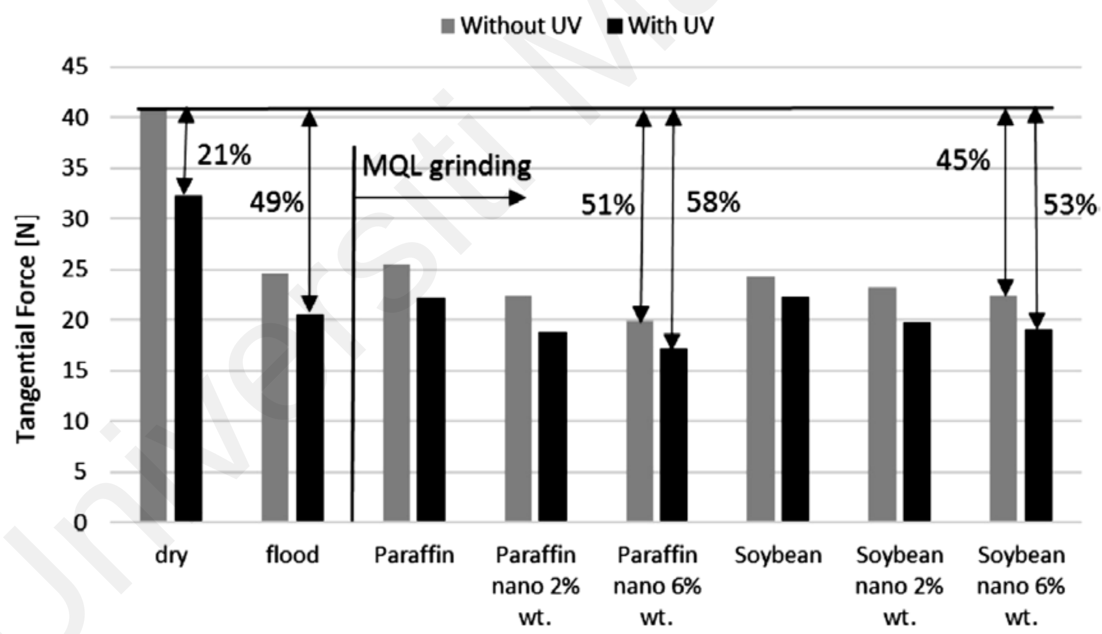

(b)

Figure 2.17: The effect of different types of biodegrable lubricants in the CG and UAG process on the (a) normal grinding forces (b) tangential grinding forces (Molaie et al., 2016).

2.6 Effects of process parameters on tool wear & micro-cracks

This section explains grinding deformations such a tool wears and microcracks on the workpiece materials. Also, the unwanted phenomenon occurring the grinding process such as, wheel loading, grain pull outs, and wear flats were analyzed, illustrating how they vary with the grinding process parameters in both CG and UAG.

Malkin (1989) explains that there are three types of wears associated with the grinding wheel during CG. These include attrition wear, grits fracture, and wheel bond rupture. However, in the UAG process, due to the different operational kinematics, the wears were found to be mainly due to macro/micro fractures (see **Figure 2.18**), grain pull outs, and cracks along grain boundaries (Ding et al., 2014; Ding et al., 2015). The microfractures which mostly occur at the tip of the tool were found to cause a great increase to the sharpness of the tool, as such the microfracture is a desired phenomenon, because it leads to improved machinability of the UAG process (Ding et al., 2014; Fathima et al., 2003; Jackson et al., 2001).

Figure 2.18: Grain macro-fracture (Ding et al., 2015).

In the investigation performed by Izman et al. (2007), it was found that the CG process was characterized by intense occurrence of lateral cracks. It was also found that the lateral cracks occur as a result of indentation on the glass, and not chipping actions. Moreover, Munoz-Tabares et al. (2011) reported that the formation of the microcracks during the CG process occurred mainly in areas close to the edges of the indentations. However, the utilization of UAG in cutting brittle materials was found to produce a great amount of reduction to these microcracks, leading to improvement in the surface profiles of the components. For instance, the surface profile produced by the CG indicates formation of brittle fractures along the length of the ground region as shown in **Figure 2.19a**. However, the cracks were seen to be significantly reduced when UAG was used as shown in **Figure 2.19b**. The texture of the surface profile observed in the UAG components illustrates that the material removal is characterised by both ductile and brittle removal modes (Liang, Z. et al., 2010; Shen et al., 2015).

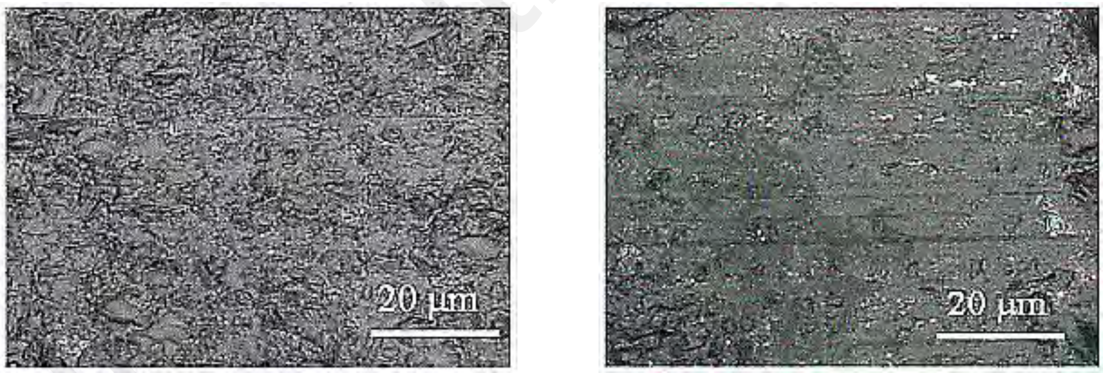

(a) (b)

Figure 2.19: Microscopic images of surface profiles (a) CG (b) UAG (Liang, Z. et al., 2010).

Similarly, Al_2O_3 ceramic has been ground with a diamond tool using both the CG and UAG processes, so as to investigate the extent of tool wear and performance of both grinding processes. Various degrees of cracks were observed in both processes, but surface and subsurface cracks on the diamond grains (illustrated in **Figure 2.20**) were more apparent in the CG system. However, in the UAG process, the wheel was characterized by high rate of grain fracture, wear of bonding material and microcracks. In addition, as the number grinding passes increases, the UAG process was reported to produce much higher propagation of the microcracks on the wheel, thereby causing excessive tool degradations. Moreover, the extent of the radial wear on the tool was found to be much higher in the UAG process as shown in **Figure 2.21** (Shen et al., 2015). However, in spite of the higher radial wears found in the UAG process, the process was found to provide extended tool life in carbide wheels by a factor of twenty (Shimada et al., 2004; Weber et al., 1984).

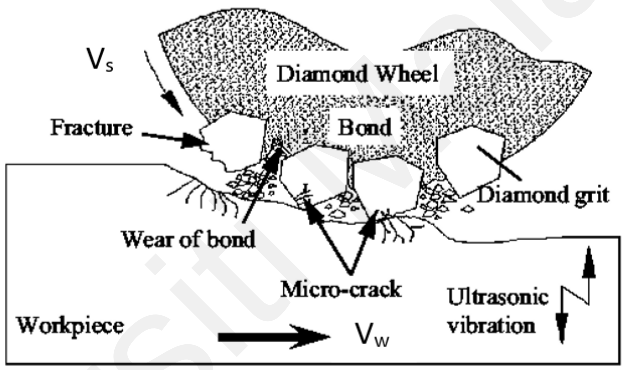

Figure 2.20: Model of the UAG process illustrating cracks and wear of tool (Shen et al., 2015).

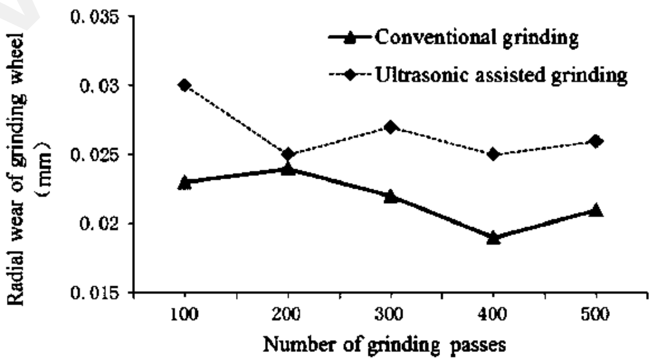

Figure 2.21: Extent of radial wear of the grinding wheel with number of passes (Shen et al., 2015).

Several types of limitations are associated with the CG process of machining superhard materials, especially the issue of wheel wear, and micro-cracking of the grinding tool, which in turn results to incessant truing/dressings (Hosokawa et al., 2006; Liang et al., 2012). However, the utilisation of ultrasonic vibrations in the process (UAG technique) was found to lower these kinds of deteriorations. During UAG, it was found that as the amplitude of vibration was increased, the deformations vary considerably. For instance, within the range of 1μm to 6.5μm amplitude of vibration, there was high rate of occurrence of microcracks and tool wear. However, between the range of vibration amplitudes of 6.5μm and 7.5μm, the microcracks were hardly noticeable on the surface and sub surfaces of the work material. Furthermore, when the amplitude was increased to 8.5μm with higher vibration frequency, there seem to be high rate of the cracking phenomenon occurring. This increased rate of crack formation was attributed to the higher momentum, which in turn results to higher impact forces during the grinding process (Jianhua et al., 2014). In addition, it is worthy to note that the cracks produced in the UAG process i.e. lateral and median cracks are often intertwined at lower depths, but become isolated at higher depths as shown in **Figure 2.22** (Chen et al., 2015).

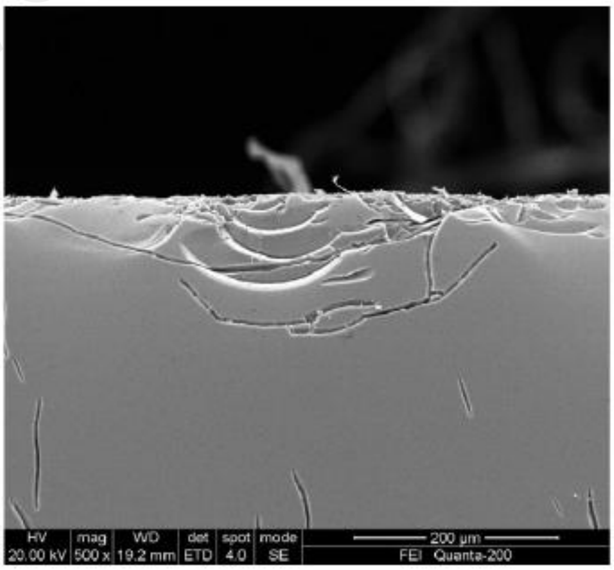

Figure 2.22: Subsurface cracks UAG process (Lv et al., 2013).

Similarly, other sources of wheel wear in CG process are abrasive activity, adhesion, and promulgations. **Figure 2.23** shows the comparisons between the extents of tool wears found in both CG and UAG processes at different feed rates. It could be seen that the higher the feed rates, the more the tool wears in both grinding process (Lauwers et al., 2010). But, the CG process was found to have higher tool wears, which confirms the findings of (Kizaki et al., 2016; Park et al., 2012; Zheng et al., 2016).

Park et al. (2012) reported that in the UAG process, the wear phenomenon was mainly caused by scrapping, edge chipping and grit macro-fractures

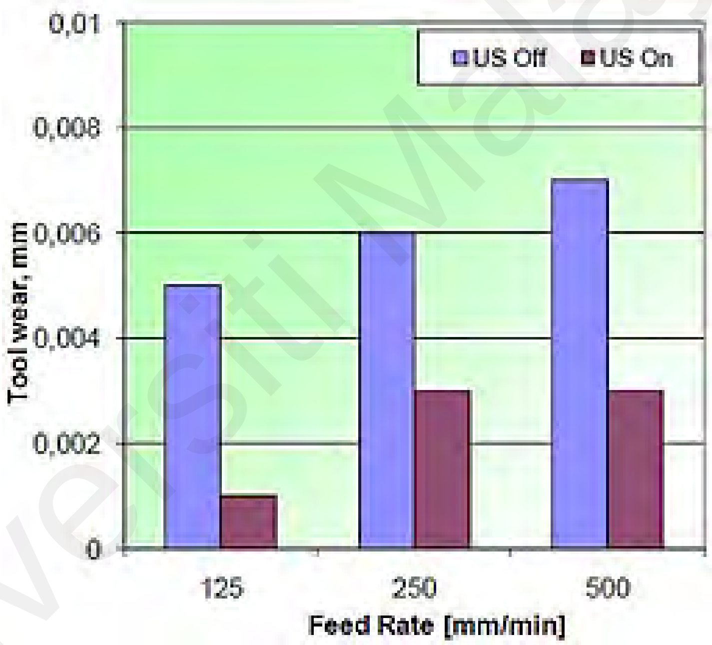

Figure 2.23: Comparison between tool wears found in CG and UAG process (Lauwers et al., 2010).

The result for the tool wears at different cutting distances, and rotational speed is shown in **Figure 2.24**. At wheel rotational speed of 4000rpm, the UAG was found to provide more than 75% reduction to the tool wears at different cutting distances. Furthermore, when the wheel's rotational speed was increased to 8000rpm with a cutting distance of 2700mm, the wear in CG was further reduced to about 8µm, while under similar conditions, the wear in the UAG process was 2µm. In general, studies have shown that the wear phenomenon in UAG process was less than in the CG process. Also, at higher wheel speed and cutting distance, the wear of the grinding tools in both CG and UAG processes decreased considerably (Park et al., 2012).

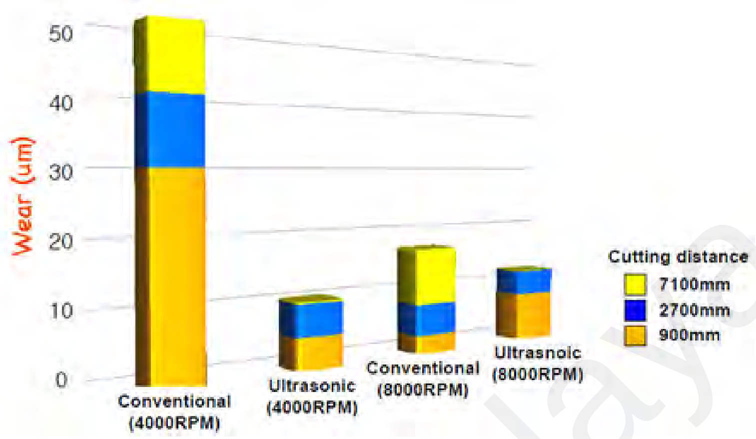

Figure 2.24: Tool wear at different wheel speed for CG and UAG processes (Park et al., 2012).

Another type of deformations often associated with the tools during the grinding operations are grain pullouts and wear flats. Studies on the grinding processes have shown that there was high rate of grain pullouts in the CG process, which depends mainly on the mechanisms of material removal. The grain pull out is illustrated in **Figure 2.25a**, and was found to occur due to higher friction and grinding force found in the CG process. However, in the UAG process, the result showed a lesser occurrence of grain pullouts, but increased existence of the micro/macro fractures on the diamond grits. The micro/macro fractures were found to produce partial wear flats on the tool, and also wheel sharpening. The wear flats, loading, and tool breakage found in UAG process are illustrated in **Figure 2.25b**. In general, it could be said that the CG process was characterized by macro-fractures, and grain pull outs as shown in **Figure 2.25c.** However, whereas the UAG process was characterized by chip adhesions, and micro fractures with less amount of grain pull outs as shown in **Figure 2.25d** (Ding et al., 2014; Liang et al., 2012; Pei, 1995; Shen et al., 2015; Uhlmann et al., 2007).

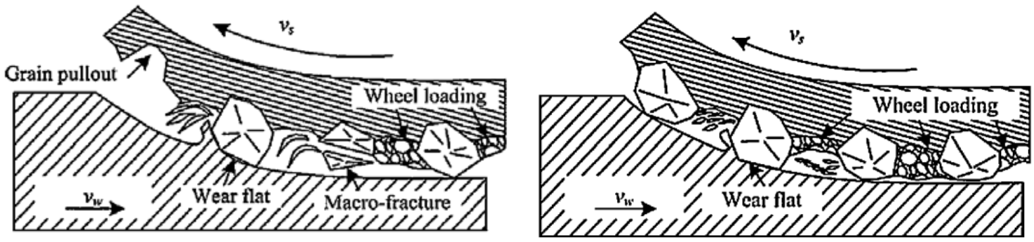

(a) (b)

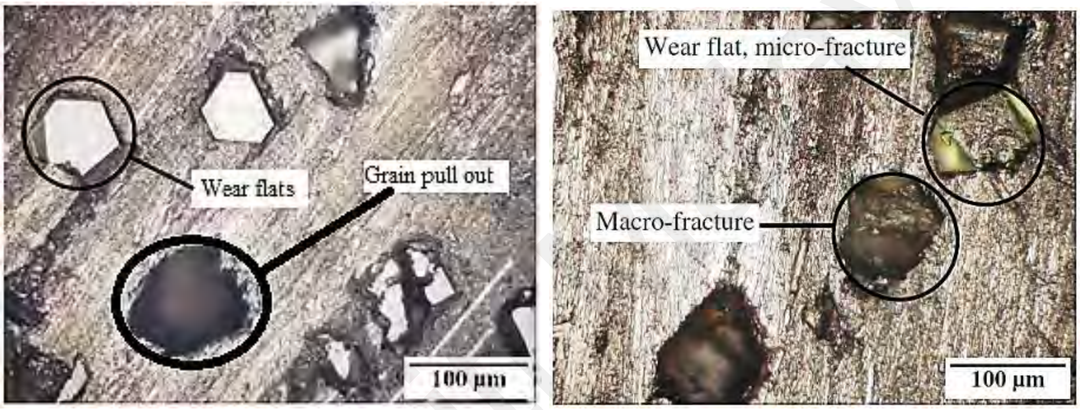

(c) (d)

Figure 2.25: (a) Mechanism of tool wear in CG (b) Mechanism of tool wear in UAG (Liang et al., 2012) (c) Wear flat and grain pull outs in CG (d) Wear flat and microfractures in UAG (Ding et al., 2014).

Furthermore, Suh et al. (2008) studied the pattern of stresses induced on a resin bonded diamond wheel. They realized that the formation of micro/macro fractures on the diamond grains depends solely on the ratio of the length of outward projection of each diamond grits to the base width of the diamond grits. It was found that the grain sizes, and type of bonds present on the grinding wheel affects the tool wear during the grinding process (Uhlmann et al., 2010).

The thermo-chemical reactions happening during the grinding process have also been found to be among the principal causes of tool wears, in certain wheel types during grinding of ceramics and super alloys. Paul et al. (1996) built a tool wear prediction model based on the number of free valence electrons in the metallic materials. The mobile electrons in the metallic materials were found to break off the C-C bond in diamond or B-N in CBN tools. It was also found that during machining of ferrous materials, the 4-valence electrons in iron forms graphite layers by oxidation, leading to graphitization of the surface of the diamond tool (Shimada et al., 2004). Also, nickel and titanium were observed to cause much more wear in diamond tools due to the presence of two D-orbital electrons in these metals. Although, diamond and CBN are extremely hard, this chemical activity often causes wear of these tools, which subsequently leads to deterioration of the surface quality of the workpiece. Improving on this limitation during grinding of super alloys with the UAG process is still actively being researched on (Feng et al., 2009; Moneim et al., 1997; Shamoto et al., 1999; Shen et al., 2015; Weber et al., 1984; Zhou et al., 2002). Another cause of tool wear is the chemical action often found at high temperatures during machining with CBN wheels. Even though the CBN grains are chemically inactive, yet they tend to be hydrolyzed by water vapor, thereby producing compounds of B_2O_3 and ammonia. This chemical action in which the CBN grits are degraded was explained by (Hitchiner, 1999). The B_2O_3 film formed in the hydro-oxidation process tends to dissolve in water at high temperatures. This oxidation and dissolution process (illustrated by **Equation 2.15, 2.16, and 2.17**) was found to produce a chain of degradable reactions during the CBN grinding.

$$2BN + 3H_2O \rightarrow B_2O_3 + 2NH_3 \uparrow \tag{2.15}$$

$$4BN + 3O_2 \rightarrow 2B_2O_3 + 2N_2 \uparrow \tag{2.16}$$

$$B_2O_3 + 3H_2O \rightarrow 2H_3BO_3 \tag{2.17}$$

2.7 Surface integrity and subsurface characteristics

Surface integrity is referred to the improvements or deteriorations found on the surface of a workpiece material after machining operations. Nowadays, the surface integrity obtained by different machining techniques is receiving keen attentions. This is as a result of the effects which part quality has on the performance of machined components (Bellows, 1972). The surface integrity of machined ceramic components was found to affect their functionality, and properties such as, fatigue strength, hardness, fracture toughness etc. (Yan et al., 2011; Yanyan et al., 2009). The surface and subsurface integrities of machined ceramic/super alloy materials have been found to depend on the machining parameters such as cutting speed, depth of cut, and feed rates (Chen et al., 2015; Nik et al., 2012).

Investigations have shown that the depth of cut has a directly proportional relationship with the surface quality in both UAG and CG processes, whereas the table feed rate, spindle speed and sizes of grits on the wheel have an inversely proportional relationship with the surface quality (Chen et al., 2004; Liang, Z. Q. et al., 2010). Also, the quality of surface produced during the UAG process was found to vary with the directions in which the vibration was applied relative to the feed direction (Zhong et al., 2004).

2.7.1 Effect of process parameters on surface quality

Many research works have been conducted in order to investigate the effects of the grinding process parameters on the surface quality of the components produced. (Yanyan et al., 2009) compared the effects of the grinding process parameters on the surface roughness during the grinding of nano-ZrO_2 ceramics. In their work, they ground nano-ZrO_2 with a diamond tool using both CG, and UAG processes. Their analysis focused on the plastic and ductile cutting modes during grinding operations. The surface roughness of the ground components was found to improve by more than 20% when the UAG process was used in place of the CG process. This result was similar with that obtained by (Chen et al., 2013; Guo et al., 2011; Jianhua et al., 2014; Lee et al., 1997; Liang, Z. Q. et al., 2010; Nik et al., 2012; Nomura et al., 2007; Park et al., 2013; Pei, 1995; Tawakoli et al., 2009; Uhlmann et al., 2006; Wang et al., 1998). Furthermore, the UAG process was found to produce better surface quality than the CG process as shown in **Figure 2.26 a & b** (Jianhua et al., 2014). This finding also conforms with the results from (Peng et al., 2012; Yanyan et al., 2009).

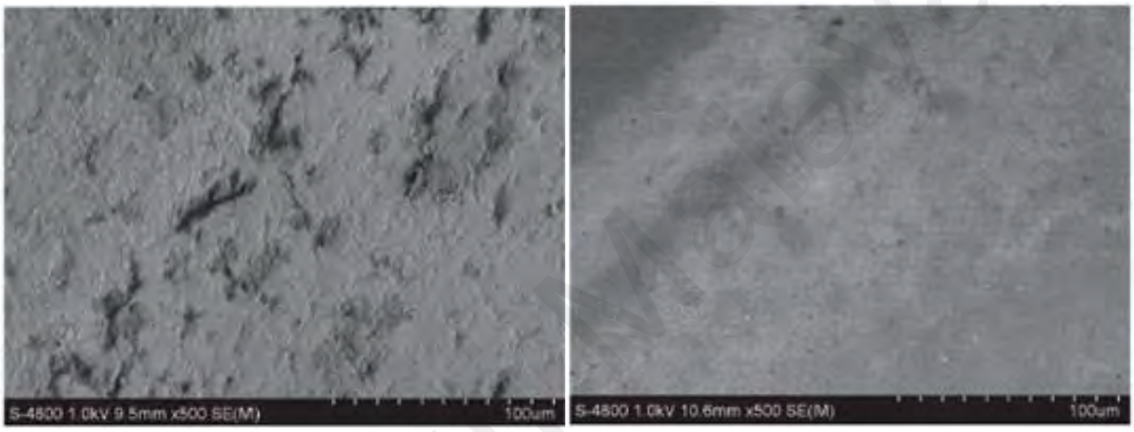

(a) (b)

Figure 2.26: Surface textures of ground components using (a) CG (b) UAG.

The components machined using the UAG process have lower surface roughness values, because they are characterized by sharp protrusions, while the CG machined parts were found to have densely ridged-like structures (Zheng et al., 2016).

Liu et al. (2008) analyzed both the ultrasonic assisted turning and ultrasonic assisted grinding of metal aluminium composites, and ceramics using SiC tools. They found that the surface quality was improved only when the ultrasonic vibrations were applied along the axial (parallel to feed) directions. This result corroborates the findings of (Nik et al., 2012). However, when the ultrasonic vibrations were along the radial or perpendicular directions, the surface quality was found to deteriorate considerably. In the UAG process, when the depth of cut was high i.e. above 2µm, it was found that there was high tendency for ductile mode cutting, which prevents the formation of spikes, thereby causing reductions of the surface roughness as shown in **Figure 2.27** (Liang, Z. et al., 2010). Also, since higher depth of cut could be achieved in the UAG process, the surface roughness was found to greatly reduce at higher depths of cut compared to the CG process (Dornfeld et al., 2006; Liang, Z. Q. et al., 2010). Furthermore, the lowest value of surface roughness was reported to occur when the amplitude of vibration was within the range of 3μm to 6.5μm. Moreover, further increase to the vibration amplitude beyond this range, shows that there was little or no change on the surface quality of the work materials (Guo et al., 2011).

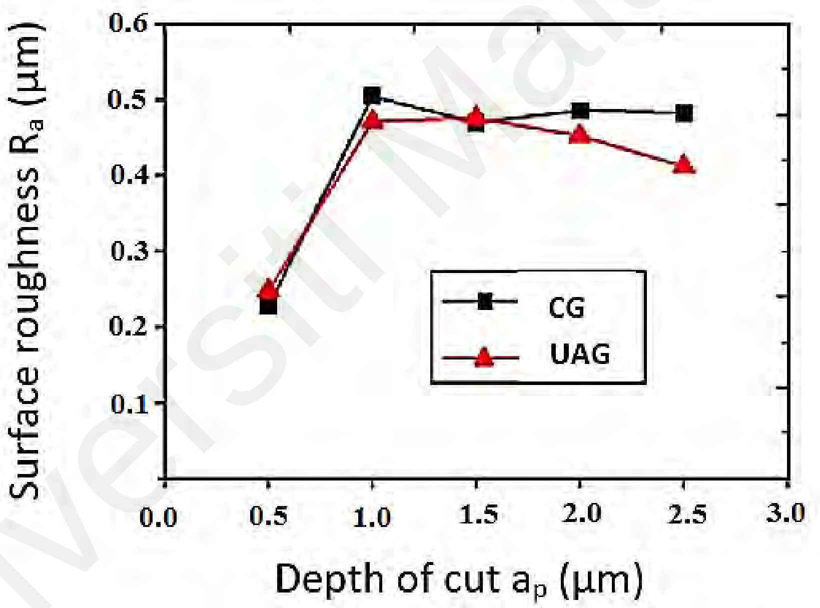

Figure 2.27: Variation of surface roughness (R_a) with depth of cut (Liang, Z. et al., 2010).

Further studies on the ultrasonic assisted grinding of Nano-zirconia ceramics, showed that at grinding depths of 1μm, the surface roughness for parts machined using CG process was 0.162μm. However, when the UAG process was used to grind the same material using the same depth of cut, the surface roughness was found to be 0.081μm. This shows that the UAG process produces enhanced surface integrity compared to the

CG process. Also, it was found that when using the UAG process, at grinding depths less than 5.2µm, there seem to occur an increase in both lateral and radial micro cracks. But at higher depths of cut, the tool material witnesses some abrasive actions, which was found to result to grain breakage on the wheel (Yanyan et al., 2009). This phenomenon of grain breakage gives rise to a much-desired phenomenon called tool re-sharpening, which has been found to cause significant improvements to the machinability, and surface quality in the UAG process (Akbari et al., 2008; Blackley et al., 1991; Klocke et al., 2000; Zhao et al., 2005).

Park et al. (2013) investigated the relationship between surface quality, and the grinding process parameters. In their work, they machined alumina ceramic (Al_2O_3) material using electroplated diamond wheel. They realized that the surface roughness R_a in the UAG process increases whenever the table feed rate, and cutting speeds were increased. **Figure 2.28** shows the variation of the surface roughness with the feed rates in both CG and UAG process. At feed rate of 1.67m/s, the surface roughness of the ground alumina material was 0.19µm and 0.16µm in both CG and UAG processes respectively. However, when the feed rate was doubled, it was found that the surface roughness decreased to 0.17µm and 0.15µm in both CG and UAG processes respectively. In general, it was found that during grinding operations, the surface roughness of the machined components could be improved by increasing the table feed rate.

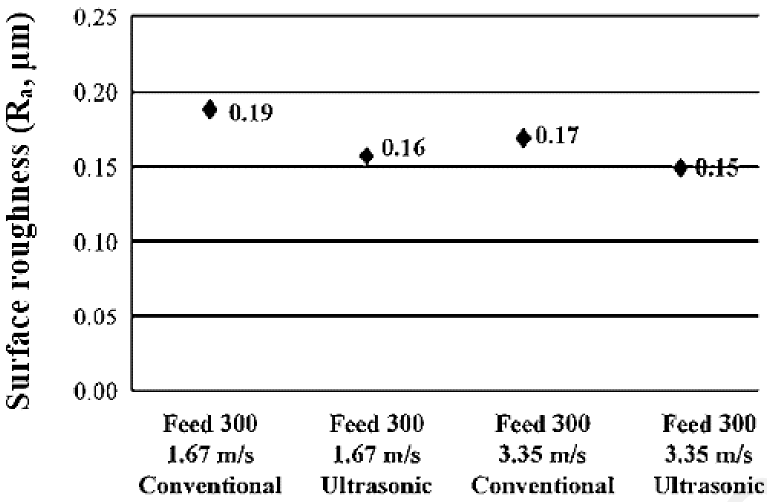

Figure 2.28: Variation of surface roughness with table feed rate (Park et al., 2013).

The surface roughness was found to reduce significantly with increase in the speed of the grinding wheel as shown in **Figure 2.29** (Zhao et al., 2005). Also, investigations have shown that there was an optimal cutting speed during UAG operations whereby the surface quality was maximum. This speed usually varies for different materials, and depends on their physical properties (Liang, Z. Q. et al., 2010). Moreover, (Jirapattarasilp et al., 2007) reports that surface roughness of cubic zirconia was greatly improved by increasing the wheel speed and grain size of the cutting tool during CG grinding.

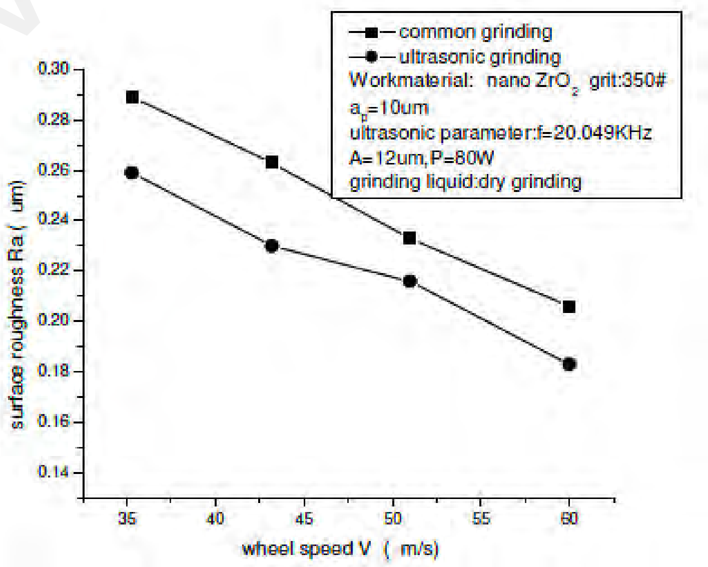

Figure 2.29: Variation of surface roughness with wheel speed (Zhao et al., 2005).

Denkena et al. (2008) investigated the machining of Al_2O_3+Ti composite using diamond wheels in both CG and UAG processes. They found that when CG was used to grind the composite, the average surface roughness R_a was about 70nm. However, when the UAG was used, the average surface roughness R_a achievable was about 20nm. This 29% decrease of surface roughness was an indication of the tremendous reduction found in the surface roughness using the UAG process in place of the CG process.

2.7.2 Effect of process parameters on sub-surface damage/ layer weakening

Sub-surface damage (SSD) is a kind of deformation which occurs beneath the ground surface as a result of the abrasive actions during the grinding operations. This defect was found to affect the properties of the machined components, as such it is necessary to investigate how it is generated, and its relationship with the grinding parameters.

Several procedures have been utilized by past researchers to detect the SSD's in ceramic materials such as Si_3N_4, Al_2O_3, and ZrO_2. They include hypothetical inspections, numerical simulations, and exploratory tests (Munoz-Tabares et al., 2011; Wang et al., 2015). Microscopic images obtained from scanning electron microscopy (SEM) and transmission electron microscopy (TEM) shows that there are two categories of subsurface damages i.e. micro cracks and pulverized layers (Li et al., 2011; Zhang et al., 2003). In addition, the amount of the sub-surface damages induced on the ceramic components was found to depend on the properties of the material, and the mechanism of material removal being employed (Agarwal et al., 2008; Rekow et al., 2005). For example, when the grinding mode was ductile, there was higher possibility of obtaining a crack-free surfaces, and minimal subsurface damages. However, the brittle fracture mode results in high rate of formations of cracks (Bifano, Dow, et al., 1991; Qu et al., 2000).

The grinding process, in general, was found to inflict various degrees of subsurface damages, which in turn reduces the strength, and reliability of the machined component. Most of the damages result from the propagation of microcracks within the workpiece materials. Pfeiffer et al. (1993) used the X-ray diffraction method to investigate the subsurface damages inflicted on SiC, and Al_2O_3 workpiece during CG. They found that there are several kinds of deformations present in the successive sub-layers of the ground surface. However, this non-destructive process was observed to be unable to distinguish between the different types of deformations and their causes.

Agarwal et al. (2008) studied the high-speed diamond grinding of silicon carbide. They found that the subsurface damages in the sub-layers occur as a result of microchipping, and the surface was characterized by microcracks. Also, the SSD's were found to reduce with distance further away from the ground surface. **Figure 2.30** shows the enormous amount of deformations found around the grain boundaries of the SiC ceramic. Also, the microchipping action was found to cause considerable propagation of the microcracks.

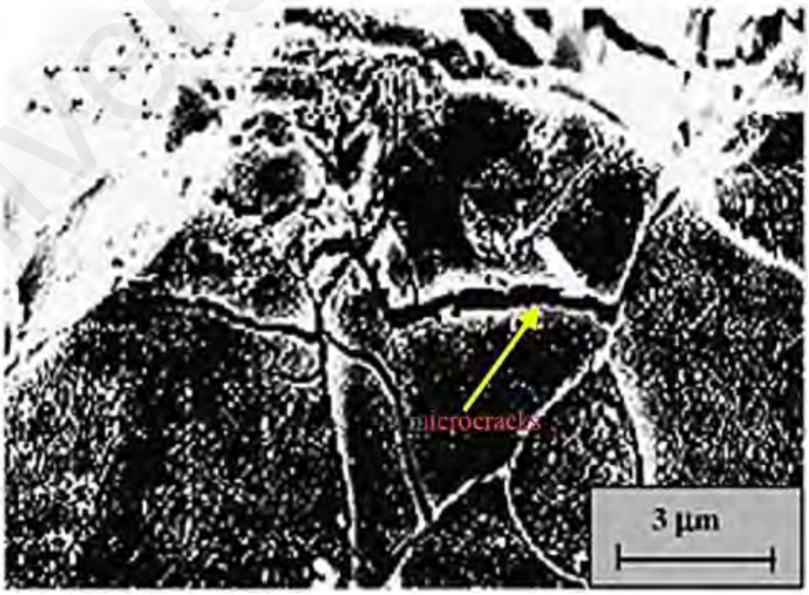

Figure 2.30: SEM image of surface damages and microcracks formed along the grain segments (Agarwal et al., 2008).

Further analysis have shown that the use of ultrasonic vibrations on the workpiece during the grinding process could cause higher SSD’s. Experimental investigations have shown that the generation of SSD’s during UAG was proportional to the feed rate, depth of cut and amplitudes of vibration. However, the higher spindle speed and amplitude of vibration were found to have insignificant effect on the formation of the SSD’s (Chen et al., 2015; Park et al., 2012).

Su et al. (2014) came up with a theoretical model to determine the size, and length of cracks produced during the grinding of ceramic materials. Their model considers the indentation fracture characteristics, which was found to depend on the properties of the ceramic material, and also the process parameters. From the developed crack model, they illustrated that the crack depth during grinding of ceramics components was proportional to the depth of cut and feed rates, whereas it was found to be inversely proportional to the speed of grinding wheel. Similar relationship was also reported by (Wang et al., 2015; Wang et al., 2008).

2.8 Grinding fluid and lubrications

Grinding fluids are used to provide different kinds of assistance during the grinding process ranging from flushing of microchips, to wheel cleaning, and in some cases coating of the newly formed sub-layer against corrosion. As such the grinding fluids are regarded as an essential part of the grinding process (Oliveira et al., 2006). Moreover, it has been revealed that during the grinding operations, majority of the grains on the wheel do not partake in the cutting actions, rather they just rub over and plow the surface of the workpiece. This rubbing and ploughing action was found to be the source of the high amount of heat in the grinding operations. The heat can be reduced significantly by using the grinding fluids (Tawakoli, et al., 2009). In general, the main purpose of the grinding fluids was to act simultaneously as a lubricant and pseudo-cooling system (Mao et al., 2012).

A great improvement to the surface quality was reported during wet grinding (grinding fluid present) as compared to dry grinding (grinding fluid absent). The cause of the poor surface quality found in dry grinding was attributed to the increase in thermal deteriorations, and frequent chip redeposition onto the workpiece materials (Arunachalam et al., 2004). The dry grinding method was also characterized by many drawbacks such as burning, high G-ratios, and high grinding forces (Uhlmann et al., 2010). However, the wet grinding has shown to be promising with improved machining performance, and better workpiece surface quality.

The grinding fluids are classified as either biodegradable or non-biodegradable. Even though the non-biodegradable grinding fluids have numerous advantages, they are yet accompanied by many limitations such as posing health risks to the operators, and menace to the environment. Recently, there have been increased usage of the biodegradable fluids as lubricants in grinding operations, due to the production of non-hazardous wastes (Fratila et al., 2011). Hence, the biodegradable grinding fluids were found to be environmentally friendly, and have less effect on the operators' health. As such, they are more preferred for use in the machining process (Chen et al., 2000). Some of these biodegradable grinding fluids include water, liquefied nitrogen, oils, etc. (Nik et al., 2012).

The biodegradable grinding fluids were subdivided into either mineral-based, or water based oils. The former being characterized by high cleaning ability while the latter has high convection property, and is often used for cooling purposes. Moreover, the grinding forces produced by the water-based grinding fluids were found to be less than those found when mineral oils were used. However, certain wheel types such as CBN tools are easily dissolved by water vapor as explained by (Hitchiner, 1999). This dissolution process was found to cause deterioration of the CBN wheels when the water-based fluids were used in the grinding operations. Thus, the mineral based oils are preferable as lubricants when grinding with such kinds of tool (Alves et al., 2006; Hu et al., 2011; Oliveira et al., 2006).

Similarly, previous research works have further classified the types of lubrication processes (based on the amount of lubricant used) as either minimum quantity lubrication (MQL) or flood cooling. The MQL grinding involved using high pressured air and oil mixture. Recently, the MQL oil mixture is composed of mineral oils with suspended nano-particles such as SiO_2, MoS_2 (Molaie et al., 2016; Tawakoli et al., 2011).

Balan et al. (2013) studied the effect of MQL process parameters on the grinding of Inconel 751 material. They found that the MQL lubrication method produces a great reduction to the grinding energy, and thermally induced deformations. Moreover, it was found that by steadily increasing the MQL fluid flow rates, the surface roughness of the Inconel workpiece could be greatly reduced from 7.25µm to 2.36µm. **Figure 2.31a & b** shows the difference of surface quality found in CG process when dry grinding was conducted (see **Figure 2.31a**), and when the MQL was used (see **Figure 2.31b**). As seen from both figures, it could be confirmed that the MQL helps to achieve better surface integrity in the machined materials.

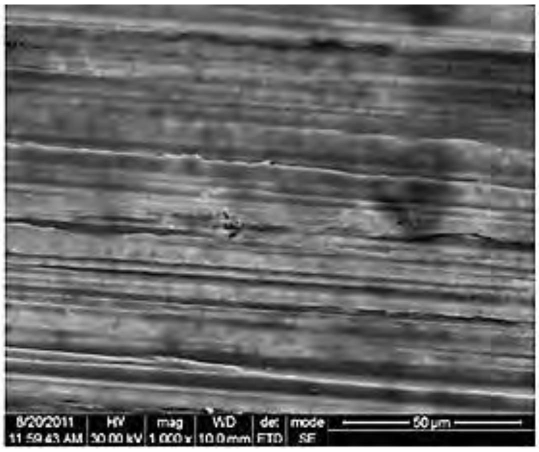 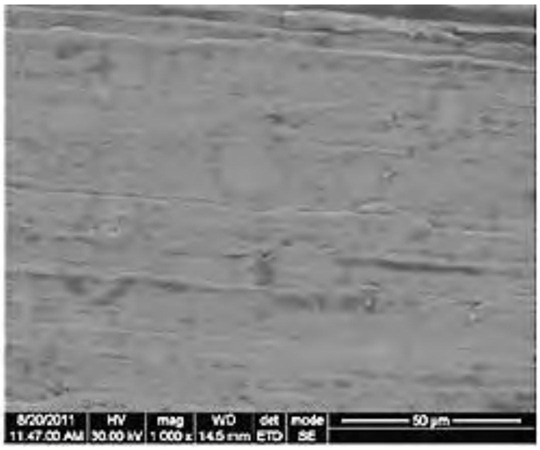

(a) (b)

Figure 2.31: Surface quality in CG grinding process (a) without MQL fluid (b) with MQL fluid (Balan et al., 2013).

Sadeghi et al. (2009) compared the performance of the MQL with flood cooling lubrication process during the grinding of titanium alloy (Ti_6Al_4V) using mineral oil based lubricants. They found that when the mineral based oils were used as lubricants, there was a high reduction in the grinding forces and grinding energy, with resultant increase in surface integrity. Also, the synthetic oils were found to produce higher reductions of the grinding forces and surface roughness. Oliveira et al. (2006) came up with a composition of mineral oil grinding fluids which was made up of sulfonate castor oil (40%), water (35%), bactericide (5%), synthetic ester (15%), emulsifier agent (5%). The fluid was found to perform greatly just like the synthetic nano-fluids. It was found that the attrition wears were greatly reduced when the grinding operation was performed with this composition of fluid. The surface roughness and grinding forces were also found to decrease significantly.

The introduction of ultrasonic vibrations into the grinding process was seen to result in even distribution of the grinding fluids around the grinding region (Peng et al., 2012). Moreover, Akbari et al. (2008) explained that in the wet UAG process, there was more than 30% reductions of grinding force, and about 40% decrease of grinding temperatures.

Molaie et al. (2016) explained that there was need for more awareness on the effect of grinding fluids to the environment, and risks to humans. In their work, they proposed the use of vegetable oil-based nano-fluids for the lubrication and cooling purposes. They investigated the effect of using MQL and oil based nano-fluids (MoS_2) in the UAG process. They found that by using the vegetable oil nano-fluids in the grinding process, the grinding forces could be reduced significantly as a result of lower wears, and attritions on the tool. Similar investigations shows that the penetration of the grinding fluids into the contact area was higher in the UAG process. Also, there was substantial reduction of the grinding forces due to the even distribution of the lubricants around the grinding region (Jian-Hua et al., 2015). Generally, the improved lubrication due to ultrasonication was found to produce lower thermal damages, and lower grinding forces (Kalita et al., 2012; Molaie et al., 2016; Qin et al., 2009; Verma et al., 2008; Zhang et al., 2015).

Figure 2.32 shows the results from the experimental investigations carried out to compare the performance of different types of grinding fluids in both the CG and UAG processes. Different surface roughness values were obtained during grinding with dry grinding, flood cooling, and minimum quantity nano-lubrications. The dry grinding in the CG process was found to have the least surface quality of 1.3µm, and the flood cooling in the UAG process was found to give the best surface quality of about 0.28µm. This was attributed to the enhanced flushing of debris, and higher penetration of grinding fluids across the grinding region in the UAG process. Moreover, it was found that the Minimum quantity nano fluids gave almost similar results for surface quality as the flood cooling technique (Alves et al., 2006; Molaie et al., 2016). In general, it could be seen that the ultrasonic vibrations in the UAG process caused higher fluid penetration, and produced improved surface quality in the machine components.

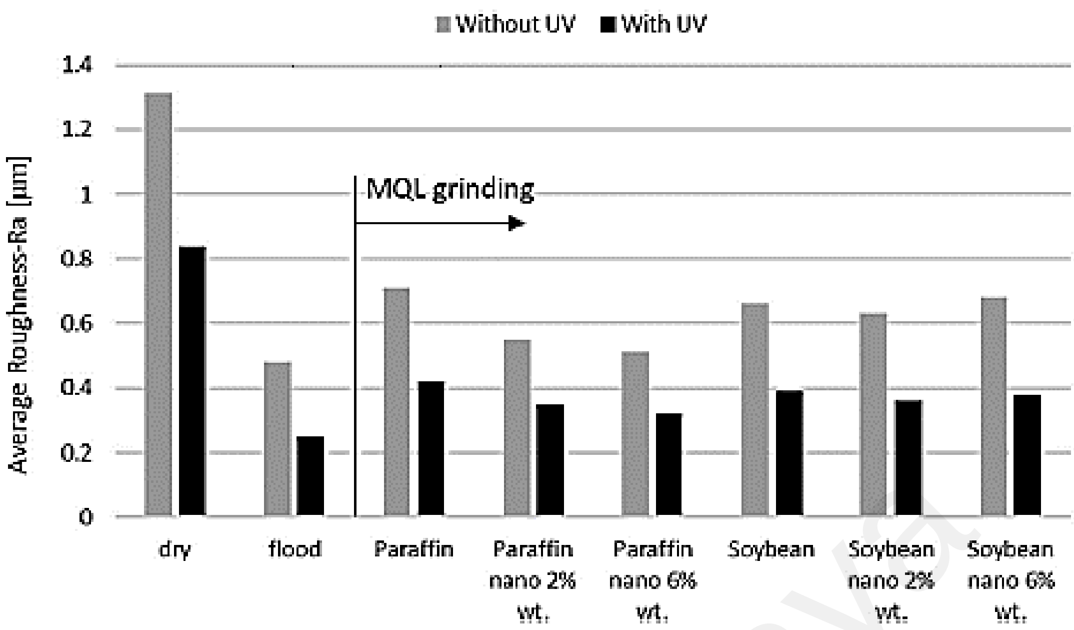

Figure 2.32: Performance of CG and UAG on the surface roughness of ground components (Molaie et al., 2016).

Investigation of the effects of fluid delivery techniques on the grinding of ceramic materials also revealed that the flow parameters of the MQL process, affects the performance of the ceramic grinding. For example, it was found that by synchronizing the jet speed of the MQL fluid with the speed of the grinding wheel, it would result to higher machining efficiency, and lower wheel loading. Also, effective fluid delivery could result to more than 80% increase of the MRR. However, when the quantity of fluid supplied was too high, the performance of the process was found to be highly reduced, producing higher tangential grinding forces, and non-uniform lubrications. As such the quantity and flow rate of the grinding fluid used should be moderate (Emami et al., 2014; Irani et al., 2007; Rowe, 2013).

2.9 Summary

The use of advanced ceramics in biomedical and aerospace applications would bring about a great improvement to the components being used in these fields, due to the exceptional properties of these advanced materials which includes high hardness, high thermal strength, high corrosion resistance and resistance to chemical attacks.

The conventional grinding of the advanced materials has so far been the most economic method of machining these materials. However, this process was found to be accompanied with many deformations such as surface/subsurface cracks, tool wears and high grinding forces. This unwanted phenomenon was found to produce negative effects on the performance of the ceramic materials. As such it is necessary to use other economical, and improved manufacturing techniques to machine these materials. The UAG system which is a hybrid process consisting of an ultrasonic system merged with the conventional grinding system has shown to be an alternative to the CG of advanced materials. Studies on the performance of the UAG process during the machining of brittle and ductile materials have shown that the introduction of ultrasonication into the grinding process significantly enhances the material removal rates and surface integrity. Moreover, the UAG process was also found to greatly reduce the grinding forces (Molaie et al., 2016).

In this section, the performance of machining advanced materials using UAG and CG processes from previous works have been reviewed. The findings show that the grinding forces decreases by about 50% in the UAG process as compared to the CG process, with about 45% increase in the G-ratio. Also, it was found that the ultrasonication process produces different kinds of effect on the individual grinding forces. The ultrasonication was found to produce more than 32% reductions in the normal grinding forces, and about 34% reductions of the tangential grinding forces (Molaie et al., 2016). The UAG process was found to achieve higher depths of cuts, up to 64% of that which was achievable in the CG process. Moreover, the findings from previous research works indicate that the surface roughness of the components produced using the UAG process was found to be greatly improved by more than 20%. However, the extent of the residual stress in the UAG process was found to be higher than in the CG process.

Studies have shown that the UAG process parameters such as feed rate, grain size, wheel speed, depth of cut, and most importantly, amplitude of vibration, were found to have a huge effect on the properties of the machined components. The results obtained from previous works show that the effects of the process parameters on the performances for both the CG and UAG process has been analyzed critically. It was found that rate of formation of subsurface damages during the UAG process was directly proportional to the feed rate, depth of cut and amplitude of vibration. Moreover, at higher cutting speeds and lower amplitudes of vibration, the subsurface damages from the UAG process was found to reduce significantly. Furthermore, for optimal performance of the UAG process in terms of reduced tool wear, the vibration amplitudes should be within the range of 6.5μm and 7.5μm. In other to obtain better surface integrity, the table feed rate should not exceed 3m/s during the grinding process because better surface roughness are achieved at lower feed rates.

Also, the use of biodegradable lubricants was found to improve the machining performance during the UAG operations. The biodegradable lubricants were seen to perform remarkably well just like the non-biodegradable ones. Due to the inexpensive and environmentally friendly nature of the biodegradable lubricants, they were considered to provide great advantage in terms of economic benefits without posing any environmental hazards or risks.

From the above general literature review, it could be seen that many studies have been conducted on investigating the effect of grinding operations on several engineering ceramics and super-alloys. However, there was no study conducted on the grinding of Si_3N_4 ceramic using UAG technique. Hence, this work involves studying the effect of different types of lubrication systems, and the effect of applying ultrasonication on the work material during grinding of Si_3N_4 ceramic.

CHAPTER 3: COMPARATIVE STUDY ON THE PERFORMANCE OF THE MQL NANO-LUBRICANT AND CONVENTIONAL FLOOD LUBRICATION TECHNIQUES DURING GRINDING OF Si_3N_4 CERAMIC

3.1 Introduction

The minimum Quantity Lubrication (MQL) process has been explained by in previous works to be a better alternative to the flood cooling lubrication system during grinding of advanced engineering ceramics. In this section, a comparison between the performance of the MQL and flood cooling lubrication techniques during grinding of Si_3N_4 ceramic is presented. The MQL nano-lubricant was formed by suspending silicon dioxide (SiO_2) nanoparticles in environmentally friendly vegetable oil (canola oil). The effect of the input parameters i.e. feed rate, depth of cut, type of diamond wheel and lubrication type, were investigated on the output parameters i.e. grinding forces, work piece surface roughness, surface damages and wheel wear. Taguchi mixed level parameter experimental design (L16) was used in the design of experiment, and the signal to noise ratio was used to optimize the grinding process. Furthermore, adaptive neuro fuzzy inference system (ANFIS) prediction method was used to predict and analyze the variation of the input parameters with the grinding forces and surface roughness.

3.2 Literature Review

Silicon nitride (Si_3N_4) is a precious advanced engineering ceramic that is highly desired for different applications in various fields due to its excellent mechanical and physical properties. The excellent properties of the Si_3N_4 ceramic makes it highly applicable in engineering applications such as cutting tools, bearings, thermal resistors, and combustion chambers (Zhang et al., 2012). Moreover, the Si_3N_4 ceramic is also highly biocompatible and characterized by low wear rates. This makes it a perfect candidate in hip joint replacement surgeries and biomedical applications. Furthermore, studies have shown that the tiny worn out debris of the Si_3N_4 could be gradually liquefied and resorbed in vivo, thereby decreasing the possibility of aseptic loosening (Olofsson et al., 2012).

However, the high strength and high brittleness of the Si_3N_4 ceramic makes it very difficult to cut, thereby causing great increase in its machining cost (Desa et al., 2001). An economical method of machining the Si_3N_4 ceramic requires the utilization of diamond grinding. This is because grinding ceramics using diamond wheels is still the most effective method of machining the Si_3N_4 ceramics and achieving high surface quality in highly precise sizes and shapes. In fact, the major limitation that is currently being encountered in the widespread usage of the Si_3N_4 ceramic is the need for efficient grinding of the ceramic material (Garshin, 2009). Also, the incessant wear experienced by the diamond wheel during the grinding of Si_3N_4 results in both surface and subsurface damages on the workpiece. As such, the wear of the diamond wheel during grinding of the advanced ceramics was among the widely analyzed areas in previous works (Dambatta et al., 2017). Also, the porosity and wheel loading ability of the grinding wheel have been found to significantly affect the performance of the grinding process. This is because high wheel porosity have been found to increase the wheel loading and embedment of nanoparticles inside the wheel's bond (Kuffa et al., 2016).

Studies have shown that the machining and finishing of advanced engineering ceramics constitutes more than 50% of the total manufacturing cost of the fabricated components. While the cost of grinding Si_3N_4 could constitute over 80% of the cost of the ceramic components (Lee et al., 2014). Moreover, literatures have indicated that the main obstacle to the widespread usage of the advanced engineering ceramics are the various degrees of damages inflicted on the ceramics during the grinding process (Spur et al., 1985). Also, it has been reported that the subsurface damages induced by the grinding process on the manufactured ceramic affects its quality by reducing the fracture strength and abrasion wear resistance (Desa et al., 2001).

Much effort has been channeled into improving the machinability of the advanced engineering ceramics aimed at reducing the machining costs, through investigation of the material removal modes, wheel wear, optimization of the machine variables, and utilization of more effective lubrication systems (Gates et al., 1999). Recent studies have shown that although the advanced engineering ceramics are brittle, their machinability could still be done in a ductile mode thereby achieving high quality surface finish. As such, achieving ductile machining mode is one the key ways of improving the machining of the advanced engineering ceramics (Sreejith, 2005). Investigations by Wang et al. (1997) indicates that the main types of surface damage during grinding operations are microplastic deformations, exfoliation, microcracks and macrocracks. Furthermore, small median cracks are also types of subsurface damages often developed below the plastic deformation zone, vertical to the ground surface. Moreover, the lateral cracks which are developed around the median cracks, are usually parallel to the ground surface. These subsurface cracks are often created by residual elastic stress as a result of contraction or relaxation of the deformed layers around grinding zone (Dambatta et al., 2017).

There have also been many studies focused on decreasing the grinding wheel wear and cost of machining, and simultaneously increasing the efficiency of the grinding process during diamond grinding of the advanced engineering ceramics. Two identified methods of achieving improved efficiency and reducing cost are improvement in the lubrication and optimization of the parametric settings of the grinding process (Emami et al., 2014). Studies have shown that the type of lubrication utilised in the grinding operations greatly affects the performance of the machining process such as wheel life, surface quality and energy expended (Fratila, 2010). Lubricants have been found to improve the material removal rates and subsequently lowering the subsurface damages compared to the dry grinding process (Desa et al., 2001). Furthermore, the grinding fluids help in evacuation of debris/heat around the grinding zones.

Boswell et al. (2017) reported that the dry grinding process is characterized by intense wheel wear, while the flood cooling process helps to reduce wheel wear. Although the Castrol oil used in the flood cooling possess many benefits, the fact that it is non-biodegradable is a major setback because it is hazardous to both the operators and the environment. Recently, studies are being focused on the use of biodegradable vegetable oils as lubricants in the grinding process (Nik et al., 2012).

Studies have shown that the minimum quantity lubrication (MQL) helps to reduce the grinding forces significantly, wheel wear and surface roughness of the workpiece materials compared with the conventional flood cooling systems. The MQL system using suspended nano-particles in oil has so far been found to out-perform the conventional flood cooling system (Kuffa et al., 2016). Several investigations have been conducted to study the performance of SiO_2 nanoparticles as a solid lubricant in machining operations. This is because the SiO_2 nanoparticles have a very high hardness and relatively costs lesser than other nanoparticles (Sarhan et al., 2012a). From the findings of various works, it could be seen that the SiO_2 nanolubricant performs greatly in machining of superhard materials. This is because the solid lubricant is capable of withstanding high impact pressure and temperatures of the grinding zones.

Analysis of the morphology and geometrical shapes of grinding chips has also shown that the lubrication/cooling method employed in the machining process significantly affects its overall performance (Wang et al., 2016). In addition, the use of solid lubricants which are transported into the grinding zone with environmentally friendly oils in the MQL process has been established to be highly economical and efficient technique of improving the efficiency of the grinding process (Molaie et al., 2016). Further studies have shown that that the properties of the oil, and the nature of the grinding wheel used in the MQL process significantly affects the outcome of the machining process (de Souza Ruzzi et al., 2017).

According to the previous review of literature, there are many reports on grinding of advanced engineering ceramics using different types of lubrication techniques. However, the report about application of SiO_2 nanolubricant in Minimum Quantity Lubrication (MQL) for grinding silicon nitride (Si_3N_4) using ANFIS modelling analysis approach has not been reported.

In this work, an experimental analysis using Taguchi design of experiment has been done to analyze the effects of grinding parameters, and different kinds of lubricants during grinding of Si_3N_4 advanced engineering ceramics. The effects of the process parameters on the grinding forces and surface quality have been studied. In addition, the effects of the type of wheel bonding on the response parameters were also investigated. Also, the performance of the MQL nano lubricant (SiO_2 based) was compared with the flood cooling lubricant. Moreover, the signals to noise ratio of the results from the Taguchi based experiment were used to obtain the optimum parameter settings. Lastly, an ANFIS prediction model was developed in other to analyze the relationship between the input and output parameters.

3.3 Mechanism of material removal

Studies have shown that the material mechanism in brittle materials is characterized by crack propagation. These cracks can be either median cracks or lateral cracks. During the material removal process, there seem to occur an elastic region which is formed due to plastic deformations as illustrated in **Figure 3.1**. The edge of the elastic region is also characterized by high residual stress and is called the plastic zone (Wang et al., 2015).

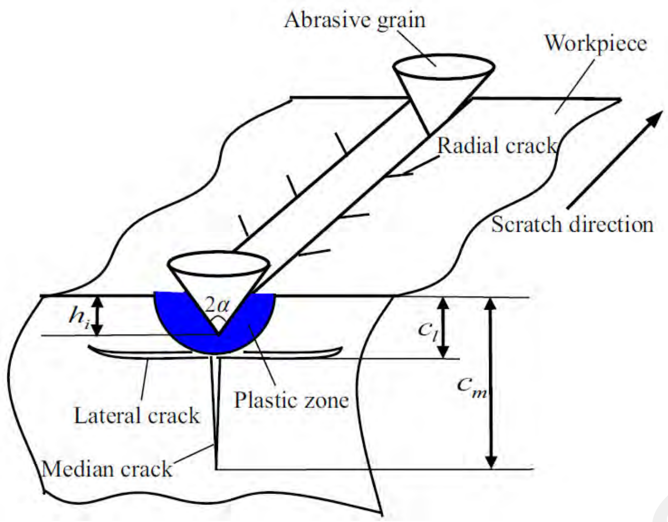

Figure 3.1: Material removal in brittle materials.

Previous works have shown that when the nanoparticle concentration of the nanofluid is increased, the coefficient of friction and grinding energy decreases significantly. Due to SiO_2 nanoparticles characterized by high bending strength and good lubrication capability (Sayuti et al., 2013), it is expected that the nanofluid would improve the lubrication by creating tribo-films in the grinding zone, thereby improving workpiece surface quality, wheel life and reducing the grinding forces significantly. The lubrication mechanism of the nanoparticle is characterized by deformation and fracture of the nanoparticles, which lead to the formation of the thin tribo-films, thus significantly reducing the asperities in the grinding region (see **Figure 3.2**). The mechanically formed tribofilm is often developed between two or more interfaces at low temperatures. The tribofilms are often formed from the nanoparticles, the debris from the work material and the wheel bond material. The composite formed by these materials is often referred to as mechanically mixed layer. The tribofilm, now a principal player in tribology helps to significantly reduce the frictional forces, thereby reducing the tangential forces (Biswas, 2000).

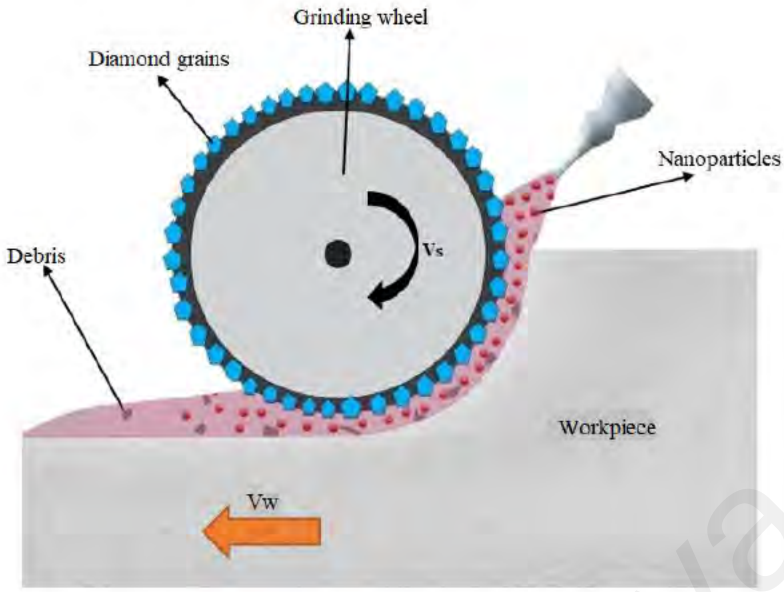

Figure 3.2: Lubrication phenomenon of SiO_2 nanoparticles during grinding operations.

3.4 Methodology

The grinding experiments were performed on using the Naga Ichi model (NI-450AV2) surface grinding machine at a constant rotational speed of 3000rpm. The experimental set up is shown in **Figure 3.3**.

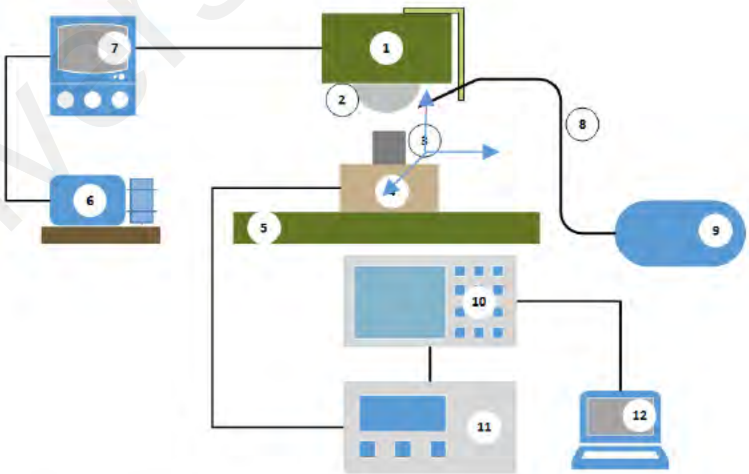

Figure 3.3: Experimental set-up: 1. Grinding machine head, 2. Grinding wheel, 3. Workpiece material, 4. Kistler Dynamometer, 5. Work table/feed, 6. Air-compressor, 7. Controller of high speed surface grinding, 8. Lubrication-nozzle, 9. MQL system, 10. 11. 12. Data acquisition system.

Furthermore, two types of diamond grinding wheels (each with a wheel speed of 63m/s) were used to conduct the experimental investigation. The specifications of the diamond grinding wheels are SD120M100M and SD120M100B for the metallic and resinoid bonded wheels respectively. Prior to performing each experimental run, the diamond wheels were dressed well using Norton's 38A150-I8VBE handheld diamond wheel dresser. The diameter, thickness and hole-diameter of grinding wheel are 200mm, 5 mm and 31.8mm respectively. Sintered Si_3N_4 ceramic blocks of sizes 50mm×20mm×10mm and properties given in **Table 3.1** were used as the workpiece material.

Table 3.1: Properties of Si_3N_4 material

Material type	Si_3N_4 >98%
Flexural strength (MPa) @ RT	700-800
Density (g/cc)	3.2
Dielectric constant	8
Coefficient of thermal expansion at RT-1000°C	3.1
Thermal shock parameter (°C)	610
Thermal conductivity at 25 °C ($W\ m^{-1}\ K^{-1}$)	42
Hardness – HV (0.3) kg/mm^2	1450
Fracture toughness ($MPa/m^{1/2}$)	6
Poisson's ratio	0.28
% Open porosity	0

The two types of lubricants used in the grinding process are conventional flood cooling (20% castrol oil mixed with water), and MQL nano-fluid (produced by suspending 4% by weight of pure silicon dioxide nanoparticles in canola vegetable oil. The mechanical properties of the SiO_2 nanoparticle used in this work are listed in **Table 3.2**. In addition, the nano fluid was formed by mixing the SiO_2 nanoparticles with vegetable oil followed by sonication in an ultrasonic bath with settings 240 V, 40 kHz, 500W for 45mins. The mixing procedure was done according to (Ooi et al., 2015).

Table 3.2: Mechanical properties of SiO_2

Properties	**SiO_2**
Size	5-15nm
Structure	Amorphous
Specific heat	1.0J/g-K
Thermal expansion coefficient	5.6×10^{-7}/K
Melting point	~1600 ºC
Density	2.2 g/cm^3
Dielectric constant	3.9
Dielectric strength	10^7
Thermal conductivity at 330K (W/cm-K)	0.014

The factors and levels of the process parameters considered in this work were chosen based on the limits of the surface grinding machine, and are summarized in **Table 3.3**. An L_{16} (4^2 2^2) Taguchi orthogonal array design formed on the Minitab-17 software was used to reduce the number of experimental runs. The Taguchi experimental design is shown in **Table 3.4**. Additionally, studies have shown that effectiveness of MQL process depends on the size and incident angle of the MQL droplets. As such, the WINMIST WT-01 MQL equipment was used to effectively deliver the nano fluid into the grounding region with nozzle inclination angle of 30°. Also, previous works have shown that the size of nanofluid delivered into the grinding zone depends on the air pressure and flow rates (Balan et al., 2013). Thus, the process parameters such as air pressure, lubricant and airflow rates were kept constant at 0.8MPa, 150ml/h and 30L/min respectively according to the optimal settings obtained by (Sayuti et al., 2013).

Table 3.3: Experimental parameters (factors and levels)

Symbol	Parameter	Level – 1	Level - 2	Level – 3	Level – 4
A	Feed rate (m/min)	10	15	18	23
B	Depth of cut (μm)	5	10	20	30
C	Wheel type	Metallic	Resinoid		
D	Lubrication type	MQL	Flood cooling		

Table 3.4: Taguchi experimental design

S/N	**Parameter**			
	A	**B**	**C**	**D**
1	1	1	1	1
2	1	2	1	1
3	1	3	2	2
4	1	4	2	2
5	2	1	1	2
6	2	2	1	2
7	2	3	2	1
8	2	4	2	1
9	3	1	2	1
10	3	2	2	1

Table 3.4, continued

S/N	A	B	C	D
11	3	3	1	2
12	3	4	1	2
13	4	1	2	2
14	4	2	2	2
15	4	3	1	1
16	4	4	1	1

The experimental runs were conducted according to the Taguchi design shown in **Table 3.4**. The average grinding force from each grinding pass was acquired with Kistler type- 9272 dynamometer. The signals acquired were channeled through a Kistler 5019 charge amplifier. The final intensified force data was the acquired with a Tektronix TDS-2001C oscilloscope. Furthermore, the surface roughness of each run was acquired using the Mitutoyo SJ-210 profilometer at 0.8mm cut-off value.

Also, the grinding induced surface damages were investigated using a field emission scanning electron microscope (FESEM). Before each FESEM analysis, the samples were cleaned prior to examination, the ground specimens were cleansed using acetone solution.

3.5 Experimental results and analysis

The results obtained from the grinding process after each experimental run for the grinding forces and surface roughness are provided in **Table 3.5**.

Table 3.5: Measured Grinding Forces and Surface Roughness.

Exp. no.	A	B	C	. D	F_n (N)	F_t (N)	R_a (μm)
1	1	1	. 1	1	69.33	22.33	0.16
2	1	2	1	1	78.93	30.13	0.19
3	1	3	2	2	92.20	49.40	0.46
4	1	4	2	2	120.27	70.73	0.50
5	2	1	1	2	78.93	34.13	0.31
6	2	2	1	2	88.00	40.72	0.47
7	2	3	2	1	82.73	29.20	0.42
8	2	4	2	1	94.60	34.53	0.45
9	3	1	2	1	64.53	26.67	0.30
10	3	2	2	1	68.40	41.60	0.45
11	3	3	1	2	126.53	96.20	0.51
12	3	4	1	2	132.60	108.80	0.63
13	4	1	2	2	92.00	40.00	0.53
14	4	2	2	2	118.00	55.00	0.69
15	4	3	1	1	108.67	90.00	0.73
16	4	4	1	1	112.60	110.44	0.77

3.5.1 Analysis of results

The Taguchi experiment design process is an important tool that is used to significantly reduce the number of the experimental runs in a given investigation. The technique is used to analyze orthogonal arrays and investigate the effects of various variables on output parameters. The Signal to noise (S/N) is defined as the ratio of the desired signal to undesired noise, and it indicates levels of disparity of the desired results as an objective function. Moreover, the S/N ratio could be used to obtain the variation of the input variables via the analysis of variance. To optimize a given process, the S/N ratio as an objective function could be selected as either smaller is better, higher is better or nominal is better.

In this work, since the aim is to obtain optimal values for the grinding process parameters, an optimal setting of the input parameters will result in smaller values of grinding forces and also the surface roughness. As such, the smaller the better response was selected to optimize the grinding process parameters. **Equation 3.1** gives the formula for the S/N ratio for the smaller-is-better S/N ratio condition.

$$S= -10\mathrm{Log}\frac{1}{n}\sum_{1}^{n} Y^2 \tag{3.1}$$

Where n is the number of runs and Y is the result obtained from the experiment.

Table 3.6 shows the results obtained from each experiment. It could be seen that the maximum value of S/N ratio for normal grinding force was obtained in experimental run 9 i.e. when the settings are feed rate of 18m/min (level 3), depth of cut of 5µm (level 1), resinoid bond (level 2) and MQL lubrication (level 1). Hence, experimental run 9 is considered the optimal setting for normal grinding force

Table 3.6: Experimental Results

Run no.	F_n (N)			F_t (N)			R_a (µm)		
	F_n	SNRA1	PSNRA1	F_t	SNRA1	PSNRA1	R_a	SNRA1	PSNRA1
1	69.33	-36.82	-36.45	22.33	-26.98	-27.60	0.16	15.70	15.71
2	78.93	-37.95	-37.63	30.13	-29.58	-30.29	0.19	14.38	12.99
3	92.2	-39.30	-40.27	49.4	-33.88	-33.84	0.44	6.68	7.51
4	120.27	-41.60	-41.31	70.73	-36.99	-35.69	0.5	6.11	6.66
5	78.93	-37.95	-38.17	34.13	-30.66	-29.42	0.21	10.16	10.45
6	88	-38.89	-39.35	40.72	-32.20	-32.11	0.25	6.62	7.72
7	82.73	-38.36	-38.07	29.2	-29.31	-29.78	0.42	7.49	6.93
8	94.6	-39.52	-39.12	34.53	-30.76	-31.63	0.45	6.92	6.09
9	64.53	-36.20	-36.20	26.67	-28.52	-28.44	0.30	10.55	10.76
10	68.39	-36.70	-37.38	41.6	-32.38	-31.13	0.45	6.86	8.03
11	126.53	-42.04	-41.38	96.2	-39.66	-39.94	0.21	5.83	4.63
12	132.6	-42.45	-42.43	108.8	-40.73	-41.80	0.23	3.97	3.78
13	92	-39.28	-39.42	40	-32.04	-32.75	0.53	5.56	5.06
14	118	-41.44	-40.61	55	-34.81	-35.44	0.69	3.22	2.33
15	108.67	-40.72	-40.69	90	-39.09	-38.38	0.29	2.69	3.62
16	112.6	-41.03	-41.74	110.44	-40.86	-40.23	0.26	2.31	2.77

The Taguchi analysed results for the normal grinding force from the experiments is shown in **Table 3.7**. It was found that the depth of cut has the highest delta value. This means it has the highest effect on the normal grinding force. The type of lubrication system employed during the grinding experiment has the second highest influence on the normal grinding force. The feed rate and the type of grinding wheel have the least effects on the normal grinding force. In addition, the mains effect plot of the S/N ratio for normal grinding force is shown in **Figure 3.4**. The characteristics of the S/N ratio of the normal grinding force relative to each process parameter and the corresponding levels are given in **Table 3.7**. It shows the effect and rank of the parameters according to delta statistics which involves comparing the relative magnitude of the effects from each parameters. In other to obtain a delta value, the maximum value obtained from each parameter is subtracted from the minimum experimental value obtained.

Table 3.7: Response Table for Signal to Noise Ratio for normal grinding force.

Level	Feed rate (m/min)	Depth of cut (µm)	Wheel type	Lubrication
1	-38.92	-37.56	-39.73	-38.41
2	-38.68	-38.74	-39.05	-40.37
3	-39.35	-40.10	-	-
4	-40.62	-41.15	-	-
Delta	1.94	3.59	0.68	1.96
Rank	3	1	4	2

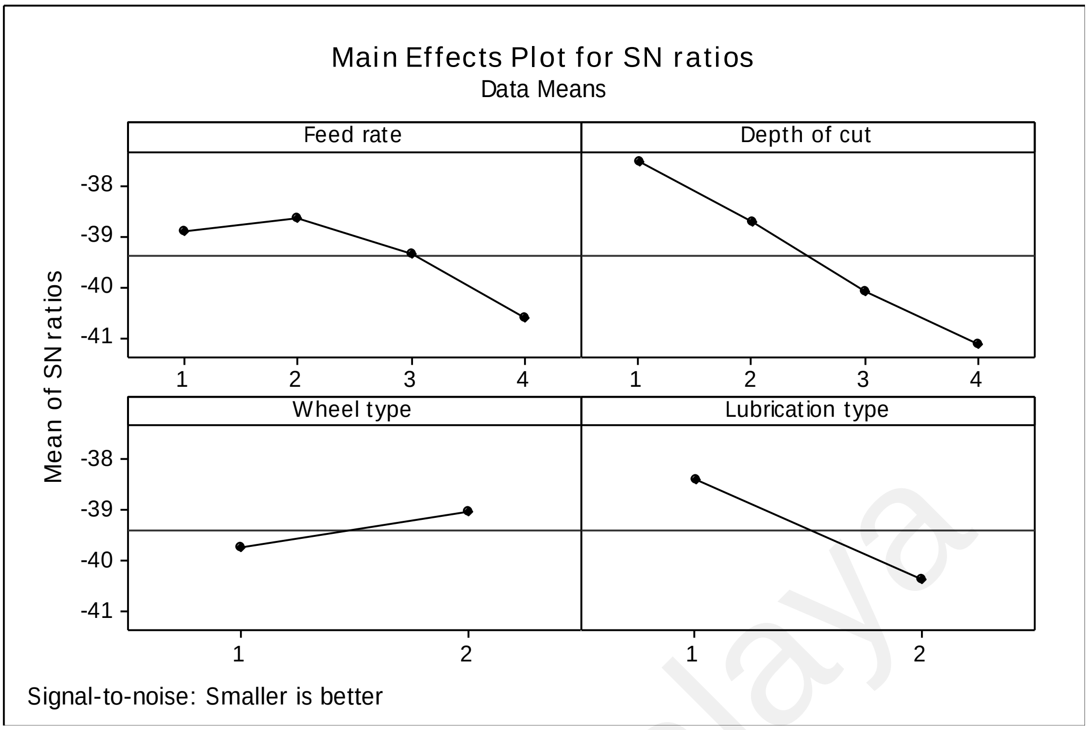

Figure 3.4: Main effect plot for SN ratio- normal grinding force.

The results of the analysis of variance for the tangential grinding force are given in **Table 3.8**. It could be seen that that the depth of cut has the highest effect on the tangential grinding force. The feed rate has the second highest influence on the tangential grinding force. The kind of lubrication system and type of grinding wheel utilized have the lowest effect on the tangential grinding force. Furthermore, the mains effect plot of the S/N ratio for tangential grinding force is illustrated in **Figure 3.5**. The results of S/N ratio shows that the maximum value of S/N ratio for the tangential grinding force occurred in the experimental run 1 i.e. when the settings are feed rate of 10m/min (level 1), depth of cut of 5µm (level 1), resinoid bond (level 1) and MQL lubrication (level 1).

Table 3.8: Response Table for Signal to Noise Ratio for tangential grinding force.

Level	Feed rate (m/min)	Depth of cut (µm)	Wheel type	Lubrication
1	-38.86	-29.55	-34.97	-32.18
2	-30.73	-32.24	-32.34	-35.12
3	-35.32	-35.48	-	-
4	-36.70	-37.34	-	-
Delta	5.97	7.79	2.63	2.94
Rank	2	1	4	3

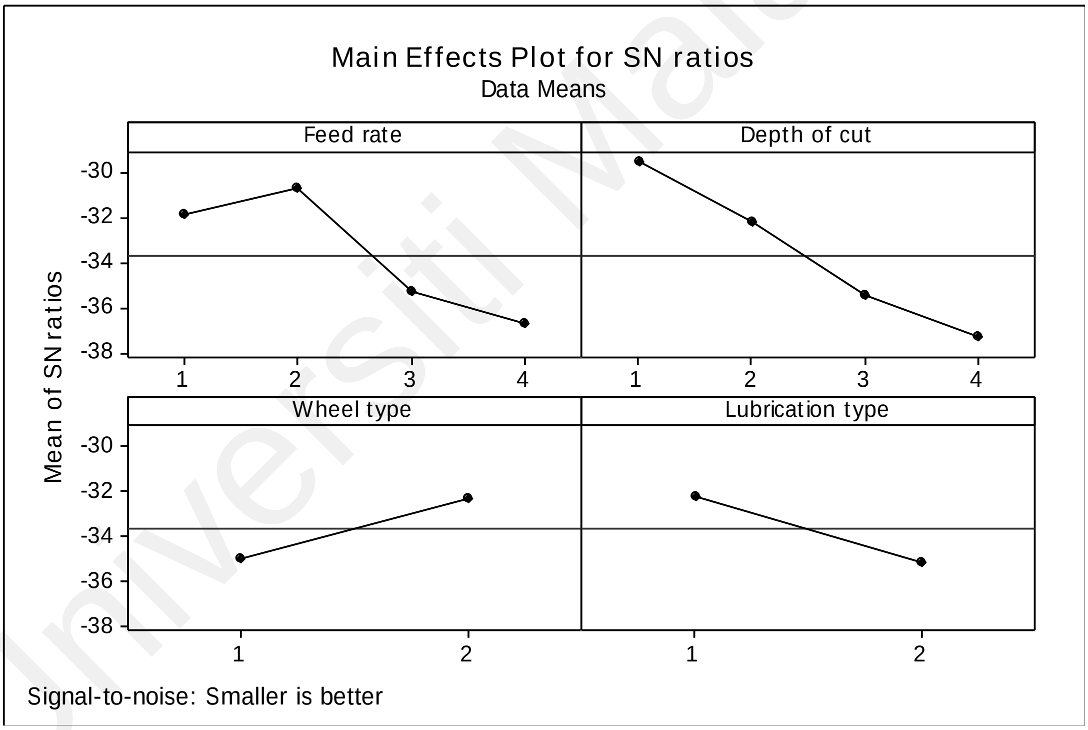

Figure 3.5: Main effect plot for SN ratio-Tangential grinding force.

Also, as shown in **Table 3.9**, the maximum value of S/N ratio for the surface roughness results was in experimental run 1. The mains effect plot of the S/N ratio for surface roughness is illustrated in **Figure 3.6**. It could be concluded that the optimum parameter setting for the surface roughness is feed rate of 10m/min (level 1), depth of cut of 5µm (level 1), resinoid bond (level 1) and MQL lubrication (level 1). Also, the table of signal to noise ratio presented in **Table 3.9** indicated that most influential parameter is the feed rate, followed by the depth of cut and then the lubricant employed in the process. The type of grinding wheel used has the least significant effect on the surface roughness of the machined parts.

Table 3.9: Response Table for Signal to Noise Ratio for surface roughness

Level	Feed rate (m/min)	Depth of cut (µm)	Wheel type	Lubrication
1	10.718	10.492	7.708	8.361
2	7.797	7.769	6.672	6.018
3	6.799	5.672		
4	3.445	4.825		
Delta	7.273	5.668	1.036	2.343
Rank	1	2	4	3

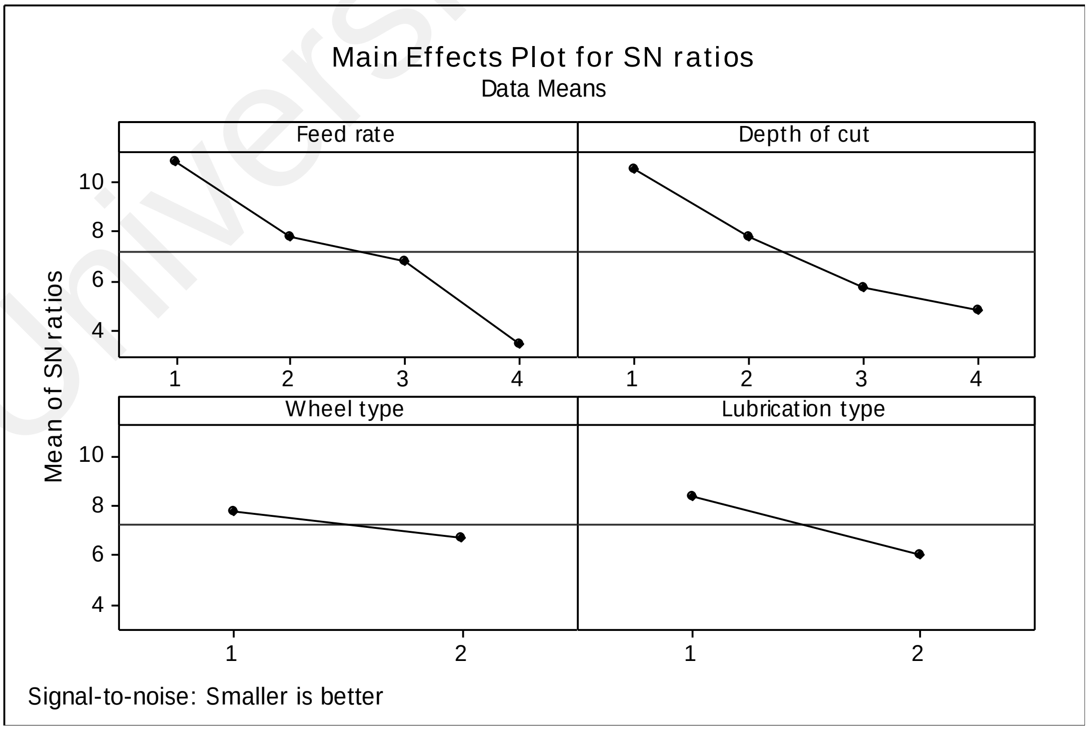

Figure 3.6: Main effect plot for SN ratio-surface roughness.

3.5.2 ANFIS Modelling

The ANFIS is an artificial intelligence technique which is used to represent the relationship between non-linear data by hybridizing intelligent algorithms in other to achieve optimum values of chosen membership functions (Jang et al., 1997). ANFIS is built by combining the learning capabilities of artificial neural network with the variability fuzzy logic as illustrated in **Figure 3.7**.

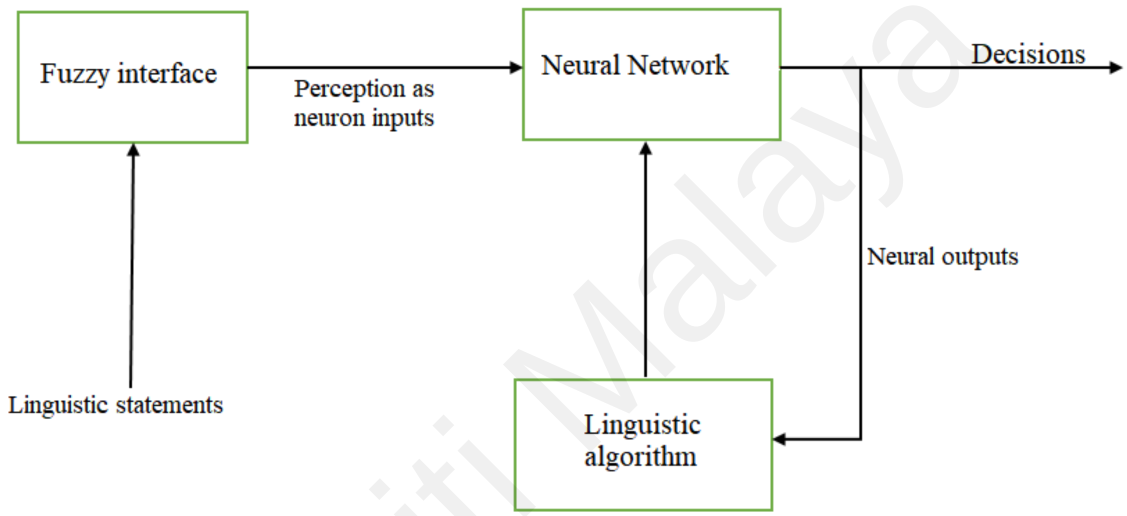

Figure 3.7: Neuro-fuzzy system.

The ANFIS model in this work was built on the ANFIS editor of MATLAB-R2015a software. The Sugeno inference system was used to construct the ANFIS model for the four set of input parameters with the response parameters. An example of the ANFIS structure is shown in **Figure 3.8** for the tangential grinding force (F_t).

Moreover, the constructed ANFIS inference system consists of five layers as illustrated in **Figure 3.9a**. The developed layers were used to in the learning process of the Sugeno-type fuzzy interface system (FIS) to develop the knowledge base and integration of the intelligent process. The actual architecture of the Sugeno ANFIS model is shown in **Figure 3.9b**.

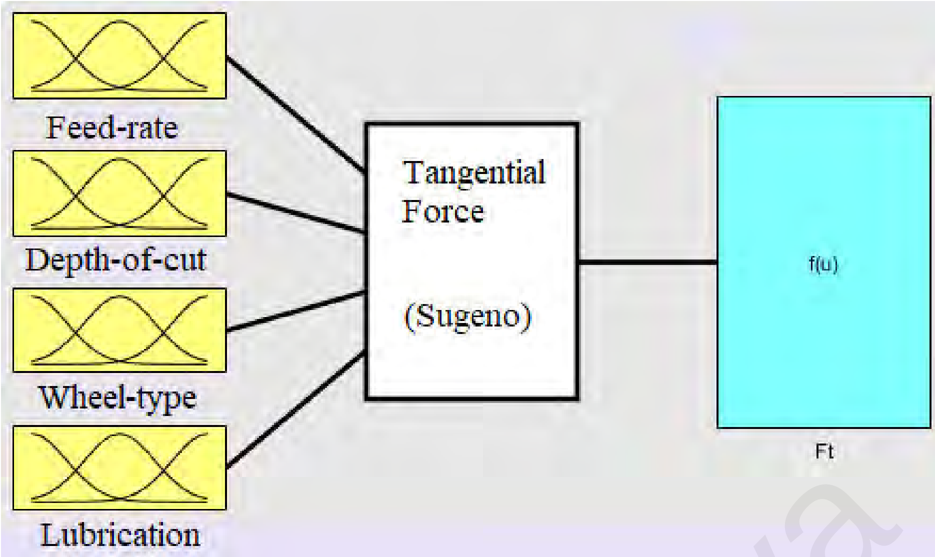

Figure 3.8: An example of the Sugeno Fuzzy inference system for the Tangential force.

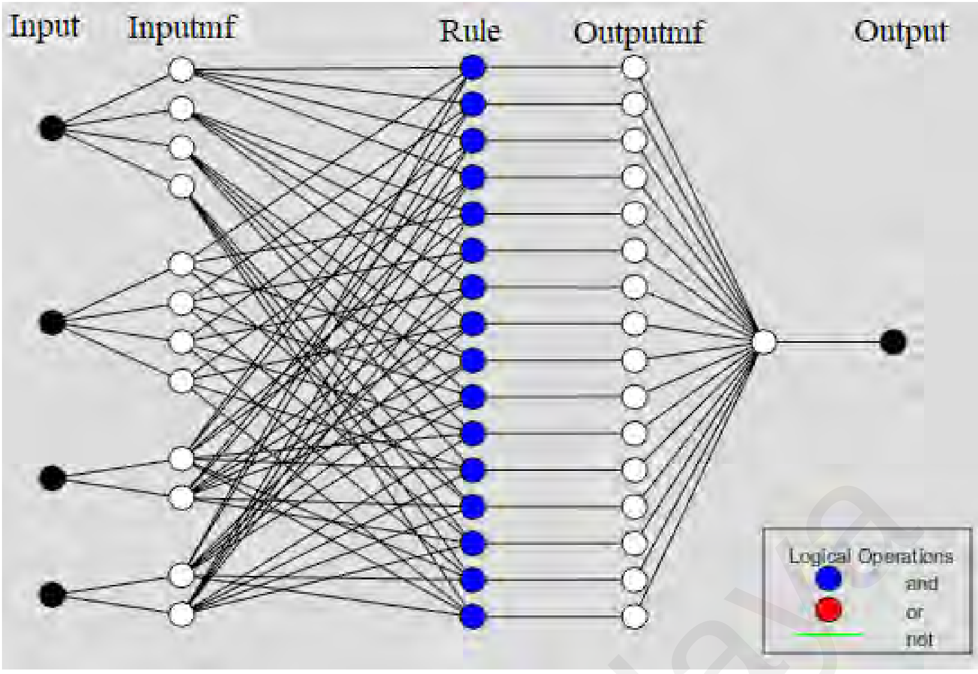

(a)

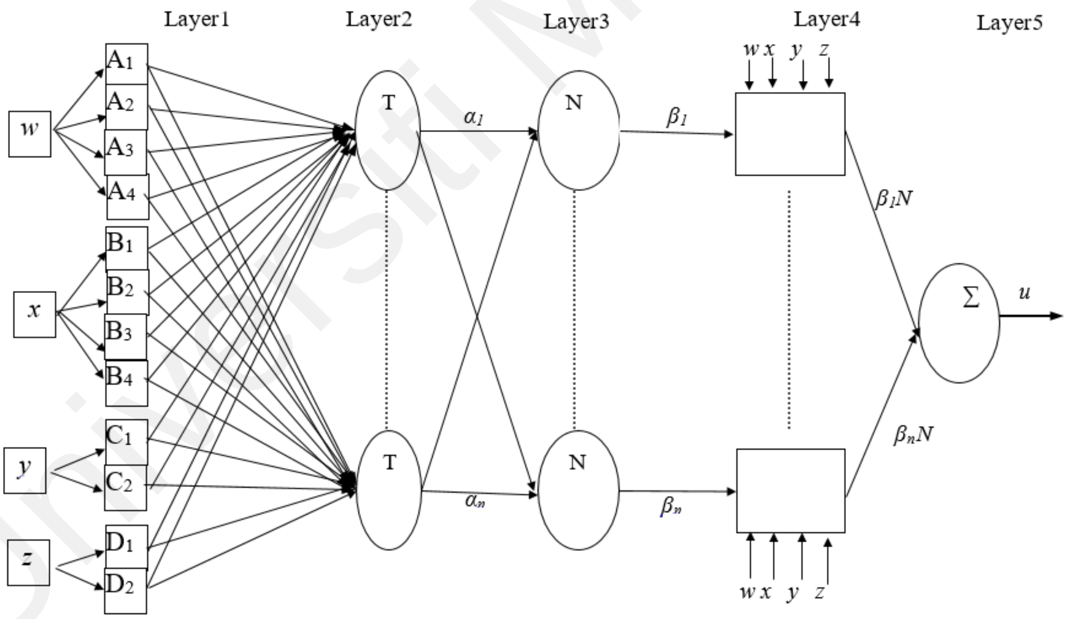

(b)

Figure 3.9: (a) Trained ANFIS model (b) Architecture of the Sugeno ANFIS model.

Layer 1

The input fuzzification is carried out in this region, and it is made up of nodes and junctions. The closeness of the input with the linguistic labels is indicated by the output of each node. In this work, due to the non-linear relation existing between the grinding parameters and the output responses, the generalized bell-shaped membership structure was selected. The mathematical representation of the membership functions is shown in **Equation 3.2, 3.3, 3.4 and 3.5** considering the input parameters.

$$A_i(w) = \exp\left[-0.5\left(\frac{w-a_{i1}}{b_{i1}}\right)^2\right] \quad (3.2)$$

$$B_i(x) = \exp\left[-0.5\left(\frac{x-a_{i2}}{b_{i2}}\right)^2\right] \quad (3.3)$$

$$C_i(y) = \exp\left[-0.5\left(\frac{y-a_{i3}}{b_{i3}}\right)^2\right] \quad (3.4$$

$$D_i(z) = \exp\left[-0.5\left(\frac{z-a_{i4}}{b_{i4}}\right)^2\right] \quad (3.5)$$

Where ai_1, ai_2, ai_3, ai_4, bi_1, bi_2, bi_3 and bi_4 denotes the set of input variables

A full transformation is observed in the structure of the generalized bell membership functions (MF) as compared to its initial form due to the change in input variables. The principle parameters represented by the linguistic symbols Ai, Bi, Ci, and Di are the components of MF.

Layer 2

The developments of the database of the fuzzy set are performed in this layer. In this region, the computation of the weights, based on prescribed rules is done in each node. These nodes are considered as the rule nodes. **Equation 3.6-3.8** show the response in the top and bottom neurons.

$$\alpha_1 = A_1(w) \times B_1(x) \times C_1(y) \times D_1(z) \quad (3.6)$$

$$\alpha_2 = A_2(w) \times B_2(x) \times C_2(y) \times D_2(z) \quad (3.7)$$

. . . . .

. . . . .

$$\alpha_n = A_n(w) \times B_n(x) \times C_n(y) \times D_n(z) \quad (3.8)$$

Layer 3

Layer 3 is responsible for building the base of the fuzzy rule. The firing weights of each node in this layer is normalized by labelling each node as N. The result obtained from the top and bottom neurons is normalized using **Equation 3.9-3.12** respectively.

$$\beta_1 = \frac{\alpha_1}{\alpha_1+\alpha_2+\alpha_3+\alpha_4} \quad (3.9)$$

$$\beta_2 = \frac{\alpha_2}{\alpha_1+\alpha_2+\alpha_1+\alpha_2} \quad (3.10)$$

$$\beta_3 = \frac{\alpha_3}{\alpha_1+\alpha_2+\alpha_3+\alpha_4} \quad (3.11)$$

$$\beta_4 = \frac{\alpha_4}{\alpha_1+\alpha_2+\alpha_3+\alpha_4} \quad (3.12)$$

Layer 4

Layer 4 is the decision-making region. To obtain outputs in this layer, the previous results/nodes are multiplied as shown in **Equation 3.13, 3.14 and 3.15**. This is simply the product of the normalized firing weights and the rules of each output.

$$\beta_1 z_1 = \beta_1 (a_1 w + b_1 x + c_1 y + d_1 z) \quad (3.13)$$

$$\beta_2 z_2 = \beta_2 (a_2 w + b_2 x + c_1 y + d_2 z) \quad (3.14)$$

. . .

. . .

$$\beta_n z_n = \beta_n (a_n w + b_n x + c_n y + d_n z) \quad (3.15)$$

Layer 5

Layer 5 is known as the output defuzzification region. This is the region where the ANFIS model represents each input by using two rules and two linguistic variables. Moreover, in this layer, the calculated weighted value for the output in terms of the preceding signals is indicated by a single node. **Equation 3.16** shows the mathematical representation.

$$U=\beta_1 N_1 + \beta_2 N_2+\beta_3 N_3 + \beta_4 N_4 \tag{3.16}$$

Since the crisped training data $((a^k, b^k), k=1, \ldots ,k)$ are provided, the developed hybrid neural network model could learn using the back propagation method. Also, **Equation 3.17** presents the error developed during the training process.

$$E_k= (b^k-o^k)^2 \tag{3.17}$$

Where b^k is the expected output value and o^k is the calculated output value obtained from the developed hybrid neural network (Azar, 2013).

The experimentally measured result of grinding forces and surface roughness obtained from the experiment was used as the input training data of the ANFIS model. The ANFIS model was then developed according the method explained by authors' (Maher et al., 2015). The generalized bell (gbell) membership function was selected for establishment of fuzzy rules, due to the non-linear relationship between the input and output variables. The ANFIS models for the normal grinding force, tangential grinding force and surface roughness were trained for 100 epochs using 16 set of rules obtained from the Taguchi design. Lastly, the average epoch error of the developed model for normal grinding force, tangential grinding force and surface roughness were obtained as 1.287×10^{-4}, 6.1113×10^{-5} and 4.844×10^{-7} respectively.

3.5.2.1 Verification of ANFIS Model

The accuracy of the ANFIS model was confirmed from four additional experiments. The parametric settings of the validation experiment are given **Table 3.10**. The accuracy of the ANFIS model was obtained using **Equation 3.18**. In addition, a the responses obtained in the ANFIS predicted and experimental runs for the normal grinding force, tangential grinding force, and surface roughness in the verification experiments are shown in **Figures 3.10, 3.11 and 3.12** respectively. The ANFIS models for the normal grinding force, tangential grinding force and surface roughness were found to have accuracies of 98.45%, 98.58% and 96.31% respectively. This indicates high prediction accuracy of the developed ANFIS models.

$$\text{Accuracy A} = \frac{1}{N}\sum_{i=1}^{N}\left(1 - \frac{V_{exp.}-V_{pred.}}{V_{exp.}}\right) \times 100\% \qquad (3.18)$$

Where N is the total number of experiments conducted for the verification.

Table 3.10: Settings for validation experiments

Exp. no.	**A**	**B**	**C**	**D**	**Measured**			**Predicted**		
					F_t (N)	**F_n (N)**	**(R_a) µm**	**(F_t) N**	**(F_n) N**	**(R_a) µm**
1	1	1	2	2	45	34	0.33	43.9	33.4	0.32
2	2	2	1	1	36	82	0.312	35.6	83.5	0.335
3	3	1	1	2	38	95	0.33	37.4	94.5	0.323
4	4	2	1	2	57	128	0.667	56.4	126	0.682

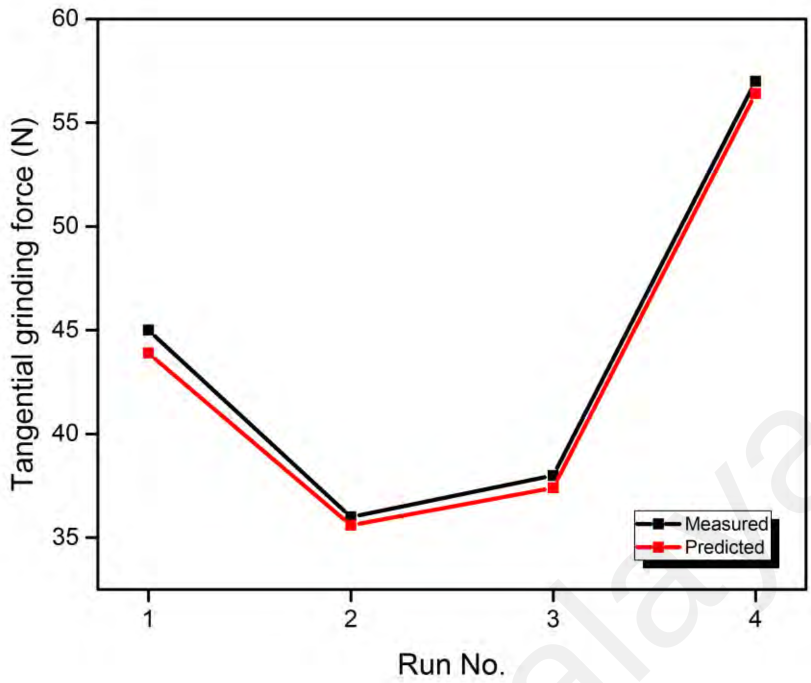

Figure 3.10: Tangential grinding force - ANFIS predicted vs measured.

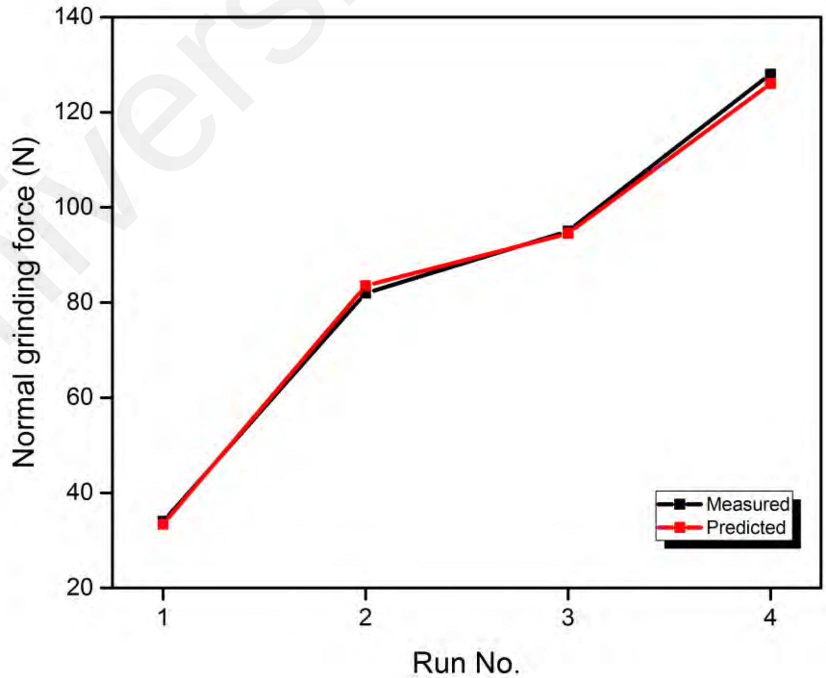

Figure 3.11: Normal grinding force - ANFIS predicted vs measured.

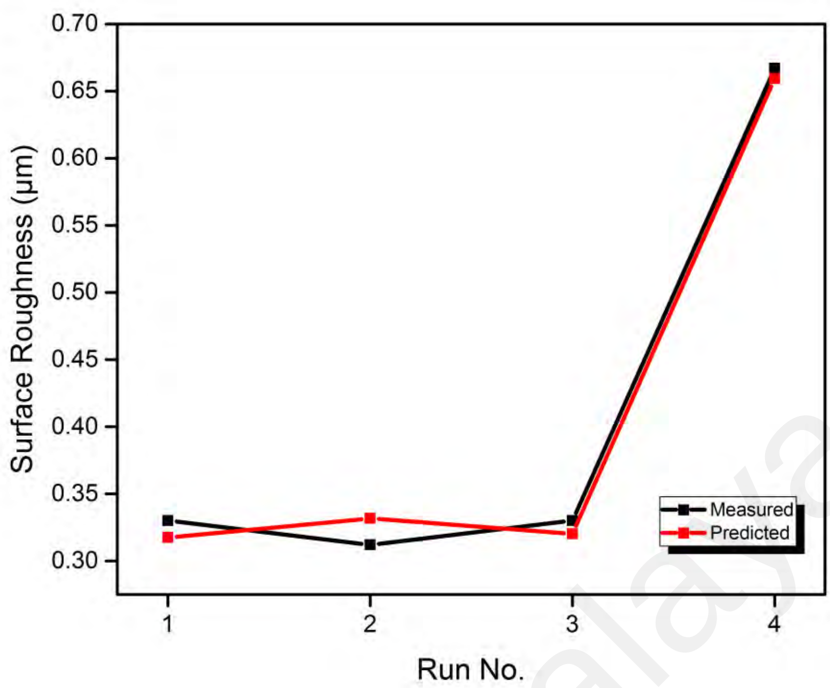

Figure 3.12: Surface roughness - ANFIS predicted vs measured.

3.6 Discussions

This study involves an experimental investigation of the grinding process using different kinds of diamond wheels and lubrication system. Moreover, the effect of the grinding process parameters, type of diamond wheels, and the lubrication system on the grinding forces and the surface quality during grinding of advanced engineering ceramics has been studied critically. Furthermore, an ANFIS modelling approach was used to analyze the grinding forces and the surface roughness.

3.6.1 Effect of parameters on normal grinding force

The effect of the grinding process parameters on the normal grinding force during grinding of Si_3N_4 engineering ceramic was investigated. The normal grinding forces occur as a result of the impact of the perpendicular pressure exerted from grinding wheel onto the workpiece material. Previous studies have shown that during grinding operations, the MQL lubrication technique has the ability to improve the tool life, surface quality and significantly reducing the energy expended during the grinding operations. The resultant increase in lubrication action results in significant reduction of the normal grinding forces (Kalita, et al., 2012) . Specifically, MQL nano lubrication has been seen to reduce the normal grinding force by about 25%, through the formation of thin tribo-films around the grinding region (Dambatta et al., 2017; Molaie et al., 2016). However, when the depth of cut is increase and the grinding wheel has to cut deeper, the performance of the lubrication oils tends to reduce significantly. This reduced performance could be as a result of both ineffective delivery of the lubricants into the grinding zone and increased frictional activity. Poor lubrication has been to result in increased mechanical overstress on both the wheel and work material during impacts, thereby causing several deformations to occur on both the wheel and the workpiece material. These deformations include reduction of the surface quality, grain break-off from the grinding wheels, and abrasive grits detachment from the bond. The deformations on the grinding leads to intense wear thereby resulting to increase in normal grinding force. Furthermore, due to difference in wear-ability between different types of grinding wheels, the rate of increase in the normal grinding force differs. For instance, it was observed that the rate of wear on the resinoid bonded diamond wheel is greater than the on metallic bonded wheel. This is due to the difference in both the bond strength and toughness of both bond types.

The main intention of using the MQL system is to reduce the amount of lubricant used in the grinding operations. Although the MQL system uses pressurized air to create a mist of cooling lubricant which is directly sprayed on the wheel's surface, yet only a thin film of lubricant spreads across the wheel's surface. This makes the MQL grinding to be a near dry grinding phenomenon. However, due to the presence of the suspended nanoparticles in the MQL oil, the tribological of the properties of the oil is highly increased thereby enhancing the lubricity of the MQL process.

In this work, the normal grinding forces have been found to have little dependence on the kind of lubrication system used in the grinding operations. Using the ANFIS model analysis, the viewer shown in **Figure 3.13a** shows that the type of lubricant employed in the grinding process significantly affects the process. The process involving the MQL nano lubrication has much lower normal grinding force compared to when the flood coolant was used. Similarly, the Phenolic resinoid bonded wheel have lower normal grinding force compared to the metallic bonded ones. Although, the normal grinding force exerted by wheel types increases with increase in both the depth of cut and feed rate, the force observed in the resinoid bonded wheels is much lower than the metallic bonded ones at high depths and speed. Furthermore, the resinoid bonded wheels exhibit higher deformation such as bond softening and deeper embedment of the diamond grains, which results in reduced number of cutting edges, thereby resulting in higher forces and bond wear at high depth of cuts. Moreover, the bond wear was found to be higher in the resinoid bonded wheels because of lower grain retention forces compared to the metallic bonded wheels. In addition, as seen in **Figure 3.13b**, both the feed rate and depth of cut have direct proportional relationship with the normal grinding force.

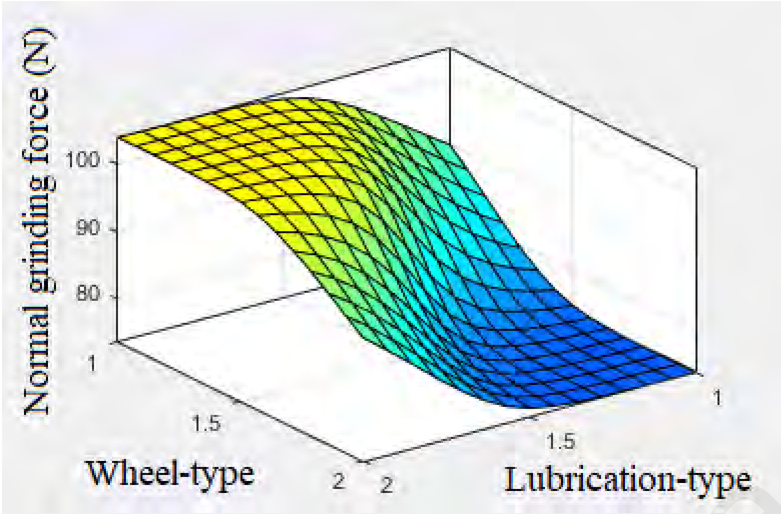

(a)

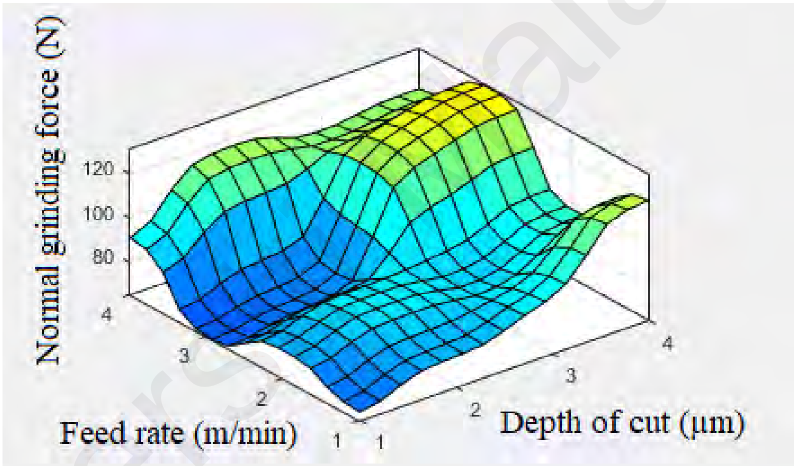

(b)

Figure 3.13: Effect of process parameters on normal grinding force (a) Type of lubrication vs wheel type (b) Feed rate vs depth of cut.

3.6.2 Effect of parameters on tangential grinding force

The tangential grinding force and the grinding power are two response parameters that are mainly dependent on the lubrication system. Previous reports have shown that the heat generated during grinding operations can be reduced by significantly reducing the friction using lubricants with a strong lubricating ability. Although the MQL process does not have a better cooling action compared with the flood coolants, the SiO_2 nano particles due to their high bending strength and stability were capable of decreasing the frictional forces around the grinding zone (Sarhan et al., 2012b).

In this section, it has been found that the tangential grinding force was significantly reduced by the MQL lubrication technique. This indicates that the silicon dioxide nano particle helps to lower the frictional force and allows for ease sliding of the wheel over the workpiece material i.e. increased lubrication. This observation could be seen from the ANFIS model results shown in **Figure 3.14**. Similarly, in the experiments conducted using the flood cooling, it was found that the tangential grinding force increases steadily from 35N at 5µm depth to over 100N at 30µm. However, from **Figure 3.14b** it could be seen that when the MQL technique was utilised, the rise in the recorded tangential grinding forces from the lower to higher depths was not so significant. This shows that the MQL system helps to significantly reduce the frictional force even at higher depths. This is because the nano particles were able to form a tribo-film on the surface of the grinding wheel which helps to reduce friction. In general, the MQL nano-lubrication system was found to offer greater reduction to the tangential grinding force than the flood cooling process. This results agrees with the findings of authors' (Molaie et al., 2016).

Furthermore, the feed rate was observed to significantly affect the tangential grinding force. As shown in **Figure 3.14a**, the feed rate exhibits a directly proportional relationship with the tangential grinding force. The same trend was observed in both the metallic and resinoid grinding wheels. However, the tangential grinding forces at higher feed rates in the metallic bond wheel than the resinoid bond wheel.

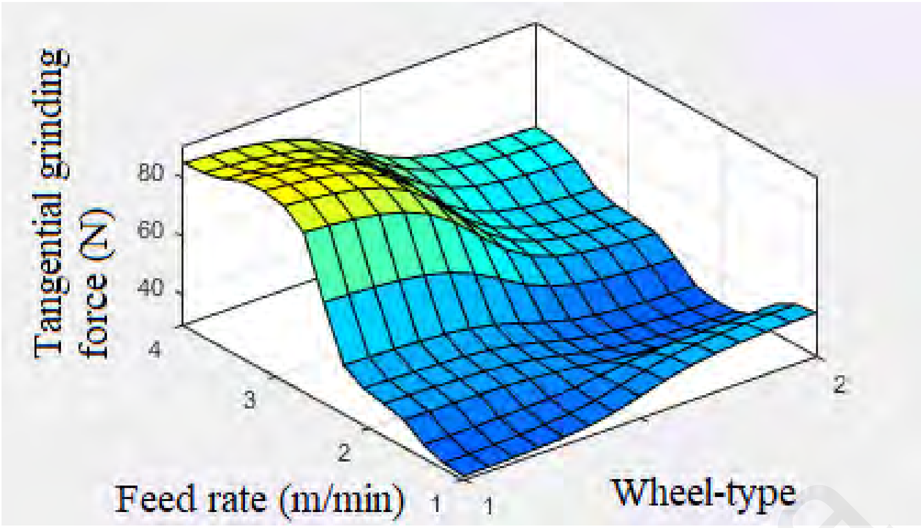

(a)

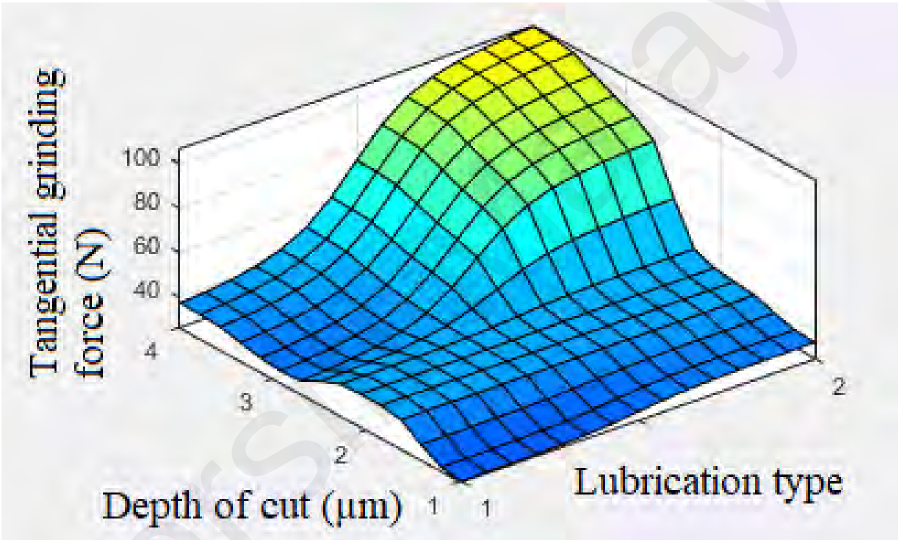

(b)

Figure 3.14: Effect of process parameters on Tangential grinding force (a) Feed rate vs Wheel type (b) Lubrication vs Depth of cut.

3.6.3 Effect of parameters on surface quality

Additionally, several studies have been conducted to investigate the effect of the grinding process parameters on the surface roughness. **Figure 3.15a** shows the ANFIS viewer which illustrates the variation of the surface quality with the wheel type and the feed rate. From the ANFIS model, it could be seen that surface roughness is directly proportional to the feed rate. Moreover, at lower feed rates, the surface roughness obtained in the resin bonded wheel was found to be higher than the metallic bonded one. This observation could be attributed to the superior toughness, strong grain retention and higher wear resistance of the metallic bonded wheel compared to the resin bonded wheel (Linke, 2016). Also, the better performance of the metallic bonded diamond wheel could be as result of increased wear flats, grain pull out and loss of cutting edges in the resinoid bonded wheels. However, at higher feed rates, the surface obtained was almost the same in wheel types. In **Figure 3.15b**, it could be seen that the surface roughness is directly proportional relation with the grinding depth. Also, in the flood cooling experiments, the surface roughness could be seen to increase from an average of about 0.3µm when the depth of cut is 5µm up to 0.6µm at 30µm depths. Moreover, when the depth of cut and feed rates are high, the samples were found to contain median cracks, exfoliations and lateral cracks as seen in the samples from experimental runs 4, 8 and 12 (see **Figure 3.16a, b & c**). The damages could be attributed to non-continuous grain trajectory due to increase in the friction forces. However, the MQL was found to produce better surface finish of about 0.2µm at 5µm depth of cut, to 0.44 µm at the depth of cut of 30µm. This indicates that the surface finish can be improved by grinding the Si_3N_4 ceramic using the nanofluid in the MQL system.

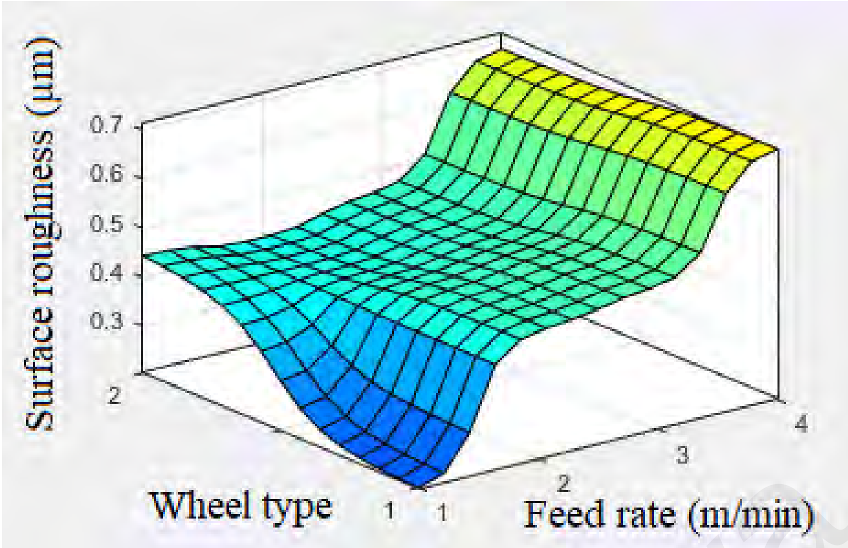

(a)

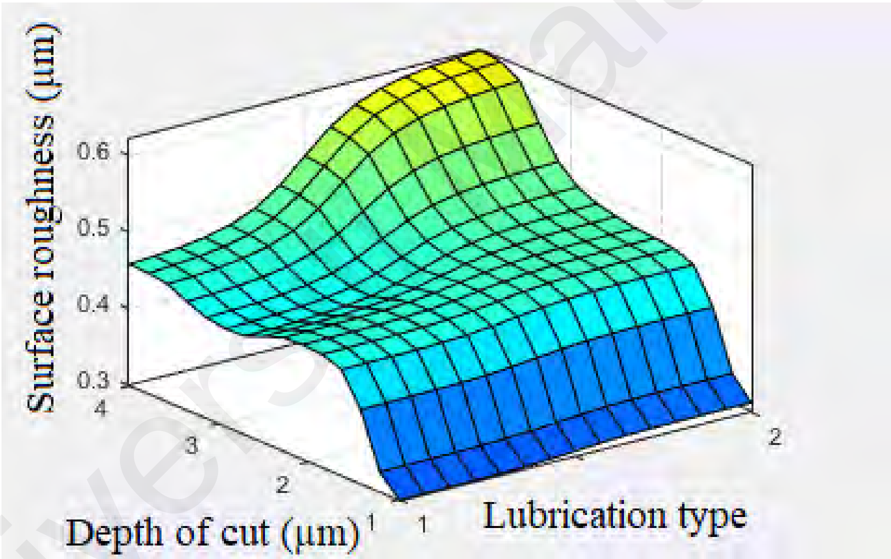

(b)

Figure 3.15: Effect of process parameters on the surface roughness (a) Wheel type vs Feed rate (b) Depth of cut vs Lubrication.

3.6.4 Surface analysis

The surface morphology after the experimental runs was obtained using the FESEM. The surface of the samples shown in **Figure 3.16** could be seen to vary according to the parameter settings. The following deliberations were made from the surface morphologies obtained:

The MQL system produces better surface quality than the flood cooling system. Although the effectiveness of the MQL process is mostly at lower depth of cut and feed rates, it still performs better than the flood cooling system at high depths and feed rates. Furthermore, the samples machined with the metallic bonded diamond wheel are seen to have better surface morphology than the ones machined with the resin bonded wheel. Qualitative comparison between the samples obtained from experimental runs 5 & 12, 4 & 14, and 8 & 9 (shown in **Figure 3.16**) indicates that a combination of low depth of cut and low feed rates produces the best surface quality.

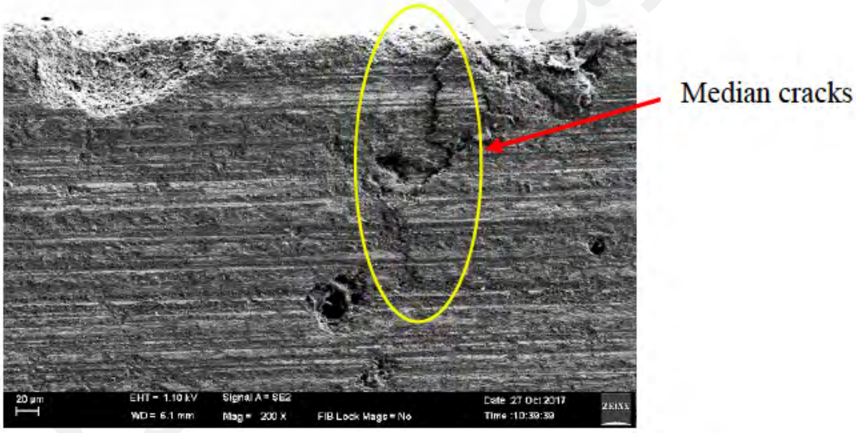

(a)

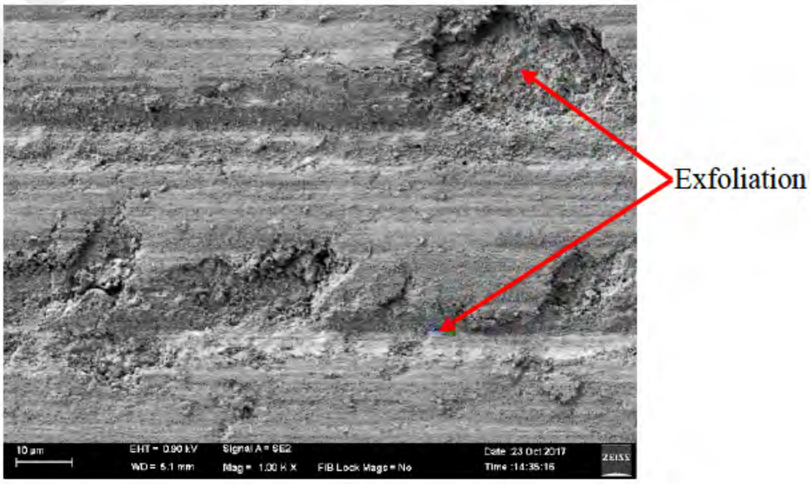

(b)

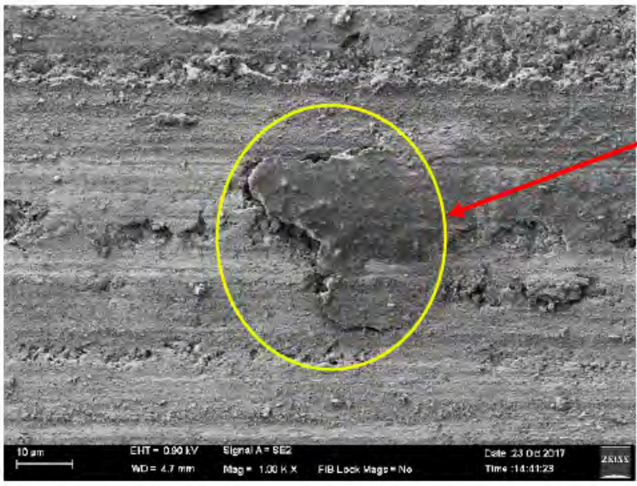

Lateral cracks and radial crack on the workpiece's surface.

(c)

Figure 3.16: Damages inflicted on the Si_3N_4 ceramic in experimental run (a) 4 (b) 8 (c) 12.

In addition, from **Figure 3.17**, it could be seen that the sample from experimental run 1 has the best surface quality, with absence of defects such cracks, scratches and/or furrows. This could be attributed lower impact forces and efficient material removal mode, and also good lubrication capability of the MQL nanofluid. This finding supports the S/N ratio results obtained in the Taguchi analysis in section 3. Also, in comparison with the sample from experimental run 16, the sample from experimental run 1 could be seen to have a much better surface quality. The sample from experimental run 16 has poor surface quality characterized by shallow and wide furrows. This shows that when both the feed rate and depth of cut are very high, the surface quality deteriorates significantly. Even though the experimental runs 5 & 12 have the same type of lubrication and grinding wheel (metallic bond), it is apparent from **Figure 3.17** that run 5 has a better surface quality because of the lower values of the depth of cut and feed rate.

However, the experiments done with the resin bonded wheel could be seen to have very poor surface quality. This could be observed by comparing experimental runs 8 & 9. This shows that the performance of the MQL system reduces when the depth of cut is very high. Similarly, as seen in the images from experimental runs 4 & 13, when either of the depth of cut or feed rate is very high, the surface becomes very poor. This could be attributed to increased wear of the resin bonded wheel, which in turn causes deterioration and defects on the ceramic workpiece.

Previous studies have indicated that the MQL nano-lubricant system significantly helps to lower the forces, surface roughness and wheel wear. Specifically, investigations have shown that by utilization of vegetable oils which are both cheap and environmentally friendly, the performance of grinding process can be improved significantly (Goindi et al., 2018). Furthermore, the capability of the SiO_2 nanoparticle in providing lubrication as a solid lubricant could be affirmed from the experimental investigation. The surface quality and grinding forces were both lowered when using the MQL nanolubricant. This could be attributed to the formation of thin tribofilm on the surface of the grinding, which in turn allows for better slewing action and material removal (Sayuti et al., 2014).

Since the canola oil is composed of fatty acids and glycerol, studies have shown that the fatty acids usually create a thin layer/lubricating films via physical and chemical adsorptions, which is adsorbed onto the surface of the wheel. Though the adsorption capability of the castrol oil is much higher than the vegetable oil, the Castrol oil is supposed to undergo some intermolecular esterification reactions that produces a frictional polyester with higher frictional ability (Jia et al., 2017). Nevertheless, the results obtained in this work have shown that the canola oil when mixed with the SiO_2 has better lubrication ability than pure castrol oil mixed with water.

Additionally, the wear of the diamond wheel depends on a number of factors such as the properties of the workpiece and grinding conditions. Others sources of wear could include chemical effects and physical/abrasive effects (Dambatta et al., 2017). Similar works have also shown that three kinds of wears often occur during grinding of advanced materials i.e. attrition wear, grain fracture, and bond excoriation. Moreover, other types of deformations on the wheel can be in form of macro fracture, micro fracture, grain ejection, wear flats and cracks (Dambatta et al., 2017).

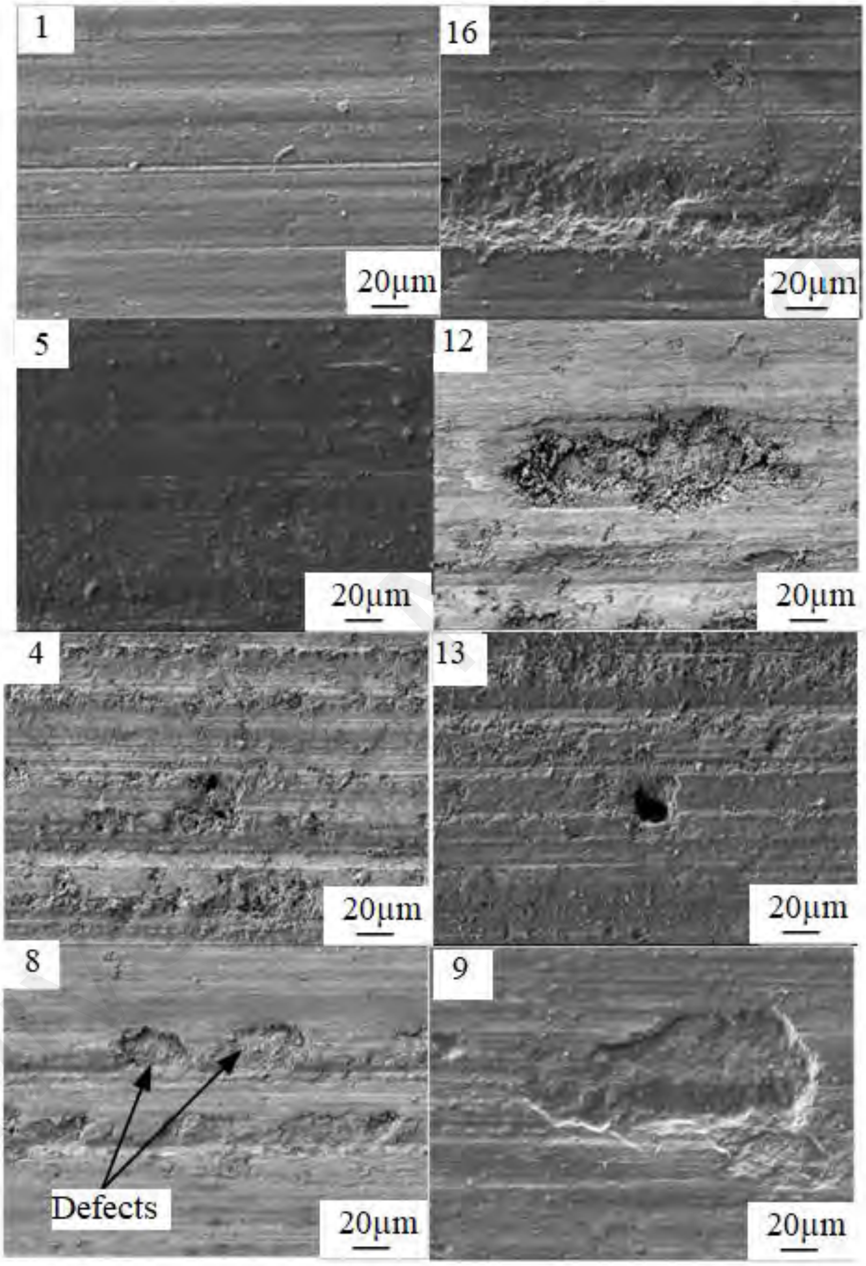

Figure 3.17: FESEM images showing the surface damage obtainable under different grinding experiments runs.

Furthermore, at high feed rates, the chatter frequency becomes high thereby causing high amplitude vibrations. In fact, the chatter marks which are visible on the surface of the workpiece material occur due to work regenerative effects. The grinding chatter is also highly affected by the rate of elastic deformation of the grinding wheel. Thus, it is expected that the chatter and vibration during grinding with the resin bonded wheel is smaller than in the metallic bonded wheel. However, the high rate of deformation and porosity of the resin bonded wheel leads to increase wheel wear. Another defect is presence of micro-welds and wheel loading, microcrystalline grain splintering, grain breakage, grain pull out and grain flattening.

Figure 3.18 shows the image of the grinding wheels before and after the grinding operations. By comparing the wheel appearance of the wheels, it could be seen that the experiments conducted using MQL are characterized by both microwelds and grain fractures. This could be attributed to insufficient debris evacuation in the MQL process, which leads to reduction of performance high feed rates and depth of cuts. However, in the flood cooling machined samples, there occurs in-process cleaning of the grinding wheel. Also, in the resin bonded wheel could be seen to have wear flats, grain breakage/pull outs, bond wear and cracks of the diamond grains. There is no definite trend observed for the wheel wear in the resin bond wheels, however the wheel was severely damaged when grinding was done at 30 μm compared to the 5 μm. For instance, comparing the image in experiment 8 & 9, it could be seen from experiment no. 8 that the wheel experience intense wear flats and pull out of the grains. Whereas in comparison, the wheel from experiment no. 9 is relatively wear free. Although the feed rate is increased, the reduction in the wheel wear seen in experiment no. 9 could be attributed to the reduction of depth of cut from 30μm to 5μm. Also, comparing the images from experiment no. 5 & 12, it could be seen that there is high rate of grit lost in experiment 12 accompanied by wear of the edges of the grinding wheel. Although, the wheels from the flood cooling experiments experiences less loading, the rate of grits pull out can be seen to be much higher than the wheels from the MQL process. In addition, the wheels from the MQL experiments due to the high rate of grit fracture, there is increase in the number of active cutting edges. This form of sharpening of the wheel is among the reason for the reduction of the grinding forces.

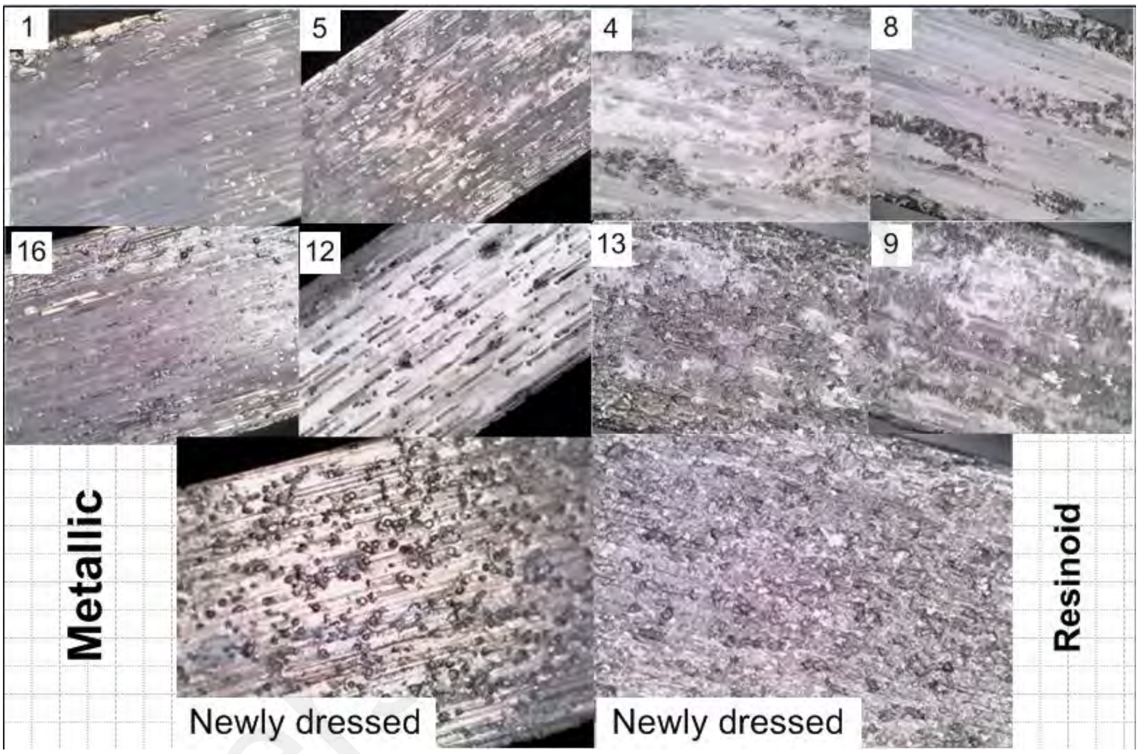

Figure 3.18: Microscopic image of the surface of the diamond wheel.

3.7 Summary

This study investigates the effect of the grinding parameters such as depth of cut, feed rate, wheel bond type and lubrication technique on the grinding forces and surface quality during surface grinding of Si_3N_4 ceramic. The findings show that the normal and tangential grinding forces were lower during grinding with the MQL technique compared to the flood cooling system. This indicates that the SiO_2 nanoparticles possess good lubrication capability on the grinding process when mixed with canola vegetable oil in the MQL process. Also, the grinding forces were found to be directly proportional to the feed rates and depth of cut. The metallic bonded wheel was also found to perform better in terms of wear and surface quality, than the resin bond wheel. Moreover, at high depth of cuts and feed rates, the surface roughness of the workpiece material becomes extremely poor in both wheels. This could be attributed to increase in wear flats, diamond grain pull out, macrocracks and loss of cutting edges. The rate of wear was also found to be more apparent in the resinoid bonded wheels. The technique illustrated in this work involves making experimental analysis to predict the outcome of the machined workpiece surface roughness based on the input process parameters. The Taguchi S/N ratio analysis was used to obtain the optimum grinding conditions for lowest grinding forces and surface roughness. The findings show that the process parameters greatly affect the outcome of the grinding experiments. As seen, the surface and subsurface damages are a major limitation of the grinding process. Thus, the cost of grinding the silicon nitride ceramic could be reduced significantly, if the process parameters are chosen using the optimized settings obtained in this work. The prediction model and the optimized values could also be used lower the cost of grinding by determining the force and roughness values prior to experimentation. The efficiency of the grinding of the Si_3N_4 ceramic could be increased, which could in turn lead to its widespread application in various engineering fields. Finally, the validation experiments also indicate that the ANFIS models for the normal grinding force, tangential grinding force and surface roughness have accuracies of 98.45%, 98.58% and 96.31%, respectively

CHAPTER 4: INVESTIGATING THE EFFECTS OF MINIMUM QUANTITY LUBRICATION GRINDING OF SILICON NITRIDE CERAMIC USING SILICON DIOXIDE BASED NANOFLUID

4.1 Introduction

Lubrication methods are a significant part of grinding process. Recently, there is increased need for alternative lubrication techniques in grinding of advanced engineering ceramics. Several findings from previous works indicate that minimum quantity lubrication (MQL) nanolubrication method is a viable option as lubricant in the grinding process. In addition to enhancing tribological properties, the MQL technique was found to be less hazardous and inexpensive. It was also found to be sustainable, eco-friendly and economical. This section entails an experimental investigation of grinding the Si_3N_4 ceramic using MQL with vegetable-oil-based silicon dioxide (SiO_2) nanofluid. The nanofluid was produced by suspending 0.2wt.% to 2wt.% of the nanoparticles in canola oil. In this section, the grinding experiment were conducted using different grinding and MQL parameters based on Taguchi L_{16} design of experiments. The results of the tangential and normal grinding forces, surface quality were analyzed using Taguchi analysis and ANFIS modelling technique. Lastly, the subsurface damages inflicted on the Si_3N_4 ceramic at higher grinding depths was also analyzed.

4.2 Literature Review

Si_3N_4 ceramic is an engineering ceramic which has been extensively used in aerospace, refractory, biomedical and manufacturing industries (Klemm, 2010; Zhang et al., 2012). The extensive utilization of the ceramic is due to its exceptional properties such as high hardness, high wear, temperature and corrosion resistance (Riley, 2000). The high hardness and brittleness of the Si_3N_4 ceramic has been found to be a major setback to its machining, because these properties lead to higher energy expended and poor surface quality.

Grinding with superhard fine abrasives has been the most common and economical method used for machining of advanced engineering ceramics (Malkin et al., 1996). In spite of various findings from previous research works on machining of engineering ceramics, there is still much to understand about the defects, deformations and the energy expended during the grinding operations (Emami et al., 2014; Liu et al., 2017; Xu et al., 1996). Also, the deformations inflicted on the Si_3N_4 ceramic during machining could impact negatively on its performance and applicability (Dambatta et al., 2017; Liu et al., 2017). Thus, it is important to improve on the grinding efficiency and surface quality while grinding of the ceramic.

An established technique of increasing the efficiency and the surface quality during machining involves proper selection of the process parameters (Liu et al., 2017). Previous research works have also shown that whenever lower roughness and cutting forces are desired, an in-depth analysis of the machining parameters is required (Abellan-Nebot et al., 2010; Maher et al., 2015). Similarly, studies have shown that during the grinding of Si_3N_4 ceramic, there is an optimal grinding depth whereby the material removal rate is maximum, and the amount of deformations inflicted on both the grinding wheel and the work material are minimal (Li et al., 2007). This indicates that the process variables significantly affect the responses from the grinding operations. Furthermore, Dambatta et al. (2018) found that the lubrication type and process parameters were among the factors that affect the grinding power, surface integrity and sub-surface damages.

Recently there is increased utilization of the nanofluids in the MQL process. The nanofluids are produced by mixing nanoparticles with eco-friendly fluids. Literatures have shown that the use of MQL nanofluids in grinding operations helps to significantly reduce the grinding forces and improves both the tool life and surface quality (Dambatta et al., 2017; Kuffa et al., 2017). The nanofluids were found to proffer tremendous benefits during machining such as better lubrication/antifriction and heat evacuation (Fratila et al., 2011; Li et al., 2013; Molaie et al., 2016). Additionally, the nanofluids have been found to significantly improve the efficiency of machining processes (Agarwal et al., 2015; Yu et al., 2013). Moreover, the use of MQL (nano-lubricants) was found to cause 25% reduction of normal forces and over 50% reduction in tangential grinding forces (Molaie et al., 2016).

In addition, the nanofluid MQL process which is a sustainable technology, has been found to considerably reduce machining costs (Wang et al., 2016). Studies have shown that the use of the MQL nanofluids in grinding of advanced engineering materials could decrease lubrication costs by about \$184.6 billion yearly. It could also reduce the waste disposal costs by about \$3.8 billion (Holmberg et al., 2013).

Recent studies have indicated that there is increased utilization of the SiO_2 nanoparticles in nanofluids (Ooi et al., 2015; Sayuti et al., 2014). The nanoparticles are very cheap, with high strength and hardness (Sarhan et al., 2012b). From various literatures reviewed, it was found that there are limited studies conducted on optimizing and studying the performance of the SiO_2 nanoparticle during grinding of Si_3N_4 ceramic. To address this concern, this work investigate the effect of the grinding process parameters during the grinding operations. The MQL nanofluid was produced by suspending pure SiO_2 nanoparticles in canola vegetable oil using similar mixing method described by (Sayuti et al., 2014). The canola vegetable oil was selected due to its ability to retain its characteristic high viscosity at high and room temperatures. The results from the grinding experiments were optimized using Taguchi signal to noise (SN) ratio analysis. Finally, we constructed a prediction model of adaptive neuro fuzzy inference system (ANFIS) in other to analyze and predict the effects of process variables parameters on grinding force, surface and subsurface quality.

4.3 Methodology (materials, equipment and experimentation)

The workpiece material used in this study is the sintered Si_3N_4 ceramic. The grinding machine shown in **Figure 4.1** was used to grind the Si_3N_4 ceramic. A resinoid bonded diamond wheel (SD120M100B) was used to perform the grinding experiments. The diamond wheel has a diameter of 200mm, thickness of 5mm and slot diameter of 31.8mm. The diamond wheel was dressed properly before each experimental run (using the Norton's 38A150-I8VBE wheel dresser with machine settings of grinding depth-15μm and feed-5mm/min).

The combination of the SiO_2 nanoparticles and the vegetable oil was thoroughly mixed for 1hr using ultrasonic bath (sonicator). The MQL equipment (WINMIST WT-01) was used to spray the nanolubricant into the grinding zone during the machining process. The Kistler type- 9272 dynamometer was used to obtain the grinding forces via a Kistler charge amplifier (model no.:5019). The amplified force results were then acquired using an oscilloscope. Lastly, the surface and subsurface quality was measured using a surface profilometer and a field emission scanning electron microscope (FESEM).

Figure 4.1: Grinding process set up.

Taguchi method was used to conduct the experimental design. The method has the advantage of producing an experimental design with the minimum amount of experiments (Emami et al., 2013). The parametric factors and their corresponding levels are given in **Table 4.1**. The Taguchi L_{16} (4^4) design of experiment (**Table 4.2**) was developed using Minitab-17 software. The MQL nozzle stand-off distance and nozzle horizontal angle were kept at 55mm and 22º, respectively, as obtained by (Molaie et al., 2016). In addition, the nozzle exit diameter was 2mm and the lubricant flow rate was kept constant at 150ml/h.

Each experiment was repeated three times in order to achieve high accuracy. Thereafter, the average grinding force for each experimental run was recorded after 10 grinding passes. Also, the roughness of the Si_3N_4 ceramic after each experiment was measured using a profilometer in parallel direction to the grinding directions at 0.8mm cut-off values.

Table 4.1: Experimental variables and levels

Symbol	Parameter	Level			
		1	2	3	4
A	MQL nanoparticle concentration (%)	0	0.5	1	2
B	Extrusion pressure (MPa)	0.2	0.4	0.6	0.8
C	Grinding depth (μm)	10	20	30	40
D	Table speed (m/min)	10	15	18	23

Table 4.2: Taguchi experimental design

S/N	A	B	C	D
1	1	1	1	1
2	1	2	2	2
3	1	3	3	3
4	1	4	4	4
5	2	1	2	3
6	2	2	1	4
7	2	3	4	1
8	2	4	3	2
9	3	1	3	4
10	3	2	4	3
11	3	3	1	2

Table 4.2, Continued

S/N	A	B	C	D
12	3	4	2	1
13	4	1	4	2
14	4	2	3	1
15	4	3	2	4
16	4	4	1	3

4.4 Results

Taguchi's SN ratio analysis was used to obtain the optimal parameter settings for the process variables. The SN ratio, which is the ratio of the desired to undesired data, was used to indicate the characteristics of the analyzed data. To optimize the machining process, the grinding forces and roughness should be minimum. As such, the smaller-the-better analysis was used in this work, as done by (Emami et al., 2014). The results of the calculated SN ratios for the response parameters (i.e. tangential grinding force-F_t, normal grinding force-F_n and surface roughness-R_a) are provided in **Table 4.3**. The performance of nanofluid concentration was studied extensively.

The main effect plots of SN ratio for the F_n, F_t and R_a are given in **Figure. 4.2, 4.3 and 4.4**, respectively. As shown in **Figure 4.2**, based on the SN ratio, the optimum grinding process parameters for the F_t were found to be: 1% nanoparticle concentration (level 3), 0.8MPa extrusion pressure (level 4), 10µm grinding depth (level 1) and 15m/min table speed (level 2). Furthermore, as shown in **Figure 4.3**, the optimum parameters for F_n were found to be: 2% nanoparticle concentration (level 4), 0.2MPa Air pressure (level 1), 10µm grinding depth (level 1) and 10m/min table speed (level 1). Lastly, as shown in **Figure 4.4**, the optimum parameters for the R_a were found to be 2% nanoparticle concentration (level 4), 0.8MPa Air pressure (level 4), 10µm grinding depth (level 1) and 10m/min table speed (level 1)

Table 4.3: Experimental results.

Exp. No	F_t (N)	SN ratio for F_t	F_n (N)	SN ratio for F_n	R_a (µm)	SN ratio for R_a
1	28.00	-28.94	36.62	-31.13	0.51	5.85
2	40.21	-32.04	52.43	-34.32	0.64	3.88
3	54.16	-34.65	86.28	-38.69	0.88	1.11
4	68.33	-36.65	112.09	-40.98	0.91	0.82
5	38.42	-31.60	49.15	-33.80	0.74	2.62
6	41.02	-32.26	67.21	-36.52	0.82	1.73
7	64.11	-36.12	70.37	-36.90	0.59	4.58
8	48.30	-33.63	75.04	-37.50	0.6	4.44
9	46.00	-33.26	70.30	-36.90	0.77	2.27
10	54.15	-34.65	68.81	-36.65	0.72	2.85
11	22.28	-26.85	48.42	-33.63	0.52	5.68
12	30.46	-29.54	37.07	-31.34	0.44	7.13
13	48.20	-33.63	65.52	-36.26	0.41	7.74
14	40.00	-32.04	41.11	-32.04	0.37	8.64
15	36.32	-31.13	44.06	-32.87	0.61	4.29
16	28.44	-28.94	32.25	-30.10	0.41	7.74

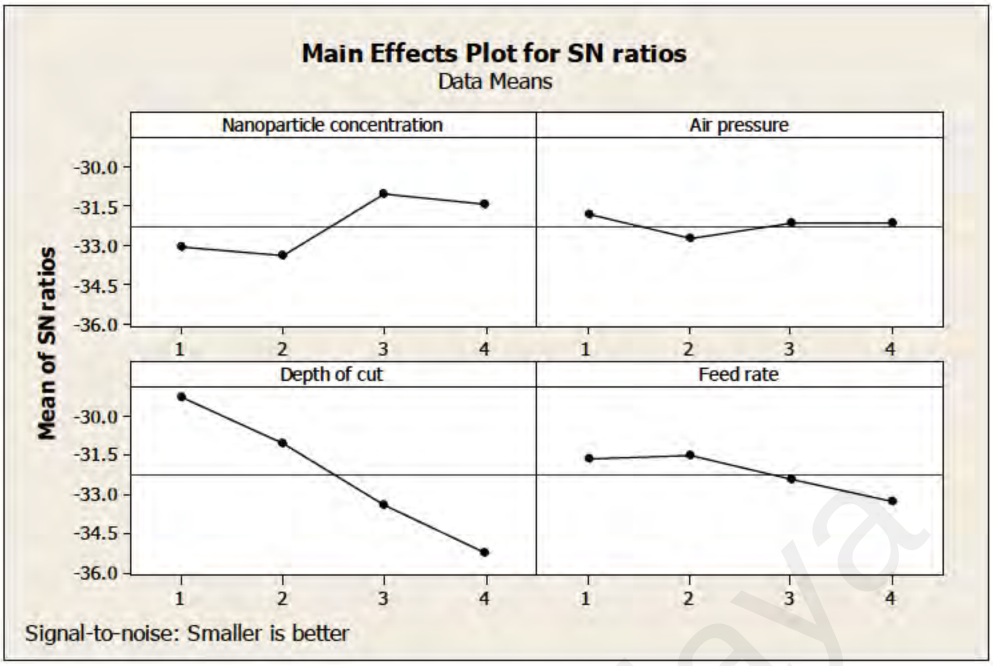

Figure 4.2: Effect of process variables on the force F_t.

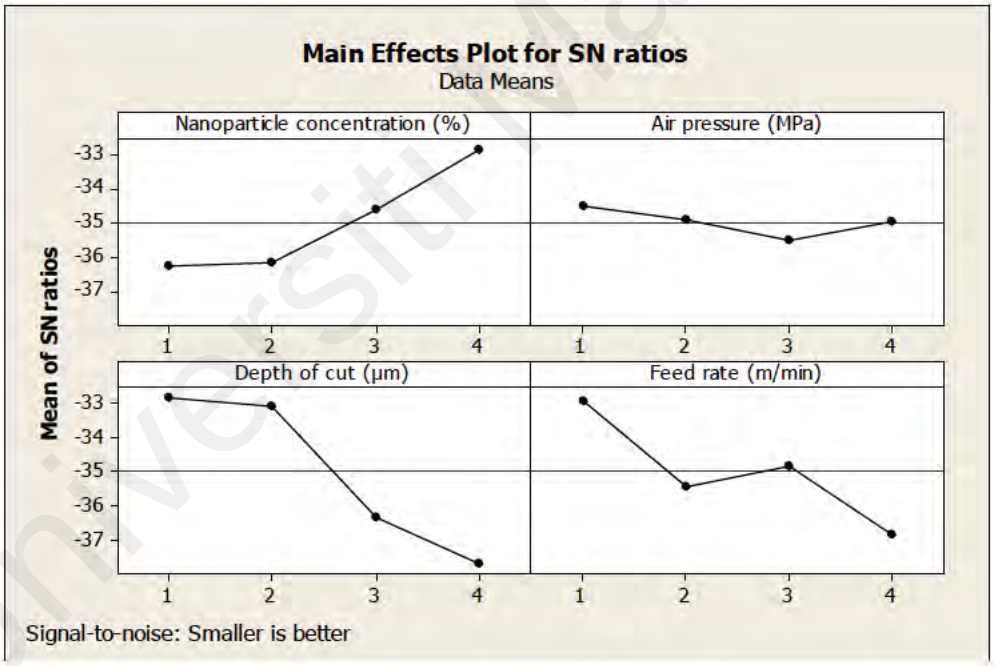

Figure 4.3: Effect of process variables on the force F_n.

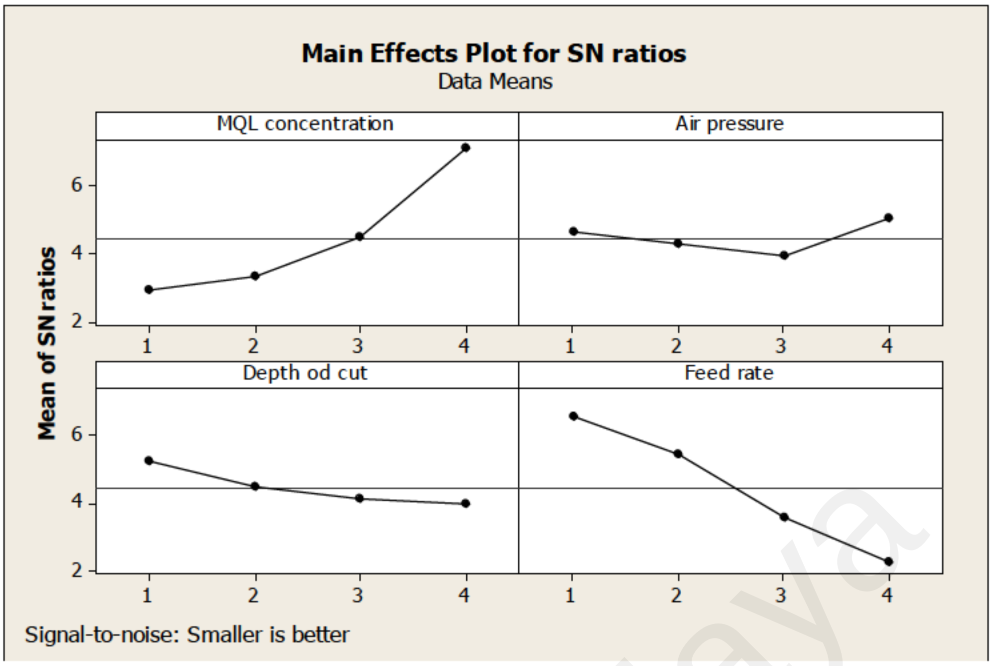

Figure 4.4: Effect of process variables on R_a.

4.4.1 Taguchi analysis of response parameters

The Taguchi analyzed results for F_n and F_t are shown in **Tables 4.4 and 4.5**, respectively. The results from **Table 4.4** show that the grinding depth exhibit the greatest influence on the F_t, followed by nanoparticle concentration, then the table speed. The results also show that the air pressure has the least influence. A similar trend was observed for the force F_n, as shown in **Table 4.5**. Generally, the hierarchy of influence of the process parameters on the grinding forces is: grinding depth > nanoparticle concentration> table speed > air pressure. The result of R_a for each experiments is given in **Table 4.6**. Moreover, as shown in the ranking from **Table 4.6**, the hierarchy of influence of the process parameters on the R_a is table speed >nanoparticle concentration> grinding depth > air pressure.

Table 4.4: Results of table of means from Taguchi analysis for F_t.

Level	**A**	**B**	**C**	**D**
1	-33.07	-31.85	-29.25	-31.66
2	-33.40	-32.75	-31.08	-31.53
3	-31.07	-32.19	-33.39	-32.46
4	-31.43	-32.19	-35.26	-33.32
Delta	2.33	0.89	6.01	1.79
Rank	2	4	1	3

Table 4.5: Results of table of means from Taguchi analysis for F_n.

Level	**A**	**B**	**C**	**D**
1	-36.28	-34.52	-32.84	-32.91
2	-36.18	-34.94	-33.09	-35.43
3	-34.64	-35.52	-36.34	-34.81
4	-32.87	-34.99	-37.70	-36.82
Delta	3.41	1.00	4.85	3.91
Rank	3	4	1	2

Table 4.6: Results of table of means from Taguchi analysis for R_a.

Level	**A**	**B**	**C**	**D**
1	2.914	4.620	5.249	6.550
2	3.340	4.272	4.479	5.434
3	4.484	3.917	4.113	3.581
4	7.105	5.033	4.000	2.277
Delta	4.191	1.116	1.249	4.273
Rank	2	4	3	1

4.4.2 ANFIS Modelling

Fuzzy logic was first introduced by (Zadeh, 1996) as a mathematical representation of data sets containing different solutions. Contrary to conventional mathematical theories whereby data sets are subsets of one larger system or another, in fuzzy logic the data sets are defined by linguistic variables instead of numeric numbers. Also, the fuzzy logic uses the fuzzy inference system (FIS) to express linguistic terms (Kar et al., 2014). ANFIS modelling was first proposed by (Jang, 1993). It was previously referred to as Takagi-Sugeno-Kang (TSK) system, and involves merging the learning and adaptive capabilities of the artificial neural network (ANN) with the linguistic expressions of fuzzy inference system (Lin, 1996). Moreover, the ANFIS consists of graphical representation of the FIS consisting of ''if-then'' rules. Prediction models for cutting forces and roughness are also being developed using artificial intelligent (AI) techniques (Chandrasekaran et al., 2010). The AI techniques have been used when there is no established certainty or linear relationships between input and output variables (Zalnezhad et al., 2013). The ANFIS is one of the artificial intelligent methods used to predict and relate between input and output responses (Asiltürk et al., 2012; Baseri, 2011; Kumanan et al., 2008). The architecture of the developed ANFIS model consists of five layered feed forward neural network as shown in **Figure 4.5**. The layer of the developed ANFIS model is made up of different nodes which are described as follows;

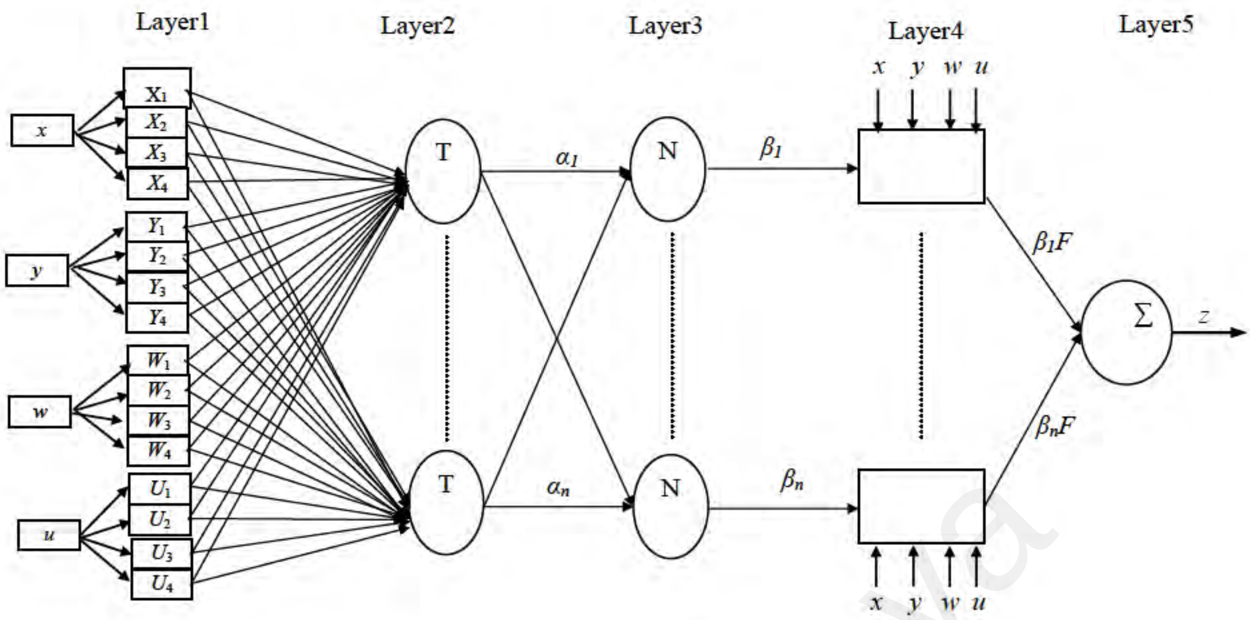

Figure 4.5: Architecture of ANFIS model.

Layer 1

This layer consists of several nodes in which input variables are fuzzified. The generalized bell membership function was chosen to relate the linguistic variables. The mathematical relationship between the membership function and the input parameters are given in **Equation 4.1, 4.2, 4.3 and 4.4**. Also, the MF Ai, Bi, Ci, and Di are referred to as the principle learning parameters.

$$X_i(x) = \exp\left[-0.5\left(\frac{x-a_{i1}}{b_{i1}}\right)^2\right] \tag{4.1}$$

$$Y_i(y) = \exp\left[-0.5\left(\frac{y-a_{i2}}{b_{i2}}\right)^2\right] \tag{4.2}$$

$$W_i(w) = \exp\left[-0.5\left(\frac{w-a_{i3}}{b_{i3}}\right)^2\right] \tag{4.3}$$

$$U_i(u) = \exp\left[-0.5\left(\frac{u-a_{i4}}{b_{i4}}\right)^2\right] \tag{4.4}$$

Where ai_1, ai_2, ai_3, ai_4, bi_1, bi_2, bi_3 and bi_4 are the input variables.

Layer 2

In the second layer of the ANFIS model, the knowledge base of the fuzzy set is established. Here, the weights of each term in the nodes is calculated according to the established rules. The output in the neurons is given by **Equation 4.5-4.7**.

$$\alpha_1 = X_1\,(x) \times Y_1\,(y) \times W_1\,(w) \times U_1\,(u) \tag{4.5}$$

$$\alpha_2 = X_2\,(x) \times Y_2\,(y) \times W_2\,(w) \times U_2\,(u) \tag{4.6}$$

. . . . .

. . . . .

$$\alpha_n = X_n\,(x) \times Y_n\,(y) \times W_n\,(w) \times U_n\,(u) \tag{4.7}$$

Layer 3

The 3rd layer is the region where the fuzzy rules are developed. The individual nodes are normalized (N) using the weights from the previous layer. **Equation 4.8-4.11** represent the variables in the neurons.

$$\beta_1 = \frac{\alpha_1}{\alpha_1+\alpha_2+\alpha_3+\alpha_4} \tag{4.8}$$

$$\beta_2 = \frac{\alpha_2}{\alpha_1+\alpha_2+\alpha_1+\alpha_2} \tag{4.9}$$

$$\beta_3 = \frac{\alpha_3}{\alpha_1+\alpha_2+\alpha_3+\alpha_4} \tag{4.10}$$

$$\beta_4 = \frac{\alpha_4}{\alpha_1+\alpha_2+\alpha_3+\alpha_4} \tag{4.11}$$

Layer 4

This is the region where the decision making is conducted. The response in this region is calculated by multiplying the normalized weights with the rules of the fuzzy. The output of the fourth layer is shown in **Equation 4.1** to **4.14**.

$\beta_1 z_1 = \beta_1 (a_1 x + b_1 y + c_1 w + d_1 u)$ (4.12)

$\beta_2 z_2 = \beta_2 (a_2 x + b_2 y + c_1 w + d_2 u)$ (4.13)

. . .

. . .

$\beta_n z_n = \beta_n (a_n x + b_n y + c_n w + d_n u)$ (4.14)

Layer 5

In this layer, the ANFIS model utilises the rules and linguistic variables to represent each input variable. It is made up of one node only, which is obtained by de-fuzzifying the calculated variables. The mathematical representation of the fifth layer of the ANFIS model is shown in **Equation 4.15**.

$$Z = \beta_1 z_1 + \beta_2 z_2 + \beta_3 z_3 + \beta_4 z_4 \quad (4.15)$$

The experimental results were used as the training variables for the ANFIS model on MATLAB (R2015a) software. Sixteen set of rules were used to develop the ANFIS model, and the model was trained using 100 epochs. The ANFIS model consist of 16 linear parameters and 48 nonlinear parameters. The final structure of the developed ANFIS model is presented in **Figure 4.6**.

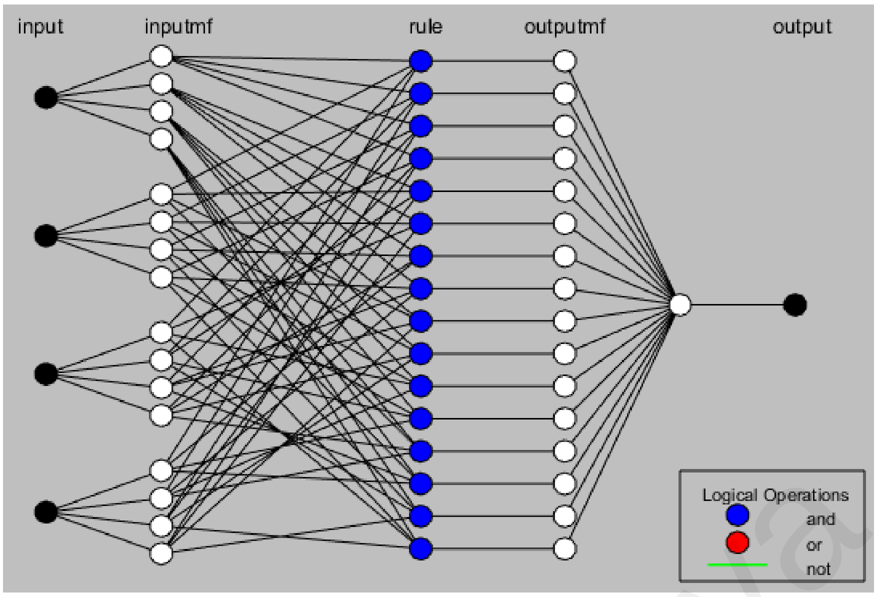

Figure 4.6: Structure of ANFIS Model from Matlab.

Lastly, the developed models for F_n, F_t and R_a was found to have epoch errors of 6.196 × 10^{-5}, 4.4619 × 10^{-5} and 6.4332 × 10^{-7} respectively.

4.4.2.1 Validation of ANFIS Model

In this section, confirmation tests were done in order to compare the experimentally obtained values and the ANFIS predicted ones. **Table 4.7** gives the experimental and predicted values of the grinding force and surface quality for different parameter settings. Comparison of the results indicates that the ANFIS model was capable of accurately predicting the grinding force and the R_a. **Figure 4.7** illustrates a comparison between the measured values and the predicted ones for each of the validation experiment runs. Furthermore, the accuracy of the ANFIS model (A), defined as the mean of all the average accuracies, was obtained using **Equation 4.16**. It was found to be 98.1%, 97.82%, and 96.4% for the F_t, F_n and R_a models, respectively.

$$\text{Accuracy A} = \frac{1}{n}\sum_{i=1}^{n}\left(1 - \frac{|N_{exp.} - N_{pred.}|}{N_{exp.}}\right) \times 100\% \tag{4.16}$$

Where n= total number of experimental runs, $N_{exp.}$ =experimentally measured values, $N_{pred.}$ =ANFIS predicted values.

Table 4.7: Settings and results for verification of the ANFIS model.

Exp. no.	A	B	C	D	F_t (N) Exp.	F_t (N) Pred.	F_n (N) Exp.	F_n (N) Pred.	R_a (µm) Exp.	R_a (µm) Pred.
1	1	1	1	2	29.00	28.40	37.12	36.50	0.462	0.514
2	1	2	1	2	40.30	39.70	52.50	51.60	0.608	0.636
3	1	3	1	1	28.08	28.30	36.27	37.00	0.522	0.514
4	1	4	2	2	45.36	43.80	64.31	63.40	0.706	0.622
5	2	1	2	2	38.02	38.10	48.16	49.10	0.744	0.737
6	2	1	1	3	40.22	38.10	50.00	49.60	0.758	0.742
7	2	2	4	2	60.14	58.40	70.62	69.40	0.663	0.651
8	2	3	3	2	50.27	48.70	76.05	75.20	0.612	0.608
9	3	3	1	1	22.60	22.20	47.14	47.70	0.526	0.518
10	3	1	3	2	48.37	46.90	60.33	58.20	0.588	0.601
11	3	2	2	2	32.88	32.10	51.52	50.00	0.592	0.581
12	3	4	1	3	28.30	27.80	36.08	34.00	0.420	0.413
13	4	3	3	1	41.15	40.00	42.21	40.00	0.404	0.37
14	4	4	3	3	30.28	28.90	34.44	33.70	0.433	0.423
15	4	2	2	1	40.01	40.00	38.64	40.00	0.368	0.37
16	4	4	1	1	30.00	28.80	35.00	34.60	0.410	0.426

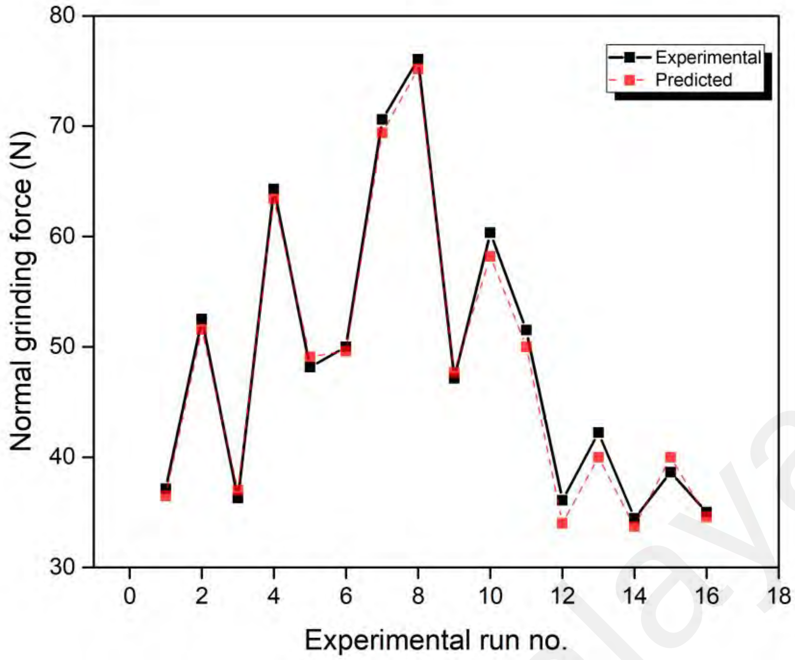

Experimental
Predicted
Normal grinding force (N)
Experimental run no.

(a)

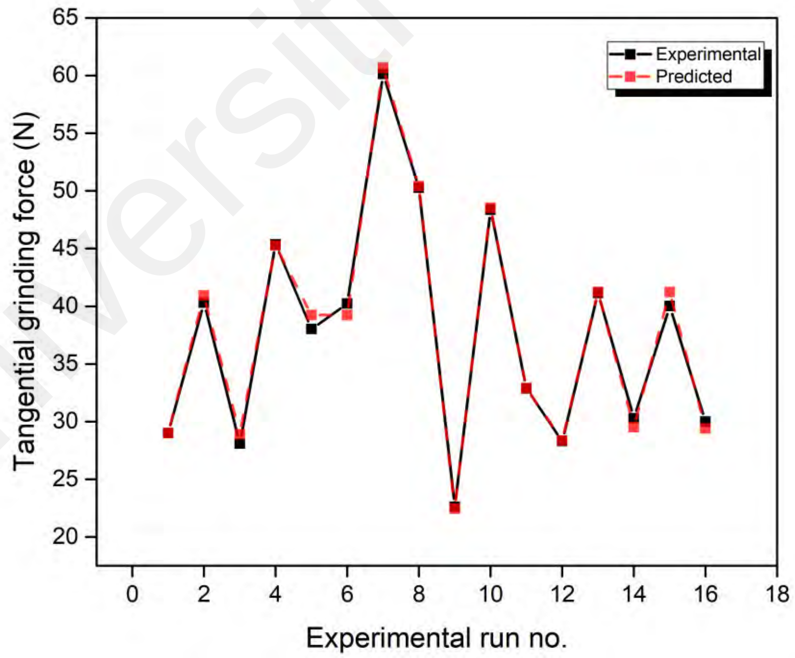

Experimental
Predicted
Tangential grinding force (N)
Experimental run no.

(b)

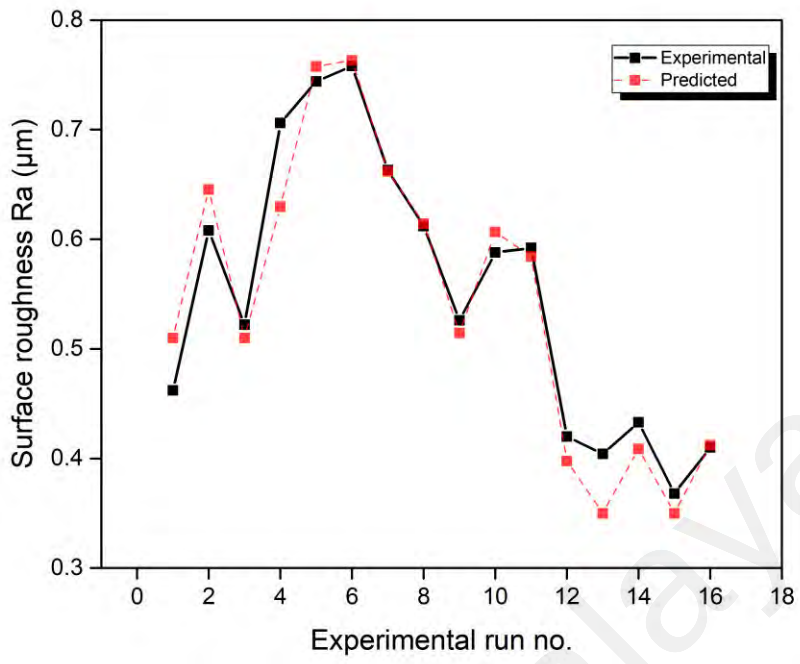

(c)

Figure 4.7: Experimentally measured vs ANFIS predicted values: (a) F_n, (b) F_t, and (c) R_a.

4.5 Discussions

The experiments were performed according to the design of experiment. The optimum parameter settings have been obtained using the SN ratio analysis. In this section, the ANFIS prediction models developed on MATLAB were used to analyze the variation of the output parameters with the input parameters. The ANFIS prediction model tends to adjust the membership functions according to the linguistic rules. The following sections explain the variation of the process variables with each response variable.

4.5.1 Tangential grinding force

The force F_t is the main force which is associated with material removal (by ploughing and rubbing). The type of lubricant employed significantly affects the magnitude of F_t (Rowe, 2013). Hence, the MQL nano-lubrication technique is expected to significantly reduce F_t, especially at low grinding depths. This is in agreement with the findings of authors (Dambatta et al., 2017; Molaie et al., 2016). The analyzed results of the ANFIS model shown in **Figure 4.8** show the variation between the process variables and F_t. From **Figure 4.8a**, it was found that the F_t is inversely proportional to the percentage concentration of nanoparticles. Thus, a higher amount of nano particle concentration can increase the efficiency of the grinding process by reducing F_t. This is because the F_t is directly involved with the power consumed during material removal. Also, it could be seen that the grinding depth varies directly with F_t, whereby the result shows a 30% increase of the F_t from grinding depth 10μm to 40μm. Similarly, the results indicate that at high depths of cut, the F_t was very high irrespective of the kind of the nanofluid used. As can be seen from **Figure 4.8b**, the air pressure has an inverse relation with the F_t. Lastly, the table speed was found to exhibit a direct relationship with F_t at smaller grinding depths, as shown in **Figure 4.8c**. But, at high grinding depths, an increase in the table speed has little influence on F_t.

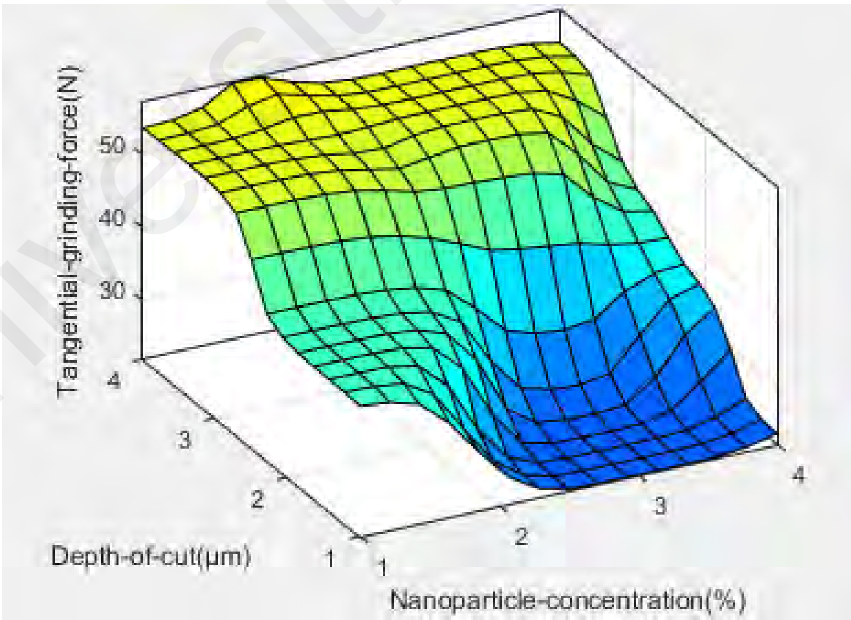

(a)

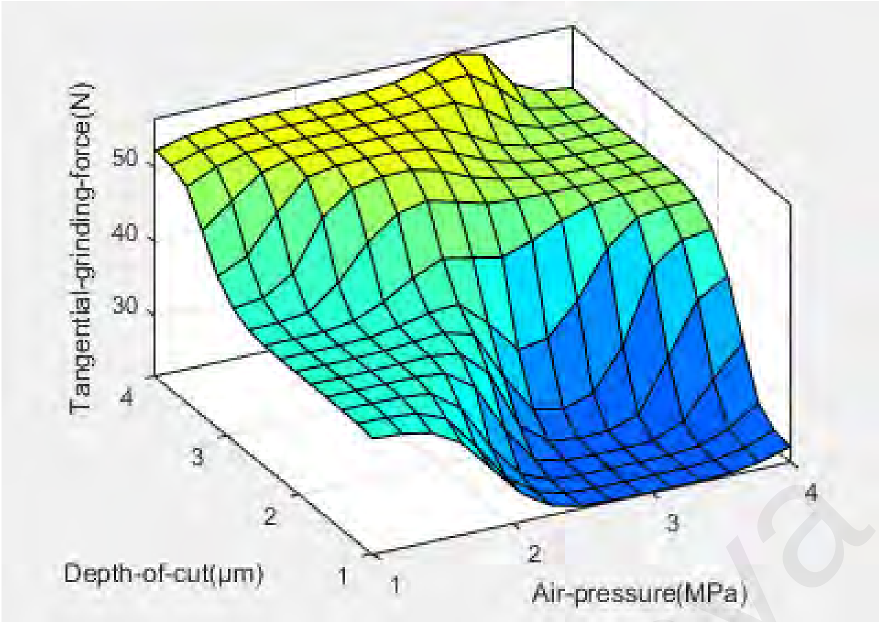

(b)

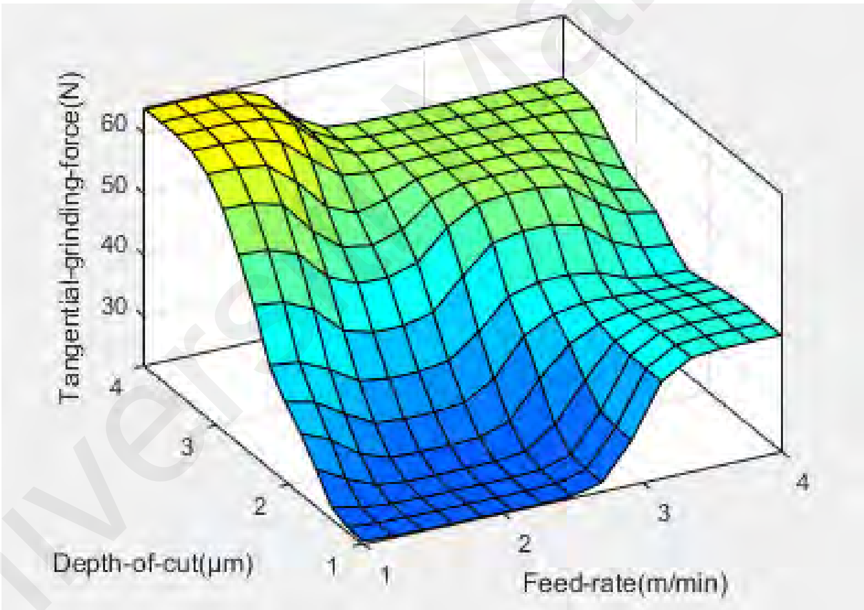

(c)

Figure 4.8: Variation of process parameters with F_t: (a) grinding depth (µm) vs nanoparticle concentration (%) (b) grinding depth (µm) vs air pressure (MPa) (c) grinding depth (µm) vs table speed (m/min).

4.5.2 Normal force

According to **Figure 4.9a**, the table speed and nanoparticle concentration have significant effects on the F_n. It is observed that the force F_n decreases with increase in the nanofluid concentration. An increase in the nanoparticle concentration from level 1 (0%) to level 4 (2%) led to significant reduction of the F_n (about 40%). The performance was similar to that of Molybdenum disulphide based nanofluid reported by (Molaie et al., 2016). Thus, the use of high concentration of the SiO_2 nanofluid during grinding of the Si_3N_4 ceramic is highly recommended. The grinding depth was also found to exhibit a directly proportional relationship with F_n. However, as can be seen in **Figure 4.9b**, the air pressure has negligible effect on F_n. Hence, in other to obtain a lower F_n, smaller grinding depth and table speed should be used in the grinding operations.

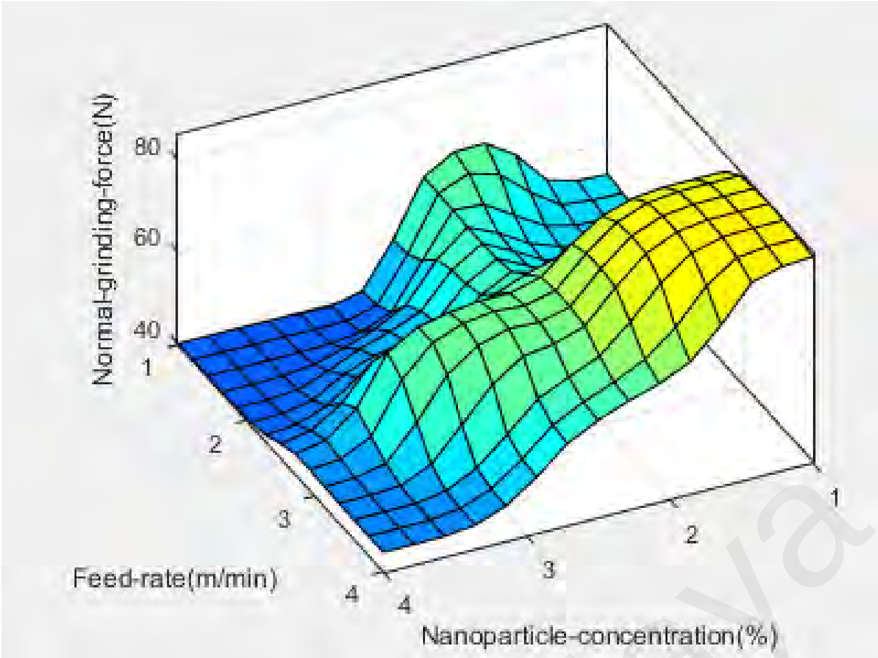

(a)

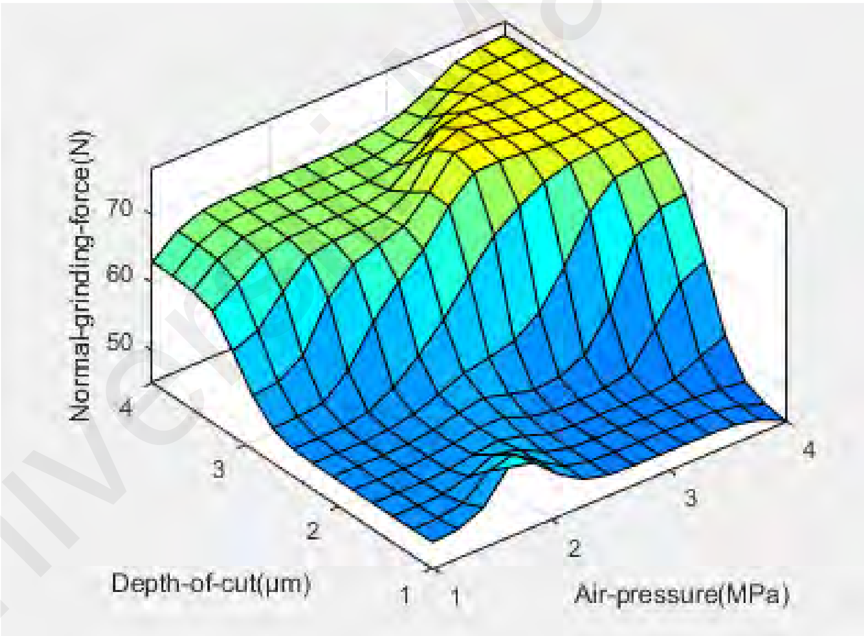

(b)

Figure 4.9: Variation of process parameters with F_n : (a) Table speed vs nanoparticle concentration (%), (b) grinding depth (μm) vs air pressure (MPa).

4.5.3 Surface Quality

From **Figure 4.10a**, it can be seen that R_a has an inverse relationship with the nanoparticle concentration, and a linear variation with the table speed. The results at 10m/min table speed show that when the nanoparticle concentration was increased from 0% to 2%, the R_a decreases by 28%. At higher table speed (i.e. 23m/min), the R_a was also found to reduce by 32% with increase in nanofluid concentration from 0% to 2%. This shows that the use of nanofluid significantly improves the surface quality of the machined ceramic workpiece. Similarly, in **Figure 4.10b**, the air pressure was found to have an inverse relationship with the R_a. This shows that higher air pressure produces better delivery of the nanofluid into the grinding zone, thereby enhancing the lubrication effect. When the air pressure was low i.e. 0.2MPa, the surface was generally poor. However, as the air pressure was increased to 0.8MPa, the R_a of the machined part was lower at low grinding depths.

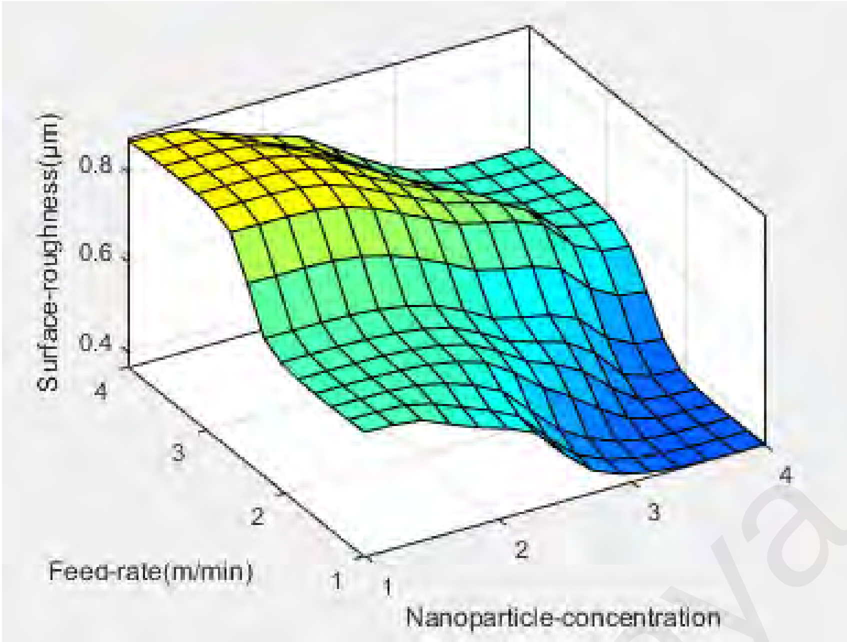

(a)

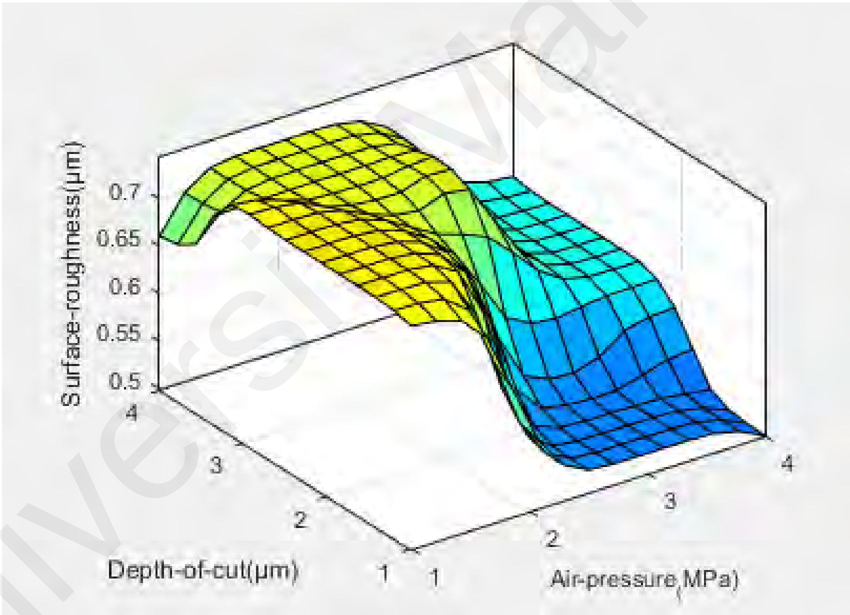

(b)

Figure 4.10: Variation of process parameters with R_a : (a) table speed (m/min) vs nanoparticle concentration (%) (b) grinding depth (μm) vs air pressure (MPa).

4.5.4 Analysis of surface morphology

Studies have indicated that the SiO_2 nanofluids have excellent lubrication capability, with good anti-friction (Dambatta et al., 2018) and heat evacuation abilities (Sayuti et al., 2014). The surface morphology is also an essential index of qualitatively evaluating the surface quality of the machined parts. FESEM images after each experimental run are shown in **Figure 4.11**. The results from the qualitative analysis corroborates the measured R_a. Different nanofluid concentrations were found to give different kinds of surface and subsurface damages (SSD). Since the Taguchi analysis indicates that the R_a is most affected by the table speed and then followed by the nanoparticle concentrations. It is imperative to make comparisons between the experimental runs based on the input parameters. Thus, from the experimental results, it could be seen that the 2% nanofluid concentration has the lowest roughness values, and smallest SSD. Furthermore, the acquired images shown in **Figure 4.11** demonstrates that nanoparticles can effectively lower the friction by effective lubrication actions, thereby improving the workpiece surface quality. The micrographs from experimental runs 3 & 4, indicates that the surface quality obtained in these experimental runs is very poor. The samples were found to contain intense grinding marks, macro/micro cracks, intermittent furrows, and discontinuity in the grinding path. The specimens from experimental runs 14 and 16, clearly shows that higher amount of nanoparticles in the nanofluid coupled with low table speed and grinding depth, produces an almost defect-free surface. However, in experimental runs 3, 4 and 6, the surface quality were found to be very poor, characterized by high surface deformation and surface cracks. This observation results from the high grinding depth and table speed used in the experiments. Moreover, it was also found that, as the table speed was increased from 10m/min to 23m/min, the surface deformations and damages were seen to increase significantly. Also, although the table speed in experimental runs 9 & 15 have similar table speed and grinding depths, their respective R_a values of 0.77 and 0.61 shows that the increasing the nanoparticle concentrations helps to greatly reduce the R_a. The same result is evidently shown in the micrographs shown in experimental runs 9 and 15. Generally, it could be concluded that, the grinding experiments should be conducted using low table speed, high concentration of nanofluid, low grinding depth, and high air pressure.

Additionally, it was found that the SSD and lateral cracks were found to become more prominent at the grinding depths of 40μm. The median and lateral cracks were found to occur beneath the ground surfaces as illustrated in **Figure 4.12**. From the micrographs, it can be seen that there is intense formation SSD when the MQL nanofluid concentration was 0%. However, an increase in the nanoparticle concentration indicates that the SSD decreases significantly. At 0% nanoparticle concentration, the length of SSD's were found to be between 258-265μm in experimental run-4 (see **Figure 4.12a**). However, the SSD were seen to decrease to 65μm-102μm at 2% nanoparticle concentration as seen in experimental run 15 (see **Figure 4.12d**).

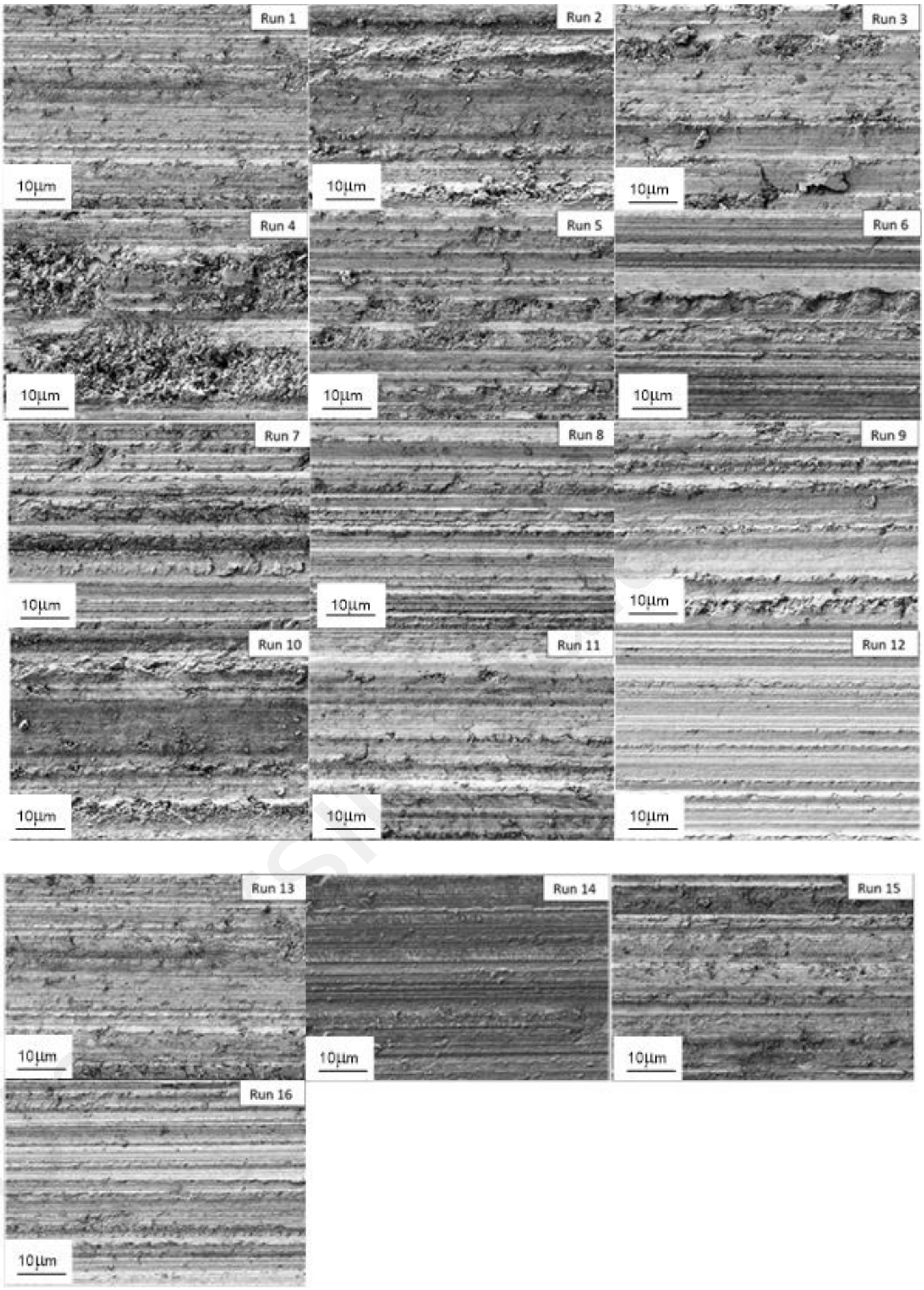

Figure 4.11: Surface morphology of each experiment run as obtained using FESEM.

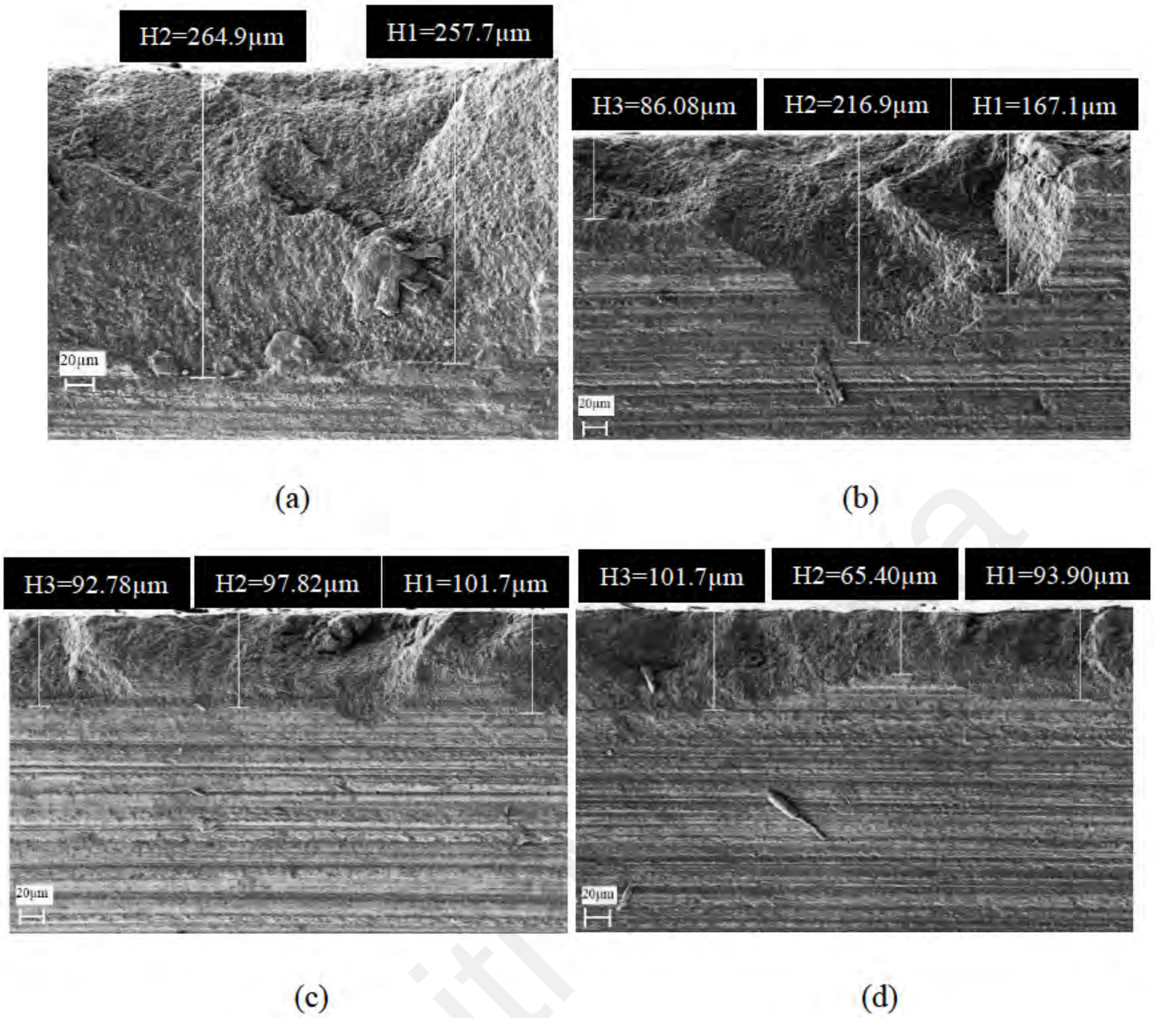

Figure 4.12: Micrographs of machined specimen SSD in experiment (a) 4 (b) 7 (c) 10 (d) 15.

4.6 Summary

This study involve investigating the performance of process variables on the forces and surface quality during MQL grinding of Si_3N_4 ceramic. The experimental settings were optimized using Taguchi signal to ratio analysis on Minitab software. In addition, ANFIS modelling was used to analyze and predict the grinding forces and R_a using process variables such as nanofluid concentration, nozzle extrusion pressure (air pressure), grinding depth and table speed. Finally, the following conclusions could be drawn;

a) The optimum process variables for F_n were found to be 2% nanofluid concentration, 0.2MPa Air pressure, 10µm grinding depth and 10m/min table speed. Moreover, the optimum process variables for F_t was obtained as 1% nanoparticle concentration, 0.8MPa Air pressure, 10µm grinding depth and 15m/min table speed. Also, the optimum process variables for R_a was found to be 2% nanoparticle concentration, 0.8MPa Air pressure, 10µm grinding depth and 10m/min table speed.

b) The accuracy of the developed ANFIS model for F_n, F_t and R_a was found to be 97.82%, 98.1% and 96.4% respectively.

c) The use of SiO_2 nanofluid in the MQL provides reduced friction via generation of tribofilm around the contact region. Higher nanofluid concentration was found to significantly decrease the grinding forces and surface roughness. Also, the surface deformations such as microcracks, furrows, SSD's were observed to decrease significantly when high nanofluid concentration was used in the MQL process.

d) Lastly, analysis of SSD's at 40µm grinding depth shows that, the SSD's was between 258µm-265µm at 0% nanoparticle concentration and reduces to between 65µm-102µm at 2% nanoparticle concentration.

CHAPTER 5: INVESTIGATING THE EFFECTS OF ULTRASONIC ASSISTED GRINDING ON Si_3N_4 CERAMIC WITH MINIMUM QUANTITY NANOLUBRICATION USING SiO_2-BASED NANOFLUIDS.

5.1 Introduction

The Minimum Quantity Lubrication (MQL) is recently gaining prominence in grinding operations due to its high performance, eco-friendliness and economic benefits. The MQL technique has been found to proffer higher performance than the conventional flood cooling as a lubrication system for grinding of ceramics. Recently, there has been increased use of nanofluids in the MQL technique. The nanofluids were found to have excellent lubricity and heat evacuation capability, thereby eradicating the main limitation of the MQL process. In addition, the surface quality and energy expended during grinding operations were found to improve significantly with the use of MQL nanofluid. Moreover, the properties of the base oil used to produce the nanofluids also significantly affects the outcome of the grinding experiments. Hence, it is necessary to investigate the performance of the different oils. Previous studies have indicated that ultrasonic assisted grinding (UAG) also helps to significantly improve the performance of the grinding process. In this section, we have presented an experimental analysis to study the effect of applying ultrasonication and MQL with SiO_2-based nanofluid. The performance of the grinding process was measured in terms of tangential, normal grinding forces and surface quality. The results obtained show that both the UAG and nanofluid MQL process helps to considerably reduce the grinding forces. However, the UAG process was found to slightly decrease the surface quality when flood cooling lubrication technique was used. The surface quality of the machined parts was seen to improve significantly, when higher concentrations of the nanofluid was used. Lastly, the canola oil was found to give the optimum performance.

5.2 Literature Review

Ceramic materials (such as Al_2O_3, ZrO_2, SiC and Si_3N_4) are popular in several manufacturing industries because of their superior properties. Superb corrosion resistance, high wear resistance, heat resistance and chemical resistance characterize the ceramic materials. However, their extensive application suffers huge setbacks as result of the high cost of machining and defects inflicted on the ceramic materials during the machining process. Hence, it is imperative to develop a cheaper method of machining the ceramic materials (Emami et al., 2013).

Conventional grinding (CG) is among the most utilized techniques for processing ceramic materials. However, due to the very brittle and hard nature of the ceramic materials, the energy consumed during the machining have been found to be very high. In addition, the machining process is characterized by high tool wear and poor surface quality. As such, it is inevitable to conduct further research towards the improvement of the ceramics grinding (Inasaki et al., 1986; Shih et al., 2000). Similarly, previous studies on grinding of ceramics materials have shown that high speed grinding is an appropriate method of machining ceramic materials (Inasaki et al., 1986). The CG of ceramics involves the abrasion process whereby the grinding wheel removes materials from the ceramic at specific depths and speed using the crack propagation technique. However, during the machining process, not all the grits on the wheel participate in the material removal process, most of the grains only performs rubbing and ploughing actions, thereby increasing the grinding power (Tawakoli et al., 2010). This causes great reduction in the grinding efficiency due to loss of energy in form of heat (Marinescu, 2006).

Previous research works have shown that applying high frequency oscillations (above 16kHz) onto the workpiece material during the grinding operation helps to significantly reduce the grinding forces, energy expended and improves the surface quality.

The process of applying the lateral ultrasonic vibrations onto the workpiece material during grinding operations is called the UAG. Most of the previous findings on studies of the UAG process found that the ultrasonication helps to improve the surface quality by about ~20% and reduce the grinding forces by about ~30-70% (Dambatta et al., 2017; Molaie et al., 2016). The UAG process has been found to enhance grinding of both ductile and brittle materials. It has been reported that the UAG helps to reduce tool wear, material removal rate, and higher number active diamond grits in grinding region (Emami et al., 2013; Molaie et al., 2016; Nik et al., 2012; Nomura et al., 2009).

Lubricants are often utilised in the grinding process to flush off the debris, evacuate heat from the grinding zone and to significantly reduce friction (Dambatta et al., 2017; Mao et al., 2012). The conventional flood coolants are the most popular kind of lubricants used during grinding operations. This is because they are associated with many advantages such as good lubricity, wheel cleaning ability, cooling and reduction of wear.

Despite the various benefit associated with conventional flood cooling process, studies have indicated that the fluids are hazardous to both the environment and the machinists. In fact, it is reported that about 80% of human disease infection on machinists arise from the direct contact with the grinding fluids (Dambatta et al., 2018). Moreover, the lubricants have been shown to account for about 20% of total manufacturing cost (Kalita, Malshe, & Rajurkar, 2012). As such, in other to improve the grinding process, it is vital to introduce a lubrication system that is less hazardous and also economical.

Accordingly, researchers proposed some eco-friendly methods such as dry grinding and minimum quantity lubrication (MQL) and the use of nanofluids in the MQL process (Sinha et al., 2017). The dry grinding process was found to significantly reduce lubrication costs. However, the dry grinding method is associated with excessive deterioration of the grinding wheels and poor workpiece surface integrity. Most findings indicate that the dry grinding method is characterized by poor lubrication, surface and subsurface damages (Rao, 2007). Recent research reports have shown that the setbacks found in the dry grinding process could be overcome using the MQL nanolubrication technique.

The MQL nanolubrication method utilizes nanofluid in the MQL process which is supplied into the grinding zone at flow rates between ~10 to 100 ml/h. Droplets of the nanofluid are sprayed at pressures between ~4.0 to 6.5 bar (Tawakoli, T et al., 2009). Also, the MQL process is environmentally friendly and helps to decrease consumption of grinding fluids by 1000 times, with subsequent increase in the grinding efficiency and enhancement wheel life (Kalita, Malshe, & Rajurkar, 2012). Emami et al. (2014) reported that the MQL process helps to increase lubrication during CG which leads to effective decrease of the grinding energy and wears on the grinding wheel. However, there have been some reports of deterioration in the surface roughness (at high grinding depths) of MQL machined parts (da Silva et al., 2007; Dambatta et al., 2018).

The hybridization of MQL technique and UAG process was found to be an alternative technique to machine superhard materials (Emami et al., 2014; Molaie et al., 2016). Studies have shown that during UAG, the ultrasonic vibrations are applied either on the work piece or wheel (Dambatta et al., 2017; Molaie et al., 2016; Park et al., 2013).

Different kinds of nanoparticles are being used to form oil-based nanofluids for the MQL process. The nanoparticles often utilised include SiO_2, MoS_2, graphene, Al_2O_3, diamond, carbon nanotube (CNT), etc. compared to the other nanoparticles, the SiO_2 was found to be inexpensive and possess very good lubrication and tribological behaviors (Dambatta et al., 2018; Rabiei et al., 2017; Sarhan et al., 2012a). In addition, the properties of the base oils used for the nanofluid also have significant effect on the outcome of the machining operations. The viscosity, functional groups present, flash and smoke points of the oil also has significant effect on the performance of the nanofluid during lubrication (Zhang et al., 2015).

In this section, we have conducted experimental investigation on the effect of different concentrations of SiO_2 based nanofluid (produced using different vegetable oil types) during CG and UAG processes. Finally, The performance of the grinding process was analyzed based on the surface roughness, tangential and normal grinding forces.

5.3 Methodology

5.3.1 Ultrasonic-assisted grinding process

The layout of the experiment for the UAG system is shown in **Figure 5.1**. The ultrasonic system was modelled such that high frequency vibrations at low amplitude were applied onto the Si_3N_4 work material. The transducer was used to generate the ultrasonic vibrations, which was then amplified and channeled onto the work material via an ultrasonic horn and a booster (See **Figure 5.1**). The workpiece holder comprises of a moveable structure, which is designed to ensure rigidity and motility of the vibrating parts along the table feed direction.

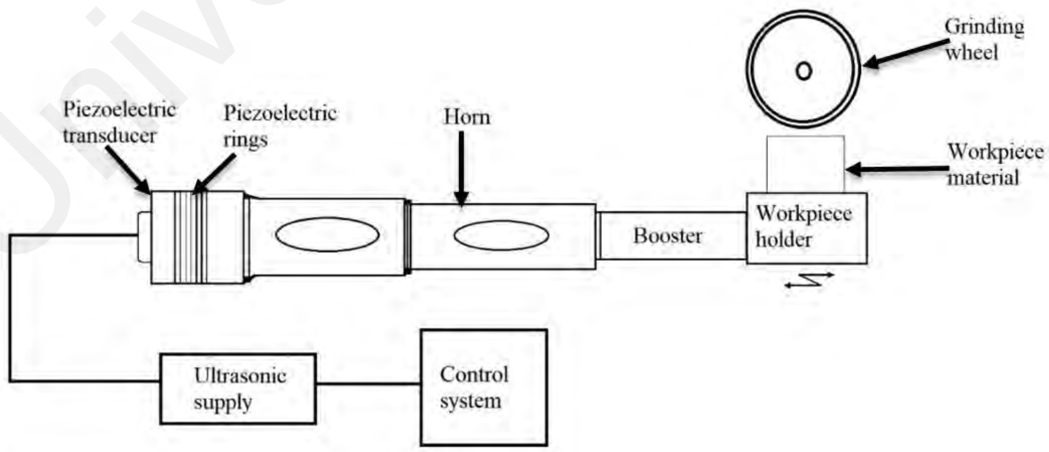

Figure 5.1: Ultrasonic grinding set up.

The grinding experiments were conducted using the surface grinding machine shown in **Figure 5.2**. The ultrasonic oscillation was produced using an ultrasonic signal generator/counter and transferred through a 20-kHz transducer on to the horn/workpiece set-up. The resonance frequency of the transducer was found to be 20.4-kHz. Thus, an ultrasonic horn of 20.4-kHz was designed and manufactured according to steps explained by (Choi et al., 2013). High frequency ultrasonic vibrations of 20.4 kHz were generated using ultrasonic generator with source voltage of 230V and frequency of 50 Hz. The ultrasonic system was designed such that the whole set-up resonates at the resonance frequency of the transducer.

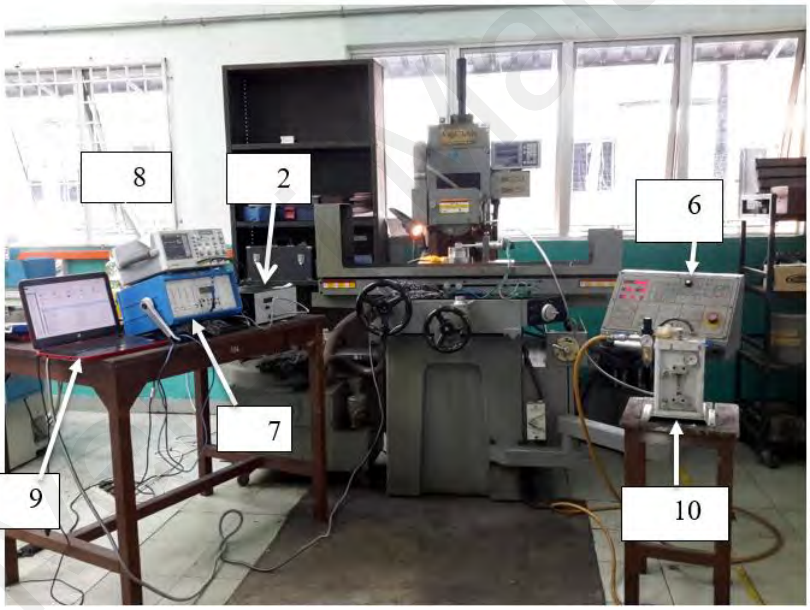

(a)

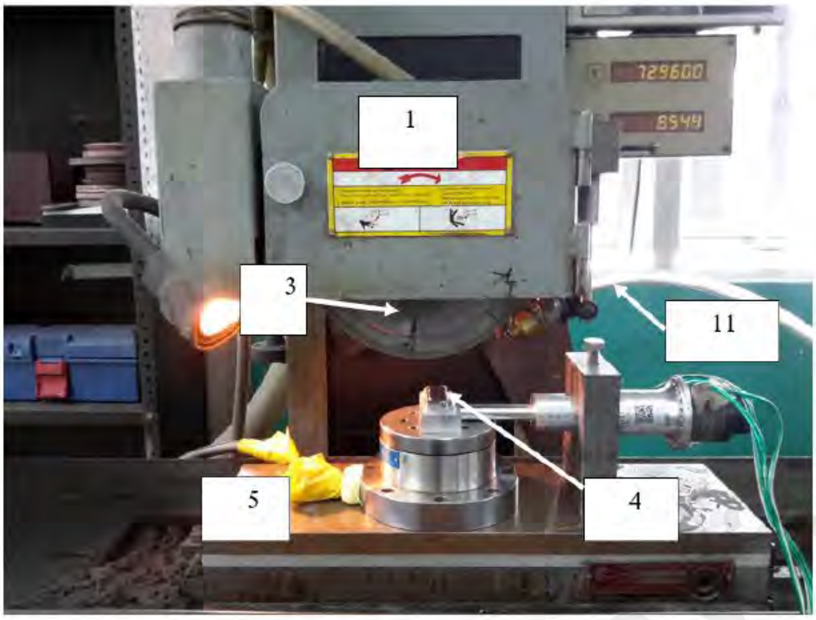

(b)

(1) Grinding wheel, (2) Ultrasonic pulse generator, (3) Workpiece, (4) Dynamometer, (5) Work table, (6) Machine controller, (7) Amplifier, (8) Oscilloscope, (9) Computer, (10) MQL equipment, (11) MQL extrusion nozzle.

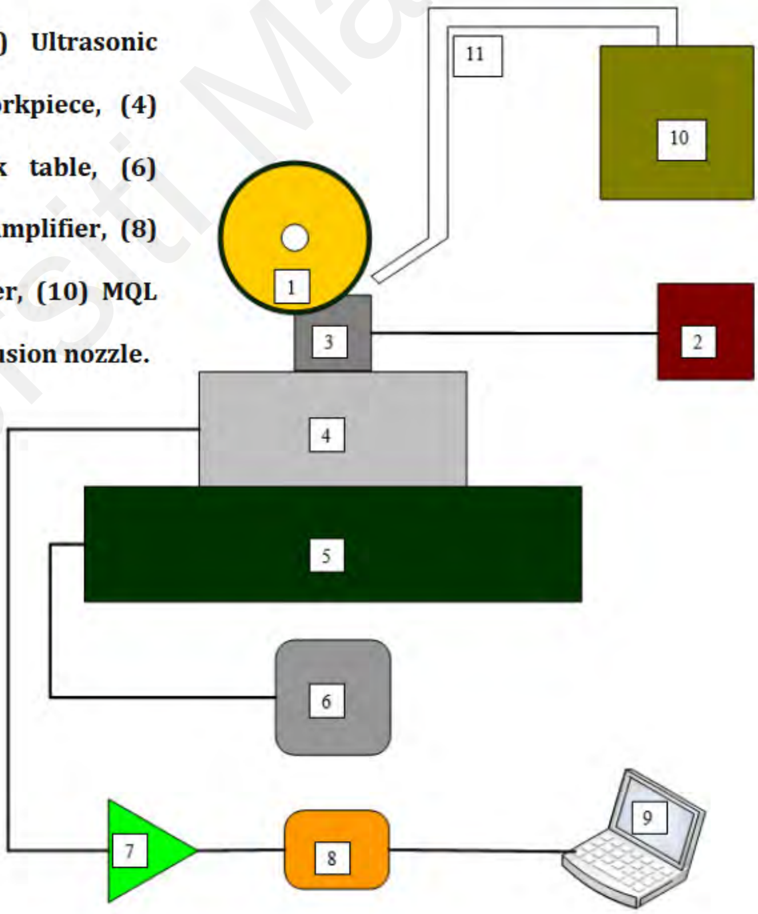

(c)

Figure 5.2: Experimental set up (a) Set-up of grinding machine (b) grinding region (c) Schematic of the experimental set-up.

The mechanism of the UAG process is such that the workpiece oscillates in a 2D-trajectory along the xy-axis. Due to the intermittent contact between the grinding wheel and workpiece in the 2D UAG process, the material removal process would therefore involve both brittle and ductile removal techniques. An illustration of the material removal mechanism (crack propagation) during grinding of superhard materials for single diamond grit is shown in **Figure 3.1**. In addition, a comparison of the path traced out during UAG and CG process is illustrated in **Figure 5.3**.

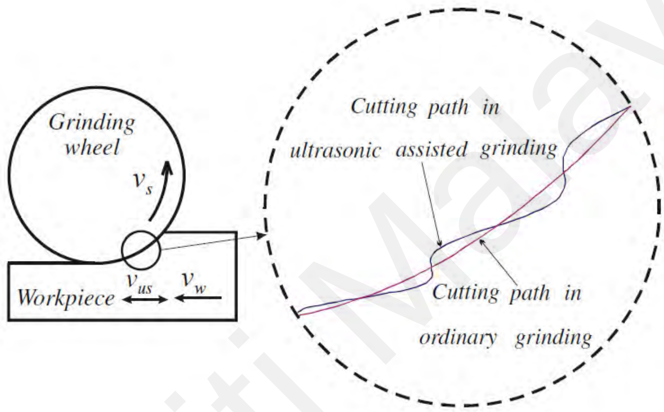

Figure 5.3: Trajectory of the diamond grains during UAG and CG processes (Abdullah et al., 2012).

5.3.2 Nanofluid: preparation and application

SiO_2 nanoparticles have high strength, high thermal stability, are cheap and readily available (see properties of SiO_2 in **Table 5.1)**. SiO_2 based nanofluids have been found to be good in terms of lubrication and tribology (Dambatta et al., 2018; Rabiei et al., 2017). Previous works have shown that the oil-based SiO_2 nanofluid proffer good lubrication in machining processes (Sayuti et al., 2014). The SiO_2 oil-based nanofluid was found to perform well in both lubrication and heat evacuation during machining operations (Lv et al., 2018; Peng et al., 2010).

The MQL technique which involves the spraying a minute quantity of the nanofluid in form of mist lubrication into the grinding region is illustrated in **Figure 5.4**. MQL grinding involve utilization of a combination of compressed air and oil as lubricant which is sprayed directly into the grinding zone. Nevertheless, the performance of the MQL nanofluid depends solely on the tribological properties of the nanofluid. This tribological property depends on the chemical and thermal characteristics of the nanoparticles. Peng et al. (2009) reported that the silicon dioxide nanoparticles have very good anti-wear characteristics, heat removal capacity and prevents burning. Thus, the nanoparticle can effectively help to improve sliding actions between the surfaces in contact by creation of a thin layer of mechanically formed tribofilm on the wheel's surface.

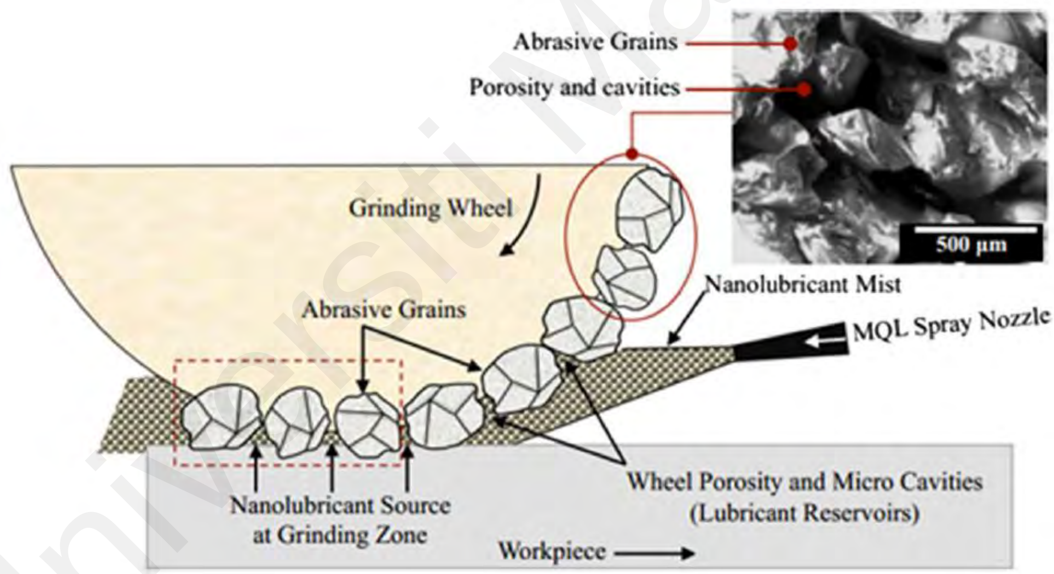

Figure 5.4: Illustration of lubricant spraying during MQL grinding process (Rabiei et al., 2017).

The nanofluids are recently being utilized in manufacturing processes due to the various benefits they proffer. The nanofluids are produced by making a suspension of the nanoparticles in base fluids that are either oil-based or water-based. The nanofluid MQL process is an effective technique that is capable of decreasing the friction due to effective increase in lubrication and tribology. This is evident from formation of tribofilm and effective delivery of lubricant into the grinding zones. The tribofilms formed depend on the tribological properties of the nanoparticles/nanofluid, whereas the delivery of the nanofluid is attributed to the high-pressure propulsion of the mist particles into the grinding region.

Table 5.1: Mechanical properties of SiO_2

Properties	**SiO_2**
Size	5-15nm
Structure	Amorphous
Specific heat	1.0J/g-K
Thermal expansion coefficient	5.6×10^{-7}/K
Melting point	~1600 ºC
Density	2.2 g/cm^3
Dielectric constant	3.9
Dielectric strength	10^7
Thermal conductivity at 330K (W/cm-K)	0.014

The vegetable oil-based SiO_2 nanofluid was prepared in steps similar to the ones taken by authors' (Sayuti et al., 2013). The process of preparing the SiO_2 based nanofluids involves adding SiO_2 nanoparticles into the oils followed by sonication. The oils used in this work were selected due to their high viscosity even at high temperatures. The oils also have good lubrication capacities and are environmentally friendly. They include corn oil, canola oil and sunflower oil. The properties of these oils are summarized in Tables 5.2, 5.3 and 5.4. The nanofluid was produced by mixing the nanoparticle with the fluids in an ultrasonic mixer. Ultrasonic homogenizer (Sonics vibra-cell) with titanium made sonotrode was used to vibrate the nanofluid mixture for a period of 20mins with machine settings of 750watt and 20-kHz. Afterwards, the fully suspended nanofluid was then used as the lubricant for the MQL grinding operations. An example of the prepared nanofluid is shown in **Figure 5.5**.

Figure 5.5: Preparation of nanofluid using sonicator.

Table 5.2: Properties of Canola oil.

S/N	Parameter	Value
1	Relative Density (g/cm3; 20°C/water at 20°C)	0.914 - 0.917
2	Refractive Index (nD 40°C)	1.465 - 1.467
3	Crismer Value	67 - 70
4	Viscosity (Kinematic at 20°C, mm2/sec)	78.2
6	Smoke Point (°C)	220 - 230
7	Flash Point, Open cup (°C)	275 - 290
8	Specific Heat (J/g at 20°C)	1.910 - 1.916
9	Thermal Conductivity (W/m°K)	0.179 - 0.188

Table 5.3: Properties of Corn oil.

S/N	Parameter	Value
1	Density/Specific Gravity	0.916-0.921 at 25°C
2	Melting (solidification) point	Solidifies at −18 to −10 °C
3	Boiling (smoke) point	230 to 238° C
4	Flash point	254°C
5	Solubility	Slightly soluble in alcohol
6	Vapor pressure	3.18 x 10-11
7	Octonol/Water (Kow) coefficient	1.86
8	Viscosity	η = 70 mPa·s at 20°C

Table 5.4: Properties of Sunflower oil.

S/N	Parameter	Value
1	Smoke point (refined)	232 °C
2	Smoke point (unrefined)	107 °C
3	Density (25 °C)	918.8 kg/m3
4	Refractive index (25 °C)	≈1.4735
5	Saponification value	188-194
6	Iodine value	120-145
8	Viscosity (25 °C), unrefined	0.04914 kg/(m*s)

5.3.3 Experimental settings and data acquisition

The grinding experiments were conducted on a high precision surface grinding machine (NI 450AV2) (shown in **Figure 5.2a**). The process parameters used in this work are given in **Table 5.5**. A full factorial experimental design was used to conduct the experiments (see **Table 5.6**).

Table 5.5: Experimental settings

S/n	Lubricant		Concentration (%)	Frequency (kHz)
	Conventional lubrication	MQL Oil-based		
1	Flood cooling	Canola	0	0
2		Corn	0.5	20
3		Sunflower	2	

Table 5.6: Experimental design

Experiment no.	Run no.	Lubricant	Concentration (%)	Frequency (kHz)
1	5	Canola	0	0
2	10	Sunflower	0	20
3	3	Corn	0	0
4	6	Canola	0	20
5	9	Sunflower	0	0
6	4	Corn	0	20
7	17	Canola	0.5	0
8	14	Sunflower	0.5	20
9	7	Corn	0.5	0
10	18	Canola	0.5	20
11	13	Sunflower	0.5	0
12	8	Corn	0.5	20
13	19	Canola	2	0
14	16	Sunflower	2	20

Table 5.6, continued

Experiment no.	Run no.	Lubricant	Concentration (%)	Frequency (kHz)
15	11	Corn	2	0
16	20	Canola	2	20
17	15	Sunflower	2	0
18	12	Corn	2	20
19	1	Flood cooling	-	0
20	2	Flood cooling	-	20

The wheel type, workpiece material (See **Figure 5.7** and **Table 5.8** for elemental composition), experimental settings used in this study are presented in **Table 5.7**. During each grinding run, the x and z-axis components of the grinding forces were measured using the KISTLER-9272 dynamometer. The forces were acquired using a three-channel amplifier (Kistler 5019 charge amplifier) and the four-channel GDS-2204-oscilloscope. In addition, the surface roughness was measured along the grinding feed direction using a profilometer. An example of the forces and surface roughness measurement are respectively shown in **Figures 5.6 a & b**.

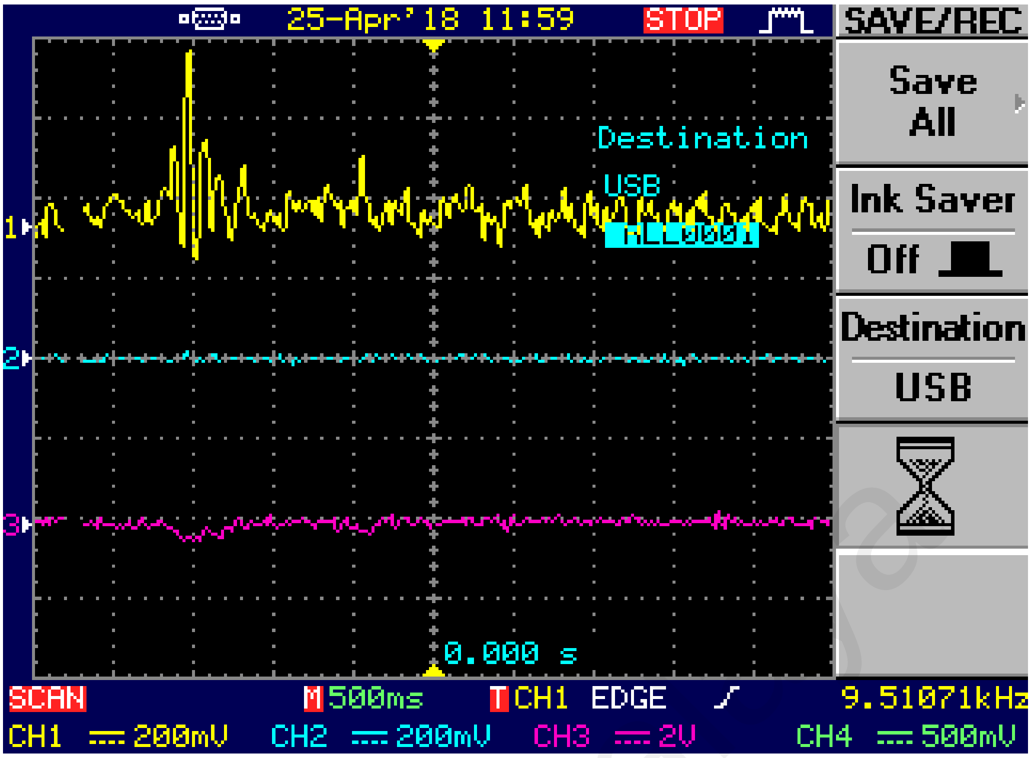

(a)

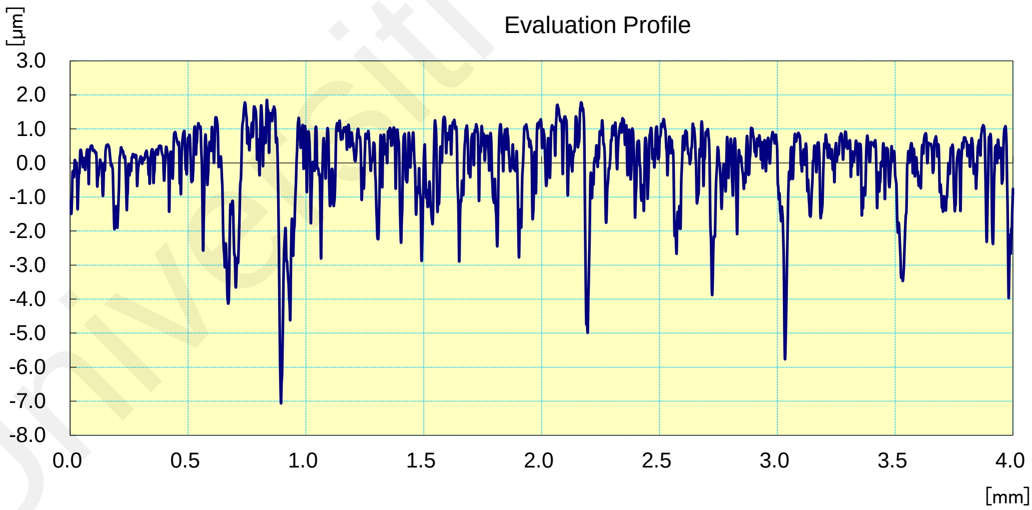

(b)

Figure 5.6: Example of (a) grinding force (b) surface roughness.

Table 5.7: Experimental settings

Grinding Conditions	
Wheel speed (V_s)	31.42 m/s
Table speed (V_f)	10 m/min
Depth of cut (a_e)	20 µm
Grinding wheel	Diamond SD120M100M
MQL flow rate, pressure, stand-off distance	150 ml/hr, 10Bar, 55mm
MQL flow rate, Q	30 L/min
MQL nozzle horizontal angle, ɵ	30º
Workpiece material	Silicon nitride ceramic
Total Dressing depth	20µm
Dressing feed	500mm/min

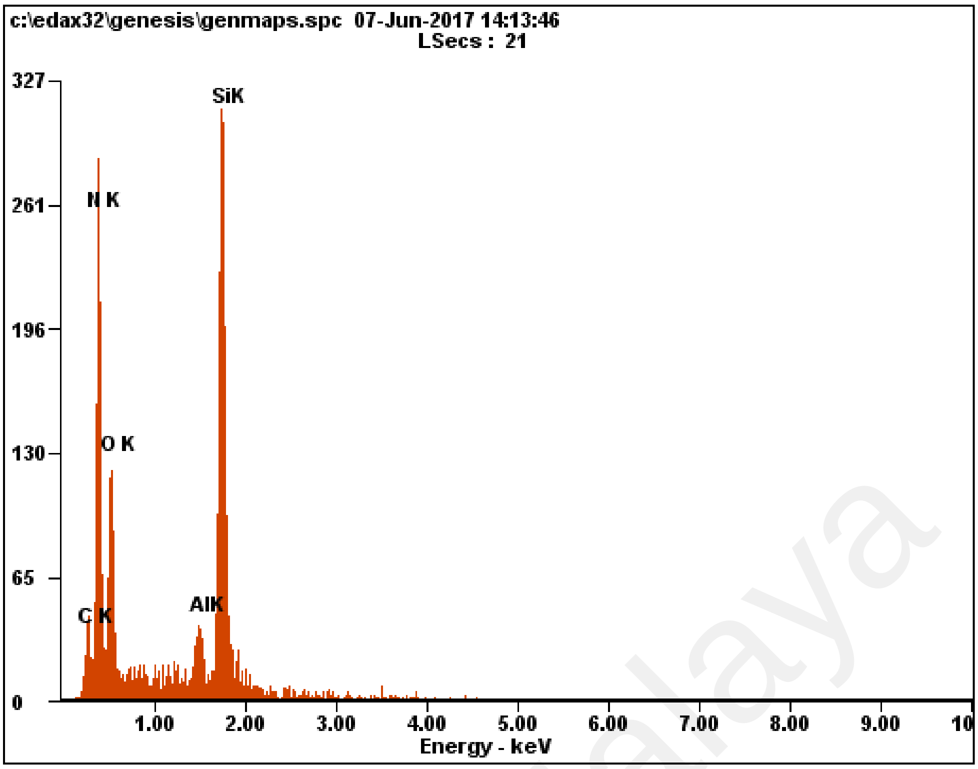

(a)

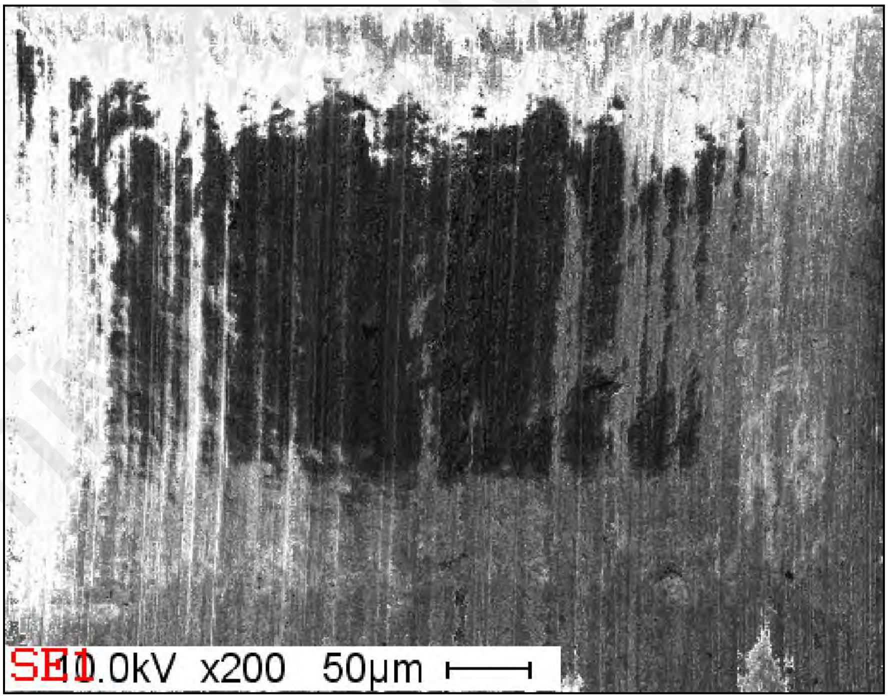

(b)

Figure 5.7: EDX analysis of element composition of Si_3N_4.

Table 5.8: Elemental composition of Si_3N_4 ceramic.

Element	***Wt%***	***At%***
C_K	07.21	10.04
N_K	41.63	49.69
O_K	21.70	22.67
Al_K	02.58	01.60
Si_K	26.89	16.01
Matrix	Correction	ZAF

5.4 Results and discussions

The results were measured after each experimental test run. An example of the result for grinding forces from experimental run 7 & 8 is given in **Figure 5.8**. The average values of normal grinding force (F_n), tangential grinding force (F_t) and surface roughness (R_a) are presented in **Figures 5.9**.

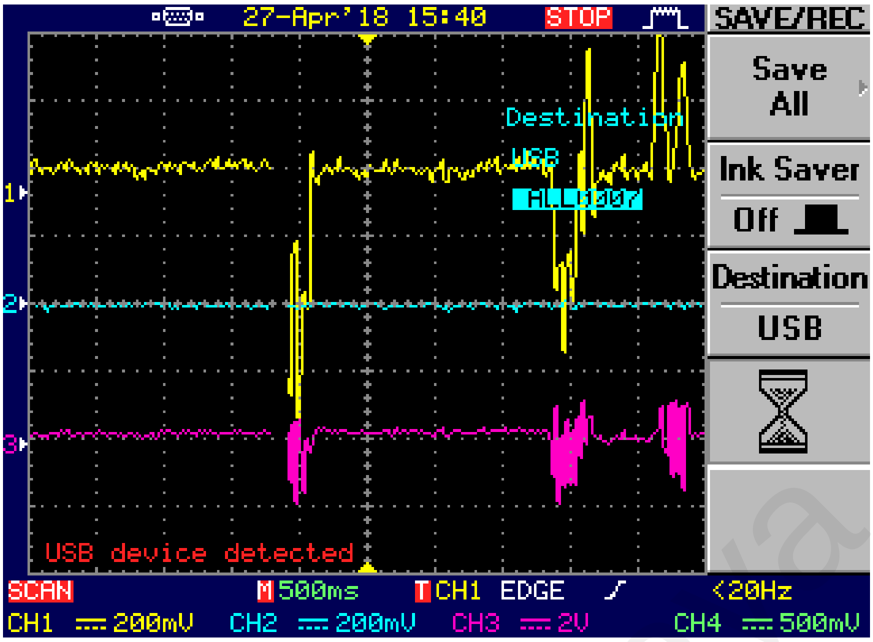

(a)

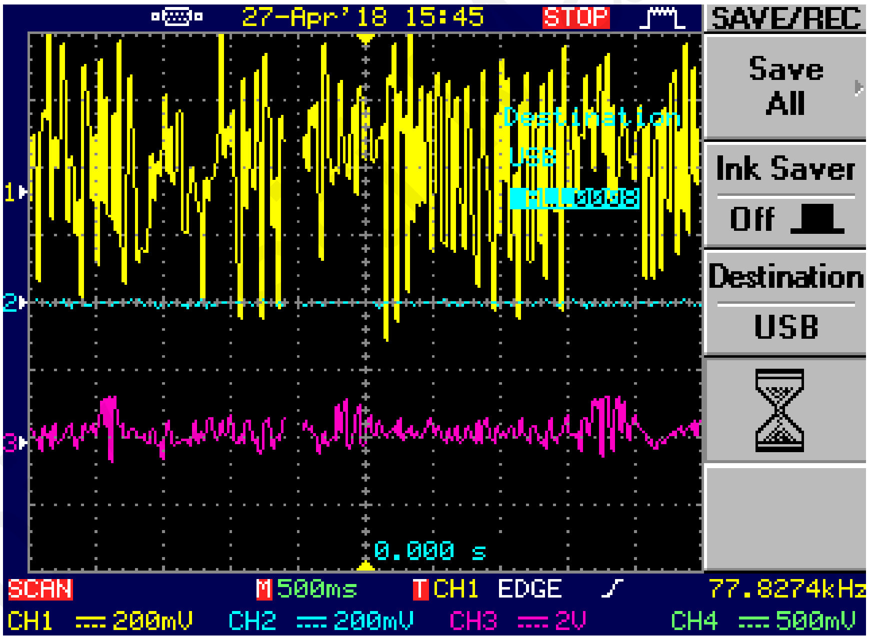

(b)

Figure 5.8: Signal of grinding forces obtained from oscilloscope for experimental runs 7 and 8 with setting: lubricant type=corn oil; nanofluid concentration 0.5% (a) frequency= 0-kHz (b) frequency= 20-kHz.

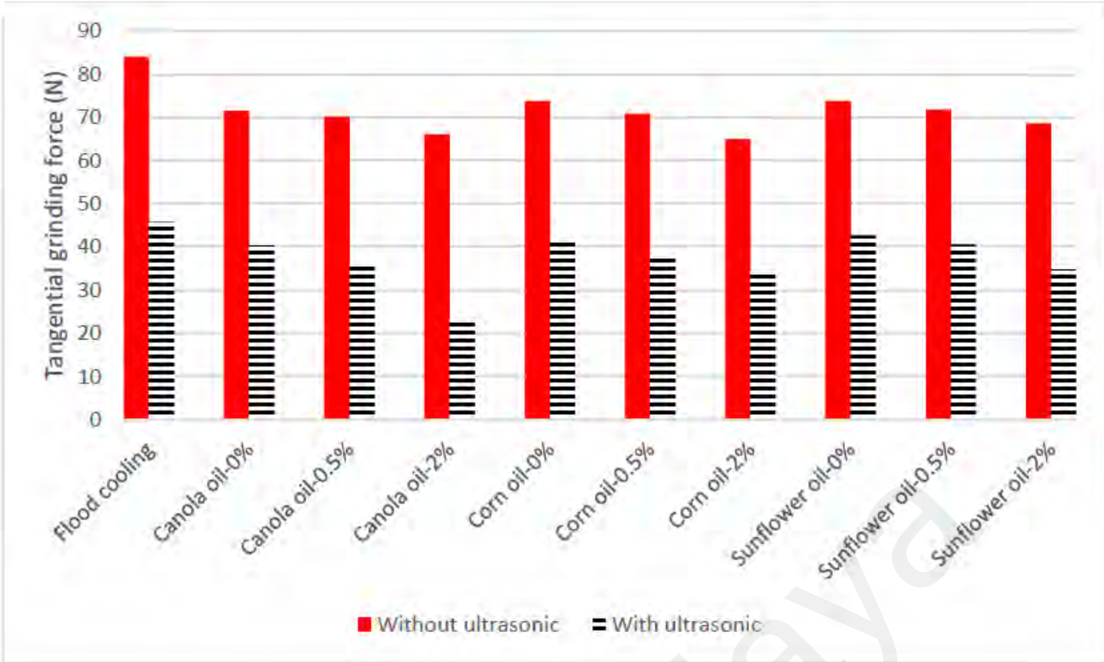
Tangential grinding force (N)
90
80
70
60
50
40
30
20
10
0
Flood cooling
Canola oil-0%
Canola oil-0.5%
Canola oil-2%
Corn oil-0%
Corn oil-0.5%
Corn oil-2%
Sunflower oil-0%
Sunflower oil-0.5%
Sunflower oil-2%
Without ultrasonic
With ultrasonic

(a)

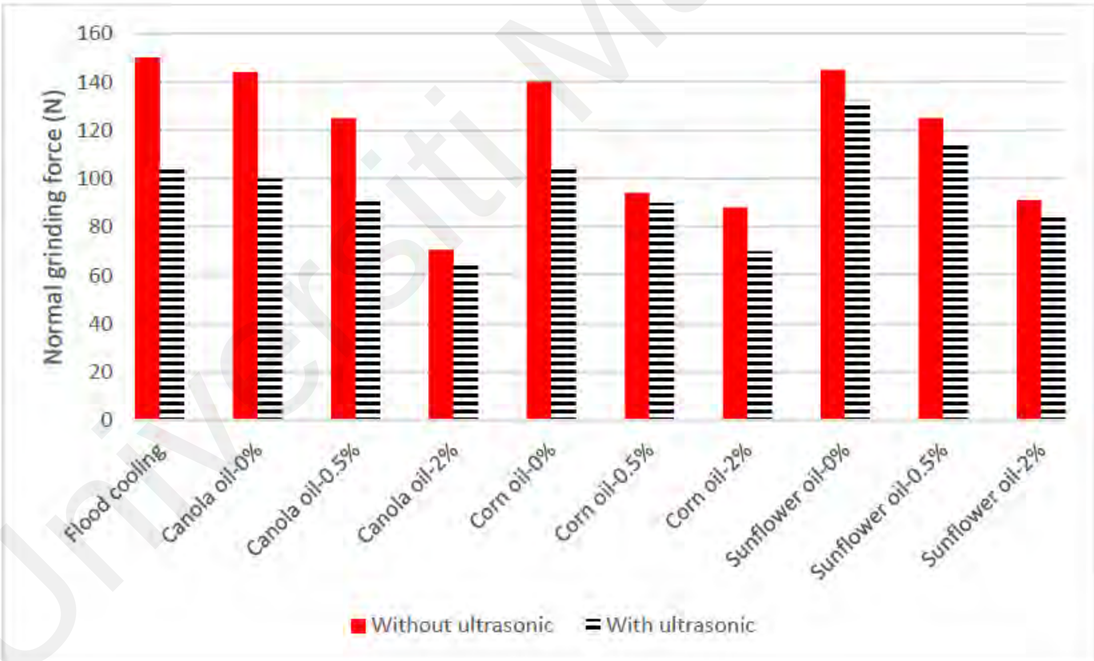
Normal grinding force (N)
160
140
120
100
80
60
40
20
0
Flood cooling
Canola oil-0%
Canola oil-0.5%
Canola oil-2%
Corn oil-0%
Corn oil-0.5%
Corn oil-2%
Sunflower oil-0%
Sunflower oil-0.5%
Sunflower oil-2%
Without ultrasonic
With ultrasonic

(b)

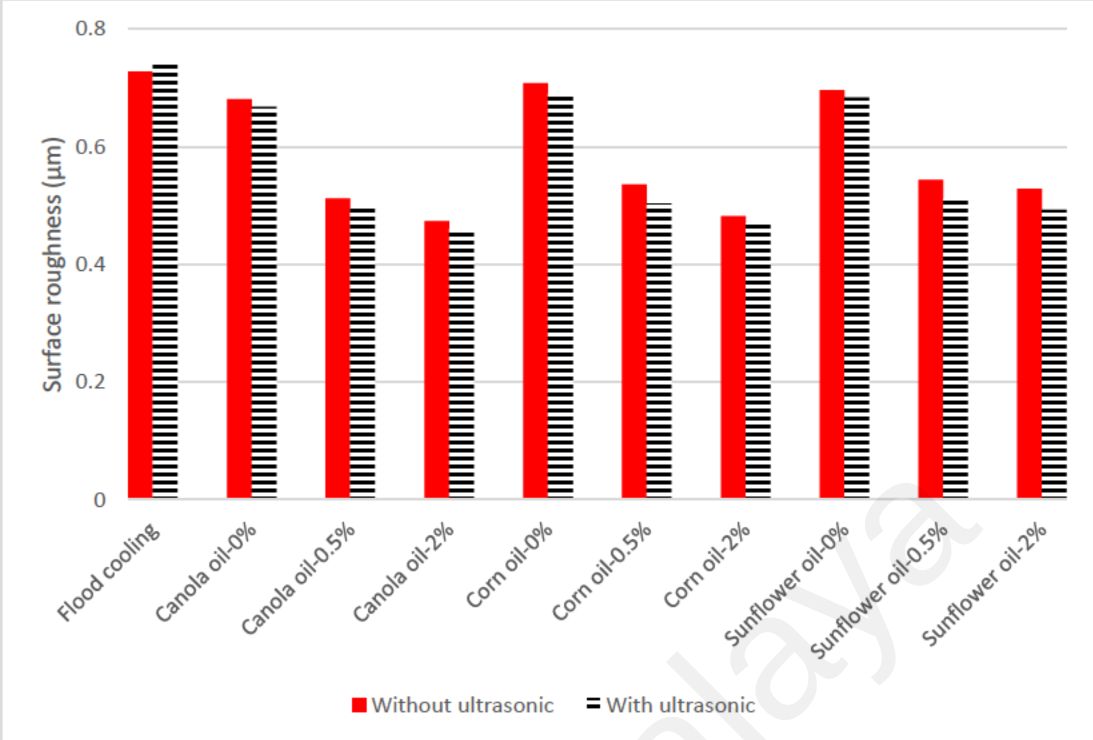

Figure 5.9: Experimental results (a) F_t (b) F_n (c) R_a.

5.4.1 Effect of MQL nanofluids

The effect of the nanofluids as lubricant of the grinding process is analyzed in this section. The results of grinding forces F_t, F_n and also the surface roughness R_a from each experimental run are respectively given in **Figures 5.9 a, b and c**. The force F_n was generally found to be higher than F_t in all the experimental runs. The force F_t which is associated with the grinding power and energy expended during grinding is highly affected by the lubrication process (Dambatta et al., 2018; Rowe, 2013). As can be seen from **Figure 5.9a**, when the nanofluid concentration was increased from 0% to 2%, there was about 60% reduction of the force F_t and more than 40% decrease in the force F_n. Thus indicating better lubrication actions at higher nanofluid concentrations. This shows that the SiO_2 nanoparticles effectively perform the desired lubrication. At 0% concentration of the nanofluid, the grinding forces were observed to be very high, indicating absence of efficient lubrication. Also, the nanofluid MQL process with higher amount of nanofluid concentration performed much better than the flood cooling system. This result agrees with the findings of authors (Dambatta et al., 2018; Molaie et al., 2016; Rabiei et al., 2017). According to the results shown in **Figure 5.9**, it can be seen that among the vegetables oils used as the MQL fluids, the canola oil produced the lowest grinding forces, whereas the sunflower has the highest forces. The nanofluid formed with corn oil was also found to perform very well with about the same performance as the canola oil. The finding also shows that the effective performance of the SiO_2 nanofluid in an MQL process highly depends on the properties of the base oil utilised in the nanofluids. Furthermore, the formation of thin layer of tribofilms through pulping and grinding of the nanoparticles could be attributed to the high reduction in friction and deformations inflicted on the workpiece material. This finding corroborates the reports of author's (Dambatta et al., 2018; Sayuti et al., 2014).

Furthermore, the results obtained also show that the 2% nanoparticle concentration has better performance than both the lower concentrations and the flood cooling technique. Also, the flood cooling samples were observed to be cleaner and without redeposition of removed chips, indicating effective evacuations of debris. However, the workpiece machined with the 0% nanofluid concentration was found to contain extremely poor surface quality with severe deformations. This indicates that the vegetable oils on its own does not perform much lubrication. However, upon addition of the SiO_2 nanoparticles, the surface quality of the machined surface greatly improves. The trend was observed such that when high concentration of the nanofluid was used, the surface quality increases significantly. The canola and corn oils were observed to produce superior surface quality compared to the sunflower oil. This can be attributed to the lower viscosity (at high temperatures) and smoke point of the sunflower, which makes it difficult for the formation of tribofilms around the grinding region. This finding agrees with the obtained by author (Li, B. et al., 2016).

The result for R_a measured along the feed direction for experimental condition is shown in **Figure 5.9c**. It was found that when only the base oils were used as the MQL lubricant, the surface roughness obtained were similar to the flood cooling conditions. In fact, the lateral vibrations were seen to cause some amount of deterioration of the surface quality. However, with increase in the concentration of the nanofluids, the surface roughness was observed to be decreased. The UAG experiments conducted using highly concentrated canola oil based nanofluid were observed to proffer the lowest surface roughness.

5.4.2 Effect of lateral ultrasonic vibration

The effect of applying high frequency ultrasonic vibrations of 20-kHz on the workpiece material was also investigated. The results obtained from the UAG experiments were compared with those of the CG process.

Figures 5.9a & b respectively show the results of the grinding forces F_t and F_n. It can be seen that the UAG experiments have lower grinding forces compared to the CG experiments. It was found also fund that during the UAG, the normal force obtained for the different MQL lubricants was reduced from 38% to 58% compared to the flood cooling lubrication. The 2% nanofluid concentration was found to have the highest reduction to normal forces. The results show that when the nanofluid and the UAG process are hybridized into the grinding system, it results in significant reduction of the normal grinding forces. This desired grinding performance can be attributed to the intermittent separations occurring at the grinding zone due to the high frequency oscillations.

Similarly, the results the tangential force obtained in the UAG process were found to be lower by 49% to 70% compared to the CG. Generally, the ultrasonication helps to significantly lower the grinding forces during the grinding operations. The resultant reduction of the grinding forces due to ultrasonication can be attributed to better penetration of the diamond grits into the work material as a result of the complex material removal mechanism in the ultrasonic grinding process. Also, the self-sharpening phenomenon explained by (Molaie et al., 2016) also helps to significantly reduce the grinding forces and improves the tool life. The rate of reduction of the grinding forces was found to be highly concentrated MQL nanofluids were used as the lubrication technique in the grinding process.

Among the vegetable oils used in the study, the canola oil was found to give the best surface quality from the UAG process. The samples machined using the CG systems were found to have poor surface quality. In general, the lubricant with higher concentration of nanofluid combined with ultrasonic assistance was found to have the best performance during the grinding operations.

Compared with the conventional flood cooling lubrication system, the canola oil was found to have the highest rate of reduction of the grinding forces amongst the vegetable oils used in this work. Similar trend was observed in surface roughness of the machined parts. The performance of the oils were found to improve significantly with addition of the SiO_2 nanoparticles. The tangential grinding force from the UAG and MQL process was found to be lowered by about 49-69% compared to the flood cooled operations. Similarly, with the hybridization of the MQL nanofluids and UAG process, there was about 38-58% reduction in the normal force and 10-37% reductions in surface roughness. As seen from the results obtained, although the SiO_2 nanoparticles were seen to significantly improve the outcome of the grinding process, the properties of the base oils contributes significantly to the enhancement of the process. The viscosity and composition of oils play a significant role in their tribological performance during the grinding operations. Previous studies have shown that the lubricity of the nanofluid during machining depends on the tribofilm produced by the nanofluids. The tribofilm consists of different kinds of chemical layers around the grinding zone. The superior tribological properties observed in the Canola nanofluid could be attributed to the higher viscosity of the canola base oils, and the outstanding performance of the tribofilms formed. Previous studies have shown that some base oils are capable of maintaining their viscosities at high temperature which helps them perform better in terms of lubrication during MQL grinding operations (Molaie et al., 2016).

5.5 Summary

The MQL process has been shown in previous research works to be an alternative to traditional flood cooling lubrication methods for machining hard materials. The flood coolants are mostly synthetic hydrocarbon-based, and were found to be hazardous to the environments, in addition to being expensive. The MQL process was found to help reduce the energy consumed during grinding operations, increase the surface quality and wheel life. In terms of cost, the MQL process helps to significantly reduce lubricant consumption by a thousand times. As such, the cost of machining superhard materials can be greatly reduced when the MQL process is used. Previous works have shown that the efficiency of the MQL process can be improved by utilization of nanofluids as the lubricant of the process. Proper selection of the base oils and nanoparticles will result in optimum performance and better efficiency of the machining process. The nanoparticles when added into the oils, have been found to enhance tribology of the oils and increase their lubricity. In addition, the introduction of lateral ultrasonic vibrations onto the workpiece material during grinding was found to also help improve the efficiency of the process. In this work, the CG and UAG of Si_3N_4 ceramic was performed using flood cooling and MQL techniques. Eco-friendly vegetable oils (i.e. corn, canola and sunflower oils) were used as the base oils for the nanofluid in the MQL process. SiO_2 nanoparticles were used as additives to the vegetable oils in other to produce the nanofluid. The SiO_2

nanoparticles were selected because they very cheap, are readily available and, have high heat evacuation/lubrication ability. The grinding experiments were performed using the same machine parameter settings. The results from the experiments indicate that the MQL technique was better than the flood cooling process. Also, the UAG process has much higher process efficiency than the CG process. The lowest value for grinding forces and surface roughness were found in the experiments performed using the hybrid of MQL (2% nanofluid concentration) and the UAG process. The canola oil was found to have better performance than both the sunflower and corn oils. In addition, the results obtained show that when corn oil was used as the base oil of the MQL lubricant, an increase in the concentration of the nanofluid from 0% to 2%, will lead to reduction of the normal grinding force by 58%. Under the same condition, the tangential force was found to reduce by more than 69%. Furthermore, compared to the results obtained from the flood cooling technique, when the canola oil was used as the MQL base oil, the 2% nanofluid concentration was found to result in the highest average reduction of the grinding forces and surface roughness. Lastly, the sunflower oil was found to have the poorest lubrication ability among the base oils used in this work. It was also found that the process of ultrasonication helps to increase the surface quality in the ground samples during MQL grinding. The samples ground using the hybridized MQL and UAG techniques were found to have the best surface integrity.

CHAPTER 6: CONCLUSIONS AND FUTURE RECOMMEMDATION

6.1 Conclusion

The applicability of advanced ceramics in various engineering fields has recently seen tremendous increase due to their desirable properties. Their superior physical strength and chemical stability them highly desirable.

The CG process being the most popular method of machining the advanced ceramic materials has many limitations such as high grinding forces and poor surface quality. The CG process has been found to be characterized by surface/subsurface damages and intense tool wears. This unwanted outcomes are a major setback to the applicability of the ceramic materials.

In this study, we have proposed the use of ultrasonic assisted grinding and SiO_2-based nanofluid in MQL technique to machine Si_3N_4 ceramic. The MQL process was found to be a better lubrication technique than the traditional flood cooling method. The MQL process has been found to decrease the grinding energy with resultant increase in surface qualities of the machined components.

Furthermore, the introduction of lateral ultrasonic vibrations onto the workpiece material during grinding was found to also help improve the efficiency of the process.

Generally, the following conclusions could be drawn;

- ✓ The use of eco-friendly oils in MQL process was found to improve the machining performance of the grinding process.
- ✓ The utilization of SiO_2 nanofluid in the MQL process was found to provide effective lubrication during grinding Si_3N_4 ceramic. This is evident from the lower grinding forces and improved workpiece surface roughness obtained in

this research. The excellent performance of the SiO_2 based nanofluid can be attributed to the formation of tribological films by the SiO_2 based nanofluid.

- ✓ Higher concentration of the nanofluid was found to have the best performance during MQL grinding operations. In addition, the existence of surface deformations such as microcracks, furrows, SSD's were found to decrease significantly when the MQL nanofluid was used in the grinding operations.
- ✓ The canola oil was found to have better performance as a base oil due to its high viscosity.
- ✓ Compared to the flood cooling lubrication, the MQL lubricants were found to bring about 40% reduction to the normal grinding force. Moreover, there was up to 70% reduction of the tangential grinding force F_t. Also, surface roughness was found to decrease by 30%.
- ✓ Lastly, the ANFIS prediction models were found to have very high prediction accuracies, as such they can be used to effectively predict the outcomes of the grinding experiments using only the process variables.

6.2 Future recommendation

Recently, advanced engineering ceramics such as Si_3N_4, zirconia, silicon carbide and alumina, have gained much relevance in various manufacturing industries. Studies have shown that the machining of these materials requires higher part quality, precision and increased efficiency.

The extensive application of the advanced engineering ceramics into the different engineering fields highly depends on their machinability. Hence, it is crucial that the manufactured materials be defect-free, and have high reliability.

The ultrasonic assisted grinding technique has been found to have high MRR, better surface and sub-surface quality, and highly economical. The UAG process has shown great capacity in grinding of advanced ceramics. However, it needs to be further scrutinized for optimal performance and higher efficiency. Thus, it would be of great importance to make a thorough investigation to analyze effects of the UAG parameters (such as vibration amplitude and vibration frequency) on different performance indicators such the grinding energy, flexural strength, bending strength, and phase transformations.

High grinding forces pose the greatest threat to the efficiency, and quality of components produced during the grinding process. The excessive grinding force also leads to increase in heat generation. As such, a thorough investigation of any potential technique that could lead to the reduction of the heat generated & grinding forces should be explored on. For instance, the use of cryogenic gases instead of air in the MQL process should be investigated. Since phase transformation is among the main source of residual stress, the phase transformation during grinding of the ceramic materials as a result of generated residual stress should also be studied extensively.

REFERENCES

Abdullah, A, Farhadi, A, & Pak, A. (2012). Ultrasonic-assisted dry creep-feed up-grinding of superalloy Inconel738LC. *Experimental mechanics, 52*(7), 843-853.

Abellan-Nebot, Jose Vicente, & Subirón, Fernando Romero. (2010). A review of machining monitoring systems based on artificial intelligence process models. *The International Journal of Advanced Manufacturing Technology, 47*(1-4), 237-257.

Adibi, H, Rezaei, SM, & Sarhan, Ahmed AD. (2014). Investigation on using high-pressure fluid jet in grinding process for less wheel loaded areas. *The International Journal of Advanced Manufacturing Technology, 70*(9-12), 2233-2240.

Agarwal, Deepak Kumar, Vaidyanathan, Aravind, & Kumar, S Sunil. (2015). Investigation on convective heat transfer behaviour of kerosene-Al2O3 nanofluid. *Applied Thermal Engineering, 84*, 64-73.

Agarwal, S, & Rao, P Venkateswara. (2005). A new surface roughness prediction model for ceramic grinding. *Proceedings of the Institution of Mechanical Engineers, Part B: Journal of Engineering Manufacture, 219*(11), 811-819.

Agarwal, Sanjay, & Rao, P Venkateswara. (2008). Experimental investigation of surface/subsurface damage formation and material removal mechanisms in SiC grinding. *International Journal of Machine Tools and Manufacture, 48*(6), 698-710.

Ahmed, Yasser, Cong, WL, Stanco, Matthew R, Xu, ZG, Pei, ZJ, Treadwell, C, . . . Li, ZC. (2012). Rotary Ultrasonic Machining of Alumina Dental Ceramics: A Preliminary Experimental Study on Surface and Subsurface Damages. *Journal of Manufacturing Science and Engineering, 134*(6), 064501.

Akbari, Javad, Borzoie, Hassan, & Mamduhi, Mohammad Hossein. (2008). Study on ultrasonic vibration effects on grinding process of alumina ceramic (Al2O3). *World Academy of Science, Engineering and Technology, 41*, 785-789.

Alves, Salete Martins, & de Oliveira, Joao Fernando Gomes. (2006). Development of new cutting fluid for grinding process adjusting mechanical performance and environmental impact. *Journal of materials processing technology, 179*(1), 185-189.

Arif, Muhammad, Rahman, Mustafizur, & San, Wong Yoke. (2011). Analytical model to determine the critical feed per edge for ductile–brittle transition in milling process of brittle materials. *International Journal of Machine Tools and Manufacture, 51*(3), 170-181.

Arunachalam, RM, Mannan, MA, & Spowage, AC. (2004). Residual stress and surface roughness when facing age hardened Inconel 718 with CBN and ceramic cutting tools. *International Journal of Machine Tools and Manufacture, 44*(9), 879-887.

Asiltürk, İlhan, Tinkir, Mustafa, El Monuayri, Hazim, & Çelik, Levent. (2012). An intelligent system approach for surface roughness and vibrations prediction in cylindrical grinding. *International Journal of Computer Integrated Manufacturing, 25*(8), 750-759.

Azar, Ahmad Taher. (2013). Neuro-fuzzy applications in dialysis systems *Modeling and Control of Dialysis Systems* (pp. 1223-1274): Springer.

Balan, ASS, Vijayaraghavan, L, & Krishnamurthy, R. (2013). Minimum quantity lubricated grinding of Inconel 751 alloy. *Materials and Manufacturing Processes, 28*(4), 430-435.

Baseri, Hamid. (2011). Design of adaptive neuro-fuzzy inference system for estimation of grinding performance. *Materials and Manufacturing Processes, 26*(5), 757-763.

Bellows, G. (1972). Applying surface integrity principles in jet engine production. *Metals Engineering Quarterly, 12*, 55-58.

Bhaduri, D, Soo, SL, Aspinwall, DK, Novovic, D, Harden, P, Bohr, S, & Martin, D. (2012). A study on ultrasonic assisted creep feed grinding of nickel based superalloys. *Procedia CIRP, 1*, 359-364.

Bifano, Thomas G, Dow, Thomas A, & Scattergood, Ronald O. (1991). Ductile-regime grinding: a new technology for machining brittle materials. *Journal of engineering for industry, 113*(2), 184-189.

Bifano, Thomas G, & Fawcett, Steven C. (1991). Specific grinding energy as an in-process control variable for ductile-regime grinding. *Precision engineering, 13*(4), 256-262.

Biswas, SK. (2000). Some mechanisms of tribofilm formation in metal/metal and ceramic/metal sliding interactions. *Wear, 245*(1-2), 178-189.

Blackley, WS, & Scattergood, Ronald O. (1991). Ductile-regime machining model for diamond turning of brittle materials. *Precision engineering, 13*(2), 95-103.

Boswell, Brian, Islam, Mohammad Nazrul, Davies, Ian J, Ginting, YR, & Ong, Ai Keem. (2017). A review identifying the effectiveness of minimum quantity lubrication (MQL) during conventional machining. *The International Journal of Advanced Manufacturing Technology, 92*(1-4), 321-340.

Brecher, Christian, Schug, Ralf, Weber, Andreas, Wenzel, Christian, & Hannig, Sophia. (2010). New systematic and time-saving procedure to design cup grinding wheels for the application of ultrasonic-assisted grinding. *The International Journal of Advanced Manufacturing Technology, 47*(1-4), 153-159.

Brehl, DE, & Dow, TA. (2008). Review of vibration-assisted machining. *Precision engineering, 32*(3), 153-172.

Brinksmeier, E, & Glabe, R. (1999). *Elliptical vibration cutting of steel with diamond tools.* Paper presented at the Proc. of the 14th Annual ASPE Meeting, Monterey, California, USA.

Buhl, Horst. (2012). *Advanced aerospace materials*: Springer Science & Business Media.

Campbell Jr, Flake C. (2011). *Manufacturing technology for aerospace structural materials*: Elsevier.

Cao, Jianguo, Wu, Yongbo, Lu, Dong, Fujimoto, Masakazu, & Nomura, Mitsuyoshi. (2014). Material removal behavior in ultrasonic-assisted scratching of SiC ceramics with a single diamond tool. *International Journal of Machine Tools and Manufacture, 79*, 49-61.

Chandrasekaran, M, Muralidhar, M, Krishna, C Murali, & Dixit, US. (2010). Application of soft computing techniques in machining performance prediction and optimization: a literature review. *The International Journal of Advanced Manufacturing Technology, 46*(5-8), 445-464.

Chattopadhyay, AK, Chollet, L, & Hintermann, HE. (1991). On performance of brazed bonded monolayer diamond grinding wheel. *CIRP Annals-Manufacturing Technology, 40*(1), 347-350.

Chen, Haifeng, Tang, Jinyuan, & Zhou, Wei. (2013). An experimental study of the effects of ultrasonic vibration on grinding surface roughness of C45 carbon steel. *The International Journal of Advanced Manufacturing Technology, 68*(9-12), 2095-2098.

Chen, JB, Fang, QH, Wang, CC, Du, JK, & Liu, F. (2016). Theoretical study on brittle–ductile transition behavior in elliptical ultrasonic assisted grinding of hard brittle materials. *Precision Engineering*.

Chen, Jianbin, Fang, Qihong, & Li, Ping. (2015). Effect of grinding wheel spindle vibration on surface roughness and subsurface damage in brittle material grinding. *International Journal of Machine Tools and Manufacture, 91*, 12-23.

Chen, Jianyi, Huang, Hui, & Xu, Xipeng. (2009). An experimental study on the grinding of alumina with a monolayer brazed diamond wheel. *The International Journal of Advanced Manufacturing Technology, 41*(1), 16-23.

Chen, Ming Jun, Li, Dan, Dong, Shen, & Zhang, Fei Hu. (2004). *Factors influencing the surface quality during ultra-precision grinding of brittle materials in ductile mode.* Paper presented at the Key Engineering Materials.

Chen, Zhong, Atmadi, Alexander, Stephenson, David A, Liang, Steven Y, & Patri, K Venuvinod. (2000). Analysis of cutting fluid aerosol generation for environmentally responsible machining. *CIRP Annals-Manufacturing Technology, 49*(1), 53-56.

Choi, JP, Jeon, BH, & Kim, BH. (2007). Chemical-assisted ultrasonic machining of glass. *Journal of materials processing technology, 191*(1), 153-156.

Choi, Young-Jae, Park, Kyung-Hee, Hong, Yun-Hyuck, Kim, Kyeong-Tae, Lee, Seok-Woo, & Choi, Hon-Zong. (2013). Effect of ultrasonic vibration in grinding; horn design and experiment. *International Journal of Precision Engineering and Manufacturing, 14*(11), 1873-1879.

Cook, Robert F, & Pharr, George M. (1990). Direct observation and analysis of indentation cracking in glasses and ceramics. *Journal of the American Ceramic Society, 73*(4), 787-817.

Cotton, James D, Clark, Larry P, & Phelps, Henry R. (2002). Titanium alloys on the F-22 fighter airframe. *Advanced materials & processes, 160*(5), 25-28.

da Silva, Leonardo Roberto, Bianchi, Eduardo Carlos, Fusse, Ronaldo Yoshinobu, Catai, Rodrigo Eduardo, Franca, Thiago Valle, & Aguiar, Paulo Roberto. (2007). Analysis of surface integrity for minimum quantity lubricant—MQL in grinding. *International Journal of Machine Tools and Manufacture, 47*(2), 412-418.

Dai, Jianbo, Ding, Wenfeng, Zhang, Liangchi, Xu, Jiuhua, & Su, Honghua. (2015). Understanding the effects of grinding speed and undeformed chip thickness on the chip formation in high-speed grinding. *The International Journal of Advanced Manufacturing Technology, 81*(5-8), 995-1005.

Dambatta, Yusuf S, Sarhan, Ahmed AD, Sayuti, M, & Hamdi, M. (2017). Ultrasonic assisted grinding of advanced materials for biomedical and aerospace applications—a review. *The International Journal of Advanced Manufacturing Technology*, 1-34.

Dambatta, Yusuf S, Sayuti, M, Sarhan, Ahmed AD, & Hamdi, M. (2018). Comparative study on the performance of the MQL nanolubricant and conventional flood lubrication techniques during grinding of Si 3 N 4 ceramic. *The International Journal of Advanced Manufacturing Technology*, 1-18.

de Souza Ruzzi, Rodrigo, de Mello Belentani, Rafael, de Mello, Hamilton José, Canarim, Rubens Chinali, D'Addona, Doriana M, Diniz, Anselmo Eduardo, . . . Bianchi, Eduardo Carlos. (2017). MQL with water in cylindrical plunge grinding of hardened steels using CBN wheels, with and without wheel cleaning by compressed air. *The International Journal of Advanced Manufacturing Technology, 90*(1-4), 329-338.

Denkena, Berend, de Leon, Luis, & Hahmann, Dennis. (2008). *Ultrasonic assisted grinding of brittle materials–surface topography and process forces.* Paper presented at the Proceedings of the 23rd Annual Meeting of the ASPE and the Twelfth ICPE, ASPE/ICPE.

Desa, O, & Bahadur, S. (2001). The effect of lubricants in single point scratching and abrasive machining of alumina and silicon nitride. *Wear, 251*(1), 1085-1093.

Ding, Kai, Fu, Yucan, Su, Honghua, Gong, Xiaobei, & Wu, Keqin. (2014). Wear of diamond grinding wheel in ultrasonic vibration-assisted grinding of silicon carbide. *The International Journal of Advanced Manufacturing Technology, 71*(9-12), 1929-1938.

Ding, Wenfeng, Zhu, Yejun, Zhang, Liangchi, Xu, Jiuhua, Fu, Yucan, Liu, Weidong, & Yang, Changyong. (2015). Stress characteristics and fracture wear of brazed CBN grains in monolayer grinding wheels. *Wear, 332*, 800-809.

Dornfeld, David, Min, Sangkee, & Takeuchi, Y. (2006). Recent advances in mechanical micromachining. *CIRP Annals-Manufacturing Technology, 55*(2), 745-768.

El-Meliegy, Emad, & van Noort, Richard. (2011). *Glasses and glass ceramics for medical applications*: Springer science & business media.

Emami, M, Sadeghi, MH, & Sarhan, Ahmed AD. (2013). Investigating the effects of liquid atomization and delivery parameters of minimum quantity lubrication on the grinding process of Al 2 O 3 engineering ceramics. *Journal of Manufacturing Processes, 15*(3), 374-388.

Emami, Mohsen, Sadeghi, Mohammad Hossein, Sarhan, Ahmed Aly Diaa, & Hasani, Farshid. (2014). Investigating the minimum quantity lubrication in grinding of Al 2 O 3 engineering ceramic. *Journal of Cleaner Production, 66*, 632-643.

Fan, Xiaorui, & Miller, Michele H. (2006). Force analysis for grinding with segmental wheels. *Machining science and technology, 10*(4), 435-455.

Fathima, K, Kumar, A Senthil, Rahman, M, & Lim, HS. (2003). A study on wear mechanism and wear reduction strategies in grinding wheels used for ELID grinding. *Wear, 254*(12), 1247-1255.

Feng, J, Kim, BS, Shih, A, & Ni, J. (2009). Tool wear monitoring for micro-end grinding of ceramic materials. *Journal of Materials Processing Technology, 209*(11), 5110-5116.

Feng, Pingfa, Liang, Guiqiang, & Zhang, Jianfu. (2014). Ultrasonic vibration-assisted scratch characteristics of silicon carbide-reinforced aluminum matrix composites. *Ceramics International, 40*(7), 10817-10823.

Feucht, Florian, Ketelaer, Jens, Wolff, Alexander, Mori, Masahiko, & Fujishima, Makoto. (2014). Latest machining Technologies of hard-to-cut materials by ultrasonic Machine Tool. *Procedia CIRP, 14*, 148-152.

Fratila, Domnita. (2010). Macro-level environmental comparison of near-dry machining and flood machining. *Journal of cleaner production, 18*(10), 1031-1039.

Fratila, Domnita, & Caizar, Cristian. (2011). Application of Taguchi method to selection of optimal lubrication and cutting conditions in face milling of AlMg 3. *Journal of Cleaner Production, 19*(6), 640-645.

Gao, GF, Zhao, B, Xiang, DH, & Kong, QH. (2009). Research on the surface characteristics in ultrasonic grinding nano-zirconia ceramics. *Journal of materials processing technology, 209*(1), 32-37.

Gao, Guofu, Kong, Qinghua, Zhao, Bo, & Liu, Chuanshao. (2006). *Research on Plastic Removal Mechanism of engineering ceramics grinding with ultrasonic assistance.*

Paper presented at the Technology and Innovation Conference, 2006. ITIC 2006. International.

Garshin, AP. (2009). Boron and silicon nitrides as mechanical engineering ceramics. *Refractories and Industrial Ceramics, 50*(5), 363-367.

Gates, Richard, Wang, You, Ying, Tse-Neng, & Hsu, Stephen. (1999). A grinding map concept for optimization of ceramic machining. *Tribology transactions, 42*(4), 715-722.

Goindi, GS, Sarkar, P, Jayal, AD, Chavan, SN, & Mandal, D. (2018). Investigation of ionic liquids as additives to canola oil in minimum quantity lubrication milling of plain medium carbon steel. *The International Journal of Advanced Manufacturing Technology, 94*(1-4), 881-896.

Gong, Hu, Fang, FZ, & Hu, XT. (2010). Kinematic view of tool life in rotary ultrasonic side milling of hard and brittle materials. *International Journal of Machine Tools and Manufacture, 50*(3), 303-307.

Guo, B, Zhao, QL, & Jackson, MJ. (2011). Ultrasonic vibration-assisted grinding of microstructured surfaces on silicon carbide ceramic materials. *Proceedings of the Institution of Mechanical Engineers, Part B: Journal of Engineering Manufacture*, 0954405411423574.

Gupta, R, Shishodia, KS, & Sekhon, GS. (2001). Optimization of grinding process parameters using enumeration method. *Journal of Materials Processing Technology, 112*(1), 63-67.

Hammel, EC, Ighodaro, OL-R, & Okoli, OI. (2014). Processing and properties of advanced porous ceramics: An application based review. *Ceramics International, 40*(10), 15351-15370.

Hanasaki, S, Fujivara, J, Wada, T, & Hasegawa, Y. (1994). Vibratory creep feed grinding. *Nippon Kikai Gakkai Ronbunshu C Hen, 60*(573), 1829-1834.

Hitchiner, MP. (1999). *Technological advances in creep feed grinding of superalloys with CBN.* Paper presented at the 3rd International Machining and Grinding Conference SME, Cincinnati, Ohio, October.

Holmberg, Kenneth, Siilasto, Roope, Laitinen, Tarja, Andersson, Peter, & Jäsberg, Ari. (2013). Global energy consumption due to friction in paper machines. *Tribology International, 62*, 58-77.

Hosokawa, Akira, Ueda, T, & Yunoki, T. (2006). Laser dressing of metal bonded diamond wheel. *CIRP Annals-Manufacturing Technology, 55*(1), 329-332.

Hu, Kun Hong, Huang, Fei, Hu, Xian Guo, Xu, Yu Fu, & Zhou, Yi Qun. (2011). Synergistic effect of nano-MoS2 and anatase nano-TiO2 on the lubrication properties of MoS2/TiO2 nano-clusters. *Tribology Letters, 43*(1), 77-87.

Huang, Han, & Liu, YC. (2003). Experimental investigations of machining characteristics and removal mechanisms of advanced ceramics in high speed deep grinding. *International Journal of Machine Tools and Manufacture, 43*(8), 811-823.

Inasaki, Inasaki, & Nakayama, K. (1986). High-efficiency grinding of advanced ceramics. *CIRP Annals-Manufacturing Technology, 35*(1), 211-214.

Irani, Rishad A, Bauer, Robert J, & Warkentin, Andrew. (2007). Development of a new cutting fluid delivery system for creepfeed grinding. *International journal of manufacturing technology and management, 12*(1-3), 108-126.

Isaev, A, & Anokhin, V. (1961). Ultrasonic vibration of a metal cutting tool. *Vest Mashinos (in Russian)*.

Izman, S, & Venkatesh, VC. (2007). Gelling of chips during vertical surface diamond grinding of BK7 glass. *Journal of materials processing technology, 185*(1), 178-183.

Jackson, MJ, Davis, CJ, Hitchiner, MP, & Mills, B. (2001). High-speed grinding with CBN grinding wheels—applications and future technology. *Journal of Materials Processing Technology, 110*(1), 78-88.

Jang, J-SR. (1993). ANFIS: adaptive-network-based fuzzy inference system. *IEEE transactions on systems, man, and cybernetics, 23*(3), 665-685.

Jang, Jyh-Shing Roger, Sun, Chuen-Tsai, & Mizutani, Eiji. (1997). Neuro-fuzzy and soft computing, a computational approach to learning and machine intelligence.

Jia, Dongzhou, Li, Changhe, Zhang, Yanbin, Yang, Min, Wang, Yaogang, Guo, Shuming, & Cao, Huajun. (2017). Specific Energy and Surface Roughness of Minimum Quantity Lubrication Grinding Ni-Based Alloy with Mixed Vegetable Oil-based Nanofluids. *Precision Engineering*.

Jian-Hua, Zhang, Yan, Zhao, Fu-Qiang, Tian, Shuo, Zhang, & Lan-Shen, Guo. (2015). Kinematics and experimental study on ultrasonic vibration-assisted micro end grinding of silica glass. *The International Journal of Advanced Manufacturing Technology, 78*(9-12), 1893-1904.

Jianhua, Zhang, Yan, Zhao, Shuo, Zhang, Fuqiang, Tian, Lanshen, Guo, & Ruizhen, Dai. (2014). Study on effect of ultrasonic vibration on grinding force and surface quality in ultrasonic assisted micro end grinding of silica glass. *Shock and Vibration, 2014*.

Jirapattarasilp, Komson, & Rukijkanpanich, Jittra. (2007). The experiment of high-speed grinding of a gemstone: cubic zirconia. *The International Journal of Advanced Manufacturing Technology, 33*(11-12), 1136-1142.

Kalita, Parash, Malshe, Ajay P, Kumar, S Arun, Yoganath, VG, & Gurumurthy, T. (2012). Study of specific energy and friction coefficient in minimum quantity lubrication grinding using oil-based nanolubricants. *Journal of Manufacturing Processes, 14*(2), 160-166.

Kalita, Parash, Malshe, Ajay P, & Rajurkar, Kamlakar P. (2012). Study of tribo-chemical lubricant film formation during application of nanolubricants in minimum quantity lubrication (MQL) grinding. *CIRP Annals-Manufacturing Technology, 61*(1), 327-330.

Kalpakjian, S, & Schmid, SR. (2014). Manufacturing Processes for Engineering Materials–5th Edition. *agenda, 12*, 1.

Kar, Samarjit, Das, Sujit, & Ghosh, Pijush Kanti. (2014). Applications of neuro fuzzy systems: A brief review and future outline. *Applied Soft Computing, 15*, 243-259.

Kirchner, Henry P. (1984). Damage Penetration at Elongated Machining Grooves in Hot-Pressed Si3N4. *Journal of the American Ceramic Society, 67*(2), 127-132.

Kizaki, Toru, Ito, Yusuke, Tanabe, Shota, Kim, Yangjin, Sugita, Naohiko, & Mitsuishi, Mamoru. (2016). Laser-assisted Machining of Zirconia Ceramics Using a Diamond Bur. *Procedia CIRP, 42*, 497-502.

Klemm, Hagen. (2010). Silicon Nitride for High-Temperature Applications. *Journal of the American Ceramic Society, 93*(6), 1501-1522.

Klocke, F, & Rubenach, O. (2000). Ultrasonic-assisted diamond turning of glass and steel. *Industrial diamond review, 60*(586), 227.

Kuffa, Michal, Kuster, Fredy, & Wegener, Konrad. (2016). Comparison of lubrication conditions for grinding of mild steel with electroplated cBN wheel. *CIRP Journal of Manufacturing Science and Technology*.

Kuffa, Michal, Kuster, Fredy, & Wegener, Konrad. (2017). Comparison of lubrication conditions for grinding of mild steel with electroplated cBN wheel. *CIRP Journal of Manufacturing Science and Technology, 18*, 53-59.

Kumanan, S, Jesuthanam, CP, & Kumar, R Ashok. (2008). Application of multiple regression and adaptive neuro fuzzy inference system for the prediction of surface roughness. *The International Journal of Advanced Manufacturing Technology, 35*(7-8), 778-788.

KUO, Kei-lin, & TSAO, Chung-chen. (2012). Rotary ultrasonic-assisted milling of brittle materials. *Transactions of Nonferrous Metals Society of China, 22*, s793-s800.

Lauwers, Bert. (2011). Surface integrity in hybrid machining processes. *Procedia Engineering, 19*, 241-251.

Lauwers, Bert, Bleicher, F, Ten Haaf, P, Vanparys, Mieke, Bernreiter, J, Jacobs, T, & Loenders, J. (2010). *Investigation of the process-material interaction in ultrasonic assisted grinding of ZrO2 based ceramic materials.* Paper presented at the Proceedings of the 4th CIRP International Conference on High Performance Cutting.

Lauwers, Bert, Klocke, Fritz, Klink, Andreas, Tekkaya, A Erman, Neugebauer, Reimund, & Mcintosh, Don. (2014). Hybrid processes in manufacturing. *CIRP Annals-Manufacturing Technology, 63*(2), 561-583.

Lawn, BR, & Marshall, DB. (1979). Hardness, toughness, and brittleness: an indentation analysis. *Journal of the American ceramic society, 62*(7-8), 347-350.

Lee, Su-Jin, Kim, Jong-Do, & Suh, Jeong. (2014). Microstructural variations and machining characteristics of silicon nitride ceramics from increasing the temperature in laser assisted machining. *International journal of precision engineering and manufacturing, 15*(7), 1269-1274.

Lee, TC, & Chan, CW. (1997). Mechanism of the ultrasonic machining of ceramic composites. *Journal of materials processing technology, 71*(2), 195-201.

Li, Benkai, Li, Changhe, Zhang, Yanbin, Wang, Yaogang, Jia, Dongzhou, & Yang, Min. (2016). Grinding temperature and energy ratio coefficient in MQL grinding of high-temperature nickel-base alloy by using different vegetable oils as base oil. *Chinese Journal of Aeronautics, 29*(4), 1084-1095.

Li, CH, Li, JY, Wang, S, & Zhang, Q. (2013). Modeling and numerical simulation of the grinding temperature field with nanoparticle jet of MQL. *Advances in Mechanical Engineering, 5*, 986984.

Li, Sisi, Wu, Yongbo, & Nomura, Mitsuyoshi. (2016). Effect of grinding wheel ultrasonic vibration on chip formation in surface grinding of Inconel 718. *The International Journal of Advanced Manufacturing Technology*, 1-13.

Li, W, Wang, Y, Fan, Shouhong, & Xu, Jinfu. (2007). Wear of diamond grinding wheels and material removal rate of silicon nitrides under different machining conditions. *Materials letters, 61*(1), 54-58.

Li, Xun, & Zhang, Deyuan. (2006). Ultrasonic elliptical vibration transducer driven by single actuator and its application in precision cutting. *Journal of materials processing technology, 180*(1), 91-95.

Li, Yaguo, Zheng, Nan, Li, Haibo, Hou, Jing, Lei, Xiangyang, Chen, Xianhua, . . . Guo, Yinbiao. (2011). Morphology and distribution of subsurface damage in optical fused silica parts: Bound-abrasive grinding. *Applied Surface Science, 257*(6), 2066-2073.

Liang, Zhi Qiang, Wang, Xi Bin, Wu, Yong Bo, & Zhao, Wen Xiang. (2010). *Elliptical ultrasonic assisted grinding (EUAG) of monocrystal sapphire–surface formation characteristics.* Paper presented at the Advanced Materials Research.

Liang, Zhiqiang, Wang, Xibin, Wu, Yongbo, Xie, Lijing, Liu, Zhibing, & Zhao, Wenxiang. (2012). An investigation on wear mechanism of resin-bonded diamond wheel in Elliptical Ultrasonic Assisted Grinding (EUAG) of monocrystal sapphire. *Journal of Materials Processing Technology, 212*(4), 868-876.

Liang, Zhiqiang, Wang, Xibin, Zhao, Wenxiang, Wu, Yongbo, Sato, Takashi, & Lin, Weimin. (2010). A feasibility study on elliptical ultrasonic assisted grinding of sapphire substrate. *International Journal of Abrasive Technology, 3*(3), 190-202.

Lin, Chin-Teng. (1996). *Neural fuzzy systems: a neuro-fuzzy synergism to intelligent systems*: Prentice hall PTR.

Linke, Barbara. (2016). Bonding systems *Life cycle and sustainability of abrasive tools* (pp. 63-95): Springer.

Liu, K, Li, XP, & Rahman, M. (2008). Characteristics of ultrasonic vibration-assisted ductile mode cutting of tungsten carbide. *The International Journal of Advanced Manufacturing Technology, 35*(7-8), 833-841.

Liu, Wei, Deng, Zhaohui, Shang, Yuanyuan, & Wan, Linlin. (2017). Effects of grinding parameters on surface quality in silicon nitride grinding. *Ceramics International, 43*(1), 1571-1577.

Lv, Dongxi, Huang, Yanhua, Tang, Yongjian, & Wang, Hongxiang. (2013). Relationship between subsurface damage and surface roughness of glass BK7 in rotary ultrasonic machining and conventional grinding processes. *The International Journal of Advanced Manufacturing Technology, 67*(1-4), 613-622.

Lv, Tao, Huang, Shuiquan, Hu, Xiaodong, Ma, Yaliang, & Xu, Xuefeng. (2018). Tribological and machining characteristics of a minimum quantity lubrication (MQL) technology using GO/SiO 2 hybrid nanoparticle water-based lubricants as cutting fluids. *The International Journal of Advanced Manufacturing Technology*, 1-12.

Ma, Chun Xiang, Shamoto, Eiji, & Moriwaki, T. (2005). *Drilling assisted by ultrasonic elliptical vibration.* Paper presented at the Key engineering materials.

Mahaddalkar, Prasanna M, & Miller, Michele H. (2014). Force and thermal effects in vibration-assisted grinding. *The International Journal of Advanced Manufacturing Technology, 71*(5-8), 1117-1122.

Maher, Ibrahem, Eltaib, MEH, Sarhan, Ahmed AD, & El-Zahry, RM. (2015). Cutting force-based adaptive neuro-fuzzy approach for accurate surface roughness prediction in end milling operation for intelligent machining. *The International Journal of Advanced Manufacturing Technology, 76*(5-8), 1459-1467.

Maksoud, TMA, Mokbel, AA, & Morgan, JE. (1999). Evaluation of surface and sub-surface cracks of ground ceramic. *Journal of Materials Processing Technology, 88*(1), 222-243.

Malkin, S. (1989). Grinding Technology: Theory and Applications of Machining with AbrasivesEllis Horwood Limited. *Chichester, England*.

Malkin, S, & Hwang, TW. (1996). Grinding mechanisms for ceramics. *CIRP Annals-Manufacturing Technology, 45*(2), 569-580.

Mao, Cong, Tang, Xiaojun, Zou, Hongfu, Zhou, ZhiXiong, & Yin, Wangwu. (2012). Experimental investigation of surface quality for minimum quantity oil–water lubrication grinding. *The International Journal of Advanced Manufacturing Technology, 59*(1-4), 93-100.

Marinescu, Ioan D. (2006). *Handbook of advanced ceramics machining*: CRC Press.

Marinescu, Ioan D, Hitchiner, Mike P, Uhlmann, Eckart, Rowe, W Brian, & Inasaki, Ichiro. (2006). *Handbook of machining with grinding wheels*: CRC Press.

Marshall, David B, & Lawn, Brian R. (1985). Indentation of brittle materials *Microindentation Techniques in Materials Science and Engineering*: ASTM International.

McNamara, Declan, Alveen, Patricia, Carolan, Declan, Murphy, Neal, & Ivanković, Aloz. (2014). Micromechanical study of strength and toughness of advanced ceramics. *Procedia Materials Science, 3*, 1810-1815.

Molaie, MM, Akbari, J, & Movahhedy, MR. (2016). Ultrasonic assisted grinding process with minimum quantity lubrication using oil-based nanofluids. *Journal of Cleaner Production, 129*, 212-222.

Moneim, M Es Abdel, & Abdou, S. (1997). Comments on the wear mechanisms of impregnated diamond bits. *Wear, 205*(1), 228-230.

Moriwaki, Toshimichi, & Shamoto, Eiji. (1991). Ultraprecision diamond turning of stainless steel by applying ultrasonic vibration. *CIRP Annals-Manufacturing Technology, 40*(1), 559-562.

Moriwaki, Toshimichi, & Shamoto, Eiji. (1995). Ultrasonic elliptical vibration cutting. *CIRP Annals-Manufacturing Technology, 44*(1), 31-34.

Moriwaki, Toshimichi, Shamoto, Eiji, & Inoue, Kenji. (1992). Ultraprecision ductile cutting of glass by applying ultrasonic vibration. *CIRP Annals-Manufacturing Technology, 41*(1), 141-144.

Munoz-Tabares, JA, Jiménez-Piqué, E, Reyes-Gasga, J, & Anglada, M. (2011). Microstructural changes in ground 3Y-TZP and their effect on mechanical properties. *Acta Materialia, 59*(17), 6670-6683.

Nakamura, Masayoshi, Sumomogi, Tsunetaka, & Endo, Toshiro. (2003). Evaluation of surface and subsurface cracks on nano-scale machined brittle materials by scanning force microscope and scanning laser microscope. *Surface and Coatings Technology, 169*, 743-747.

Negishi, Nobuhiko. (2003). Elliptical vibration assisted machining with single crystal diamond tools.

Niinomi, Mitsuo. (2002). Recent metallic materials for biomedical applications. *Metallurgical and Materials Transactions A, 33*(3), 477. doi: 10.1007/s11661-002-0109-2

Nik, Mohsen Ghahramani, Movahhedy, Mohammad R, & Akbari, Javad. (2012). Ultrasonic-assisted grinding of Ti6Al4V alloy. *Procedia CIRP, 1*, 353-358.

Nomura, Mitsuyoshi, Wu, Yong Bo, Kuriyagawa, Tsunemoto, Kawashima, Takahiro, & Shibata, Takayuki. (2009). *Effects of grain size and concentration of grinding wheel in ultrasonically assisted grinding.* Paper presented at the Key Engineering Materials.

Nomura, Mitsuyoshi, Wu, Yongbo, & Kuriyagawa, Tsunemoto. (2007). Investigation of internal ultrasonically assisted grinding of small holes: effect of ultrasonic vibration in truing and dressing of small CBN grinding wheel. *Journal of mechanical science and technology, 21*(10), 1605-1611.

Oliveira, JFG, & Alves, Sale Martins. (2006). Development of environmentally friendly fluid for CBN grinding. *CIRP Annals-Manufacturing Technology, 55*(1), 343-346.

Olofsson, Johanna, Grehk, T Mikael, Berlind, Torun, Persson, Cecilia, Jacobson, Staffan, & Engqvist, Håkan. (2012). Evaluation of silicon nitride as a wear resistant and resorbable alternative for total hip joint replacement. *Biomatter, 2*(2), 94-102.

Ooi, Ming Erh, Sayuti, Mohd, & Sarhan, Ahmed AD. (2015). Fuzzy logic-based approach to investigate the novel uses of nano suspended lubrication in precise machining of aerospace AL tempered grade 6061. *Journal of Cleaner Production, 89*, 286-295.

Park, Kyung-Hee, Hong, Yun-Hyuck, Kim, Kyeong-Tae, Lee, Seok-Woo, Choi, Hon-Zong, & Choi, Young-Jae. (2013). Understanding of Ultrasonic Assisted Machining with Diamond Grinding Tool. *Modern Mechanical Engineering, 4*(01), 1.

Park, Kyung Hee, Kim, Kyeong Tae, Hong, Yun Hyuck, Choi, Hon Jong, & Choi, Young Jae. (2012). *Study on effect of ultrasonic vibration in machining of alumina ceramic.* Paper presented at the Key Engineering Materials.

Paul, Ed, Evans, Chris J, Mangamelli, Anthony, McGlauflin, Michael L, & Polvani, Robert S. (1996). Chemical aspects of tool wear in single point diamond turning. *Precision Engineering, 18*(1), 4-19.

Pei, Zhijian. (1995). *Rotary ultrasonic machining of ceramics: characterization and extensions.* University of Illinois at Urbana-Champaign.

Pei, ZJ, Ferreira, PM, & Haselkorn, M. (1995). Plastic flow in rotary ultrasonic machining of ceramics. *Journal of Materials Processing Technology, 48*(1), 771-777.

Peng, De-Xing, Chen, Cheng-Hsien, Kang, Yuan, Chang, Yeon-Pun, & Chang, Shi-Yan. (2010). Size effects of SiO2 nanoparticles as oil additives on tribology of lubricant. *Industrial Lubrication and Tribology, 62*(2), 111-120.

Peng, DX, Kang, Y, Hwang, RM, Shyr, SS, & Chang, YP. (2009). Tribological properties of diamond and SiO2 nanoparticles added in paraffin. *Tribology international, 42*(6), 911-917.

Peng, Y, Liang, Z, Wu, Y, Guo, Y, & Wang, C. (2012). Characteristics of chip generation by vertical elliptic ultrasonic vibration-assisted grinding of brittle materials. *The International Journal of Advanced Manufacturing Technology, 62*(5-8), 563-568.

Peng, Y, Wu, YB, Liang, ZQ, Guo, YB, & Lin, X. (2011). An experimental study of ultrasonic vibration-assisted grinding of polysilicon using two-dimensional vertical workpiece vibration. *The International Journal of Advanced Manufacturing Technology, 54*(9-12), 941-947.

Pfeiffer, W, & Hollstein, T. (1993). Damage determination and strength prediction of machined ceramics by X-ray diffraction techniques. *Machining of Advanced Materials*, 235-245.

Prabhakar, D, Ferreira, PM, & Haselkorn, M. (1992). An experimental investigation of material removal rates in rotary ultrasonic machining. *Transactions of the North American Manufacturing Research Institution of SME., 20*, 211-218.

Qin, Na, Pei, ZJ, Treadwell, C, & Guo, DM. (2009). Physics-based predictive cutting force model in ultrasonic-vibration-assisted grinding for titanium drilling. *Journal of manufacturing science and engineering, 131*(4), 041011.

Qu, W, Wang, K, Miller, MH, Huang, Y, & Chandra, A. (2000). Using vibration-assisted grinding to reduce subsurface damage. *Precision engineering, 24*(4), 329-337.

Rabiei, F, Rahimi, AR, Hadad, MJ, & Saberi, A. (2017). Experimental evaluation of coolant-lubricant properties of nanofluids in ultrasonic assistant MQL grinding. *The International Journal of Advanced Manufacturing Technology, 93*(9-12), 3935-3953.

Rao, R Venkata. (2007). Cutting fluid selection for a given machining application. *Decision Making in the Manufacturing Environment: Using Graph Theory and Fuzzy Multiple Attribute Decision Making Methods*, 97-114.

Rekow, D, & Thompson, VP. (2005). Near-surface damage-a persistent problem in crowns obtained by computer-aided design and manufacturing. *Proceedings of the Institution of Mechanical Engineers, Part H: Journal of Engineering in Medicine, 219*(4), 233-243.

Riley, Frank L. (2000). Silicon nitride and related materials. *Journal of the American Ceramic Society, 83*(2), 245-265.

Rowe, W Brian. (2013). *Principles of modern grinding technology*: William Andrew.

Sadeghi, MH, Haddad, MJ, Tawakoli, T, & Emami, M. (2009). Minimal quantity lubrication-MQL in grinding of Ti–6Al–4V titanium alloy. *The International Journal of Advanced Manufacturing Technology, 44*(5-6), 487-500.

Saljé, E, & Möhlen, H. (1986). Fundamental dependencies upon contact lengths and results in grinding. *CIRP Annals-Manufacturing Technology, 35*(1), 249-253.

Samant, Anoop N, & Dahotre, Narendra B. (2009). Laser machining of structural ceramics—a review. *Journal of the European Ceramic Society, 29*(6), 969-993.

Sarhan, Ahmed AD, Sayuti, M, & Hamdi, M. (2012a). Reduction of power and lubricant oil consumption in milling process using a new SiO2 nanolubrication system. *The International Journal of Advanced Manufacturing Technology, 63*(5-8), 505-512.

Sarhan, Ahmed AD, Sayuti, M, & Hamdi, M. (2012b). Reduction of power and lubricant oil consumption in milling process using a new SiO 2 nanolubrication system. *The International Journal of Advanced Manufacturing Technology, 63*(5), 505-512.

Sayuti, M, Sarhan, Ahmed AD, Fadzil, M, & Hamdi, M. (2012). Enhancement and verification of a machined surface quality for glass milling operation using CBN grinding tool—Taguchi approach. *The International Journal of Advanced Manufacturing Technology, 60*(9-12), 939-950.

Sayuti, M, Sarhan, Ahmed AD, & Hamdi, M. (2013). An investigation of optimum SiO 2 nanolubrication parameters in end milling of aerospace Al6061-T6 alloy. *The International Journal of Advanced Manufacturing Technology*, 1-17.

Sayuti, Mohd, Erh, Ooi Ming, Sarhan, Ahmed AD, & Hamdi, Mohd. (2014). Investigation on the morphology of the machined surface in end milling of aerospace AL6061-T6 for novel uses of SiO 2 nanolubrication system. *Journal of Cleaner Production, 66*, 655-663.

Shamoto, Eiji, & Moriwaki, Toshimichi. (1994). Study on elliptical vibration cutting. *CIRP Annals-Manufacturing Technology, 43*(1), 35-38.

Shamoto, Eiji, & Moriwaki, Toshimichi. (1999). Ultaprecision diamond cutting of hardened steel by applying elliptical vibration cutting. *CIRP Annals-Manufacturing Technology, 48*(1), 441-444.

Shen, JY, Wang, JQ, Jiang, B, & Xu, XP. (2015). Study on wear of diamond wheel in ultrasonic vibration-assisted grinding ceramic. *Wear, 332*, 788-793.

Shi, Donglu. (2006). *Introduction to biomaterials*: 清华大学出版社有限公司.

Shih, AJ, McSpadden, SB, Morris, TO, Grant, MB, & Yonushonis, TM. (2000). High speed and high material removal rate grinding of ceramics using the vitreous bond CBN wheel. *Machining Science and Technology, 4*(1), 43-58.

Shimada, S, Tanaka, H, Higuchi, M, Yamaguchi, T, Honda, S, & Obata, K. (2004). Thermo-chemical wear mechanism of diamond tool in machining of ferrous metals. *CIRP Annals-Manufacturing Technology, 53*(1), 57-60.

Sinha, Manoj Kumar, Madarkar, Rajeshkumar, Ghosh, Sudarsan, & Rao, P Venkateswara. (2017). Application of eco-friendly nanofluids during grinding of Inconel 718 through small quantity lubrication. *Journal of cleaner production, 141*, 1359-1375.

Speidel, Markus O, & Uggowitzer, Peter J. (1992). High manganese, high nitrogen austenitic stainless steels: their strength and toughness.

Spur, G, Stark, C, & Tio, TH. (1985). Grinding of non-oxide ceramics using diamond grinding wheels. *Machining of Ceramic Materials and Components*, 33-44.

Spur, Günter, & Holl, S-E. (1996). Ultrasonic assisted grinding of ceramics. *Journal of Materials Processing Technology, 62*(4), 287-293.

Sreejith, PS. (2005). Machining force studies on ductile machining of silicon nitride. *Journal of materials processing technology, 169*(3), 414-417.

Su, Jang Kwang, Lin, Bin, & Wang, Lei. (2014). *Study on the Model of Surface Crack Depth in Ceramics Grinding.* Paper presented at the Advanced Materials Research.

Suh, Chang-Min, Bae, Kyo-Seouk, & Suh, Min-Soo. (2008). Wear behavior of diamond wheel for grinding optical connector ferrule—FEA and wear test—. *Journal of mechanical science and technology, 22*(11), 2009-2015.

Suzuki, K, Uematsu, T, Makizaki, T, & Iwai, M. (2000). *Ultrasonic grinding utilizing a stator of an ultrasonic motor.* Paper presented at the Proceedings of JSME Conference Manufacturing and Machine Tool.

Suzuki, Kiyoshi, Uematsu, Tetsutaro, Iwai, Manabu, Ninomiya, Shinichi, Sano, Sadao, & Nakagawa, Takeo. (2007). *A New Complex grinding method for ceramic materials combined with ultrasonic vibration and electrodischarge machining.* Paper presented at the Key Engineering Materials.

Suzuki, Norikam, Nakamura, Akihiro, Shamoto, Eiji, Harada, Kanrhiro, Matsuo, Makoio, & Osada, Michio. (2003). *Ultraprecision micromachining of hardened steel by applying ultrasonic elliptical vibration cutting.* Paper presented at the Micromechatronics and Human Science, 2003. MHS 2003. Proceedings of 2003 International Symposium on.

Tan, Yuanqiang, Yang, Dongmin, & Sheng, Yong. (2008). Study of polycrystalline Al 2 O 3 machining cracks using discrete element method. *International Journal of Machine Tools and Manufacture, 48*(9), 975-982.

Tawakoli, T, Hadad, MJ, & Sadeghi, MH. (2010). Investigation on minimum quantity lubricant-MQL grinding of 100Cr6 hardened steel using different abrasive and coolant–lubricant types. *International Journal of Machine Tools and Manufacture, 50*(8), 698-708.

Tawakoli, T, Hadad, MJ, Sadeghi, MH, Daneshi, A, Stöckert, S, & Rasifard, A. (2009). An experimental investigation of the effects of workpiece and grinding parameters on minimum quantity lubrication—MQL grinding. *International Journal of Machine Tools and Manufacture, 49*(12), 924-932.

Tawakoli, Taghi, & Azarhoushang, Bahman. (2009). *Effects of ultrasonic assisted grinding on CBN grinding wheels performance.* Paper presented at the ASME 2009 International Manufacturing Science and Engineering Conference.

Tawakoli, Taghi, Azarhoushang, Bahman, & Rabiey, Mohammad. (2009). Ultrasonic assisted dry grinding of 42CrMo4. *The International Journal of Advanced Manufacturing Technology, 42*(9-10), 883-891.

Tawakoli, Taghi, Hadad, Mohammadjafar, Sadeghi, Mohammad Hossein, Daneshi, Amir, & Sadeghi, Banafsheh. (2011). Minimum quantity lubrication in grinding: effects of abrasive and coolant–lubricant types. *Journal of Cleaner Production, 19*(17), 2088-2099.

Tawakoli, Taghi, Westkämper, Engelbert, & Azarhoushang, Bahman. (2009). *Effects of vibration-assisted grinding on wear behavior of vitrified bond Al2O3 wheel.* Paper presented at the Advanced Materials Research.

Tesfay, Hayelom D, Xu, Zhigang, & Li, ZC. (2016). Ultrasonic vibration assisted grinding of bio-ceramic materials: an experimental study on edge chippings with Hertzian indentation tests. *The International Journal of Advanced Manufacturing Technology*, 1-12.

Thoe, TB, Aspinwall, DK, & Wise, MLH. (1998). Review on ultrasonic machining. *International Journal of Machine Tools and Manufacture, 38*(4), 239-255.

Uhlmann, E, & Hübert, C. (2006). *Advances in ultrasonic assisted grinding of ceramic materials.* Paper presented at the Advances in Science and Technology.

Uhlmann, Eckart, & Hübert, Christoph. (2007). *Ultrasonic assisted grinding of advanced ceramics.* Paper presented at the Proceedings of the ASPE spring topical meeting.

Uhlmann, Eckart, & Sammler, C. (2010). Influence of coolant conditions in ultrasonic assisted grinding of high performance ceramics. *Production Engineering, 4*(6), 581-587.

Vanparys, Mieke, Liu, Weidong, & Lauwers, Bert. (2008). *Influence of machining parameters and tool wear on the material removal mechanisms in the ultrasonic assisted grinding of Al2O3.* Paper presented at the Proceedings of the 3rd CIRP International Conference High Performance Cutting.

Verma, Arpana, Jiang, Wenping, Abu Safe, Husam H, Brown, William D, & Malshe, Ajay P. (2008). Tribological behavior of deagglomerated active inorganic nanoparticles for advanced lubrication. *Tribology Transactions, 51*(5), 673-678.

Vicario, Inaki, Gonzalo, Oscar, & Bengoetxea, Ion. (2007). Rotary ultrasonic machining of aluminium oxide ceramics: designed experiments. *International Journal of Machining and Machinability of Materials, 2*(2), 233-243.

Wang, Changchu, Fang, Qihong, Chen, Jianbin, Liu, Youwen, & Jin, Tan. (2015). Subsurface damage in high-speed grinding of brittle materials considering kinematic characteristics of the grinding process. *The International Journal of Advanced Manufacturing Technology*, 1-12.

Wang, Hailong, Wang, Chang-An, Yao, Xuefeng, & Fang, Daining. (2007). Processing and Mechanical Properties of Zirconium Diboride-Based Ceramics Prepared by Spark Plasma Sintering. *Journal of the American Ceramic Society, 90*(7), 1992-1997.

Wang, X, & Ren, J. (1997). Ground surface damage of structure ceramics. *J. Chin. Ceram. Soc., 25*(1), 101-105.

Wang, Yan, Lin, Bin, Cao, Xiaoyan, & Wang, Shaolei. (2014). An experimental investigation of system matching in ultrasonic vibration assisted grinding for titanium. *Journal of Materials Processing Technology, 214*(9), 1871-1878.

Wang, Yan, Lin, Bin, Wang, Shaolei, & Cao, Xiaoyan. (2014). Study on the system matching of ultrasonic vibration assisted grinding for hard and brittle materials processing. *International Journal of Machine Tools and Manufacture, 77*, 66-73.

Wang, Yan, Lin, Bin, & Zhang, Xiaofeng. (2014). Research on the system matching model in ultrasonic vibration-assisted grinding. *The International Journal of Advanced Manufacturing Technology, 70*(1-4), 449-458.

Wang, Yaogang, Li, Changhe, Zhang, Yanbin, Yang, Min, Zhang, Xianpeng, Zhang, Naiqing, & Dai, Jingjie. (2016). Experimental evaluation on tribological performance of the wheel/workpiece interface in minimum quantity lubrication grinding with different concentrations of Al2O3 nanofluids. *Journal of Cleaner Production, 30*, 1e13.

Wang, Yiding, Moon, Kee S, & Miller, Michele H. (1998). A new method for improving the surface grinding process. *Journal for Manufacturing Science and Production, 1*(3), 159-168.

Wang, Zhuo, Wu, Yulie, Dai, Yifan, & Li, Shengyi. (2008). Subsurface damage distribution in the lapping process. *Applied optics, 47*(10), 1417-1426.

Warnecke, G, Rosenberger, U, & Milberg, J. (1995). Basics of process parameter selection in grinding of advanced ceramics. *CIRP Annals-Manufacturing Technology, 44*(1), 283-286.

Weber, Horst, Herberger, Jürgen, & Pilz, Rolf. (1984). Turning of machinable glass ceramics with an ultrasonically vibrated tool. *CIRP Annals-Manufacturing Technology, 33*(1), 85-87.

Williams, James C, & Starke, Edgar A. (2003). Progress in structural materials for aerospace systems. *Acta Materialia, 51*(19), 5775-5799.

Winter, Marius, Ibbotson, Suphunnika, Kara, Sami, & Herrmann, Christoph. (2015). Life cycle assessment of cubic boron nitride grinding wheels. *Journal of Cleaner Production, 107*, 707-721.

Wu, Y, Nomura, M, Kato, M, & Tachibana, T. (2003). Study of internal ultrasonic vibration assisted grinding of small holes,-Construction of ultrasonic vibration spindle and its fundamental performances. *J. Jpn. Soc. Abras. Technol, 47*(10), 550.

Xiao, Xingzhi, Zheng, Kan, & Liao, Wenhe. (2014). Theoretical model for cutting force in rotary ultrasonic milling of dental zirconia ceramics. *The International Journal of Advanced Manufacturing Technology, 75*(9-12), 1263-1277.

Xiao, Xingzhi, Zheng, Kan, Liao, Wenhe, & Meng, Heng. (2016). Study on cutting force model in ultrasonic vibration assisted side grinding of zirconia ceramics. *International Journal of Machine Tools and Manufacture, 104*, 58-67.

Xin-honga, YANG, Jie-caib, HAN, Yu-minb, ZHANG, Hong-bob, ZUO, & Xue-junb, ZHANG. (2006). Research on ultrasonic vibration grinding of the hard and brittle materials. *Chinese Journal of Aeronautics, 19*, S9-S13.

Xu, Hockin HK, & Jahanmir, S. (1995). Microfracture and material removal in scratching of alumina. *Journal of materials science, 30*(9), 2235-2247.

Xu, Hockin HK, Jahanmir, Said, & Ives, Lewis K. (1996). Material removal and damage formation mechanisms in grinding silicon nitride. *Journal of Materials research, 11*(7), 1717-1724.

Xue, JX, An, LL, & Sun, QP. (2013). *Grinding Technology for Engineering Ceramics-A Review.* Paper presented at the Advanced Materials Research.

Yan, Yan Yan, Liu, Jun Li, & Zhao, Bo. (2011). *Study on the Prediction of Surface Roughness of ZTA Ceramics under Ultrasonic Assisted Grinding.* Paper presented at the Advanced Materials Research.

Yan, Yan Yan, Zhao, Bo, Wu, Yan, Liu, Chuan Shao, & Zhu, Xun Sheng. (2006). *Study on material removal mechanism of fine-crystalline ZrO2 ceramics under two dimensional ultrasonic grinding.* Paper presented at the Materials Science Forum.

Yanyan, Yan, Bo, Zhao, & Junli, Liu. (2009). Ultraprecision surface finishing of nano-ZrO2 ceramics using two-dimensional ultrasonic assisted grinding. *The International Journal of Advanced Manufacturing Technology, 43*(5-6), 462-467.

Yu, Helong, Xu, Yi, Shi, Peijing, Wang, Hongmei, Wei, Min, Zhao, Keke, & Xu, Binshi. (2013). Microstructure, mechanical properties and tribological behavior of tribofilm generated from natural serpentine mineral powders as lubricant additive. *Wear, 297*(1-2), 802-810.

Zadeh, Lotfi A. (1996). Fuzzy sets *Fuzzy Sets, Fuzzy Logic, And Fuzzy Systems: Selected Papers by Lotfi A Zadeh* (pp. 394-432): World Scientific.

Zahedi, Ali, Tawakoli, Taghi, & Akbari, Javad. (2015). Energy aspects and workpiece surface characteristics in ultrasonic-assisted cylindrical grinding of alumina–zirconia ceramics. *International Journal of Machine Tools and Manufacture, 90*, 16-28.

Zalnezhad, E, Sarhan, Ahmed AD, & Hamdi, M. (2013). A fuzzy logic based model to predict surface hardness of thin film TiN coating on aerospace AL7075-T6 alloy. *The International Journal of Advanced Manufacturing Technology, 68*(1-4), 415-423.

Zemzemi, F, Rech, J, Salem, W Ben, Dogui, A, & Kapsa, Ph. (2014). Identification of friction and heat partition model at the tool-chip-workpiece interfaces in dry cutting of an Inconel 718 alloy with CBN and coated carbide tools. *Advances in Manufacturing Science and Technology, 38*(1).

Zeng, WM, Li, ZC, Pei, ZJ, & Treadwell, C. (2005). Experimental observation of tool wear in rotary ultrasonic machining of advanced ceramics. *International Journal of Machine Tools and Manufacture, 45*(12), 1468-1473.

Zhang, Bi, & Howes, Trevor D. (1994). Material-removal mechanisms in grinding ceramics. *CIRP Annals-Manufacturing Technology, 43*(1), 305-308.

Zhang, Bi, & Howes, Trevor D. (1995). Subsurface evaluation of ground ceramics. *CIRP Annals-Manufacturing Technology, 44*(1), 263-266.

Zhang, Bi, Zheng, XL, Tokura, H, & Yoshikawa, M. (2003). Grinding induced damage in ceramics. *Journal of materials processing technology, 132*(1), 353-364.

Zhang, DongKun, Li, Changhe, Jia, Dongzhou, & Zhang, Yanbin. (2014). Investigation into engineering ceramics grinding mechanism and the influential factors of the grinding force. *Int J Control Autom, 7*(4), 19-34.

Zhang, Hong Li, Zhang, Jian Hua, & Huo, Meng You. (2006). *Study on ultrasonic vibration assisted grinding in theory.* Paper presented at the Materials Science Forum.

Zhang, Yanbin, Li, Changhe, Jia, Dongzhou, Zhang, Dongkun, & Zhang, Xiaowei. (2015). Experimental evaluation of MoS 2 nanoparticles in jet MQL grinding with different types of vegetable oil as base oil. *Journal of Cleaner Production, 87*, 930-940.

Zhang, Ying-Wei, Yu, Jian-Bo, Xia, Yong-Feng, Zuo, Kai-Hui, Yao, Dong-Xu, Zeng, Yu-Ping, & Ren, Zhong-Ming. (2012). Microstructure and mechanical performance of silicon nitride ceramics with seeds addition. *Wuji Cailiao Xuebao(Journal of Inorganic Materials), 27*(8), 807-812.

Zhao, Bo, Yan, Yan Yan, Wu, Yan, Jiao, Feng, & Liu, CS. (2006). *Study on motion model of abrasive particle and surface formation mechanics under two dimensional ultrasonic grinding.* Paper presented at the Key Engineering Materials.

Zhao, Bo, Zhang, XH, Liu, CS, Jiao, Feng, & Zhu, Xun Sheng. (2005). *Study on ultrasonic vibration grinding character of nano ZrO2 ceramics.* Paper presented at the Key Engineering Materials.

Zheng, Kan, Li, Zhihua, Liao, Wenhe, & Xiao, Xingzhi. (2016). Friction and wear performance on ultrasonic vibration assisted grinding dental zirconia ceramics against natural tooth. *Journal of the Brazilian Society of Mechanical Sciences and Engineering*, 1-11.

Zhong, ZW, & Venkatesh, VC. (2009). Recent developments in grinding of advanced materials. *The International Journal of Advanced Manufacturing Technology, 41*(5-6), 468-480.

Zhong, ZW, & Yang, HB. (2004). Development of a vibration device for grinding with microvibration. *Materials and manufacturing processes, 19*(6), 1121-1132.

Zhou, Ming, Wang, XJ, Ngoi, BKA, & Gan, JGK. (2002). Brittle–ductile transition in the diamond cutting of glasses with the aid of ultrasonic vibration. *Journal of Materials Processing Technology, 121*(2), 243-251.

LIST OF PUBLICATIONS

Papers published or under review in ISI indexed journals

1. **Dambatta, Yusuf S**, Sarhan, Ahmed AD, Sayuti, M, & Hamdi, M. (2017). Ultrasonic assisted grinding of advanced materials for biomedical and aerospace applications—a review. The International Journal of Advanced Manufacturing Technology, 1-34. **(Published)**.
2. **Dambatta Yusuf S**, M. Sayuti, Ahmed A. D. Sarhan, M. Hamdi, (2018). Comparative study on the performance of the MQL nanolubricant and conventional flood lubrication techniques during grinding of Si_3N_4 ceramic. The International Journal of Advanced Manufacturing Technology, 1-34. **(Published)**.
3. **Dambatta Yusuf S**, M. Sayuti, Ahmed A. D. Sarhan, M. Hamdi, S.M Manladan (2018). Prediction of Grinding Forces and Surface Roughness in Machining of AL6061-T6 alloy with Minimum Quantity nanolubrication Technique. Journal of Industrial Lubrication and Tribology **(Published)**.
4. **Dambatta Yusuf S.**, M. Sayuti, Nur Aqilah Delrahman, Ahmed A. D. Sarhan, M. Hamdi (2018). Study of Minimum Quantity Lubrication in Grinding of Al6061 Alloy Using Adaptive Neuro-fuzzy Inference System (ANFIS) Modelling Technique. International Journal of Materials and Product Technology (IJMPT) **(Accepted)**.
5. **Dambatta Yusuf S**, M. Sayuti, Ahmed A. D. Sarhan, M. Hamdi, S.M. Manladan (2018). Investigating The Effects Of Minimum Quantity Lubrication Grinding Of Silicon Nitride Ceramic Using Silicon Dioxide Based Nanofluid. Journal of Manufacturing Processes (**Under review**).

Papers Accepted In Conferences

1. M. Sayuti, Yusuf S. Dambatta, Ahmed A. D. Sarhan, M. Hamdi, SM. Manladan (2017). An experimental analysis of the effects of grinding parameters on minimum quantity lubrication-MQL grinding of AL6061-T6: ANFIS modelling approach. **2nd Advanced Research in Engineering and Information Technology International Conference (*AREITIC*) (Accepted).**
2. Yusuf S. Dambatta, M. Sayuti, Nur Aqilah Delrahman, Ahmed A. D. Sarhan, M. Hamdi (2018). Study of Minimum Quantity Lubrication in Grinding of Al6061 Alloy Using Adaptive Neuro-fuzzy Inference System (ANFIS) Modelling Technique. **(The 5th Mechanical Engineering Research Day - MERD 18') (Accepted).**